89 2011

Lenzinger Berichte

LENZING

LEADING FIBER INNOVATION

Table of Contents

METHODS, RAW MATERIALS, WEBS AND PARTICLES

IN MEMORIAM

Professor Kirill E. Perepelkin
1929 – 2011

On 15 February 2011, Professor Perepelkin, a well-known authority in the field of polymers and chemical fibers, died at the age of 81 at a hospital in St. Petersburg.

Kirill E. Perepelkin was born on December 21, 1929 in Leningrad (now St. Petersburg). In 1953 he graduated from the Leningrad Textile Institute, Faculty of Chemical Technology, was awarded a Ph.D. in 1965, and in 1966 became a D.Sc. from the Leningrad Institute of Textile and Light Industry. In 1967, he received a Professorship at the All-Union Research Institute of Chemical Fibres. Altogether from 1953 to 1983 Professor Perepelkin worked at this institute, starting from senior scientist to finally becoming the Head of the Research Department of Fibres and Fibrous Materials. Thereafter he became Deputy Director of R&D at the Leningrad Research Institute of Chemical Fibres & Composites and from 2001 was Professor at the St. Petersburg State University of Technology and Design.

K. E. Perepelkin has carried out fundamental research into the structure and properties of oriented polymer materials, fibers and films. New types of fibers, with specific high performance and functional properties – e.g. high-strength, superhigh-modulus, thermo- and chemo-resistance, inflammability – have been of central interest to him. He investigated on the reinforcing properties of chemical fibres and specific features of their application to polymer composites, made a significant contribution to the development of the theory of extreme properties of materials, and substantiated the values of theoretical and maximum attainable properties for many materials.

K. E. Perepelkin was a leading speaker at many international conferences, amongst others also at the Dornbirn Man-made Fibers congress in Austria. He was the author of more than 900 scientific publications, including 20 monographs and 35 published reviews, as well as some papers devoted to Chemical and Polymer Encyclopedias. He was a member of the editorial boards of 5 international scientific journals and some Scientific Councils in Russia.

The importance of Professor Perepelkin as a teacher resulted in 60 Ph.D. and 9 D.Sc. theses made under his scientific supervision. He was also a visiting professor at universities and institutes in Austria, Bulgaria, China, Germany, Poland, Slovakia and Sweden.

The Editorial Board of the journal would like to express his deepest sympathy on the loss of Professor Perepelkin – his death is a great loss to the scientific world.

DDr. Haio Harms, Kelheim Fibres

Lenzinger Berichte 89 (2011) 1-11

75 YEARS HIGH-TECH FIBRES FROM KELHEIM

Haio Harms

Kelheim Fibres GmbH, Regensburger Str. 109, 93309 Kelheim, Germany

Phone: (+49) 9441 99-250; Fax: (+49) 9441 99-1250; Email: haio.harms@kelheim-fibres.com

Speech Delivered to Mark the Occasion of 75 Years of Viscose Fibre Production in Kelheim on 15th July 2011 in the Presence of the Prime Minister of Bavaria, Horst Seehofer

Mr Minister President, Mr District President, Mr District Administrator, Mr Mayor, Father Bauer, Father Brandl, esteemed Members of Parliament, representatives of Public Authorities, Trade Associations, Science and Research Organisations, ladies and gentleman, dear guests,

Who would have predicted a decade ago that we would be able to celebrate our 75th anniversary with the opening of several plants and the announcement of substantial new investment as a successful company, honoured by the presence of the highest officials in the region?
I would like to thank you all for coming: your presence here is a sign that the fibre industry in Germany is anything but dead!
Mr Minister President, I am also delighted that you have made our celebration one of the stops on your "**New Start for Bavaria**" tour, which focuses on family, education and innovation. I will return later to the extent to which these are precisely the same values that are important to us.

We can look back on an **eventful history** and we have every reason to celebrate.
"Süddeutsche Zellwolle AG" in Kelheim started production in 1936, at a time when, due to the shortage of foreign exchange, importing cotton was virtually impossible for Germany. The process of creating fibres from the cellulose in wood was the only way of making sufficient material to clothe the population.
Viscose fibres are quite literally fabric made from trees – as you can see from this illustration that I discovered in an old Kelheim advertising brochure:

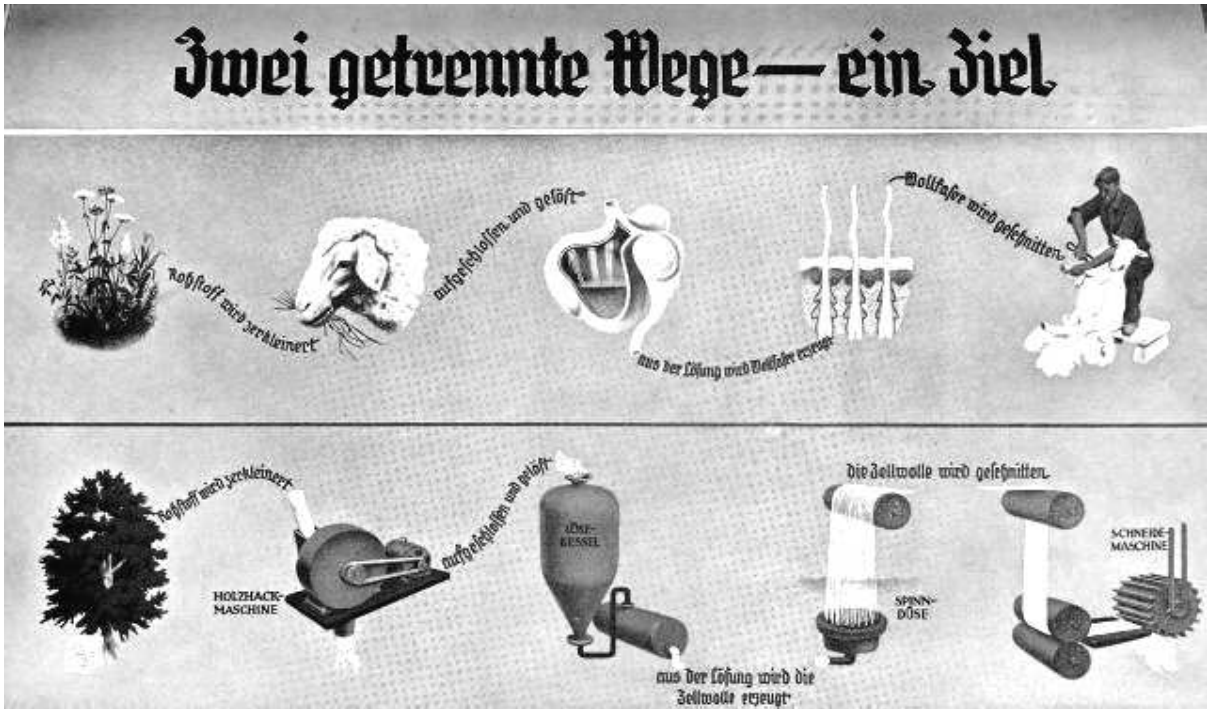

The cellulose from which our fibres are made is sustainable, natural and compatible with the human body, and some of it even comes from the beech trees in our Bavarian forests. It is hard to imagine a better way of adding value to this local resource.

Mr Minister President, I am not sure to what extent you are aware of the fact that Kelheim Fibres is a **jewel in the crown of medium-sized companies** in Bavaria – even though we do not yet produce any carbon fibre here!

Did you know, for example, that one of our products is important to more people throughout the world than all of the BMWs, Audis and Mercedes put together? Of course, our products are rather smaller in scale – but 95 % of all tampons throughout the world, used every month by women from Australia to Alaska, contain fibres from Kelheim. And do you know why? Our Galaxy® fibre is a patented, high-tech specialist product that provides better performance, greater security and more comfort than any other product made by our competitors.

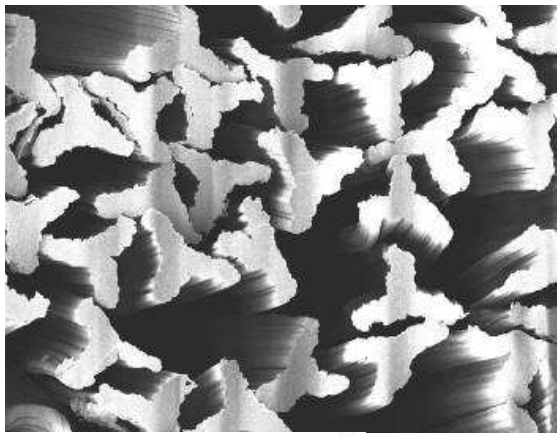

GALAXY®

Moreover, since the production of acrylic fibre began in 1960, the cars I was just talking about have also played a part: did you know that all of the premium car manufacturers use Dolan®, the acrylic fibre made in Kelheim, for the soft tops of their cabriolets, because it is the only fibre that is able to withstand the rigours of the weather and of permanent mechanical stresses over a long period of time?

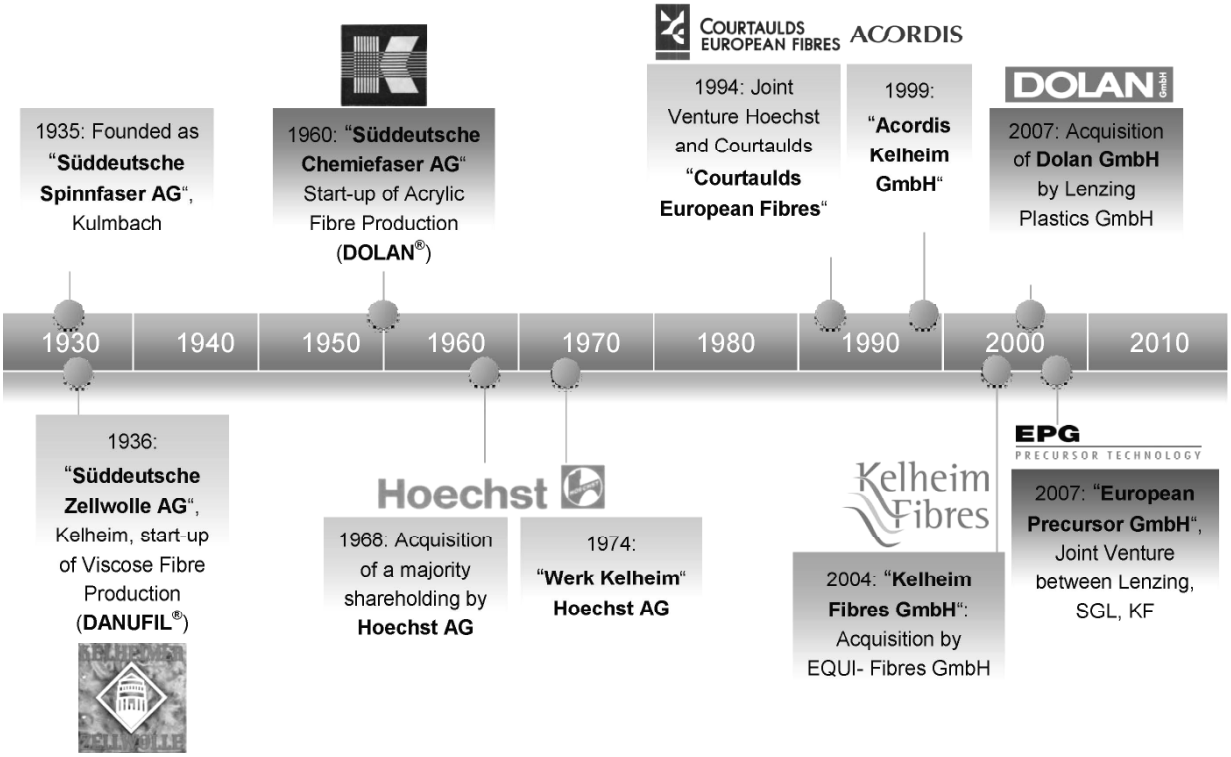

In the 1960s, chemical fibres were the flagship of the **German chemical industry** and as a result, Kelheim was taken over by HOECHST AG.

With the onset of globalisation, the fibres were first turned into a "cash cow" and then, because no effort was made to invest in them as a reaction to ongoing changes, they inevitably became "lame ducks". HOECHST gave up on fibres as part of its chemical business, then gave up altogether!
The consequences in terms of destroying value were also felt by us at our site: there were several restructuring measures and sales in the 1990s and about 15 years ago it all came close to being shut down – which certainly provides food for thought!!
But you have to look after your crown jewels! Economic and political circumstances change quickly and things can then happen very suddenly.

It was not until 2004 that Kelheim found new owners in the form of EQUI-Fibres, who were willing to work with our new identity as a medium-sized company, to turn necessity into a virtue, to turn risks into opportunities.

Of course, no one can catch up on **10 years of missing investment** in the latest technologies or operate competitively in the mainstream with small-scale machinery. Nobody can compete with commodities from the Far East in a high-cost country like Germany. But with the excellent training and expertise of our staff we are able to manufacture high-quality specialist products like nowhere else and our small machines make it possible to manufacture even tiny quantities in an efficient and flexible way.
Thanks to this willingness to invest in new processes, innovations and products, it has once again been possible to work on establishing a technological edge and a strong market position.

With a series of key investments in equipment and the establishment of EPG,

we turned the corner: from 2004 to 2010, over €100 million was invested in the site.

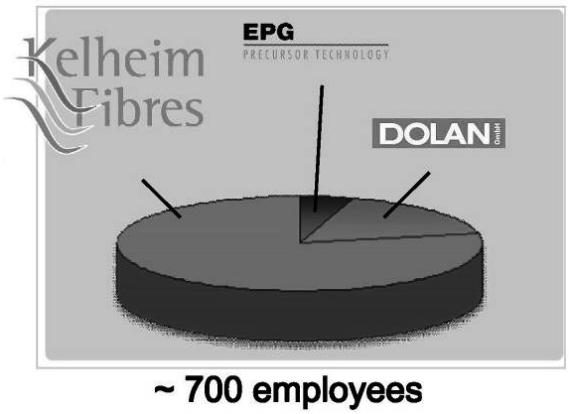

We have been able to turn the company into a "high-tech fibre" manufacturer and we feel proud of the fact that today **Kelheim Fibres GmbH** is the leading manufacturer of specialist viscose fibres in the world! With a current capacity of 80,000 metric tonnes a year and approximately 500 staff, we generate a turnover of just on €200 million.
Together with Dolan GmbH, one of the leading manufacturers of specialist acrylic fibres, and European Precursor GmbH, manufacturers of carbon fibre precursors, which have been developed as the latest specialist acrylic fibres, Kelheim is in a strong position as a fibre production site – and we are determined to build further on this position in the future.

The **Kelheim fibre site** is typical of the large sites of the chemical industry in Germany that have developed since the 1930s: using a common infrastructure and the synergies that are possible from families of products that have been adapted to complement one another has been the secret of our competitiveness. This is still true today, even though our activities have been divided among several companies!
Although each company at the site has its own production facilities, the opportunity to use the efficient infrastructure of the site, which is owned and operated by Kelheim Fibres, is essential for the competitiveness of the individual partner companies. As a service provider, Kelheim Fibres offers the other partners in the fibre association

- both specific, shared production and logistics functions
- and, above all, energy and environmental protection facilities,
- together with the majority of administrative services.

The organisation of human resources at the site is also of crucial importance to this system and this is reflected in the collective pay agreement for the site, the common operating agreements and the single works committee.
There is, however, **another side** to this model of synergies: it is very complex, because the partners still have to maintain their own autonomous positions. The loss of any one of the partners as a contributor to the costs would have far-reaching consequences for all of the others, because none would be strong enough to maintain the essential infrastructure alone.
However, the authorities and politicians are also under an obligation to help to preserve this valuable constellation; and this is frequently anything but straightforward! It is always a matter of taking special situations into consideration and a sense of proportion is always required when it comes to applying operating restrictions.

After more than ten years of severely restricted investment activity, there is naturally **a need to catch up**, particularly

as far as the infrastructure is concerned. The big challenge in this area over recent years has been the imposition of **increasingly strict requirements regarding environmental protection**.
As I mentioned, our products consist entirely of cellulose, a renewable raw material; our fibres are biologically degradable and we go to considerable lengths to ensure that our raw materials come from FSC-certified forests and that the processes used in their production are entirely chlorine-free. Sustainability is one of the most important values for us! And quite apart from our responsibility towards the environment and the local area, this naturally also includes the environmental friendliness of our processes.

Environmental protection is therefore a key value for us – and so we are particularly pleased that today we can combine our 75th anniversary celebrations with the **opening** of two large new plants specifically designed with this in mind, the BIOHOCH® Reactor III and the WSA sulphuric acid plant.

The **BIOHOCH® Reactor III** improves the position of the site as far as clean water is concerned.
BIOHOCH® reactors are based on a patented technology developed in Kelheim, which is now used throughout the world. They are used to clean the waste water from our processes biologically which is then fed back into the river. Using special air circulation systems and an specifically designed geometry, they are able to break down organic effluents with considerably more efficient space/time yields and significantly reduced energy consumption.
The new BIOHOCH® Reactor III, with a total investment of €6.5 million, will make it possible to carry out repairs on the other reactors without the need to cut back production, in general guarantee operating safety and more effective decomposition of organic matter and provide reserve capacity for possible future increases in production.

Our new **WSA sulphuric acid plant** improves the position of the site in respect of air cleanliness.
It is a plant that is fully integrated into our processes; it not only treats the waste gases containing sulphur and thereby acts as a waste gas cleaning unit; it also produces sulphuric acid, one of the most important raw materials in fibre manufacturing, as well as high-pressure steam from the excess energy produced in the process. This is then converted into electricity in the power plant, significantly reducing the consumption of fossil fuels and thus the emissions of CO_2 at the site.
This modern technology is a perfect example of being able to find innovative solutions to environmental problems that are not just a burden on competitiveness. The fact that this often comes at a high price is demonstrated by the €25 million

that we have invested; and as a result of the problems we experienced when the plant came into service, we have certainly realised that not everything is guaranteed to go smoothly with innovative, pioneering solutions.
But this is not where our **efforts in the field of environmental protection** end.
In parallel with the two projects that we are opening today, we have collaborated with the authorities to develop a **package of measures** to improve the situation of the site as far as the remaining waste air and noise emissions are concerned. Although this involves a further investment programme of about €10 million over the next few years, it is already designed to accommodate the plans for possible next stages in the site's development.

During this year we are still hoping to erect a series of buildings on the vacant site to the west of the plant which are designed to reduce the direct impact of noise on the surrounding houses. The CS_2 recovery plant is also to be improved in terms of noise and fitted with high-performance absorbers, thereby creating a certain amount of reserve capacity. After that, a variety of specific measures will be implemented to improve the situation at various sources of noise and waste gas, for example on the roof of the spinning area and in the DMF distillation plant.

The fundamental agreement of the authorities to this programme of measures to improve the environmental situation was an essential prerequisite for us to take the decision to proceed with the first stages of the **operational development of the site**, with the necessary legal guarantees in place.

I am delighted to be able to announce that our shareholders have approved the **first stage of our "UEK Programme"**, which includes measures to further improve the environmental situation of the plant, to increase the efficiency through refurbishment and to unlock capacity reserves, with an investment of approximately €25 million. Under this programme, one of our spinning lines will be refurbished, a new combined evaporation and calcination plant which will consume only 25% of the current amount of steam will be installed, and through various measures to remove bottlenecks, a capacity of 91,000 metric tonnes per year will be available to us as of the second quarter of 2012.
With the modernisation of the remaining spinning lines, in the course of the years ahead we plan to reach a total capacity of 122,000 tonnes per year in three further stages – "UEK 2 to 4", each costing about another €25 million.

After everything I said earlier about the basic market conditions we have to deal with, you will be asking yourselves whether we can be accused of setting our sights too high and trapping ourselves in **non sustainable economies of scale**.

On the one hand, given the market prices there is almost no alternative to distributing the energy costs, environmental costs, administrative, safety and ancillary wage costs, which are higher than those of our competitors and are continuing to rise here, across higher production levels in some way. If we want to survive, we have no choice other than to take this route.

But on the other hand, it is quite clear that we would not embark on a future strategy of investment, renovation of infrastructure and increase in production levels if we were not also entirely convinced that we could push forward with the **specialisation of our portfolio** at the same time: our success has come through the specialisation of our products and diversification of our markets.

I have already mentioned our leading position in the world market for **hygiene fibres** in my introductory remarks. We were recently able to file a number of key patents in this area. In addition, we are determined to provide our customers with even greater product safety in the future and we are therefore working hard on a project to establish "virtually clean room production conditions", which is a complete innovation in cellulose fibre production and is certainly not a small matter.

Cellulosic fibres: a very special material with special properties for many special applications

- physiologically neutral, skin-friendly
- hydrophilic, perfect moisture management
- restricted growth of micro organisms
- chemical stability
- chemical reactivity (dyeability, processability, adaptability)
- superb next-to-skin comfort, soft to touch
- brilliant colours
- not melting

The second market segment in which we are number one on the world market, in fact where we have a largely unchallenged position, is in **short cut fibres** for special papers such as bank notes and security papers, teabags, coffee and oil filters, and similar products. In this area, we have achieved a number of pioneering innovations over the last two years.

You will already have noticed that in all of these fields, the key is **research and development**. For our business in particular, there is no future without innovation.

It is therefore very appropriate that the third plant that we have the pleasure of opening today is the new **paper pilot plant** for our technology centre. Although it is far less costly than the other two environmental

plants, it is of crucial importance for the short cut fibres and special papers business mentioned above.

However, we need to be doing considerably more in terms of innovation to exploit our opportunities fully and to **ensure our success in the long term**. We do have a small research group, with laboratories, a pilot plant and the corresponding academic research network. But we cannot afford to do any more!

We are therefore grateful to the State of Bavaria and the federal government for their support for the work on a new generation of carbon precursor fibres, since developing them to so-called "aerospace quality" is also inconceivable without focussed R&D.

This great **demand for innovation** is fundamentally very difficult for our type of medium-sized high-tech companies to meet on their own. Above all, there is a lack of expertise built up over a long period, a lack of stable, hypercritical research groups, which, on the one hand, are able to carry out fundamental academic research in the relevant fields and on the other hand remain close to products and industrial scale production.

Particularly in Bavaria, with its large proportion of forested areas, the question arises as to why there is such a clear need to catch up on research into using the chemical components of wood to make high value added products. Simply producing energy from wood by burning it does not seem to be the most innovative way of using this valuable resource.

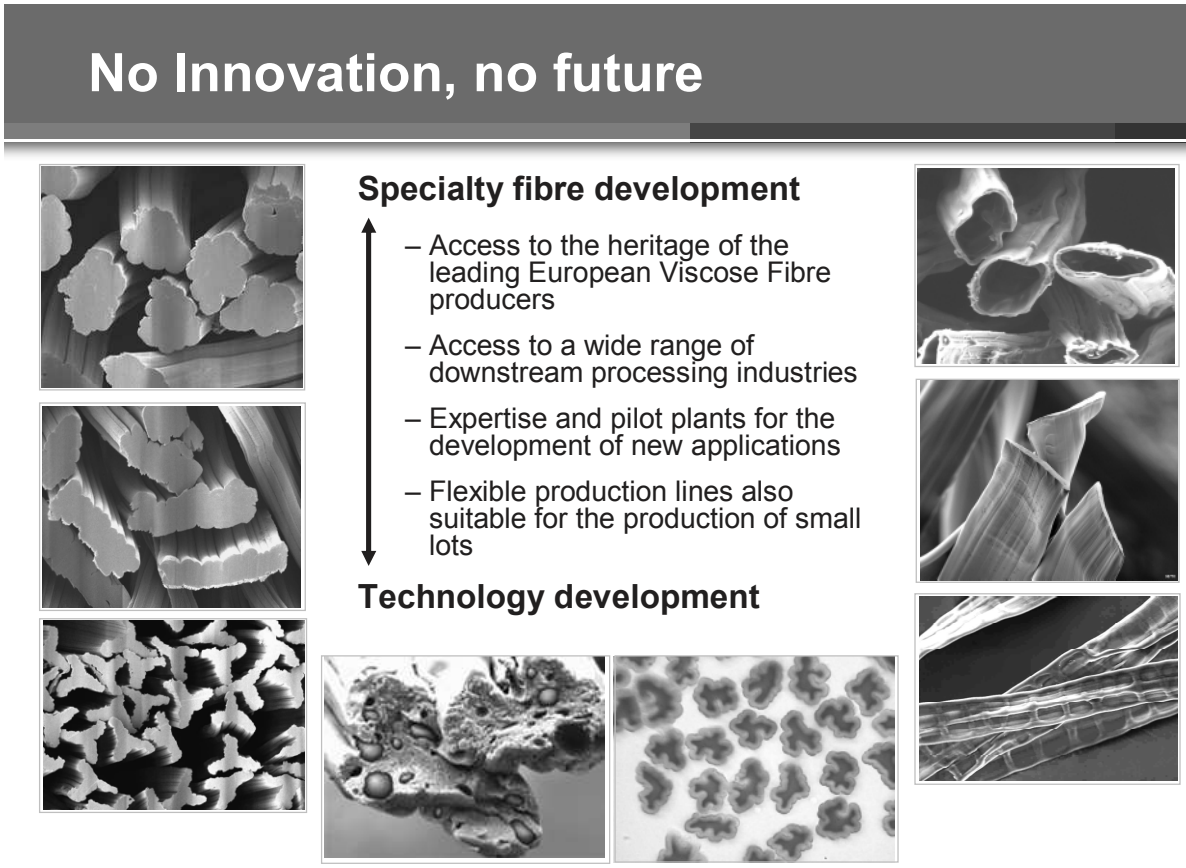

It is in this context that we are currently holding discussions with partner companies, the Munich Technical University, the University of Regensburg and the public authorities to convey to them our conviction that it would be right and proper to establish a **"centre of expertise for cellulose and high-tech fibre research**" here at the Kelheim site, which would go far beyond the interests of individual companies.
Of course, there are even broader issues on the horizon that are extremely important for the future of the site. You will recall that every additional partner who shares the infrastructure costs of the site helps to make the future more secure! Research activity would certainly also help to create favourable conditions in this context and of course, "high-tech fibres" also include the carbon fibres that have been much discussed in public in connection with Kelheim over recent months – whether these are manufactured from polyacrylonitrile, cellulose or lignin.

For many products, the availability of **cost-effective electricity** is indispensable for their competitiveness. The high demand for thermal energy all year round at the Kelheim site as a result of its continuous fibre production should in itself provide extremely favourable conditions for this: probably nowhere else in Germany can electricity be produced more cost-effectively and with lower specific CO_2 emissions based on environmentally friendly gas.

However the implementation of the **"energy transition"**, which has also become of primary importance for the **"New Start for Bavaria"** programme, naturally also requires investment in infrastructure. At the Kelheim site, this would require relatively moderate funding for a modern back pressure steam turbine, an efficient control system and connection to the public grid.
This would certainly be a prerequisite for all of the concepts that envisage an extension of precursor production and further processing of precursors into carbon fibres in Kelheim.
Moreover, it would also be a prerequisite for other plans, such as further extending fibre production capacity, an investment in a carbon disulphide production plant or a second environmentally-friendly sulphuric acid plant. Currently, however, it is impossible to foresee who would finance these infrastructure investments.

Ladies and Gentlemen, I hope that I have been able to make clear to you that, despite some extremely unfavourable conditions and not inconsiderable risks, we as a company are willing to rise to the challenges of and to commit to our strategy for the future.
Indeed, if we all stick together there is a good chance that there can be a new start in Kelheim as part of the **"New Start for Bavaria"**. And this new start will work to the benefit of the level of education we offer, of the families who are involved with Kelheim and of the innovation delivered by our company.
As a company, we have known for a long time that a new start of this sort cannot succeed without having existing education, families and innovations on which to build.
I have already explained in detail how important we consider **innovation** to be for the future of our company and what we are doing in this connection.

But of course, we also appreciate the importance of **education and training** to us: working in Kelheim is not like working on an assembly line. Particularly for us as a "specialist" manufacturer, everything revolves around well-trained staff. We rely on their high level of technical expertise, their responsibility and their identification with the commercial targets of the company and with its success.

We go to great lengths to support the delivery of this type of training and to keep it in the company.
There are good reasons why we train an exceptional number of young people in our **company apprenticeships**. We work with universities, support undergraduate studies and dissertations and offer graduates attractive employment opportunities. We hope to take a further step in this direction with the proposed research centre.
At the same time, we make every effort to ensure that our staff want to stay with us: we are happy that we have hardly any **staff turnover** and that the average length of service with us is 18 ½ years.
The criticism in Günter Walraff's latest documentary is probably justified in many cases – but it does not apply to our circumstances: neither the company nor our workforce operate on the principle of "might is right"! We have no use for lawyers who specialise in making staff redundant, nor do we need strikes or private lessons in dialectics.

Yes, individuals are important to us, and therefore so are the **families** of which they are a part: for 75 years the Kelheim fibre site has probably been the most important employer in the region. And this much is certain: to see this exclusively from the point of view of good jobs, a steady income, social stability and chances of promotion would be to underestimate its importance.

In preparation for the themes of your tour of the future, Mr Minister President, we wanted to know more about families – and so we organised a **competition** among our staff that has run over recent weeks. We asked them to write accounts that describe how many generations of their families have worked for the company and how many people from their family circle have been employed here.
The responses we received confirm what we know to be true from our everyday experience: in the 75 years of our history, a sense of identification with the company has been created that lasts over several generations and through all the members of extended families! Those 75 years correspond to four generations of working life and, as we have now discovered, we currently have a whole series of employees who are already the fourth generation of their families working for us, without interruption!

It is therefore hardly surprising that the people who are most interested in tomorrow's **open day** are pensioners, former employees who want to see how unbelievably different things are today in their former place of work and want to know how we manage to do things now that they thought were impossible in the past; and, of course, the close relatives of our current staff want to know where they spend one quarter of their lives.

We consider this sort of identity with and awareness of our own history to be very important. In place of a **glossy anniversary brochure** to mark the 75 years that we have been in existence, we have therefore decided to sponsor a PhD on the history of Kelheim as a fibre production site from 1935 to 2005 in the new Department of Industrial History at the University of Regensburg. We have signed a letter of intent with Professor Spoerer concerning the financial support for this work.

A new start requires a good foundation from which it can develop. Honoured guests: Kelheim Fibres and the Kelheim fibre production site offer just that sort of foundation. We are setting out on a new start! I hope that you will wish us every success in this, together with the good luck that every successful undertaking requires!

Lenzinger Berichte 89 (2011) 12-21

THE CELLULOSE GAP (THE FUTURE OF CELLULOSE FIBRES)

Franz Martin Hämmerle

Arenberggasse 1/5, 1030 Vienna, Austria

Phone and Fax: (+43) 1 715 1518; Mobile: (+43) 6991 712 6399; Email: fmhaemmerle@hotmail.com

Presented during the 2011 Lenzing – Nature Jeju Festival,
2nd – 4th June 2011, Jeju, South Korea

Within the next two decades the world population will grow by 1.4 billion and is moving up the food chain. By 2030 we will have an additional demand for food of 43 %. On the other hand arable land is limited and the cropland area per person will shrink. This situation will result in a food crisis.
Also the demand for textile fibres (natural as well as man-made) will increase by 84 %. But in the future cotton production will be stagnant because of the limited availability of arable land.

The experience shows that approximately one third of textile fibres have to be cellulosic fibres because of certain properties like absorbency and moisture management. This will result in a disproportionately high demand for man-made cellulosic fibres in the coming years.
The substitution of cotton by man-made cellulose fibres is also a contribution to the environmental protection.

Keywords: *Population growth, arable land, food crisis, textile fibres, cotton, man-made cellulose fibres*

Introduction

Thomas Robert Malthus, an English economist (*1766, †1834), in opposition to the popular view in 18th century Europe that saw society as improving and in principle as perfectible, wrote in his "Essay on the Principle of Population" about the increase or decrease of population in response to various factors:
The increase of population is necessarily limited by the means of subsistence. Population growth therefore generally expands in times and in regions of plenty until the size of the population relative to the primary resources causes distress. But "Population, when unchecked, increases in a geometrical ratio, but subsistence increases only in an arithmetical ratio" (see Figure 1). As a result, population sooner or later gets checked by famine, wars and disease [1].

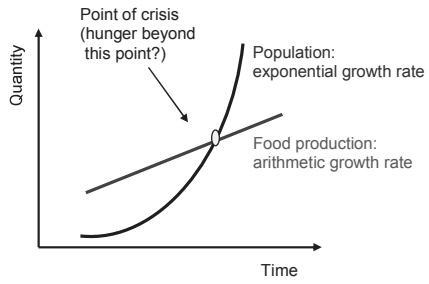

Figure 1. Th. R. Malthus: Principle of Population.

This publication roused a storm of controversy.
What Malthus failed to foresee was the astonishing development of transport and colonisation which took place in the 19th century and which increased the area from which foodstuffs and raw materials could be drawn enormously.
With the advent of the progressive agribusiness ("Post-war Green Revolution"), the use of synthetic

fertilisers, pesticides, state-of-the-art irrigation systems and today's genetic engineering were the driving forces for the exponential growth of the food production.
Today, 200 years later, we are again confronted with the comeback of the "Malthusians Misery". The world population growth is outpacing the growth of food supply and the number of malnourished people is growing again.
The following diagram (see Figure 2) shows the problems which we will face in the near future: the population is growing by 20% over the next two decades, at the same time we need more food and textile fibres, but arable land is decreasing [2].

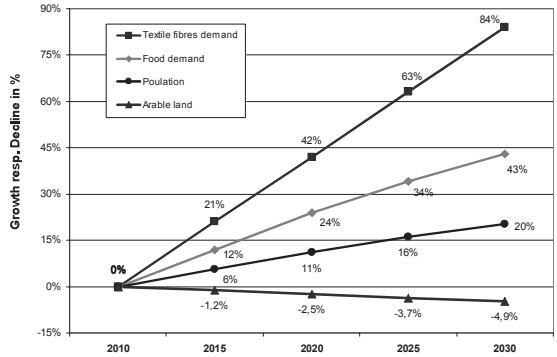

Figure 2. Development of the world population, the need for food and textile fibres and the availability of arable land.

In 1996, when the world leaders attended the World Food Summit in Rome, they committed themselves to halve the number of undernourished people by 2015 (see Figure 3).
Today, the number has already risen to more than a billion undernourished people compared to 825 million in 1996 [3].

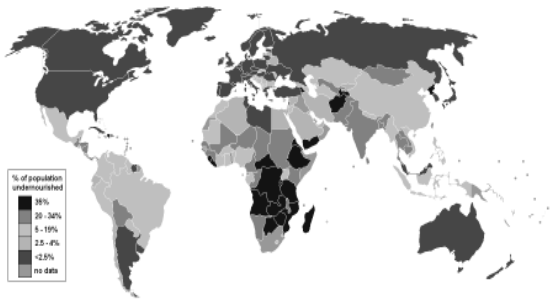

Figure 3. Percentage of Population affected by Undernutrition by Country [4].

With the current growth rate of 78.6 million persons p.a. (respectively 215,000 per day) the population will continue to grow from today 6.9 to 8.3 billion by 2030 [5]. This means that combined with the impact of rising incomes and urbanisation, the food demand will roughly double in the next 50 years. The agricultural production and yields, however, will stagnate. Since several years now the global food security situation has worsened and continues to represent a serious threat for humanity!

Availability of Arable Land and Food

Approximately 17.3 mill km² (11.6 %) of the earth's 149 mill km² of land are cultivated. This includes 15.8 mill km² (≙ 10.6 %) arable land, which is land cultivated for crops that are replanted after each harvest like all sorts of grains, sugar or cotton. It further includes 1.5 mill km² (≙ 1.0 %) permanent crop land, which is land cultivated for crops that are not replanted after each harvest like citrus, coffee or rubber. The remaining 132 mill km² include permanent pastures, forests, barren land and built-on areas [6].
About 1 % of the total arable land (10 to 20 million hectares) is currently being lost per year; urbanisation alone is responsible for about 3 - 4 million hectares [7].
The combined development of population growth and shrinking arable land means that compared to 1960, where approximately 4,400 m² of arable land per capita was available worldwide, only 30 years later, in 1990, it was merely 2,700 m² per capita, and in 2025 it most probably will only be 1,700 m² per capita [8].
It seems obvious that more arable land would be necessary to secure food production.
Historically, one of the successful ways out of this dilemma was to increase food production by an enhancement of the yield per area without expanding the area of arable land itself.
However, the intensification of production requires a much higher input of inorganic fertilisers and pesticides as well as a

substantial improvement of the irrigation systems. Ironically, all these efforts decrease the yields in the long run. The agricultural land is constantly losing fertility.
The inputs of synthetic fertilisers and pesticides can be reduced or avoided with an ecological cultivation, the yields, however, will be much lower.
The only practical method to reduce the input of pesticides and to increase the yield at the same time is the use of genetically modified crops. Genetic engineering is analogous to nuclear energy: nobody loves it, but both will be absolutely necessary for the environment!
Several of the important crops are already genetically engineered: 81 % of the soybeans, 64 % of the cotton, 29 % of the maize and 23 % of canola (variety of rapeseed) grown are genetically modified (see Figure 4).

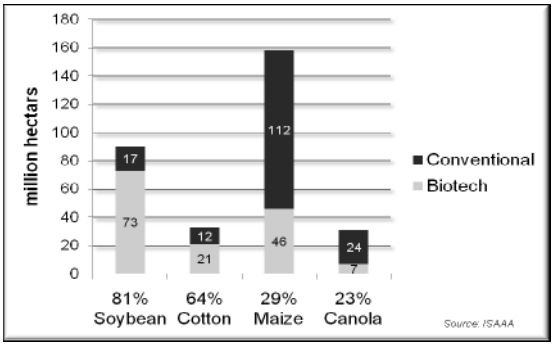

Figure 4. Global Adoption of Principal Biotech Crops 2010 – in million ha [9].

Over the last years, the area planted with gene-modified crops is growing by 10 million hectares p.a. and has reached 148 million hectares in 2010.
The benefits are immediate and obvious: Higher yields, less need for pesticides, fewer crop losses and more attractive products. Genetic engineering offers faster crop adaptation as well as a more biological rather than a chemical approach to yield increases.
People in the area of the "Fertile Crescent" have been domesticating wild plants more than 10,000 years ago, by artificial selection. Our ancestors made a fateful choice to domesticate annual and not perennial plants. The reason was that the artificial selection could be done year by year. Today, all the grains but also cotton are annual plants. Perennial plants would have some advantages (e.g. deeper roots, less soil erosion).

Maybe it's provocative, but
"Selective breeding is nothing else than genetically modifying. And genetic engineering is in other words the shortening of the evolution."

Refusing genetic engineering makes the food problem even more daunting.

Conclusions

- We will have a desperate shortage of fertile farmland in the near future.
- Arable land on which non-food crops are growing today has to be used more and more for food crops.
- Food crops should be used for feeding people, not for animal feed or bio-fuels.

Cotton: Production, Planted Areas & Yield

Over the last 60 years cotton production has continuously increased (see Figure 5).

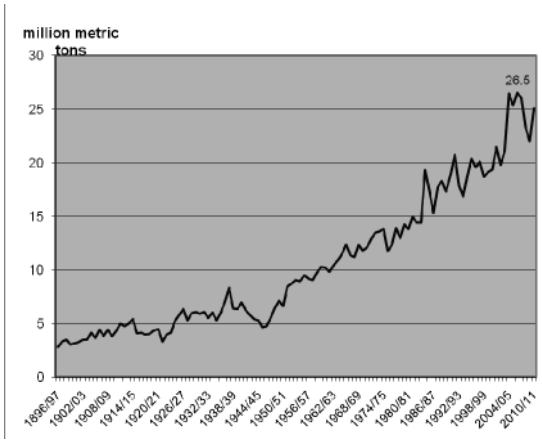

Figure 5. Cotton Production 1896-2010 [10].

The area on which cotton was grown fluctuated between 29 and 36 million hectares. At an average this is only about 2 % of the worlds arable land but the percentage in those climatic regions where cotton can be grown is of course much

higher.
During the last years the cotton growing area shrunk from 35.7 to 30.6 hectares (in 2010/11, the area was increasing because of the extreme high cotton price) and it will certainly continue to shrink further in the future. Many cotton growing countries are highly populated with a tremendous need to increase food production. The area for food has to be expanded. More and more farmers decide to cultivate plants that contribute to nutrition which brings higher and primarily safer incomes.
In the US, in China and in Europe cotton farmers receive huge amounts of subsidies (e.g. in 2009/10: 5.3 billion US-$) [11].
In addition, there is a continuous land loss by soil degradation (desertification, salinization etc.) reducing the overall arable land available.

Cotton Year	*Production*		mill. tons
2009/10	*ICAC preliminary (May 2011)*		*22.00*
2010/11	*ICAC projection (May 2011)*		*24.80*
Year	Area mill. ha (assumption)	Yield kg/ha (assumption)	Theoretical maximum production mill. tons
2015	31.0	850	26.35
2020	30.0	875	26.25
2025	29.0	900	26.10
2030	28.0	925	25.90

Figure 6. Assumption of Cotton Production for the next two Decades [12].

As a consequence, there will be less land available for cotton production. Projections indicate (see Figure 6) that the cotton planted area will drop to approximately 28.0 million hectares until 2030. Within the same period, because of an intensified cultivation of genetically modified cotton, the yield (actual: close to 800 kg/ha) however will continue to increase for the next two decades and will reach a level of about 925 kg/ha in 2030. The loss of cotton planted areas can partly be compensated. But still the overall cotton production in the foreseeable future will decrease: based on the above assumptions the maximum possible production at that time will be about 26 million metric tons of cotton per year!

Textile Consumption
Income and population growth are the major factors driving increases in textile consumption.

The world population will increase by 1.4 billion people during the next 20 years (see Figure 7).

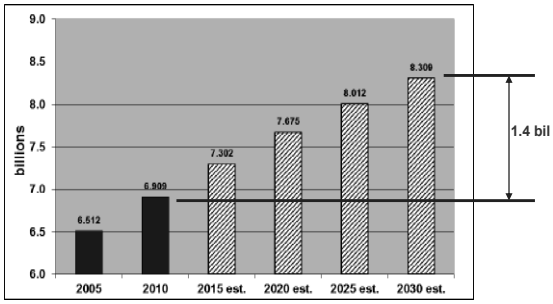

Figure 7. Growth of the Population 2005–2030 [13].

The per capita fibre consumption, more or less in parallel with the income, has grown at an average rate of 1.8 % per annum over the last 10 years (see Figure 8).

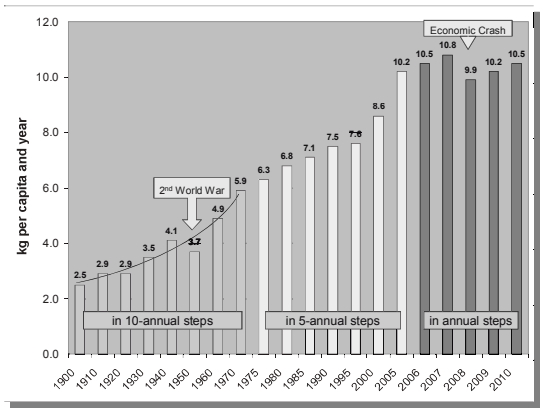

Figure 8. Fibre Consumption per Capita (1900 – 2010) [14].

It is projected to grow by 2.5 % p.a. in the coming 5 years and thereafter to decline to about 1.5 % in the following years (see Figure 9).

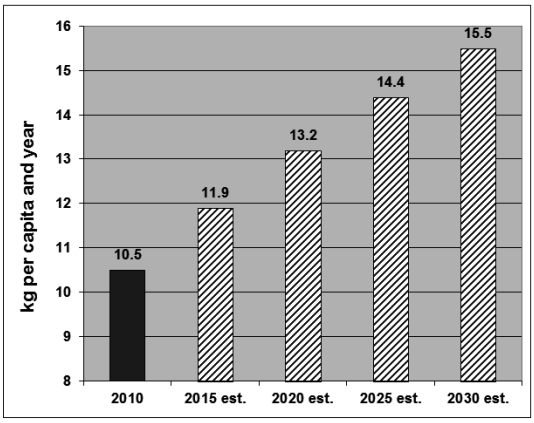

Figure 9. Per Capita Textile Fibres Consumption 2010 – 2030 [15].

Both, the population growth and the growth of the per capita textile consumption resulted in a continuous, substantial increase of the overall fibre consumption. It has reached 72.5 million tons in 2010 and is projected to grow with an average growth rate of 3.1 % p.a. to a level of 133.5 million tons in 2030 (see Figure 10).

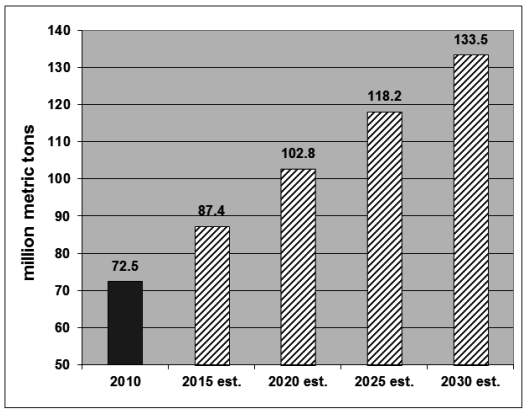

Figure 10. Textile Fibres Consumption 2010–2030 [16].

Cellulosic and Synthetic Fibres

The physiological performance of cellulose fibres - cotton or man-made - is unmatched by any other man-made fibre. They are *hydrophilic* and stand for absorbency and breathability. These inherent physiological fibre properties are ideal for the *moisture_management*. The fibres can absorb sufficient moisture, which they then release into the surrounding air. This function ensures an adequate temperature balance on the skin, especially where textiles touch the skin.

Different to petroleum-based synthetic fibres (Polyester, Polyamide, Polypropylene, Polyacrylonitrile and others) cellulosic fibres are ideal in all fields of application where moisture management and physiological performance are of high importance, whether this is in the textile and garment industry for woven and knitted fabrics or in nonwovens or industrial products.

For several decades the growing fibre demand was mainly covered by synthetic fibres (see Figure 11). They entered the fast growing applications with a lower importance of properties typical for cellulose.

Year	Wool	Cotton	Manmade cellulosic fibres	Synthetic fibres	Total	%-age of cellulosic fibres
Historical Data						
1900	0.7	3.2	0.0	0.0	3.9	82.1
1920	0.8	4.6	0.0	0.0	5.4	85.2
1940	1.1	6.9	1.1	0.0	9.1	87.9
1960	1.5	10.1	2.7	0.7	15.0	85.3
1980	1.6	13.8	3.5	10.8	29.7	58.2
2000	1.4	18.9	2.8	28.4	51.5	42.1
2005	1.2	24.8	3.3	37.0	66.3	42.4
2010	1.2	21.8	4.2	45.3	72.5	35.9
Future (assumption)						
2015 est.	1.2	*26.4**	6.2	53.6	87.4	37.2
2020 est.	1.2	*26.3**	10.3	65.0	102.8	35.6
2025 est.	1.2	*26.1**	14.8	76.1	118.2	34.6
2030 est.	1.2	*25.9**	19.0	87.4	133.5	33.6

** Possible peak production*

Figure 11. Historical and Future Development of Fibre and Filament Consumption [17].

While still growing in absolute terms until the beginning of this millennium, the share of cellulosic fibres continuously dropped. However, in the recent decade the cellulosic fibre supply, because of the limitations to increase the cotton production, also in absolute terms, could no longer meet the growing demand.

Already from 2006/07 onwards the cotton demand outweighed the supply (see Figure 12) and presently the global cotton inventories are on the lowest level in 14 years.

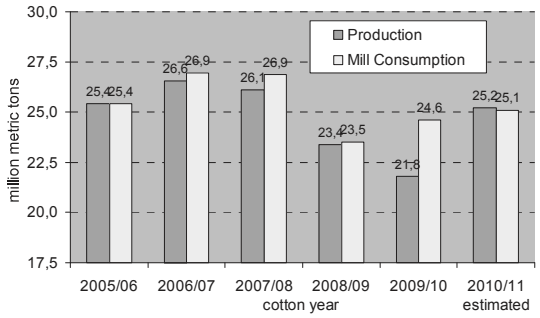

Figure 12. World Cotton Production and Consumption [18].

As a consequence, cotton prices during the last two years have risen strongly (more than 300 %) (see Figure 13) and it can be expected that they will even out on a high price level with the stagnation or the decline of the production.

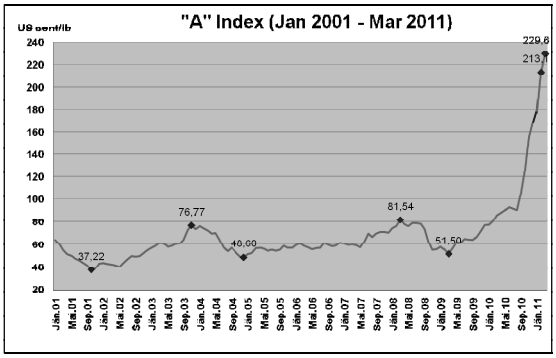

Figure 13. "A" Index (Nov 2008 – Oct 2010) [19].

The FAO Food Price Index shows a similar trend. Food prices are also exploding (see Figure 14).

Figure 14. "FAO Food Price Index" (1990 – 2010) [20].

Cellulosic fibre gap

Based on the pattern of required fibre properties in different applications it can be projected that cellulosic fibres – natural and man-made - in the future will still make 33 to 37 % of the fibre demand (see Figure 15 and 16).

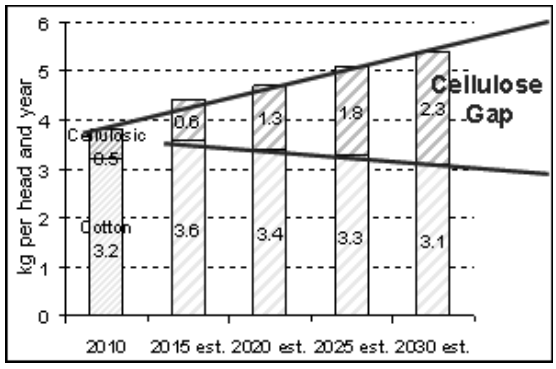

Figure 15. Per capita consumption of cellulosic fibres (in kg per head and year) 2010-2030(est) [21].

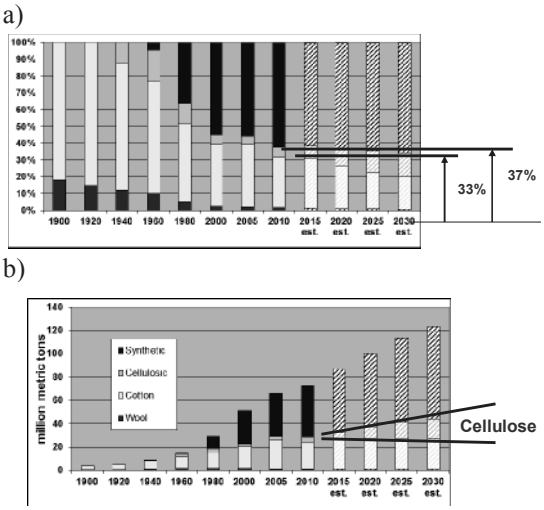

Figure 16. Consumption of different fibres 1900 – 2030: a) in % of total consumption and b) in mill. tons [22].

The annual per capita consumption of cellulosic fibres will increase from presently 3.7 kg to 5.4 kg in 2030. However, due to the limitations to increase the production, it will only be possible to cover 3.1 kg of this demand with cotton.

The only way to fill the resulting cellulosic fibre gap (see Figure 16) and to secure supplies is to increase capacities for man-made cellulosic fibre production.

This process has already started with significant investments in recent years.

Man-made cellulosic fibres are an ideal

substitute for cotton (see Figure 17)!

	Vis-cose	Vis-cose-Blends	Lyocell	Lyocell - Blends	Modal	Modal-Blends
Woven and knitted fabrics:						
Apparel:						
Underwear			√	√ √	√ √	
Knits	√	√	√	√		√
Bottom weights		√	√	√ √		√
Active wear				√ √		
Socks				√ √	√ √	
Shirts / Blouses			√	√ √		
Home textiles:						
Bed linen			√	√ √		
Towels				√	√ √	
Filling				√		
Nonwovens:						
Cleaning rags	√	√		√		
Sanitary articles	√	√		√		
Baby wipes		√		√ √		

Figure 17. Man-made Cellulosic Fibres as a Substitute for Cotton.

Companies which are mainly using cotton today will have to add man-made cellulosic fibres to their production programme.
To a large extent they can be tailored and accordingly be selected to the application. With Viscose, Lyocell, Modal, Acetate, Cupro, Triacetate, etc. several types of man-made cellulosic fibres are on the market.

Sustainability

The sustainability of products and processes is a complex, but in view of the future extremely important topic. Dimensions that need to be considered in an assessment are the relevance to the ecology (effect to the environment), the economy (value generation) and the social responsibility (enhancing the quality of life).

In comparing the sustainability of cotton with the sustainability of man-made cellulosic fibres, the main differences result from the way of cultivation (e.g. the use of scarce agricultural land, synthetic fertilisers and pesticides), from manipulation of the genom and the water consumption.
Today, 70 % of the cotton is already genetically modified and approximately 1 % is “organic cotton”.
The implications of the scarcity of prime fertile agricultural land, good for food production in densely populated developing countries have been addressed already.
Compared to cotton cultivation man-made cellulosic fibres are based on wood, which is grown in forests on marginal land. Without the need to use synthetic fertilisers or pesticides and without the need for irrigation, the yield of cellulose fibres from Central European beech forests and from fast-growing eucalyptus is much higher (see Figure 18). Life cycle analyses show that man-made cellulosic fibres have a much smaller carbon footprint compared to cotton.

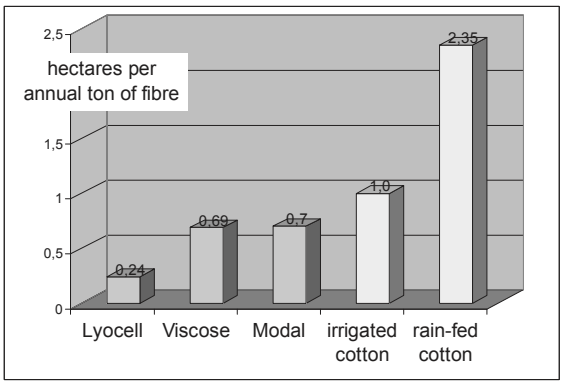

Figure 18. Land needed for the production of various cellulosic fibres [23].

Only 45 % of the cotton grows based on natural rains. Cotton production based on irrigation requires 15 to 35 times more water than cellulose fibre production based on wood pulp (see Figure 19). The water either is provided by flood or furrow irrigation (97 %), mobile irrigation (2 %) or drip irrigation (1 %).
The sustainability implication of water utilisation will substantially grow in the future. Today, already approximately one third of the world population suffers from water shortage. Until 2025, this share is likely to expand to two thirds! Several studies addressing this problem concluded

that "Water will become the oil of the future!"
Cotton already has caused the virtual disappearance of the Aral Sea, formerly the
4th biggest freshwater sea on earth. This environmental disaster, in a time-span of only three decades, resulted from excessive use of the inflowing rivers for cotton irrigation.
In spite of being a natural fibre, cotton in comparison to man-made cellulosic fibres – like Viscose, Lyocell or Modal – is not sustainable at all (see Figure 20).
The natural origin of man-made cellulosic fibres from the renewable resource wood contributes to a sustainable future.
Fibres with prefixes as "eco-", "bio-", "natural-" and "organic-" are not always sustainable. For example water consumption is not a criterion for the certification as organic cotton. This proves that even "bio" is not necessarily "eco" as well.

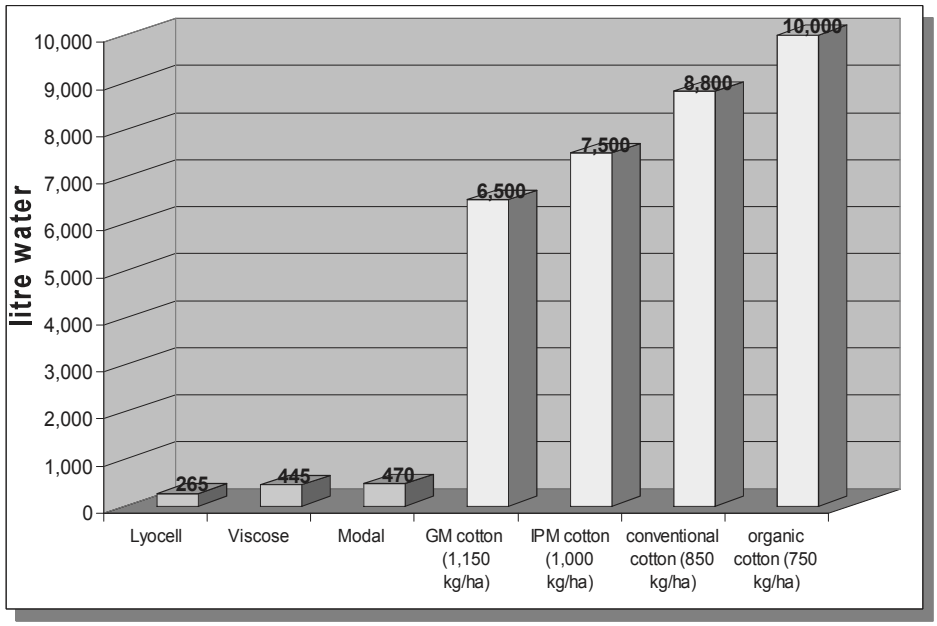

Figure 19. Water requirement for one kg of fibres [24].

		Man-made Cellulose Fibres				Cotton							
		Lenzing Viscose Austria	Lyocell (Tencel)	Lenzing Modal	Lenzing Viscose Asia	Gen-modified 70%		Organic 1%		IPM 10%		Conventional 20%	
Environ-mental impacts	Use of pesticides (+ human impact)	no	no	no	no	little		no		high		huge	
	Manure, fertilizer	no	very lttle	no	no	synthetic fertilizer (little)		only natural manure		synthetic fertilizer (high)		synthetic fertilizer (very high)	
	Soil degradation, depletition, ecoto-xicity, acidification, eutrophication, etc												
Resources	Cumulative energy demand												
	Land use, yield	forest land	forest land	forest land	forest land	agricultural land 110 -120%		agricultural land 70 – 80%		agricultural land 80 – 90%		agricultural land 100%	
	Water consumption (incl. process + irrigation water)	rain-fed	rain-fed	rain-fed	rain-fed	rain-fed	irrig.	rain-fed	irrig.	rain-fed	irrig.	rain-fed	irrig.
Fibre quality		good	good	good	good	good		reduced		good		good	
Sustainability Points		26	24	24	21	22	20	21	17	16	13	14	11
Ranking		1	2	2	5	4	7	5	8	9	11	10	12

sustainable
4 3 2 1 0
yes no

30 – 50% higher fibre price

rain-fed cotton <40%
irrigated cotton >60%

Figure 20. Sustainability Ranking of Cellulosic Fibres [25].

Final Conclusions

1. The demand for textile fibres together with the increasing world population and the per capita fibre consumption will continue to grow.
2. The production of natural fibres will remain constant or shrink. The growth of total fibre consumption therefore can only be covered by man-made fibres.
3. Certain properties of cellulosic fibres (Cotton, Viscose, Lyocell, Modal and others), especially their physiological performance, cannot be substituted by petroleum-based synthetics (Polyester, Polyamide, Polypropylene, Polyacrylo-nitrile and others).
4. Cellulosic fibres – natural and man-made - therefore also in the future will make up 33 – 37 % of the fibre market. Companies which are mainly using cotton today will have to add man-made cellulose fibres to their production programme.
5. Man-made cellulose fibres are extremely sustainable fibres. In comparison to cotton they have some important assets (see Figure 20):
   - No arable land is necessary. The trees (eucalyptus and beech) for the pulp production are growing in forests or on marginal land,
   - less water consumption,
   - no input of pesticides and fertilizers.
6. Man-made cellulose fibres are really ecological fibres: The substitution of cotton by man-made cellulose fibres is an important step in order to protect our environment.

References

[1] Malthus Th. R.; "An Essay on the Principle of Population";1798.

[2] a) United Nations Population Division; The 2008 Revision Population Database; "World Population Prospects - Medium Variant"; 2008.
b) UNEP (United Nations Environment Programme); "The environmental Food Crisis"; 2010.
c) Own calculations; 2011.
d) Sundquist, B.; "Topsoil loss – causes, effects and implications: a global perspective.", 2000.

[3] FAO (Food and Agriculture Organization); FAO Media Centre; 19 June 2009.

[4] UN (United Nations); United Nations Statistics, "Percentage of Population affected by Undernutrition by Country".

[5] UN (United Nations); United Nations Population Division; The 2008 Revision Population Database; "World Population Prospects - Medium Variant"; 2008.

[6] CIA; World Factbook; 2009.

[7] Sundquist, B. "Topsoil loss – causes, effects and implications: a global perspective"; 2000.

[8] WRI (World Resources Institute); "Arable Land per Capita".

[9] ISAAA (International Service for Acquisition of Agri-Biotec Applications) / Clive James; "Dominant Biotech Crops in 2010"; 2010.

[10] ICAC (International Cotton Advisory Committee), USDA (United States Department of Agriculture); "Cotton Production"; 2011.

[11] ICAC (International Cotton Advisory Committee), "Production and trade policies affecting the cotton industry"; Sept. 2010.

[12] ICAC (International Cotton Advisory Committee), ICAC Press Release, May 2, 2011.

[13] UN (United Nations) Population Division, "World Population Prospects (Medium Variant), The 2008 Revision Population Database"; 2008.

[14] a) FAO (Food and Agriculture Organization), "World apparel fibre consumption survey".
b) Own calculations; 2011.

[15] Own calculations; 2011.

[16] Own calculations; 2011.
[17] a) USDA (United States Department of Agriculture); “Wool and Cotton Outlook”.
b) CIRFS (International Rayon and Synthetic Fibres Committee); “World Man-Made Fibres Production”, 2011.
[18] a) NCCA (National Cotton Council of America).
b) ICAC (International Cotton Advisory Committee); 2011.
[19] NCCA (National Cotton Council of America); "A-Index"; April 2011.
[20] FAO (Food and Agriculture Organization), "Food Price Index"; May 2011.
[21] Own calculations; 2011.
[22] Own calculations; 2011.
[23] Lenzing AG/Schmidtbauer, J.; “Wie nachhaltig sind Lenzinger Cellulosefasern?”; 2008.
[24] Lenzing AG/Schmidtbauer, J.; “Wie nachhaltig sind Lenzinger Cellulosefasern?”; 2008.
[25] a) Karst Kooistra, Aad Termorshuizen (Wagenningen University/The Netherlands); "The sustainability of cotton. Consequences for man and environment.", 2006.
b) Li Shen, Martin K, Patel (Utrecht University/The Netherlands); "Life Cycle Assessment of man-made cellulose fibres", Lenzinger Berichte 88 (2010) 1-59.

Additional bibliographical references

- Lester R. Brown; "World on the Edge", 2011.
- Wolfram Mauser; "Wie lange reicht die Ressource Wasser?", 2007, Fischer Taschenbuch Verlag, Frankfurt am Main.
- Klaus Hahlbrock; "Kann unsere Erde die Menschen noch ernähren?", 2007, Fischer Taschenbuch Verlag, Frankfurt am Main.

Lenzinger Berichte 89 (2011) 22-29

THE GLOBAL VISCOSE FIBRE INDUSTRY IN THE 21ST CENTURY – THE FIRST 10 YEARS

Nick Bywater

Nick Bywater Consulting, 40, Postbridge Road, Styvechale, Coventry, CV3 5AH, England

Phone: (+44) 24 7641 7900; Email: nick.bywater@btinternet.com

The viscose fibre industry is the oldest man-made fibre business in the world with its roots stretching back to the late 19th century, although commercial production did not begin until 1905 when Courtaulds opened its first filament plant. Initially the industry enjoyed a period of substantial growth which was followed by an equally dramatic decline in the face of competition from the newer synthetic fibres. However, in more recent times the industry has shown signs of recovery, driven primarily by the commissioning of new plants in Asia. At the same time some factories in the western world and elsewhere have struggled to compete, with many closing down and others running at reduced capacity utilisation. This paper highlights developments in the latest chapter of the global viscose fibre industry by examining the regional changes that have taken place during the first ten years of the 21st century. It shows that far from being in decline, the viscose fibre business is in a healthy state with annual average growth rates exceeding many other fibres including polyester staple. Finally, and in conclusion, the prospects for the second ten years of the 21st century are reviewed.

Keywords: *viscose, market, trends*

Introduction

The first ten years of the 21st century have witnessed a resurgence in the global viscose fibre industry as production has continued to increase, following a trend first evident in only some regions of the world during the latter part of the 1900s. In the late 20th century however, the regional upward trend, which was driven by the developing industry in Asia, was masked by the more significant and frequent closure of older, less environmentally friendly plants in the western world, particularly in Eastern Europe. Now, at the end of the first decade in the 21st century with that programme of plant closures effectively finished, the previously obscured underlying trend has become clear (Figure 1).

The net result of the two opposing trends in Asia and East Europe towards the end of the 20th century was an overall net decrease in global manufacturing capacity of around 600 kt, to approximately 2.0 million tonnes by the year 2000.

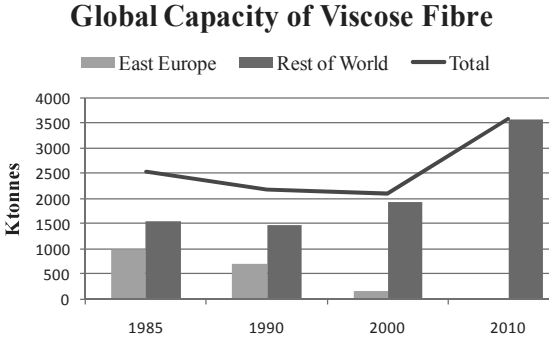

Figure 1. Global Capacity of Viscose Staple, 1985 – 2010.

During this time, more than 800 kt of capacity was lost in Eastern Europe with a further 300 kt closing in West Europe and

other smaller losses recorded in Japan and North America. However, at the same time capacity in China was increasing by more than 400 kt with a similar increase occurring in South and Southeast Asia. So, whilst the global headline figure was suggesting a decline in capacity with all the connotations of an industry in terminal decline and the associated negative public perception, a closer examination of the situation revealed an industry which far from dying was in reality growing significantly, particularly in Asia.

By the end of the first decade of the 21st century, closures of viscose staple plants had slowed almost to zero and the underlying growth pattern had become much clearer. In fact, during the first ten years of the 21st century global viscose staple capacity increased by around 1.5 million tonnes (an average of 7.7 % per annum) to more than 3.5 million tonnes, an all time record high. At the same time, production of viscose staple also increased, albeit at the more modest average pace, of 6.7 % per annum.

Increased capacity in the industry was driven by the strengthening global demand for viscose staple, not only in textile applications concentrated mostly in Asia, but also in the more technical demanding and fast expanding nonwovens industry concentrated in the West where viscose staple is the preferred fibre in many applications including wet wipes, hygiene products and surgical applications. Thus, long gone is the once popular perception that viscose staple is a cheap filler fibre to be found only in budget priced apparel – it is now in demand for the positive contribution it makes to the finished product whether that be in the more traditional textile industry or in nonwoven applications. Indeed, the old textile mills of Eastern Europe which traditionally produced large quantities of low grade textile materials mainly for domestic consumption have long since given way to the new highly automated and in many cases vertically integrated textile conglomerates located chiefly in Asia. It is no surprise therefore that high grade fibre making capacity has migrated to those markets where the textile industry has been growing fastest.

Whilst the rapid increase in capacity has been taking place in Asia, viscose staple producers in the West have taken stock and become stronger and better able to cope with competition from the newer low cost producers. Today many of the remaining producers outside Asia are reaping the benefits of decisions taken in the latter part of the 20th century to move production away from commodities towards speciality products. The continuing trend towards research driven developments of new fibre variants offering a wide range of properties to the market place is set to continue – indeed survival of the industry in West Europe and elsewhere depends an innovative approach. Never has the saying been truer than it is now – "today's speciality is tomorrow's commodity".

The Viscose Industry in Perspective

The pattern of growth in the viscose fibre industry during the past twenty years outlined above took place against a background of strengthening demand for almost all other fibre types. Thus, viscose staple was out of step in the context of other mainstream fibres because whilst production of all fibres, including wool and cotton, rose by an average annual rate of almost 3.3 % during the final decade of the 20th century, global output of viscose staple fibre declined at an average rate of -1.4 % per annum (Figure 2).

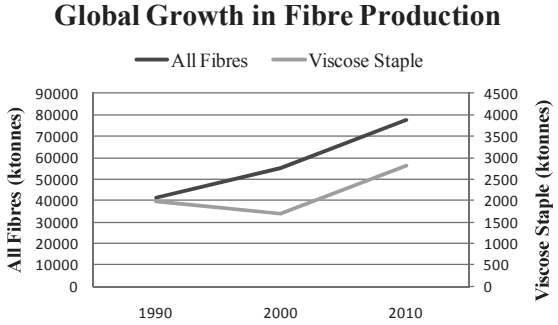

Figure 2. Global Growth in Fibre Production, 1990 – 2010.

By the beginning of this century, total fibre production had reached more than

55 million tonnes, driven particularly by higher production of polyester filament and staple which grew at average annual rates of 17.9 % and 8.0 %, respectively. Indeed the only other fibres apart from viscose that failed to increase production during the last decade of the previous century were polyamide staple (average annual decline of -3.0 %) and wool (- 3.2 %).

In the first ten years of the 21st century however, the picture was very different with the previous decline in viscose staple production reversed and growing at an average annual rate of 6.7 %, well above the all fibre average of 4.1 % per annum. In fact, the rate of growth of viscose fibre production was exceeded only by that of polyester filament which increased at an average annual rate of 10.7 %. Perhaps rather surprisingly, the growth in production of viscose staple was slightly higher than that of polyester staple (6.6 % per annum) and was well ahead of acrylic staple which went into decline at an average rate of -2.5 % per annum. By comparison, the cotton crop increased at an average annual rate of 2.8 % per annum during the same period whilst production of both wool and polyamide staple continued to decline as in the previous decade.

Regional Trends in the Viscose Fibre Industry

China

As noted above, the global viscose fibre industry grew at an average annual rate of 7.7 % (in terms of capacity to produce) during the first decade of the 21st century, driven primarily by expansion in Asian countries. Most notable amongst them was China where capacity increased by more than 1.5 million tonnes

The rate of growth of the viscose fibre industry in China has been remarkable such that today it dominates the global scene with a 58 % share of total world capacity. Only twenty years ago, that share was 8 % (Figure 3).

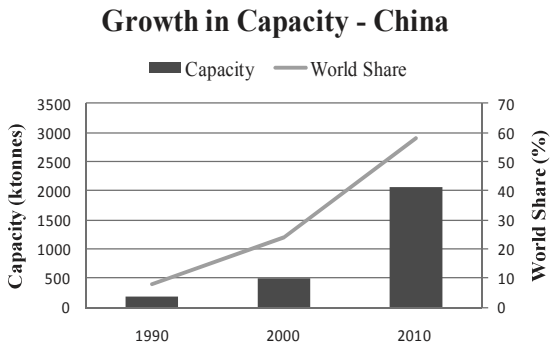

Figure 3. Growth in Capacity – China.

Historically, all producers in China were indigenous, with many using cotton linters as their raw material in plants some of which had a capacity of 10 ktpa or less. However, in more recent times as demand for viscose staple strengthened, other producers have been attracted to the market such that now the two major global players – Lenzing and Birla – both have plants in the country, as does Säteri. Although many of the smaller plants have closed, new ones have been built and older ones expanded. Thus, during the first decade of the 21st century, a total of nine new plants were opened in China with a combined capacity of 800 ktpa, the largest of which was the 180 ktpa Xiaoshan Fulida plant. Also, new lines were commissioned at a further 12 plants with a combined total of around 800 ktpa, with the largest being more than 200 ktpa at Shangdon Helon. At the same time, eight plants with an average capacity of 11 ktpa ceased production.

So, whereas in 2000 there were 26 plants in China with an average capacity of 20 ktpa (the largest plant having a capacity of 40 kt), by 2010 although there was only one more plant, the average capacity had increased to 75 ktpa with the largest plant being 230 ktpa. The rapid increase in capacity has been driven by strengthening demand for viscose staple in China from the fast expanding domestic textile industry which in turn has been feeding strong demand in export markets including Western Europe and North America.

However, despite the rapid expansion in capacity, production has failed to keep pace with strengthening demand with the result that imports have been increasing.

Whilst some fibre imports have been commodity products, much is speciality fibre not produced locally but demanded in textile products destined for export to the more sophisticated textile markets, particularly those in the West.
Viscose staple capacity is expected to continue expanding in China during this decade with both new plants and expansions continuing to be announced. For example, both Lenzing and Birla have announced plans to increase the size of their plants at Nanjing and Xiangfan, respectively whilst Xinjiang Faluda has announced a tripling of capacity to 300 ktpa and Shandong Yamei is reported to have plans for an additional 200 ktpa to its existing 60 ktpa plant. At the same time, Anhui Shumeite has announced plans to build a brand new 180 ktpa plant whilst Säteri are rumored to have plans for a new 200 ktpa plant.
Whilst export demand for textile products from China is likely to remain high, the pattern of trade is forecast to change, and at the same time domestic demand is expected to grow. The rate of growth in demand from western markets for Chinese exports is expected to slow for logistical reasons as the fashion market is increasingly demanding fast response times from garment manufacturers. Consequently, retailers in the West are increasingly turning to suppliers closer to home for the supply of fashion goods, a move that has stimulated demand in Turkey, East Europe and North Africa.

South & South East Asia
After China, South and Southeast Asia is the largest producing region in the world with plants in Indonesia (two producers with a combined capacity in 2010 of 412 ktpa), India (three plants, with a total capacity of 312 ktpa) and Thailand (a single plant of 142 ktpa). Together in 2010, capacity of all six plants accounted for almost 25 % of the global total compared with 28 % at the turn of the century (Figure 4).

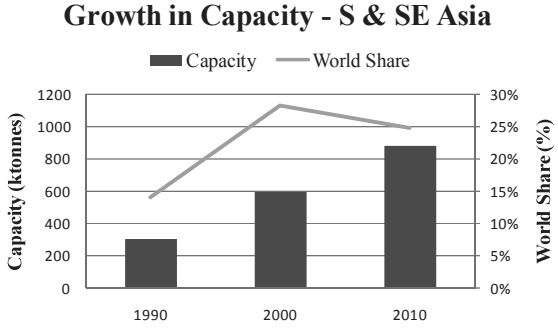

Figure 4. Growth in Capacity – South and Southeast Asia.

Thus, compared with China growth has been slower but nevertheless capacity has increased by almost 300 kt to approximately 900 ktpa.
This region is the heartland of activity for the Indian producer Birla which together with Lenzing claims to be the largest producer in the world. Birla owns all but one of the plants in the region – the exception being South Pacific Viscose (SPV) in Indonesia which is owned by Lenzing. Thus, Birla has a capacity in the region of more than 650 ktpa and Lenzing a little over 200 ktpa. Since 2000, capacity in India has grown relatively modestly by 60 ktpa, though a further 230 ktpa is planned by the end of this decade as Birla opens a new 120 ktpa plant at Vilayat and Lenzing begins production at an 80 ktpa facility in Patalganga.
Development of the industry in Indonesia has been faster than in India with almost 200 ktpa of capacity commissioned during the past decade and both Lenzing and Birla planning further expansion there such that by the end of the present decade a further 200 ktpa could be on stream. In Thailand, Birla has almost doubled the size of its plant in the past decade to 142 ktpa though no further expansion plans have been published.
During the past decade, demand for viscose staple in the region has grown at a little over half the rate of production as textile companies have struggled to compete with their lower cost competitors in China, suffering the consequences of failing to invest in more modern high speed spinning equipment in older less

well-equipped mills. Consequently, producers in the region have found it necessary to increase exports by around 170 ktpa, with Turkey the main market although significant trade has been developed elsewhere around the world including China and Western Europe. With China continuing to pose a significant threat to local textile businesses, fibre exporting is expected to continue to form an important part of the sales portfolio of producers in the region. Such is the rate of increase in export sales, that in 2011 South and Southeast Asia became the largest exporting region in the world, taking over from West Europe which had held that position for many decades.

West Europe

Despite the rapid expansion of capacity in parts of Asia described above, Western Europe has continued to hold a significant place in the league table of world viscose staple producers though in terms of volume, its importance has diminished in recent years. Nevertheless, capacity remained essentially unchanged during the first decade of the 21st century at around 370 ktpa though share of global capacity almost halved to 10 % during that time (Figure 5).

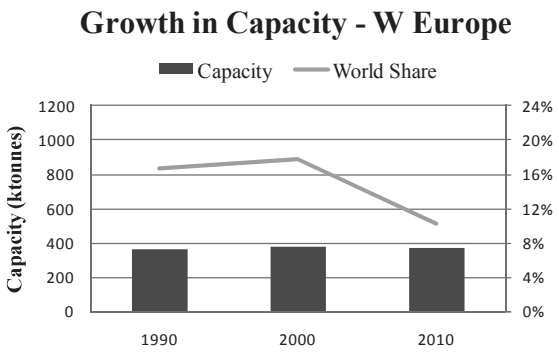

Figure 5. Growth in Capacity – West Europe.

Although total capacity in the region remained unchanged, three plants did close but others expanded. Thus, the first decade of this century saw Acordis (formerly Courtaulds) close its Grimsby plant in the UK and Svenska cease production in Sweden before Kiutu (formerly known as Kemira) ceased operations at its plant in Finland. However, on the positive side, Lenzing expanded its plant in Austria by more than 100 ktpa by debottlenecking and adding an extra line, and there is some suggestion that Kiutu may resume production again though the situation there remains uncertain.

Although as stated above, capacity and production in the region were essentially unchanged during the decade, the same was not true of demand that weakened by more than a third as the textile industry in the region suffered from the effects of competition, not only from Asia but also closer to home in Turkey. The decline in the West European textile market would have been significantly more difficult to manage by viscose staple producers however had it not been for the continuing growth of the domestic nonwovens market which by the year 2010 accounted for two thirds of total demand in the region. Thus, those producers who in the latter part of the 20th century had taken steps through research and development to engineer fibres tailor made to meet the requirements of the large multinational nonwoven companies, were able to reap the benefits of their vision whilst others found it more difficult to compete.

However, although an innovatative approach to product development proved to be an important element in a robust long term business strategy for viscose staple producers in West Europe, in itself it was not enough to ensure success – it was important also to have a good understanding of world exports markets and the products required to build market share there. That producers were successful in achieving that objective can be judged from the fact that during the first decade of this century, export trade almost tripled as business grew with nations across the globe, including Turkey, the Americas, Asia (including China) and East Europe. In many instances, exported fibre found its way back into the West European market in the form of various textile goods which formerly would have been manufactured by local industries. However, being unable to compete with

low cost producers both in Asia and closer to home in Turkey and East Europe, the spinning and fabric manufacturing industries have migrated out of the region.
Looking ahead, demand is expected to continue its slow decline as the textile industry in the region contracts further, offset to a degree by continuing growth in nonwoven applications. However, demand for locally produced fibre in export markets is expected to remain strong resulting in a positive outlook for the viscose fibre industry in the region.

Rest of the World
China, South and Southeast Asia and West Europe accounted for almost 93 % of total world production of viscose staple in 2010, an increase of 23 % on a decade earlier. Elsewhere, production continues in other parts of Asia (Taiwan and Japan) and South America (Brazil) but during the first ten years of this century output ceased in East Europe and North America (Figure 6).

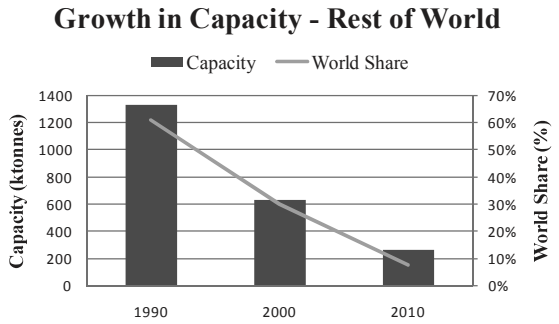

Figure 6. Growth in Capacity – Rest of the World.

Production of viscose staple in Japan, which is modest by global standards, fell by more than a half during the first decade of this century and led to the closure of three relatively small plants – Fuji Spinning, Toho Rayon and Toyobo. The closures were the result of a combination of weakening domestic demand and increased imports of viscose rayon fibre particularly from Indonesia but also of speciality fibre from West Europe. At the same time, export opportunities dwindled early in the decade but have begun to recover more recently as business in speciality fibre has grown in North America and more latterly in Asia. Although average plant utilisation in the country is below the global average and the market outlook is not good, the fact that Japan relies on sales of a high proportion of speciality fibres means that margins are good and the future more secure than if commodity fibres were the basis of the business.
Production of viscose staple by the Formosa Chemical and Fibre Company in Taiwan, the sole producer in the rest of Asia, a region that also includes South Korea, has been trending downwards during the past decade with utilisation (based on nameplate capacity) falling by 26 % to 60 % during that time. Weakening local demand in the region has been the main factor behind the decline which is the result of increasing competition in textile markets from lower cost producers in the region. The situation has been compounded by increasing imports of commodity products from close neighbours China and Indonesia and also of speciality fibres from West Europe. Furthermore, a failure to exploit fully the potential for increasing exports, particularly to Pakistan, Iran and to a lesser extent Vietnam, has contributed to the situation. With little signs of a reversal in the trends of recent years with regards to demand and export opportunities, the business situation is likely to remain tough in the short term.
The only other region in the world where the viscose fibre industry continues to have a presence is South America where Fibra produce from a single 53 ktpa plant in Brazil. During the first decade of the 21st century, production was limited with plant utilisation never exceeding 75 % and falling to a low of less than 40 % in 2010 as market opportunities diminished. Although demand for viscose staple in South America has been essentially stable during the ten year period, imports have continued to rise forcing the local producer to search for opportunities in export markets with varying degrees of success. Turkey has been the main target with the other markets in West Europe, North

America and Africa also explored. Overall though, export volumes have been small. Conversely, imports have grown as producers in South and Southeast Asia (Indonesia) and West Europe (Germany and Austria) have built stronger positions in the market.

With the economy in Brazil growing fast and expected to continue so, demand for viscose staple fibre is expected to strengthen during the present decade, though based on recent experience, it seems unlikely that the domestic producer will be in a position to satisfy the increased requirement. Rather, it is more likely that imports will continue to increase.

At the turn of the century, the industry had a significant presence in both North America and East Europe but 10 years later production in both regions had ceased. Capacity in the once powerful East Europe, which at its peak during the previous century produced almost a million tonnes of viscose staple per annum, had by the beginning of the 21st century been reduced to a total of four plants, three in Russia and one in Serbia, with a total capacity of a little over 150 ktpa.

Under political and economic pressures, the Serbian plant at Loznica closed early in the decade only to reopen three years later with the aid of new funds pumped into the business. However, the revival was short lived with the plant closing for good in 2005 but not before it had caused considerable disruption in export markets where, in an attempt to build a position, fibre was sold at low prices.

Although demand for viscose staple remained stable in East Europe, it was not sufficient to support production of the Russian plants which relied heavily on export markets, particularly Turkey. Thus, the Balacovo plant was able to stay open until 2008 when it finally closed, though prior to that utilisation had been poor, never rising much above 60 % during the decade. Meanwhile, a second plant at Ryazan operated close to capacity until 2004 when an inability to supply export markets forced it to close the following year, whilst the only other plant operational in Russia at the turn of the century, at Krasnoyarsk, operated on an intermittent basis during the first half of the decade, but after downsizing in 2000, closing and reopening, it finally ceased production for good in 2004.

At the turn of the century in North America there were two plants operational, one owned by Courtaulds at Mobile Alabama and the other by Lenzing at Lowland Tennessee with a combined capacity of 110 ktpa. In the face of weakening domestic demand and limited export opportunities, the Courtaulds plant was forced to close in 2001. Similarly, the Lowland plant, which continued to operate under difficult market conditions, was also forced to close four years later marking the end of viscose staple production in the region.

Although there was limited production of viscose staple from a very small plant in Iraq in the early part of this century, historically the industry has had no significant presence in the Near East or in Africa. However, the situation is set to change with the announcement that Birla are planning to build a plant in Egypt as part of its long term plan to increase global production of viscose staple to one million tonnes by the end of the current decade.

Turkey has no indigenous viscose industry, relying exclusively on imports for supply of the market. With demand strengthening during the decade, tripling to almost 200 ktpa by 2010, it provided an attractive prospect for viscose staple exporters. Towards the end of the last century, it was European (West and East) producers that dominated the market with some plants in Russia directing the major part of their output there. However, early in the last decade, quality issues precluded the Russians from the market (being an important factor in demise of the industry in Russia), thereby providing an opportunity for producers in West Europe and South and Southeast Asia to strengthen their positions. Indeed, it is the expanding market in Turkey that has been

of fundamental importance in producers in South and Southeast Asia taking over from West Europe the position of the world's largest exporting region. Indonesia, Thailand and India have all made significant advances in the market with the former principal supplier, Austria, being forced into third place behind Indonesia and China.
Demand in Turkey is forecast to continue strengthening, partly as a result of a shift in the supply chain of the European textile fashion industry in favour of local suppliers for logistical reasons. So although not a producer, Turkey is expected to play an important role in the future development of the global viscose fibre industry.

Future Prospects

Traditionally, and because viscose and cotton have a unique portfolio of characteristics particularly with regard to moisture absorbency and other aesthetic properties, cellulosic fibres have become the preferred option in specific sectors of the global fibres market. Late in the 20th century, approximately 50 % of total world fibre consumption was made up of cellulosic fibres but during recent times the figure has fallen, reaching 40 % at the turn of the century and 35 % by 2010. The main reason for the decline in share has been the size of the cotton crop which has been limited in recent years by various factors, including competition for the use of land from other crops including food and bio fuels and limitations in the extent and use of genetic engineering to improve yields. At the same time, the production of man-made fibres has increased rapidly. That the size of the cotton crop has been constrained has resulted in increased demand for other fibres to fill the "cellulose gap" and viscose, having similar characteristics to cotton, has been one of the fibres of choice. It is common to blend the two fibre types together in many textile applications and as long as the size of the cotton crop is constrained, viscose with its unique combination of moisture absorbency, softness and vibrancy of colour together with its green credentials can increasingly be expected to be in demand.
Related to the size of the cotton crop has been price and recent events in the futures market only serve to demonstrate the increasing volatility of commodity product prices in global markets. With demand for cotton forecast to increase during this decade, particularly in China, it is unlikely that the price of cotton will return to its long time average of around 65 c/lb, a situation that is also likely to benefit viscose and other fibres including lyocell and polyester staple.
But perhaps the most significance factor in determining the future prospects for the global viscose fibre industry will be the growth in total fibre demand, which itself is linked closely to world Gross Domestic Product (GDP). Latest forecasts suggest that by the end of this decade, total fibre demand, including natural fibres, will have risen by approximately 35 million tonnes to around 115 million tonnes, representing an average growth rate of 4.7 % per annum, slightly faster than during the first decade of the 21st century when the rate was 4.1 % per annum.
Given the cotton situation and the projected long term increase in demand for all fibres, the indicators for the viscose industry in the second decade of the 21st century are positive. However, it remains a challenge for individual viscose producers to ensure that the potential for growth is turned into reality.

Lenzinger Berichte 89 (2011) 30-36

ENVIRONMENTAL BEST PRACTICE IN DYEING AND FINISHING OF TENCEL® AND LENZING MODAL®

Jim Taylor
Lenzing AG, Werkstr. 1, 4860 Lenzing, Austria
Phone: (+43) 7672 701-3488; Fax: (+43) 7672 918-3488; Email: j.taylor@lenzing.com

Presented during the 48th Man-Made Fibers Congress, Dornbirn, Austria, 2009

This paper will report on studies carried out by Lenzing in collaboration with DyStar and Huntsman to investigate the environmental aspects of dyeing processes for TENCEL® and Lenzing Modal®.
It will report results studying the performance of different reactive dye types to Lenzing's fibres utilising batchwise and semi-continuous application techniques.
The paper will then move on to assess energy, chemical and water consumption in the fibre manufacture through dyeing and finishing processes and draw comparisons with cotton, demonstrating the reduction in environmental damage that can be delivered. The analysis is then extended to investigate the cost savings that are possible as a result of the optimised processing.

Keywords: *TENCEL, dyeing, finishing, Modal, environment*

The Requirement for Bleaching and Scouring

TENCEL® and Lenzing Modal® fibres are inherently white and will require no bleaching to achieve the majority of colours. Of course for optical whites and very pale bright pastels, some degree of bleaching may still be necessary.
The fibre is also extremely clean and contains very little in the way of impurities. In knitted structures (where this work was concentrated) the fibre contains a very small amount of water soluble spinning lubricant, applied during fibre manufacture, together with low levels of waxes that may have been introduced in the knitting process.
For the purposes of calculations made relating to process routes, it was assumed that only a mild detergent scour was required prior to dyeing although in many cases it would be feasible to use scour – dye methodologies.
Comparisons are drawn with the processing of cotton, where a thorough scouring process is needed to remove it's natural impurities and waxes. In contrast to the man-made fibres bleaching is required for many more shades, not just those of high clarity and brightness.
Cotton is prone to base colour variation and is often bleached regardless of shade being dyed to deliver a more uniform base white.

Comparison of Dye Requirements to Achieve Equivalent Shades

Exhaust Dyeing
Figure 1-4, show the chemical and dyestuff requirements to achieve equivalent shades on cotton, TENCEL® ,TENCEL® A100 and (in one instance) TENCEL® LF in an exhaust dyeing process.
The shades studied were Dark Brown, Navy, Khaki and Pink dyed using commodity dyes, Remazol RGB or Levafix CA from DyStar and Novacron LS and FN ranges from Huntsman.

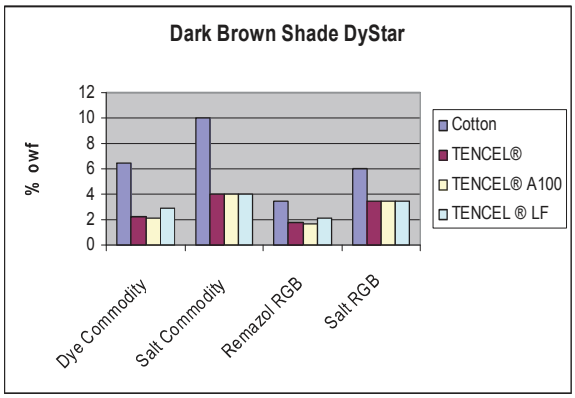

Figure 1. Dye and salt required for Dark Brown Shade – DyStar.

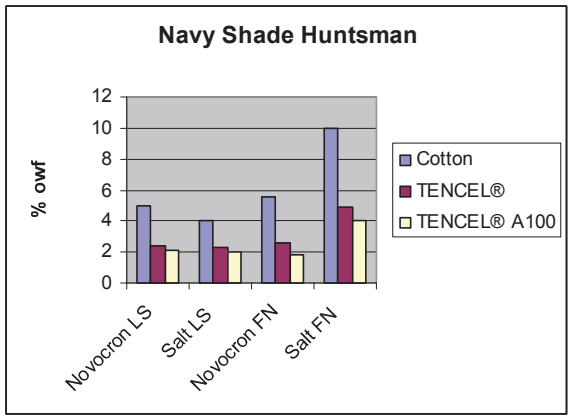

Figure 2. Navy Shade – Huntsman.

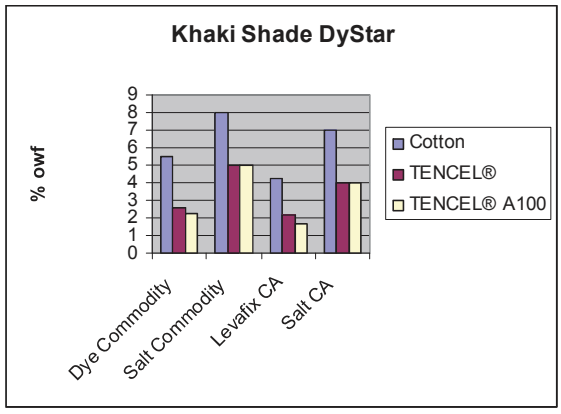

Figure 3. Khaki Shade – Dystar.

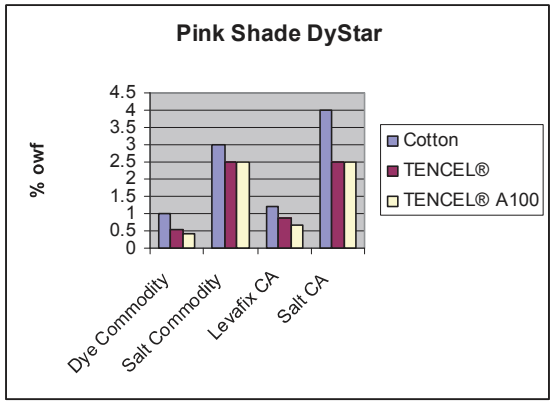

Figure 4. Pink Shade – DyStar.

The results show that:
(1) TENCEL® requires less than half of the amount of dye to achieve the same shade as cotton.
(2) You need only half the amount of salt on TENCEL®.
(3) Soda ash concentrations are also reduced by similar magnitude.
(4) The use of lower dye levels coupled with higher fixation levels means less unfixed dye on TENCEL® compared with cotton.
(5) TENCEL® results in only 30% of the level of residual colour compared with cotton.
(6) TENCEL® A100 results in only 20% of the level of residual colour.

Comparison of Wash Off Behaviour
The figures 5 and 6 show the colour remaining in the dye bath / rinsing baths after dyeing the dark brown shade.

Dye bath	50°C	50°C acid	80°C	98°C	80°C	Cold

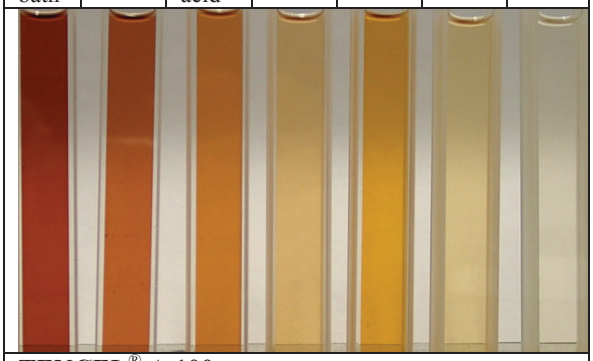

TENCEL® A 100
1.72% C.I Reactive Yellow 176
0.51% C.I. Reactive Red 239
0.51% C.I. Reactive Black 5
2,74% Total

35 g/l Na_2SO_4
7 g/l Soda

Figure 5. Wash off behaviour of TENCEL® A100.

It is clear that much less is needed to be removed from the TENCEL® A100, and it should be possible to remove at least one, possibly two washing baths.

Cold Pad Batch Dyeing

In the assessment of dyeing performance carried out, work concentrated on the results with standard TENCEL® as it is most likely to be utilised with this dyeing technique rather than the TENCEL® A100 variant which is most likely to be used in knitted fabrics.

Once again, the work was carried out over a range of shades, but only two – the Navy and Khaki are reported here. Figures 5 and 6 show the results.

Dye bath	50°C	50°C acid	80°C	98°C	80°C	Cold

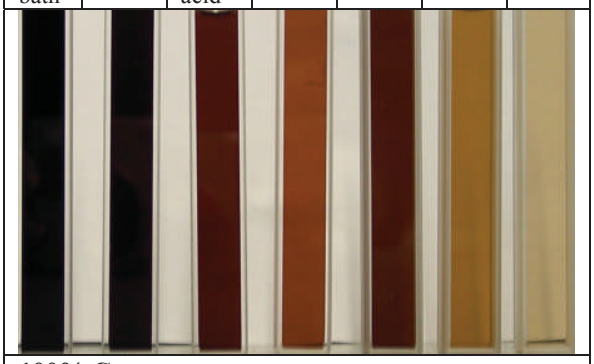

100% Cotton
3.99% C.I Reactive Yellow 176
1.2% C.I. Reactive Red 239
1.197% C.I. Reactive Black 5
6,39% Total

100 g/l Na_2SO_4
20 g/l Soda

Figure 6. Wash off behaviour of cotton dyed to the dark brown shade.

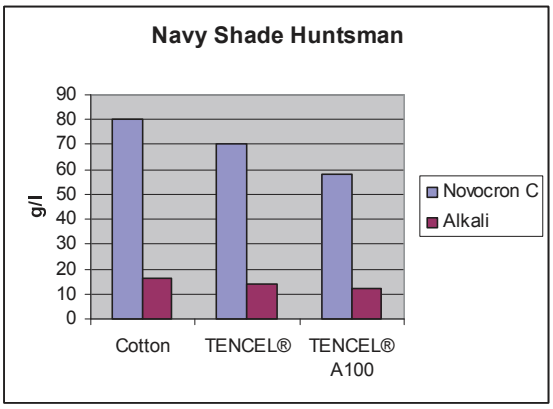

Figure 7. Dye and Alkali requirements Navy shade – Huntsman.

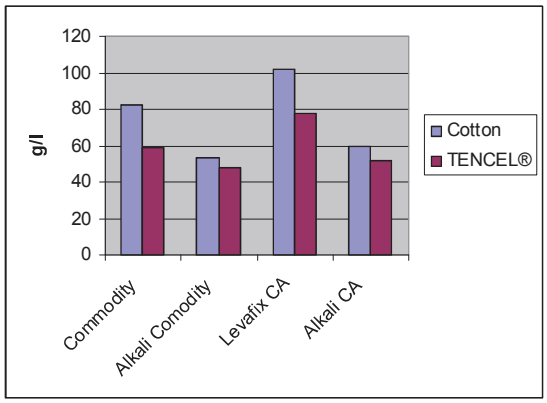

Figure 8. Khaki Shade – DyStar.

The dye yield benefits are not as large as was seen with the exhaust dyeing, but are still valuable.

(1) About 70% of the dye is required on TENCEL® to achieve the same shade as on cotton.
(2) 15% less alkali is needed.
(3) TENCEL® results in just 45% of the amount of residual unfixed colour as is seen with cotton.

Salt Sensitivity and Effect of Liquor Ratio

It is important in dyeing systems that small changes in process parameters do not result in large variations in shade.

When dyeing critical shades such as beige, grey or khaki that are based on tri-chromatic combinations, the more robust the dye combination and fibre being dyed are to process variation, the better "right first time" performance that could be expected.

Work was carried out with DyStar to change the salt and liquor ratio when dyeing the khaki shade and to measure the impact on shade reproducibility.

The results show that the impact on shade of variations in salt concentration and liquor ratio, is lower on TENCEL® A100 than with cotton.

It also shows the improved performance of the Levafix CA dye combination when compared with Commodity dyestuffs – (the last four columns are smaller than the first four).

It is interesting to note that with TENCEL® A100 even a reduction in salt concentration to 50% of it's original results, even with commodity dyes, in a shade change of less than DE 1.0, indicating that salt levels can probably be reduced further.

Comparison of Energy, Water and Chemical Consumption in Jet Dyeing the Navy Shade.

In order to make these comparisons, a number of assumptions have been made:

- 200 kg loading
- 10:1 liquor ratio
- Cold water at 20°C
- No hot fill (all heating done in machine)
- Liquor retention of 2x weight of fabric on draining
- Standard fill / drain – no parallel rinsing/draining
- 100% right first time – no additions
- All hot baths cooled to 60°C before draining
- 50% efficiency of heating (steam energy transfer)
- 50% efficiency of cooling (heat transfer to cold water)
- No water recycling
- No use of renewable energy
- No bleaching needed for TENCEL® A100

The results show that water, energy, dye and chemical consumption for a dark shade on TENCEL® A100 is half that needed for cotton.

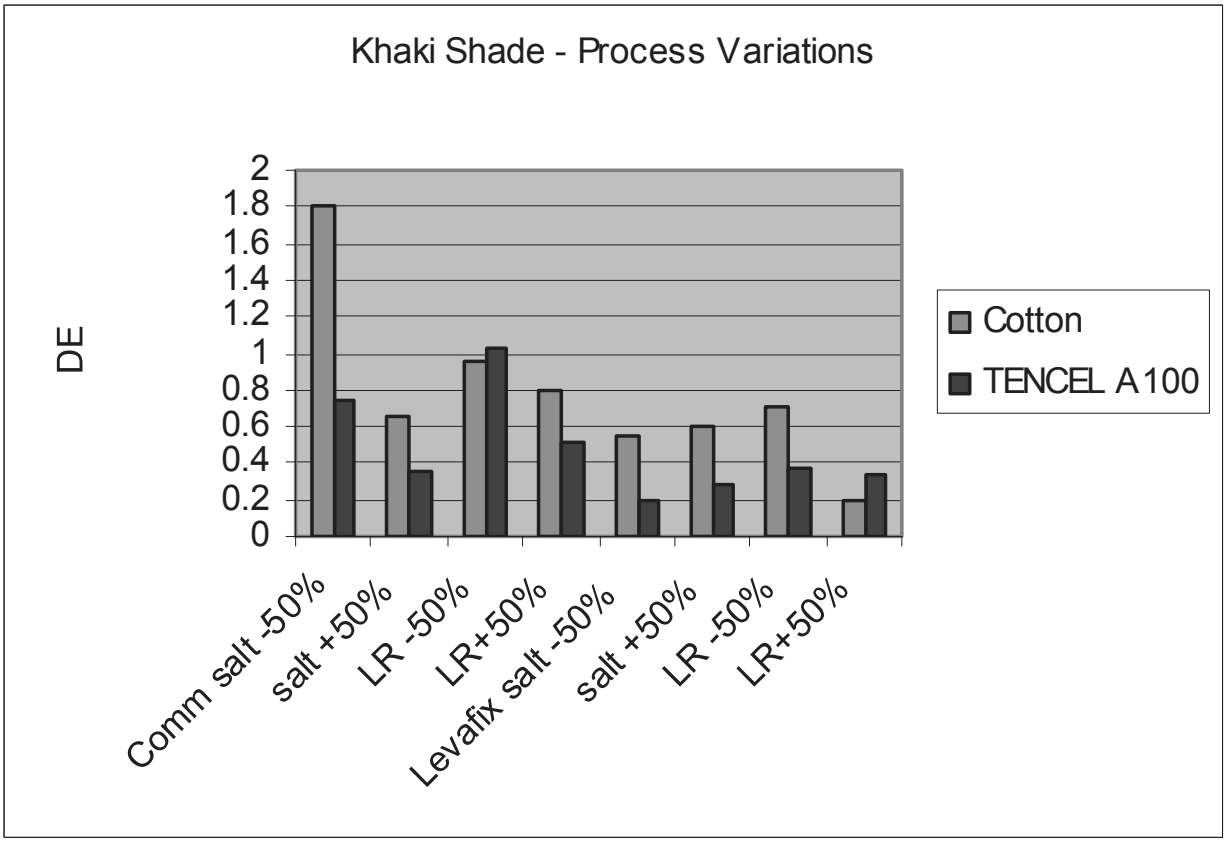

Figure 9. Effect of process parameter change on Khaki Shade.

Table 1. Comparison of Energy, Water and Chemical Consumption in Jet Dyeing the Navy Shade.

	Novocron FN Cotton	**Novocron FN TENCEL® A100**	**Remazol RGB Cotton**	**Remazol RGB TENCEL® A100**	**Remazol RGB TENCEL® LF**
Preparation	Scour/Bleach at 98°C Rinse at 80°C Rinse at 60°C	Detergent scour at 65°C	Scour/Bleach at 98°C Rinse at 80°C Rinse at 60°C	Detergent scour at 65°C	Detergent scour at 65°C
Dyeing	Migration dyeing 80/60°C	Migration dyeing 80/60°C	Isothermal Dyeing at 60°C	Isothermal Dyeing at 60°C	Isothermal Dyeing at 60°C
Wash off	Rinse at 50°C Rinse at 70°C Boil off Rinse at 80°C Rinse at 60°C Rinse at 50°C	Rinse at 50°C Rinse at 70°C Boil off Rinse at 60°C	Rinse at 50°C Rinse at 50°C Rinse at 80°C Boil off Rinse at 80°C Rinse at 25°C	Rinse at 50°C Rinse at 50°C Boil off Rinse at 50°C	Rinse at 50°C Rinse at 50°C Boil off Rinse at 50°C
Process Time (mins)	691	434	649	375	400
Bath water (l)	16400	10000	16400	10000	12000
Cooling water (l)	16380	76300	21060	4260	4750
Total water (l)	32000	17630	37460	14260	16750
Water / kg fabric (l)	**160**	**88**	**187.3**	**71.3**	**83.7**
Total Energy (MJ)	3974	2262	3639	1819	1875
Energy /kg fabric (MJ)	**19.87**	**11.31**	**18.12**	**9.10**	**9.37**
Total Chemicals (kg)	253	130	260	121	121
Chemicals/kg fabric (kg)	**1.27**	**0.65**	**1.3**	**0.61**	**0.61**
Total Dye (kg)	5.55	1.85	7.35	3.3	4.1
Dye / kg fabric (kg)	**0.028**	**0.009**	**0.036**	**0.016**	**0.021**

Costs of the Dyeing Process

If we use the information from above, it is possible to estimate the costs of the dyeing process.
The analysis has been carried out using average prices for gas, electricity and water / effluent in Europe.

Gas	0.425 Euro / m^3
Electricity	0.25 Euro / kWh
Water / effluent	2.50 Euro / m^3

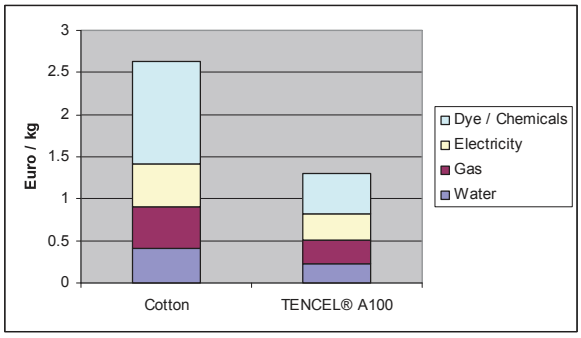

Figure 10. Cost comparison cotton with TENCEL® A100.

The calculations show that TENCEL® A100 is significantly more cost effective in processing than cotton.
For the example above, based on a Navy shade dyed with Novocron FN dyes, the total reduction in processing cost is €1.33 / kg, made up of saving €0.59 from power and water, and €0.74 in dyes and chemicals.
Of course, the saving in dyes and chemicals will be reduced in pale shades, so this result is a "good case" scenario, however it should be borne in mind that the TENCEL A100 process is shorter than that for cotton, so there will be fixed cost savings also that have not been factored in here.

The Environmental Cost of Your Black T-Shirt
A comparison between cotton, TENCEL® A100 and Lenzing Modal®

Trials at scale have been carried out to verify the results from the lab results reported above.

Dyeing of a black shade on the three fibres indicated demonstrated a 40% better colour yield on TENCEL® A100 with a 10% improvement from the modal fabric.
Information drawn from a Life Cycle Analysis Study carried out by Dr Martin Patel and Li Chen [1, 2], reported at Dornbirn conference in 2008, allows us to examine the environmental impact of the three fibre types from fibre production through to the finished fabric in terms of energy usage and water consumption.

Table 2. Fibre manufacture, impact per T-shirt (assume 250g) [1].

	Cotton	TENCEL®	Modal
Water litres)	1430	66	123
Energy (MJ)	10	11	6.2
CO2 (kg)	0.75	0.52	0.22
Land Use (m2)	3.4	0.52	1.52

It should also be noted that unless the cotton is certified organic, there will be high levels of pesticides, herbicides and fertilizers used in cotton production also.
Note that the land use for cotton growing is of agricultural quality, whereas the land used for growing of the trees is marginal land, generally unsuitable for growing agricultural crops.

Yarn Spinning
Cotton has much higher levels of waste. 30% waste is typical for a combed cotton.
This results in a 30% increase in energy requirement for spinning yarn.
Typically reducing the energy consumption from 3.7 MJ to 2.9

Knitting
No differences

Dyeing Process

Table 3. Dying process – comparison of cotton, TENCEL® and Modal.

	Cotton	TENCEL®	Modal
Energy (MJ)	4.5	1.8	2.0
Water (litres)	47	18	22
Chemical (g)	320	150	225
Dyestuff	20	12	18

Conclusions

In exhaust dyeing, when compared to cotton, TENCEL® A100 can be dyed using approximately:

- Half the amount of dye to achieve the same shade
- Half the amount of chemicals
- Half the amount of water
- Half the amount of energy

This is achieved because of very mild scouring/bleaching requirements, high dye fixation and thus less unfixed dye to remove from low salt dye liquors.

In cold pad batch dyeing a similar picture emerged for TENCEL® compared to cotton:

- Approx 66% of dye required to achieve same shade
- Less than half the amount of chemicals
- Half the amount of water
- Half the amount of energy

Again this is achieved by mild scouring/bleaching requirements, high dye fixation and less unfixed dye to wash off.

The remarkable savings on water, energy, dyes and chemicals in processing mean that the cost of processing of TENCEL® and TENCEL® A100 are significantly less than the cost of processing cotton. Further studies are needed to assess the true cost of producing a TENCEL® garment in comparison to one made of cotton over a wider range of colours.

Taking into account the improved efficiencies of TENCEL® in comparison to cotton, if best practice is adopted, the cost differential between cotton and TENCEL® will be considerably reduced if not eradicated.

Acknowledgements

The author wishes to express great thanks to the following for their help in carrying out the work and interpretation of the results:

Phil Patterson, Colour Connections Ltd,
Peter Collishaw and Roland Schamberger, DyStar,
Erwin Miosga and Mike Heaton, Huntsman Textile Effects,
Andrew Thompson, CHT for help with calculations.

References

[1] Li Chen and Martin K. Patel, Lenzinger Berichte 88 (2010) 1-59.

[2] Li Chen and Martin K. Patel, Lenzinger Berichte 88 (2010) 60-66.

Lenzinger Berichte 89 (2011) 37-42

ENGINEERED VISCOSE FIBRES DELIVERING ENHANCED WEARER COMFORT AND FABRIC PERFORMANCE

Matthew North

Kelheim Fibres GmbH, Regensburger Str. 109, 93309 Kelheim, Germany

Phone: (+49) 9441 99-368; Fax: (+49) 9441 99-1368; Email: matthew.north@kelheim-fibres.com

The modification of the cross section of viscose fibres can be used to enhance not only the properties of the fibre itself, but may also be used to improve the properties of the textile structures made from such fibres.
Recent comparative studies carried out on fabrics produced to identical specifications with different cellulosic fibres have proven that viscose fibres with a modified cross section can be used to produce fabrics with better levels of thermal resistance and better moisture transport properties than fabrics produced with standard cross-section fibres.
In tests carried out at the Hohenstein Research Institutes using their skin simulation model, fabrics produced with modified cross-section viscose fibres were also demonstrated to have very good perspiration buffering properties. In combination with the thermal resistance and moisture transport results it was concluded that the fabrics produced from such fibres could deliver higher levels of wearer comfort than, for example, identical fabrics produced from 100 % cotton.
Although the best results were achieved when 100 % modified cross-section fibres were used, it was also demonstrated that the use of such fibres in blends can also improve wearer comfort.

Keywords: *Thermal, viscose, cross-section, Viloft®, Kelheim Fibres*

Introduction

The opportunity to engineer specific fibre properties is one of the major advantages offered by man-made fibres when they are compared with natural fibres. The fibre manufacturer can adjust the production process to manufacture fibres which meet specific customer needs. Examples of the fibre properties that can be changed are:

- fibre count,
- fibre length,
- fibre strength,
- fibre colour,
- fibre cross-section.

There are many examples of modified cross sections in the fibre world, and it can even be said that the natural world has shown man-made fibre producers the way - the complex cross section of cotton, for example, lends the fibre some of its properties. However, the control and consistency offered by manufacturing processes open up many more possibilities to the man-made fibre producer.
Kelheim Fibres Viloft® fibre has been engineered with a flat cross-section (Figure 1) and is specifically designed to deliver enhanced performance in apparel fabrics.
Viloft® fibre, when used in appropriate constructions, can improve the softness of fabrics as a result of the fibre's increased flexibility, as well as delivering improved levels of thermal insulation and moisture

transport. Viloft® fibres have been successfully used in textile applications for many years, and in the past comparison work has been carried out which has proven that Viloft® fabrics offer superior thermal performance to fabrics made with cotton, hollow polyester and polypropylene.

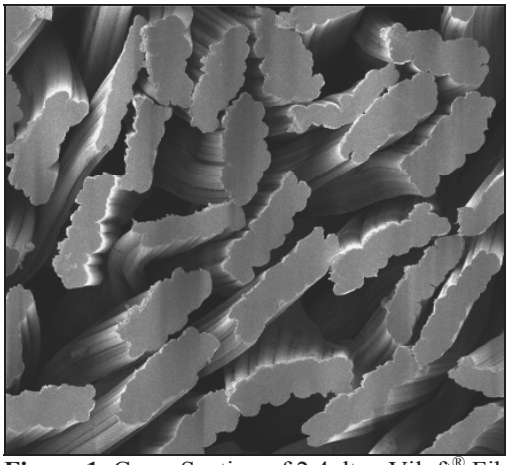

Figure 1. Cross Section of 2.4 dtex Viloft® Fibre.

The superior performance of fabrics containing Viloft® fibres is believed to be due to the flat cross-section of the fibres, for the following reasons:

- the behaviour of the individual fibres in the yarn increases the number of voids (air pockets) in the yarn,
- the amount of air in the fabric is thereby increased and contributes to the improved thermal and moisture management performance of the fabrics,
- the flat cross-section of Viloft® fibre has a significant influence on wearer comfort.

The purpose of the investigative work described here was as follows:

- investigate and confirm the behaviour of flat cross section fibres in spun yarns,
- determine the potential benefits of the use of Viloft® fibres in apparel fabrics and back these up with objective data,
- investigate the link between cross-section, yarn air content, and wearer comfort,
- validate the assumptions relating to the performance and wearer comfort of fabrics manufactured with Viloft® fibres.

Materials and Methods

Initially, the investigation was based on a comparison of fabrics containing Viloft® fibres

- in 100%,
- in blends with cotton,
- in blends with viscose,
- in blends with Modal,
- with other cellulosic fibres.

To ensure a direct comparison of the results of the fabric testing was possible, identical yarn and fabric constructions were used.

In total four ranges of fabrics were produced under industrial conditions. These were as follows:

1) Single Jersey and Single Jersey Elastic based on Nm85/1 ring yarns using 1.9 decitex Viloft fibres in 100 %, in blends with cotton at various blend ratios, in blend with micro (0.9 dtex) viscose, in blend with MicroModal and also fabrics in 100 % MicroModal, 100 % cotton and a blend of cotton and MicroModal, and
2) Single Jersey and Single Jersey Elastic based on Nm50/1 ring yarns using 1.9 decitex Viloft fibres in 100 %, in blends with cotton at various blend ratios, in blend with viscose and also fabrics in 100 % cotton and a blend of 50 %/50 % Viloft/cotton compact spun.

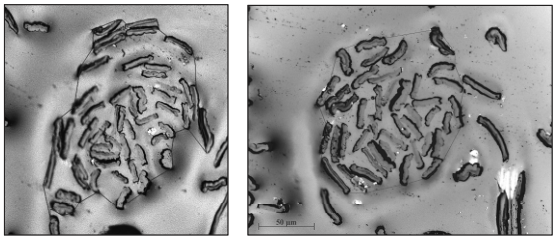

Figure 2. Determination of Yarn Cross Sectional Surface Area.

The first stage of the investigation involved the determination of the air

content of a selection of yarns used in the production of the fabrics. This was carried out using microscopy in combination with the AxioVision software from Zeiss, which allows the cross-sectional surface area of the yarn to be determined.
The air content of the yarns was determined by subtraction of the fibre cross-sectional area from the yarn area.
In order to assess the potential benefits of the use of Viloft® fibres in apparel fabrics five fabrics were selected for tests at the Hohenstein Research Institute in Germany, using their proprietary test methods and equipment, including their skin simulation model. These tests have been developed over many years and are acknowledged to deliver an objective assessment of wearer comfort [1].

All five fabrics tested were elastic single jersey E36/30 gauge S + Z using Nm85/1 ring yarns in the following blends:

- 100 % Viloft® 1.9 dtex (100 Vi),
- 67 % Viloft® 1.9 dtex/33 % Cotton (67/33 Vi/CO),
- 50 % Viloft® 1.9 dtex/50 % Cotton (50/50 Vi/CO),
- 100 % Cotton (100 Co),
- 100 % MicroModal (100CMD).

The following tests were carried out:

- Thermal Insulation ($R_{ct} * 10^3$ m^2 K/W)
  Test Equipment: The Hohenstein Skin Model
  Test Methods: see DIN EN 31 092 02/94)/ISO 11 092 (10/93)
- Water Vapour Permeability Resistance (R_{et} m^2Pa/W)
  Test Equipment: The Hohenstein Skin Model
  Test Methods: see DIN EN 31 092 02/94)/ISO 11 092 (10/93)
- Water Vapour Permeability Index (i_{mt})
  Description: see DIN EN 31 092 02/94)/ISO 11 092 (10/93), Section 2.3
- Water Vapour absorbency potential (F_i g/m^2)
  Test Equipment: The Hohenstein Skin Model
  Test Methods: see DIN EN 31 092 02/94)/ISO 11 092 (10/93)
- Perspiration Buffering Index
  Test Equipment: The Hohenstein Skin Model
  Test Methods: see Hohenstein Standard Test Method BPI 1.2 (12/93), Section 3

Results and Discussion

The results of the investigations to determine the air content of a selection of Nm85/1 ring yarns using 1.9 decitex Viloft are shown in Figure 3. The upper (light) sections of the columns represent the air content of the yarns tested, the lower (dark) sections represent fibre content.

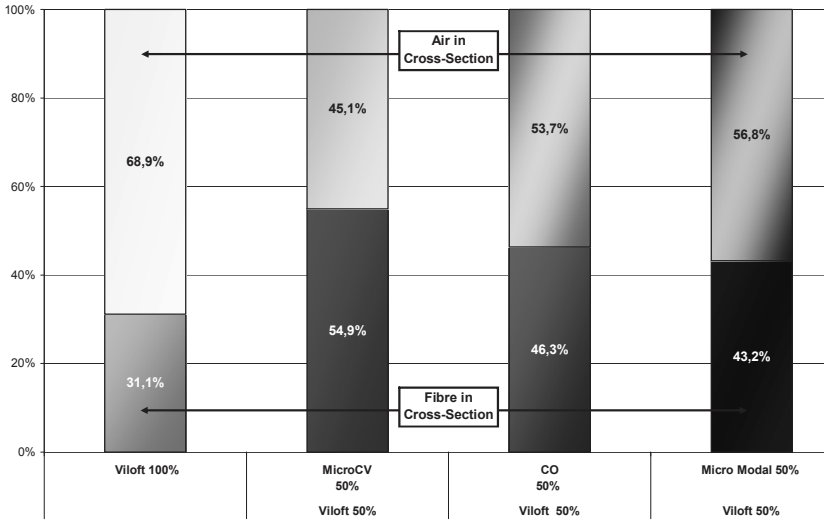

Figure 3. Results of Investigation to Determine Air Content.

The following results were obtained:

- With 68.9 % air content, 100 % Viloft® yarn showed the highest level of air content of the yarns tested.
- Viloft® in blends with MicroModal and with cotton showed similar levels of air content at between 63 and 67 %
- Viloft® in blend with micro viscose showed the poorest result, with only 46.1 % air content. It is believed that the individual microfibres pack more densely and hinder the formation of voids.

Based on these results it was concluded that the flat cross-section of Viloft® fibres enhance the formation of voids in yarns, thereby increasing the content of air in the yarn.

The results of the thermo-physiological tests carried out on the selected single jersey elastic fabrics listed above the Hohenstein Research Institute were as follows:

*Thermal Insulation (R_{ct}*10^3 m^2 K/W)*

Of the fabrics tested, the fabric with 100 % Viloft® delivered the highest thermal insulation result. It was also noted that fabrics containing man-made cellulosic fibres generally gave better thermal insulation results than the fabric containing 100 % cotton (Figure 4).

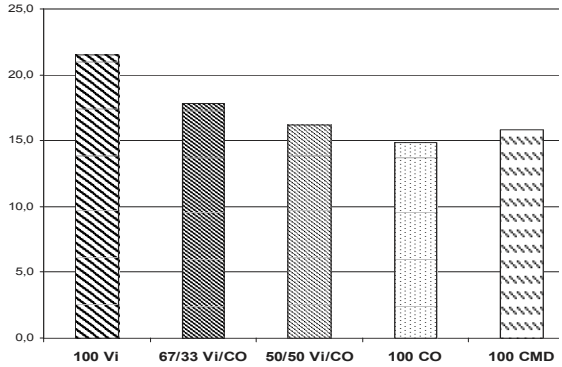

Figure 4. Thermal Insulation (R_{ct}*10^3 m^2 K/W).

It was also established that the thermal insulation performance of cotton fabrics can be increased by adding Viloft® fibre to the blend. An increase of 19 % in measured thermal performance was achieved when 67 % Viloft® was added to the blend. However, the 100 % Viloft® fabric outperformed this fabric by 20.7 % and the 100 % cotton fabric by 44.3 %.

Water Vapour Permeability Resistance (R_{et} m^2Pa/W)

Water vapour permeability resistance is a measure of the breathability of fabrics with higher values indicating a higher resistance and lower breathability (Figure 5).

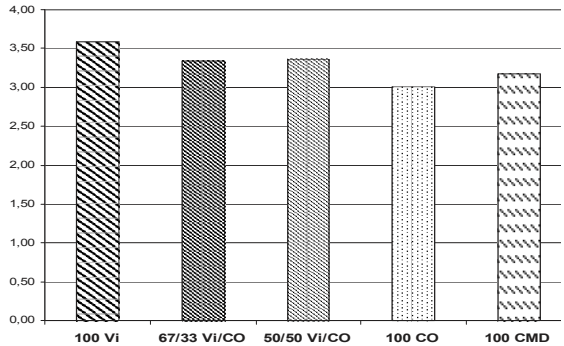

Figure 5. Water Vapour Permeability Resistance (R_{et} m^2Pa/W).

Although the 100 % Viloft® fabric delivered the highest level of resistance the results for all the fabrics tested lie within a narrow range and, in the experience of the Hohenstein Institute the differences would not be perceived as significant by the wearer of the fabrics.

Water Vapour Permeability Index (i_{mt})

The water vapour permeability index is a combination of the results of the thermal resistance and water vapour permeability resistance tests carried out on the fabrics.
Of the fabrics tested, the fabric with 100 % Viloft® delivered the highest water vapour permeability index (Figure 6).

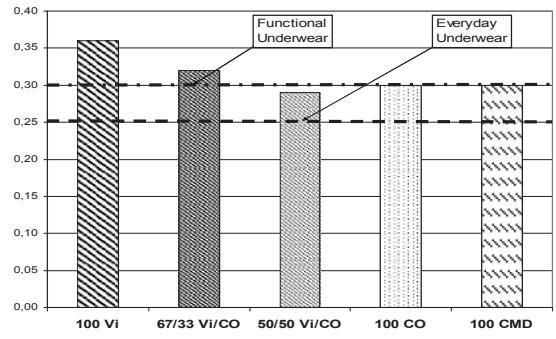

Figure 6. Water Vapour Permeability Index (i_{mt}).

The Hohenstein Institute has defined levels of performance above which fabrics may be considered to offer a degree of functionality. While the 100 % cotton and 100 % MicroModal were just able to meet this threshold, the 100 % Viloft® fabric exceeded it by 20 %.

Water Vapour absorbency potential (Fi g/m2)

The measurement of water vapour absorbency potential defines the capability of the fabric to absorb moisture from the skin (Figure 7).

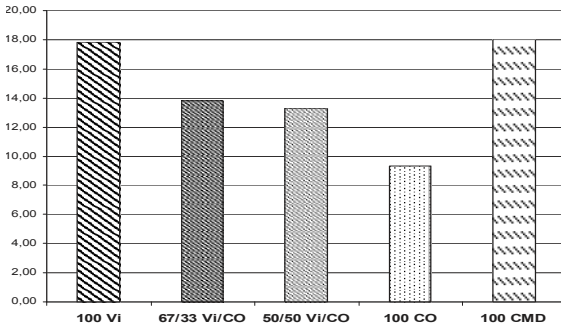

Figure 7. Water Vapour absorbency potential (Fi g/m2).

The fabric with 100 % Viloft® delivered performance comparable to the 100 % MicroModal fabric, both outperforming the 100 % cotton fabric.

Generally it was established that fabrics containing man-made cellulosic fibres outperformed fabrics containing cotton.
And as with the thermal insulation results, the results for this test for cotton blend fabrics improved as the proportion of Viloft® fibres was increased.

Perspiration Buffering Index

The perspiration buffering index is a combination of the results of tests for perspiration absorption and perspiration transportation (Figure 8).

All of the fabrics tested performed to a similar level - in this case the 50/50 blend of Viloft® and cotton performing slightly better than the other fabrics. Most of the fabrics tested met the criteria defined by the Hohenstein Institute for a "very good" result.

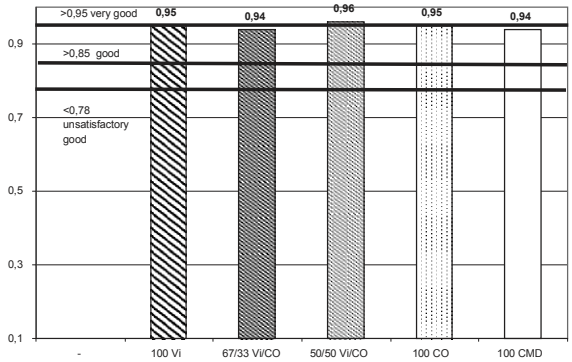

Figure 8. Perspiration Buffering Index (Index Value).

Thermophysiological Wearer Comfort

The Hohenstein Institute has developed a formula which takes the results of these tests and combines them with constants to deliver an objective measure of wearer comfort. The results of this formula have over time, been proven to be consistent with the results of wearer trials.
The fabrics tested were ranked according to this test on a scale of 1 to 6, where results less than 1.5 are considered "very good" and results between 1.5 and 2.5 as "good". Differences in ranking of more than 0.5 can be subjectively felt by test candidates.
The results of the fabrics tested are shown in Figure 9.

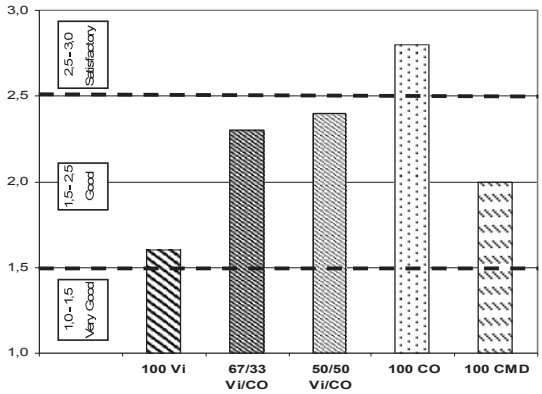

Figure 9. Thermophysiological Wearer Comfort.

The fabric in 100 % Viloft delivered the highest level of thermo-physiological wearer comfort. The 100 % cotton fabric performed worst in these tests. The level of wearer comfort of cotton fabrics was

improved by the addition of Viloft® fibre in the blend.
The results of the test work at Hohenstein can be summarized as follows:

- Fabrics containing 100 % Viloft® fibres achieve the highest wearer comfort rating of the fabrics tested.
- The incorporation of Viloft® fibres can improve the thermal insulation performance of blends.
- Fabrics containing Viloft® fibres
  - deliver high levels of thermal insulation,
  - meet the moisture management criteria for functional underwear,
  - show excellent levels of wearer comfort.

Beyond this additional testing work carried out on the fabrics based on Nm50/1 yarns outlined detailed above mirrored the results of this test series, indicating that the inherent properties of Viloft® fibres can bring similar benefits in other fabric constructions.

Conclusions

From the testing work carried out, the following conclusions have been drawn:

- Of the fabrics tested, those with a high air to fibre content ratio deliver better wearer comfort results.
- The unique flat cross-section of Viloft® fibres lead to a higher air content in yarns and fabrics.
- The results of the Hohenstein tests confirm the superior performance of Viloft® fabrics in terms of wearer comfort.

The investigations described above demonstrate that the modified cross-section of Viloft® fibres drives the superior performance of fabrics made with the fibre and confirm that the fibre is appropriate for use in garments where high levels of thermal performance and wearer comfort are desired.

Acknowledgements

Kelheim Fibres GmbH would like to thank Roger Kargel, Schiesser AG, the Hohenstein Institutes, ITV Denkendorf and Carl Zeiss AG for their support in carrying out this project.

References

[1] K. H. Umbach, Produktauszeichnung “Tragekomfort” Am Point of Sale, Lenzinger Berichte, 85 (2006) 9-16.

Lenzinger Berichte 89 (2011) 43-49

ARE FLAME RETARDANTS ALWAYS NECESSARY? BURNING BEHAVIOR OF TENCEL® IN BEDDING ARTICLES

Mohammad Abu-Rous*, Robert J. Morley, Johann Männer, Hartmut Rüf, Tom Burrow and Susanne Jary

Lenzing AG, Werkstr. 2, 4860 Lenzing, Austria

*Phone: (+43) 7672 701-3387; Fax: (+43) 7672 918-3387; Email: m.aburous@lenzing.com

Presented during the 48th Man-Made Fibers Congress, Dornbirn, 2009

Already implemented or pending amendments in the USA and the EU concerning the requirements on the flammability of commercial articles entail also in the home textile domain the necessity to develop complying materials, constructions and products.
For example, the Californian standard for mattress flammability behaviour has already been adopted on US-federal level. The so-called Technical Bulletin (TB) 603 has become the Federal Standard CRF 1633. A norm concerning comforters, mattress pads and pillows is in draft (TB604).
To comply with such standards, flame retardants are being applied. However, efficient substances are typically not always harmless in terms of health and ecology.
Such substances become especially critical in bedding articles due to the direct contact with the human body.
An economical and chemically harmless solution seems to be reached by applying TENCEL® fibers: Having an appropriate design, the article surface would carbonize and form an isolating layer, which protects the subjacent zones.
Based on TENCEL® and polyester fibers, bed articles can be developed which do comply with the requirements of the single norms (TB604, CFR1633, BS 5852, BS7177) and also maintain comfort as well as health compatibility.

Keywords: *TENCEL®, flame retardants*

Introduction

Historically known as one of the oldest fuel materials, cellulose doesn't come immediately to mind in the context of flame protection, although many daily life observations show that cellulosic material in compact construction (bulky wood, telephone book) does not burn as easily as a single paper or straw does.
The health and ecology debates, which accompany the recent developments of fire standards in industrial countries, make elegant solutions based on rather natural, chemically harmless material very desired.
The Californian standard for mattress flammability behavior has already been adopted on US-federal level. The so-called Technical Bulletin (TB) 603 [1] became the Federal Standard CRF 1633 [2].
A norm concerning comforters, mattress pads and pillows is also in draft (TB604)[3], which concerns filled and foam-based flat bed items, is also in draft and is expected to be ratified. Each of the product areas, comforters, pillows, and mattress pads are respectively addressed in Sections 1, 2 and 3 of TB604, of which each is presenting a different set of challenges [4]. The parts 1 and 2 are based

on weight loss whilst burning and apply for bed items with loose (i.e. pillows) or ordered (i.e. comforters) fills. Part 3 is based on the fire penetration and applies for mattress pads and bed items thinner than 5 cm. This work focuses on sections 1 and 3 of TB604, where the fiber aggregation is similar. Section 2 concerns items where the fibers are mostly in loose form, and is therefore worth a separate study.

The new standards require developments of complying materials, constructions and products. Initiatives of concerned US citizens are already campaigning against TB604. The expected increase of flame retardant (FR) additives brings worries in both health and ecological aspects [5, 6].

In Europe, the obligatory flammability standards make the British market special [7] and limit the options for possible materials. The British Standard 5852 was developed to assess the flammability of upholstered furniture systems by smoldering cigarettes, lighted matches and stronger ignition sources. Mattresses are regulated by the related BS 7177 [8]. It applies for mattresses, divans and bed bases Items (except comforters) sold for residential use are identified as low hazard use and must meet both a smoldering cigarette ignition test as well as a match flame equivalent ignition test.

It is unknown at this time whether the European Community will adopt the British standards. However, European standards, such as EN597 [9] are barriers to be passed in order to enter the public and hospitality segments.

The flammability standards are based on different observations on the burning behaviors (Table 1). Burning duration, extending speed, burning energy, weight loss, shape maintenance etc. are all criteria which are related to the burning process, but are not related to the same rate to each other.

Earlier studies already recommended the use of cellulosic fibers as a solution to comply with the flammability norms [10]. Having an appropriate design, the cellulosic surface would carbonize and form an isolating layer, which protects the subjacent zones. An economical and chemically harmless solution seems to be approached by applying the cellulosic TENCEL® FILL fiber and its blends with standard polyester. The 6.7 dtex fiber can easily be blended with polyester. The aim of this study is to prove the compliance of common TENCEL® FILL/polyester blends without chemical additives with the flammability standards.

Materials

All TENCEL® FILL fibers are standard Lenzing fibers (6.7 resp. 1.7 dtex; 60 mm, siliconized). The polyester fiber, M1119; 5.4 dtex, 55 mm, non-siliconized, was kindly supplied by Wellman Inc (Ireland).

Cotton/Polyester fabric (110 gsm) for TB604 was acquired from Lauffenmühle (Austria). FR-polyester fabric (220 gsm) for BS5852/2 and BS7177 testing was kindly supplied by Fogarty Ltd. (UK).

Table 1. Overview on the test parameter and the scope of the investigated flammability standards.

Standard	Main criterion	Concern	Sample form
TB604/1	Weight loss/time	Comforter, flat bed items thicker than 5 cm	Card, fleece
TB604/2	Weight loss/time	Pillows, loose fill	Fiber balls
TB604/3	Flame penetration	Mattress pads, thin flat bed items	Card, fleece
CFR1633	Burning heat	Mattress, divans, bed bases	Complete mattress
BS7177 / BS5852	Burning time, flame penetration	Pillows, Mattress pads	Stuffed as intended in use

Experimental

Technical Bulletin TB604

TB604/1

A 38x38 cm cushion made of the cotton/polyester fabric defined by the standard was prepared and stacked with multiple layers of the fiber sample to reach a thickness of approximately 89 mm under a Plexiglas plate defined by the standard. The sewn cushion was conditioned for at least 24 hours at 20°C and 50% rh. The cushion was exposed to a defined fire flame for 20 seconds, and the weight loss during the burning process was measured (Figure 1).

Figure 1. Trial setting according to TB604/1.

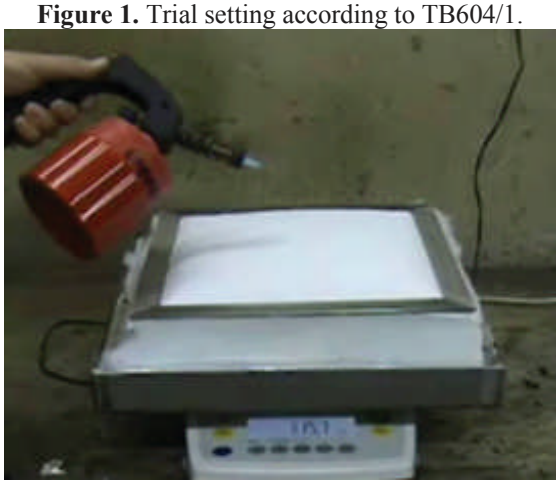

Figure 2. Trial setting according to TB604/3.

TB604/3

A 305 mm x 305 mm fiber sample fleece was tested between two cotton/polyester standard fabric double sheets. The height of the sample was set to 50 mm under the defined Plexiglas plate. A square metal frame defined in the standards was placed over the top sheeting fabric.

The surface of the test specimen was exposed to a 35 mm high gas flame oriented at 30 degree with respect to the horizontal line for 20 seconds (Figure 2). After removing the flame, the burning process was observed. After all traces of flaming and smoldering have ceased, the dimensions of largest voids in the filling material and (if existing) the two bottom fabrics were measured.

BS5852/2, BS7177

Fiber sample was filled in the back and the bottom of a "Chair" with defined dimensions, and covered with a FR polyester shell fabric (220 gsm). The lower part of the chair back was exposed for 40 seconds to a 14 cm butane gas flame (Figure 3).

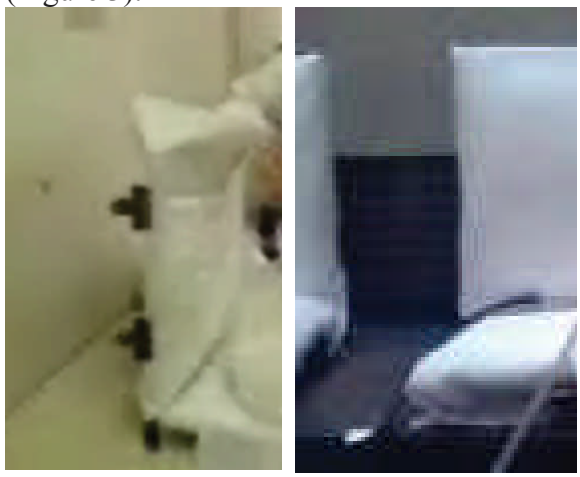

Figure 3. Trial setting according to BS5852/2.

After removing the flame source, the sample shouldn't burn for more than 120 seconds. A further failing criterion is if it burns through or until the edge of the sample, or if burning parts fall on the sitting part of the chair.

Results and discussion

Results on Californian Technical Bulletin TB604

TB604/1

Figure 4 shows the time/weigh plot at the first six minutes of the sample burning. Both commercially available, TENCEL®

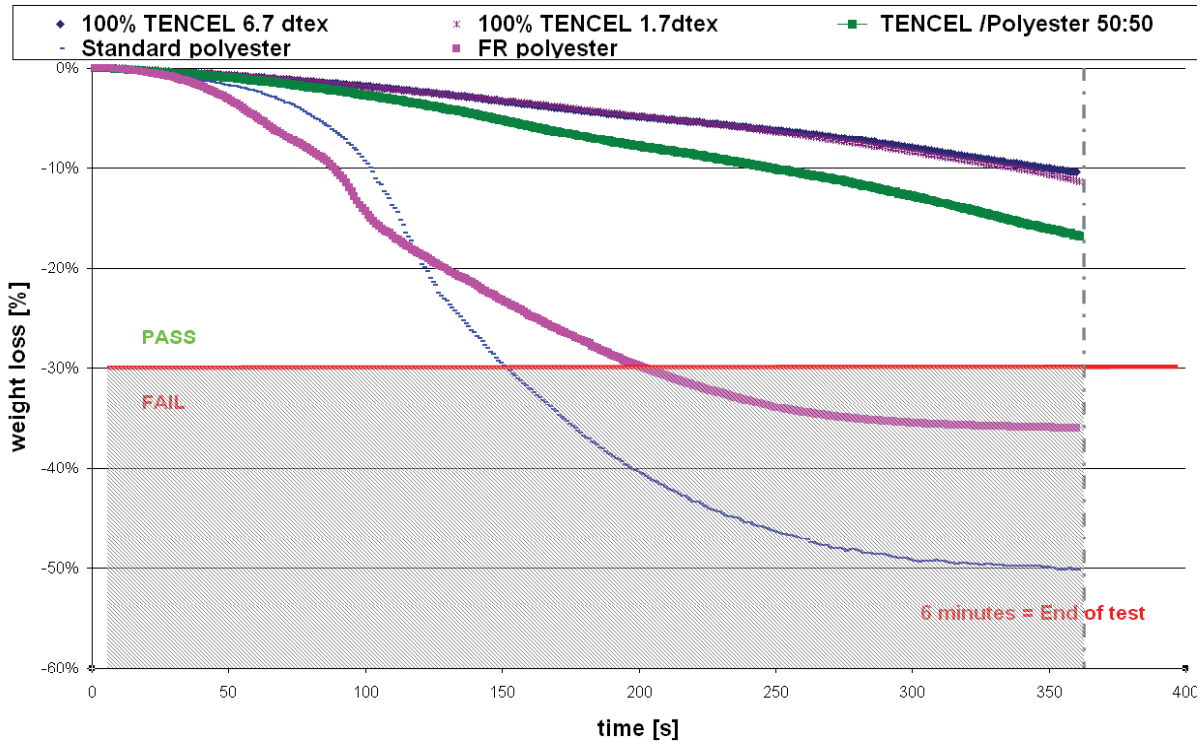

Figure 4. Time/weight plot of the burning of TENCEL® FILL in comparison to regular and FR-treated polyester, tested according to TB604/1.

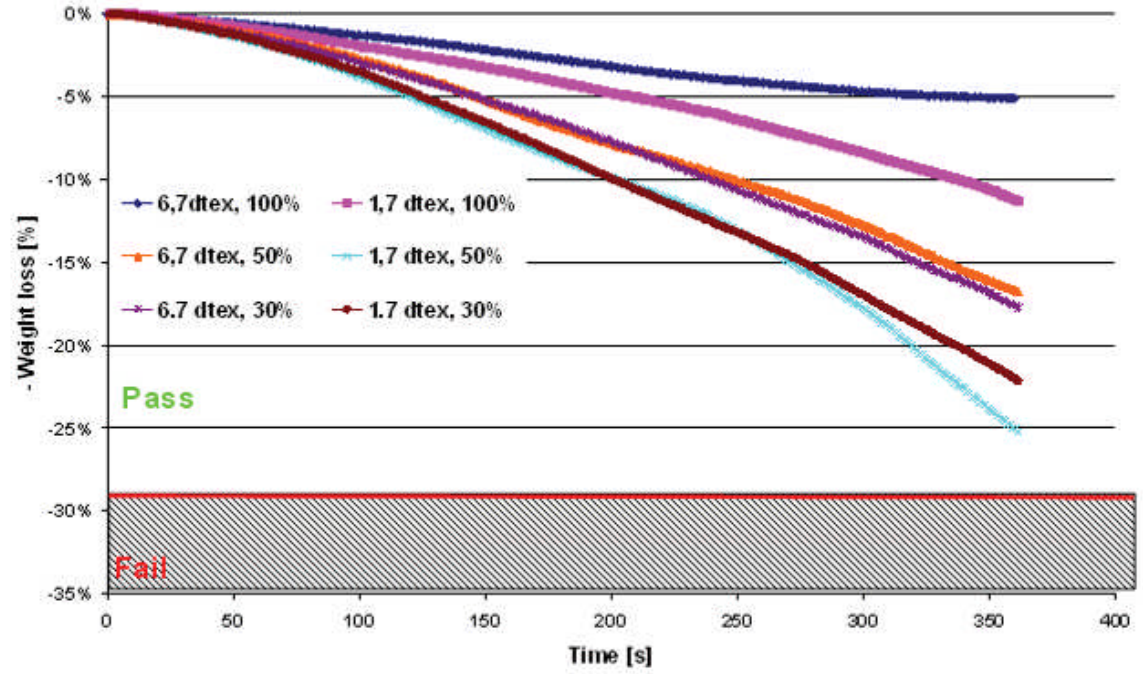

Figure 5. Time/weight plot of the burning of TENCEL® FILL fiber and fiber blends with polyester according to TB604.

fibers (1.7 and 6.7 dtex) and their 50:50 blends with polyester were able to pass, while the samples of 100% standard and FR polyester failed.

Figure 6 shows the sample situation after complete burning. Independent of the residual weight, a 100% polyester sample would melt down and completely loose shape, while a TENCEL® sample, in 100% or blended, would only burn on the surface, keeping the sample interior intact.

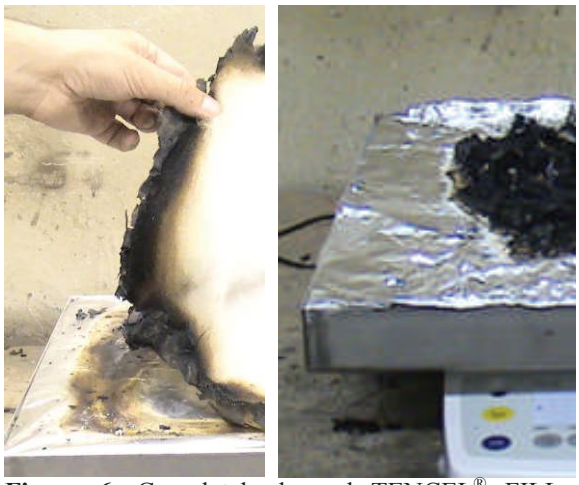

Figure 6. Completely burned TENCEL® FILL (left) and polyester (right) samples, according to TB604/1.

Figure 7 shows different blends of TENCEL® FILL with polyester. With the right fleece construction, samples containing 30% TENCEL® FILL were able to pass. It is important to consider the fleece construction, which is decisive for the outcome of the test.

TB604/3

Part three of TB604 concerns flat bed items thinner than 5 cm, such as mattress pads.

This part of the standard is considered to be the most challenging due to its thinness and cost constraints [4].

The test is based on the hole which occurs in the sample after a 20 second exposure to a high gas flame.

A sample would fail if a hole larger than 5 cm in any direction results from the completed burning process. In this test setting, even FR polyester samples failed after melting down and burning to a plastic mass. Oppositely, cellulose samples showed only a superficial burning and the carbonized surface hindered the oxygen from reaching the sample inside. The interesting point here is also the fact, that TENCEL®/Polyester blends performed similarly to 100% TENCEL®.

Figure 8 also shows the behavior padding applications, which are thinner than 5 cm. TENCEL® FILL passes even in a 50:50 blend with regular polyester.

Figure 7. A TENCEL® FILL/polyester fiber blend (left), compared to 100% polyester, burned according to TB604/3.

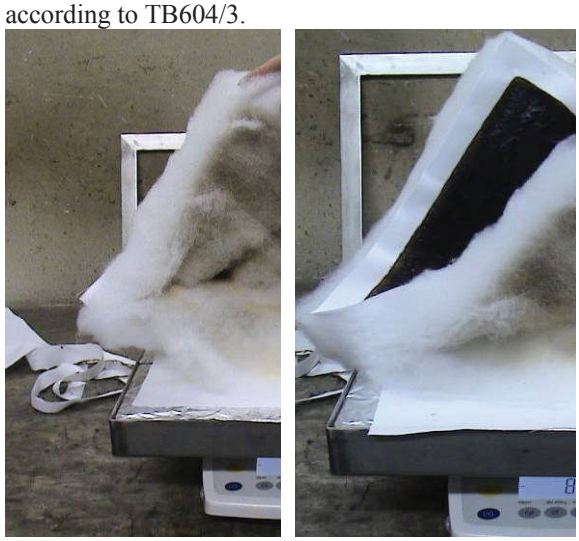

Figure 8. 2.5cm high thick samples of 100% TENCEL® FILL and a 50:50 TENCEL® FILL/polyester blend (left), burned according to TB604/3.

Figure 9. A 100% polyester sample burned according to TB604/3 using a protective barrier fabric.

Additionally, it was observed that a flame retardant barrier fabric is not always enough to make a standard polyester mattress pad pass TB604/3. The melting beneath the fabric leads to larger holes in the pad, or – in some cases – to a burn-through (Figure 9).

Results on BS7177

The main pass/fail criterion is the smoldering time after a forty second exposure to a prescribed flame. None of the two trials performed on the chair should fail. A further failing criterion is burn through, or if burning parts fall on the sitting part of the chair. Figure 10 shows a sample which passed the test.

Figure 10. Test sample burned according to BS5852/2.

The packing density was observed to be one of the most decisive factors in the burning performance. 100% standard polyester did not smolder for longer than two minutes, but a burn-through was observed and the samples failed hence. The same phenomenon was observed on wool (Figure 11).

TENCEL® FILL and its 50:50-blend with polyester do not show such a burn-through. On the other hand, the polyester blend was critical concerning the burning time. However, the 100% TENCEL® sample, where the fibers are well paralleled, passes the test showing neither long smoldering nor burn-through.

Figure 11. Burning behavior of TENCEL® FILL/polyester 50:50 blend (left) in comparison to 100% wool (right).

Conclusions

Table 2 summarizes the compliance of TENCEL® FILL and its blends with regular polyester with both standards in question. TENCEL® fibers and their 50:50 blends with regular polyester could match the requirements of TB604 for flat bed items containing fibers in an ordered (paralleled) form. Furthermore, the fibers can comply with the British standard 7177 when used in the right construction, where surface carbonization occurs and isolates.

The same phenomenon can be utilized in other filled and textile items to match other flammability standards for household and hospitality articles, such as the European cigarette and match test EN597 and similar standards. This will be the subject of a separate study.

Table 2. Summary of the results (up-to-now) on the compliance of TENCEL® FILL and its blends with standard polyester to the standards in concern.

Fiber	Fiber content [%]	BS5852/2 ; BS7177	TB604/1	TB604/3
Use		Mattress pads, divans, domestic pillows, upholstered cushions	Comforters	Mattress Pads
TENCEL FILL 6.7dtex	100%	**X**	**X**	**X**
TENCEL FILL 6.7dtex	50%		**X**	**X**
TENCEL FILL 1.7 dtex	100%	**X**	**X**	**X**
TENCEL FILL 1.7 dtex	50%		**X**	**X**

Acknowledgments

Johann Gruber, Heidrun Weissl and Gerold Riedl , Lenzing AG for the sample preparations and TB604 test performance,
Florian Justl for help in digital processing of film material,
Noel McEnroe, Wellmann for the polyester fiber,
Kevin Smithbone, Fogarty, UK for the BS 7717 testing.

References

[1] State Of California, Department of Consumer Affairs, Technical Bulletin TB603, Requirements and test procedures for resistance of a mattress/box spring set to a large open flame, July 2003.

[2] Consumer Product Safety Commission, 16 CFR Part 1633, Standard for the Flammability (Open Flame) of Mattress Sets; Final Rule, Federal Register / Vol. 71, No. 50 / Wednesday, March 15, 2006 / Rules and Regulations.

[3] State of California, Department of Consumer Affairs, Technical Bulletin TB604: Test procedure and apparatus for the open flame resistance of filled bedclothing, Draft October 2007.

[4] Jeff Vercellone, Kaneka Corporation, The regulation of bedclothing materials for Flame retardancy –A Stakeholders Perspective, NIST Barrier Fabric Workshop March 18, 2009.

[5] Arlene Blum, Averting a California toxics disaster, *Green Science Policy Institute, California Progress Report, 11.03.2009,* http://www.californiaprogressreport.com/2009/03/averting_a_cali.html

[6] Green Science Policy Institute; http://greensciencepolicy.org/regulations/

[7] British Standard BS7177:1996, Specification for resistance to ignition of mattresses, divans and bed bases.

[8] *IN TOUCH*, a regular publication of the Polyurethane Foam Association (PFA). Flammability Update: Flexible Polyurethane Foam Industry Strives to Further Reduce Fire Deaths and Injuries, http://www.pfa.org//intouch/text/v7n1.txt

[9] ÖNORM, EN597, 1995: Furniture – Assessment of the ignitability of mattresses and upholstered bases- Part 1 (smoldering cigarette) and 2 (match flame equivalent).

[10] Mc Fadyen J. P. – Wellmann Inc., Flame retardant furniture and top-of-the-bed filling applications, 44th International Man-Made Fibers Conference, September 22th 2005.

Lenzinger Berichte 89 (2011) 50 – 59

THERMAL AND SORPTION STUDY OF FLAME–RESISTANT FIBERS

Ksenija Varga[1,2], Michael F. Noisternig[3], Ulrich J. Griesser[3], Linda Aljaž[4] and Thomas Koch[5]

[1]Christian–Doppler Laboratory for Chemistry of Cellulosic Fibers & Textiles, University of Innsbruck, Austria
[2]Lenzing AG, Fiber Science & Development Department, Werkstraße 2, A–4860 Lenzing, Austria
Phone:+43 7672 701 2757; Fax:+43 7672 918 2757; E–Mail: k.varga@lenzing.com
[3]University of Innsbruck, Institute of Pharmacy, Pharmaceutical Technology, Innrain 52c, A-6020 Innsbruck, Austria
[4]Faculty of Natural Sciences & Engineering, University of Ljubljana, Slovenia
[5]TU Wien, Institute of Materials Science & Technology, Favoritenstraße 9-11, A-1040 Vienna, Austria

The characterization of FR fibers and fabrics is of crucial importance giving the main accent to the thermal behavior of materials in practical use. Since FR fabrics are often made from a very limited number of materials, it is important to use fibers which provide good physiological comfort. Lenzing FR® fibers are characterized by thermal and sorption methods in comparison with other flame–resistant materials. DSC and TGA are important means to study thermal properties of textiles. DSC spectra provide changes of heat release during decomposition while TGA show weight loss of the tested materials, but no specific pyrolysis of the products. Dynamic sorption analysis in broad humidity range show high sorption of cellulosic Lenzing FR® and lower for synthetic materials. Visualization of the residues of combusted materials by SEM confirms the theory of different decomposition mechanisms during heat exposure.

Keywords: *Lenzing FR®, FR fibers, protective wear*

Introduction

Safety of human beings has been an important issue all the time. A growing segment of the industrial textiles industry has therefore been involved in a number of new developments in fibers, fabrics and protective clothing. Major innovations in the development of heat–resistant fibers and flame–protective clothing for fire-fighters, foundry workers, military and space personnel, and for other industrial workers who are exposed to hazardous conditions have been carried out. For heat and flame protection, requirements range from clothing for situations in which the wearer may be subjected to occasional exposure to a moderate level of radiant heat as part of normal working day, to clothing for prolonged protection, where the wearer is subjected to severe radiant and convective heat to direct flame.

In the process of accomplishing flame protection, however, the garment may be so thermally insulative and water vapor impermeable that the wearer may begin to suffer discomfort and heat stress. Body temperature may rise and the wearer may become wet by sweat. Attempts have therefore been made to develop thermal and flame protective clothing which can be worn without any discomfort [1, 2].

This paper provides an overview of mostly used fibers for thermal and flame protection. The thermal behavior of such fibers is studied by using following thermal methods: thermogravimetry (TGA) and differential scanning calorimetry (DSC). Scanning electron microscopy (SEM) images showed the residues of the fibers after combustion.

Sorption study highlights the importance of using cellulosic flame–retardant fibers in the protective fiber blends.

Thermal behavior of fibers

The effect of heat on textile materials can produce physical and chemical changes. The physical changes occur at the glass transition (T_g), and melting temperature (T_m) in thermoplastic fibers. The chemical changes take place at pyrolysis temperature (T_p) at where thermal degradation occurs. The combustion is a complex process that involves heating, decomposition leading to gasification (fuel generation), ignition and flame propagation.

A self–sustaining flame requires a fuel source and a means of gasifying the fuel, after which it must be mixed with oxygen and heat. When a fiber is subjected to heat, it pyrolyses at T_p and volatile liquids and gases, which are combustible, act as fuels for further combustion. After pyrolysis, if the temperature is equal or greater than combustion temperature T_c, flammable volatile liquids burn in the presence of oxygen to give products such as carbon dioxide and water. When a textile is ignited heat from an external source raises its temperature until it degrades. The rate of this initial rise in temperature depends on: the specific heat of the fiber, its thermal conductivity and also the latent heat of fusion (for melting fibers) and the heat of pyrolysis.

In protective clothing, it is desirable to have a low propensity for ignition from a flaming source or, if the item ignites, a slow fire spread with low heat output would be ideal. In general, thermoplastic fibers such as polyamide or polyester fulfill these requirements because they shrink from the flame. If they burn, they burn with a small and slowly spreading flame and ablate.

For protective clothing, however, there are additional requirements, such as protection against heat by providing an insulation, as well as high dimensional stability of fabrics. Upon heat exposure, they are expected to support the wearer's work; they should not shrink or melt, and if then decompose, from char. These requirements cannot be met by thermoplastic fibers and so resource must be made from aramid fibers, flame–resistant cellulosics or wool. It may also be noted that the aramid fibers with their high limited oxygen index (LOI) and high thermal stability, have not been found suitable for preventing skin burns in molten metal splashes because of their high thermal conductivity. The mode of decomposition and the nature of the decomposition products (solid, liquid and gaseous) depend on the chemical nature of the fiber, and also on the type of applied finishes or coatings. If the decomposition products are flammable, the atmospheric oxygen raises ignition, with or without flame. When the heat evolved is higher than that required for thermal decomposition, it can spread the ignition to the total material destruction.

In addition to the fiber characteristics and fabric finish, several garment characteristics also influence the thermal protection. For a given fabric thickness, the lower the density, the greater is the thermal resistance. This applies on char–forming fibers such as cellulosics and wool. Hence, thicker fabric made from cellulosics or wool or other non–melting fibers give good thermal protection, whereas the thicker thermoplastic fibers–fabric produce burns. Thermal properties of some fibers are given in Table 1 [1].

Concerning the environmental point of view, Horrocks et al. developed an analytical model for understanding the environmental consequences of using flame–retardant textiles. An environmental rank value is given at each stage in the manufacturing process and product life of each flame–retardant fibers and fabrics. The results show that each of the eleven generic fibers analyzed showed an environmental index value within the range of 32–51 % where 100 denotes the worst environmental position possible [3].

Table 1. Thermal and flame–retardant properties of some fibres [1].

Fibre	T_g [°C] Glass transition	T_m [°C] Melt	T_p [°C] Pyrolysis	T_c [°C] Combustion	LOI [%]
Viscose (CV)	-	-	350	420	18.9
Cotton (CO)	-	-	350	350	18.4
Wool (WO)	-	-	245	600	25
Polyester (PES)	80-90	255	420 –477	480	20–21.5
Acrylic (PAN)	100	>320	290	>250	18.2
Modacrylic (MAC)	<80	>240	273	690	29–30
Meta–aramid (AR)	275	375	310	500	28.5–30
Para–aramid (AR)	340	560	590	>550	29

Materials for flame protection

Flame-resistant Cellulosics

Inherently flame–resistant viscose fibers are produced by incorporating FR additives (fillers) in the spinning dope before extrusion. For example: phosphorous additives, polysilicic acid or polysilicic acid and aluminum [1].

Lenzing AG currently produces Lenzing FR® which contains phosphorus / sulfur–containing additives [4].

Rüf *et* al. patented a new procedure for producing TENCEL® fibers with reduced flammability. The invention relates to a cellulosic molded body containing a cellulose / clay nanocomposite. The clay component of said nanocomposite comprises a material selected from the group consisting of unmodified hectorite clays and hydrophilically modified hectorite clays [5].
There are also viscose fibers with incorporated polysilicic acid available on the market [1].

Flame-retardant Polyester

There are three methods of rendering synthetic fibers flame retardant: use of FR co-monomers during co–polymerization, introduction of an FR additive during extrusion and application of flame retardant finishes or coating. Additives and co–monomers are halogen- or phosphorus–based [1].

Flame-retardant Acrylic

Like other synthetic fibers, acrylic fibers shrink when heated, which can decrease the possibility of accidental ignition. However, once ignited they burn vigorously accompanied by black smoke. Halogen–based and particularly bromine derivatives or halogen– or phosphorus–containing co–monomers are the most effective flame retardants used in acrylic fibers. A number of spinning dope additives are also known to render acrylic fibers flame retardant, for example esters or antimony, tin and their oxides, SiO_2, halogenated paraffins, halogenated aromatic compounds and phosphorus compounds [1].

Aramids

Aromatic polyamides char above 400 °C and can be exposed to temperatures up to 700 °C. Meta–aramid fibers have been developed for protective clothing for fighter pilots, tank crews and astronauts.

The meta–aramid nonwovens are also used for hot gas filtration and thermal insulation. Para–aramid fibers are used for ballistic and flame protection. Generally, meta–aramides are used in heat protective clothing. However, para–aramid fibers are added to improve the mechanical stability [1].
Meta–aramid fibers are blended with Lenzing FR® and FR–treated wool.

Polyimide
Another aromatic copolyamide fiber is polyimide (brand name P84®; produced by Evonik Industries). The fiber does not melt but becomes carbonized at 500 °C with LOI value 36–38 %. The application of high–performance P84® fibers include protective clothing, as a sealing or packing material, for hot gas filtration and in aviation and space including aircraft seats [1].

Phenolics
Melamine polymer is obtained by condensation reaction between melamine and formaldehyde. The cross–linked polymer is then spun to melamine fibers. They can be used in continuous service at 200 °C. Above 370 °C, thermal degradation result in char formation rather then molten drip [1].

Modacrylic
FR modacrylic fiber is a copolymer of acrylonitrile, vinyl–chloride or vinyliden–chloride in ratio of 60:40 wt% along with a sulphonated vinyl monomer [1].

Aim of our work
DSC and TGA are important means to study thermal properties of textile materials, fabrics and fibers. However, DSC spectra provide changes of temperature of the material in pyrolysis and the changes of heat release, but no other thermal properties. TGA can show weight losses of fibers and fabrics under different temperature, but not the concrete pyrolysis processes and products. In this study, DSC and TGA were employed to study the energy and mass changes of various FR fibers during temperature increase. The use of these FR fibers in clothing requires sufficient physiological comfort. Therefore, FR fibers have to provide good sorption properties. Additionally to the thermal study, moisture sorption isotherms and WRV (water retention value) measurements were done on FR samples to have a notion about the physiological behavior of FR fibers in use. By SEM, the visualization of fiber residue after burning was conducted.

Experimental

Materials

In this work, thermal behavior of Lenzing FR® fibers was compared with flame–retardant polymers. The characteristics of used samples are given in Table 2.

Table 2. Fibres used for thermal and sorption study.

Fibre Type	Characteristics Titer [dtex] / Length [mm]
Lenzing FR®	2.2 / 51
Lenzing Modal®	1.3 / 38
TENCEL®	1.3 / 38
Meta–aramid	1.7 / 50
Para–aramid	Fabric
Modacrylic	2.8 / 38
Polyimide	2.2 / 53
Melamine	2.2 / 90
Flame–retardant polyester	7.0 / 60

Methods

Thermal analysis
Thermogravimetric Analysis (TGA)
Approximately 20 mg of compressed fibers rolled in a small ball were placed in

the sample pan. The temperature programme was set from 23 °C until 600 °C with a heating rate 10 $Kmin^{-1}$. All measurements were done under air atmosphere to get more realistic results since oxygen is needed to burn the fibers. Before measurements all fibers were carded to ensure maximum homogeneity of the fibers and better reproducibility of the results. A TA instruments TGA 2050 was used.

Differential Scanning Calorimetry (DSC)
10–12 mg of fibers were compressed and placed in the sample pan. Four holes were made in the sample lid to allow the off–gases to escape. Heating rate was set at 10 $Kmin^{-1}$. For these experiments, standard pan and standard lids were used (pan 900786.901; lid 900779.901). Preparation of samples for DSC is more sensitive than for TGA and more attention had to be paid to the sample preparation. Two parallel measurements were done and the average value was calculated. An untreated sample was also measured in parallel in order to investigate the effect of the incorporated polymers on the temperature stability.

Sorption study
Dynamic Sorption Analysis
Moisture sorption measurements were done on dynamic sorption analyzer (SPS 11 Analyser, Projekt–Messtechnik, Ulm, Germany). The measurements of the fiber samples by dynamic sorption analyzer were described in detail by Okubayashi et al. [6]. In brief, the atmosphere in the analyzer was conditioned at 25 °C and 0 % relative humidity (RH) until equilibrium was achieved. Then, the moisture cycle was started increasing the RH in 10 % RH steps (interval method). The maximal achieved RH was 90 % for measurements at 25 °C.

Water Retention Value
The WRV value denotes the amount of water held inside the fiber after wetting and centrifuging. The measurements were performed following a Lenzing protocol *TIIL–PRÜFANWEISUNG 092/00*. The fiber sample (0.35 g) was weighed in the centrifuge glass and wetted for 10 minutes in deionized water (15 mL). After that, the sample was centrifuged for 15 minutes at 3000 rpm and weighed immediately (m_w). Then the samples were dried for 24 h at 105 °C and weighed again (m_d). The WRV was calculated according to Equation (1). The value expresses the water amount held in the pores inside the fibers.

$$WRV[\%] = \frac{m_w - m_d}{m_d} \cdot 100$$

(Eq. 1)

Visualization of burned fibers
Lenzing FR®, modacrylic, FR polyester and meta–aramid fibers were burned and viewed under SEM. The samples were Au–coated for 60 s. A Hitachi S–400 SEM was used with a relatively low accelerating voltage of 5 kV to prevent beam damage of the samples.

Results and discussion

Thermal analysis
Mass change by TGA
TGA is a basic method for characterization of flame–retardant materials under high–temperature environments. By the first derivation of the mass change curve it is possible to determine the temperature at which the degradation rate is the highest (the peak of the first derivation). In this work this temperature is defined as degradation point [7].
The TGA plots of examinated fibers are shown in Figure 1, Figure 2 and Figure 3.
Plots of standard and modified cellulosics are summarized in Figure 1. There are no differences in degradation point between TENCEL® and Lenzing Modal® (305 °C). At 450 °C the whole cellulose is burned. Very good results in heat protection show Lenzing FR® fibers. The thermal decomposition of Lenzing FR® fibers occurs in two steps: the first point is at 250 °C (most of the FR–agent reacts) and the second degradation point is 458 °C. At

the temperature 250 °C to 700 °C, the material degrades slowly with a residue of 8 % (w/w) at 700 °C.

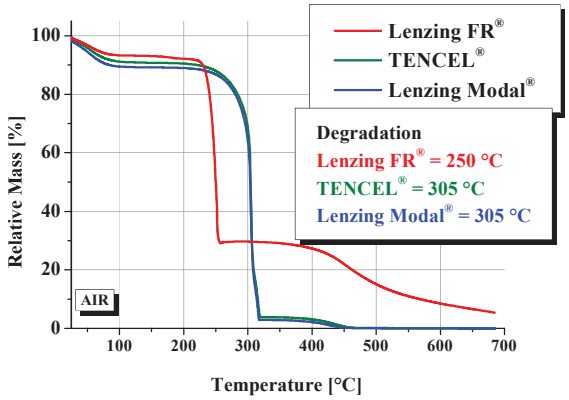

Figure 1. TGA graph of cellulosics.

Phosphorous containing FR agents incorporated in Lenzing FR® fibers work according to following principle: during burning, a protective layer is formed on the surface of fabric by the production of polyphosphoric acid and carbonization, e.g. by release of water. These P–containing FR agents have to decompose before the cellulose decomposes. If the decomposition of cellulose occurs at 305 °C (derived from TGA curves), then the P–agents have to decompose below this temperature to form a protective layer [8].

In Figure 2 the traces of synthetic polymers show significantly higher degradation points than measured for cellulosics. The role of high–performance polymers is not to react before the basic material (like in the case of cellulose), then to postpone the melting point to higher temperatures. The heat energy is spent on melting of polymer or on radical reaction like in FR polyester. The tested samples degrade at two major points: 431 °C and 517 °C which indicate that various modifications are present in the polymer. Para–aramid degrades at 521 °C.

Meta–aramid, due to the meta–position of aromatic rings is less stable then para–aramid. Meta–aramid degrades at 476 °C. The physical action of the meta–aramid fiber when exposed to a heat source is that the fiber itself absorbs heat energy during the carbonization process. The fiber swells and thickens in size and seals openings in the garment fabric helping to eliminate air movement and heat transfer to the interior skin area. As both the fiber and the fabric thicken together this increases the insulating barrier and therefore reduces heat transfer to the wearer.

Polyimide (brand name P84®) is more stable then meta–aramid and FR polyester. It degrades at 510 °C.

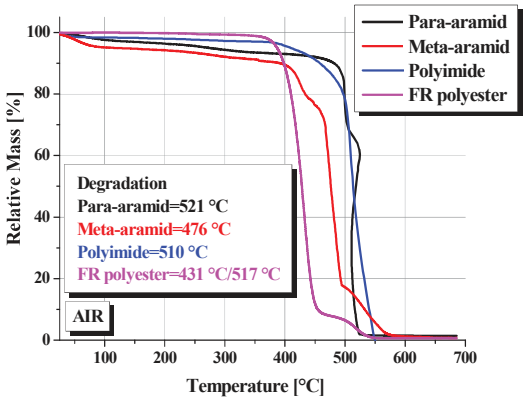

Figure 2. TGA plots of synthetic FR fibers.

TGA plots of other high–performance synthetic fibers melamine and modacrylic are shown in Figure 3. Both melamine and modacrylic fibers degrade in two major steps. Modacrylic is less stable than melamine. Modacrylic degrades at 236 °C (first point) and 503 °C (second point). The two–step degradation of this polymer is explained by the formation of acrylic and modacrylic (halogen containing) components in a ratio approx. 60:40 wt%. Halogens contained in modacrylic work on the principle of radical reaction. The acrylonitrile component works on the principle of char formation. Melamine also degrades in two steps: 363 °C and 617 °C. The thermal degradation in melamine results in char formation rather than molten drip.

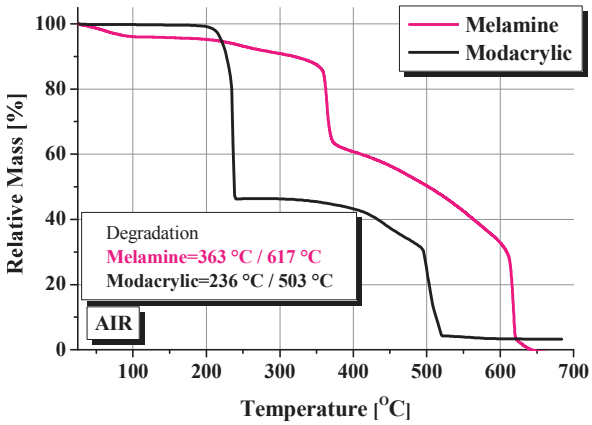

Figure 3. TGA plots of melamine and modacrylic fibers.

Energy changes by DSC

The heat released or absorbed during the thermal conversion is measured by DSC.

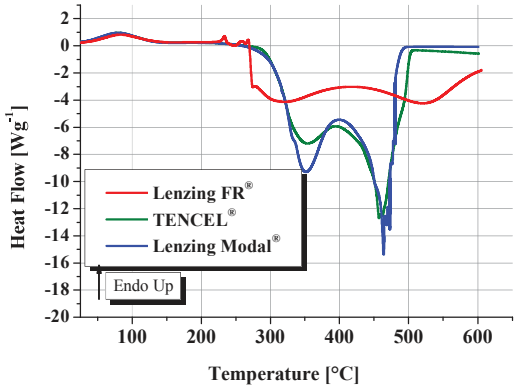

Figure 4. DSC Plots of cellulosics.

In Figure 4, DSC traces of cellulosics are shown. At the beginning of the measurement, there is a small endothermic peak due to the water evaporation.

Both standard and Lenzing FR® show exothermic peaks while those for Lenzing FR® are significantly smaller and narrower due to the phosphorous/sulfur based agents.

DSC plots of high–temperature polymers are shown in Figure 5. Exothermic peaks are not measured at these samples, which indicate that the exothermic reaction which started at 350 °C is still ongoing at 600 °C.

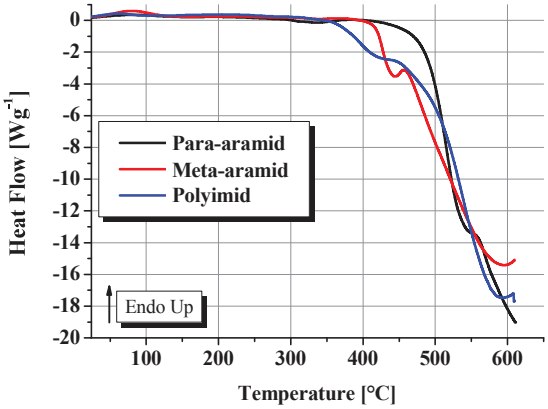

Figure 5. DSC Plots of synthetic FR fibers.

The DSC traces of melamine and modacrylic show first smaller peaks (where char is formed) and the reaction is finished (Figure 6). The second part of the thermal degradation is melting. Like in other high–performance fibers, the melting of melamine occurs at the beginning of the reaction.

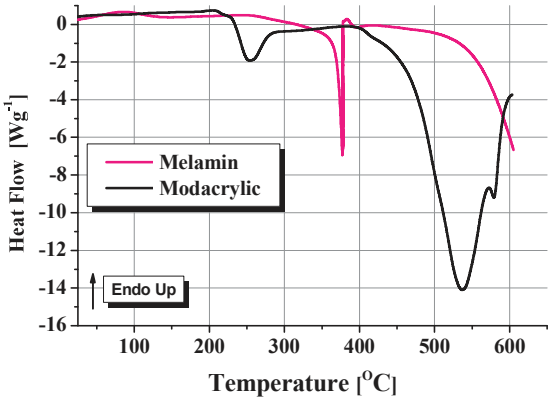

Figure 6. DSC plots of melamine and modacrylic fibers.

If we compare TGA and DSC data, the correlation of the degradation points of the temperatures show exact fitting. The combination of these two analytical methods provides a very useful tool in fiber characterization and product development.

Sorption study

Water vapor sorption

Dynamic sorption analysis is a very precise method for material characterization. It covers the whole range

of relative humidities, where the 50–70 % RH range is relevant for physiological comfort. So the comparison of the materials in this paper focuses on this humidity range. All isotherms show sigmoid–shaped curves, which are typical for hygroscopic materials. In Figure 7, TENCEL® and Lenzing Modal® show the highest sorption (9 – 13 %) where the sorption capacity of Lenzing FR® is slightly lower due to the incorporated additives (7 – 11%). The isotherms of synthetic fibers are rather linear (Figure 8). In the humidity range 50 – 70 %, meta–aramid and melamine absorb 5 – 6% H_2O. Para–aramid and polyimide absorb 2 – 3 % and the lowest sorption is measured for modacrylic – only 0.5 to 1 %.

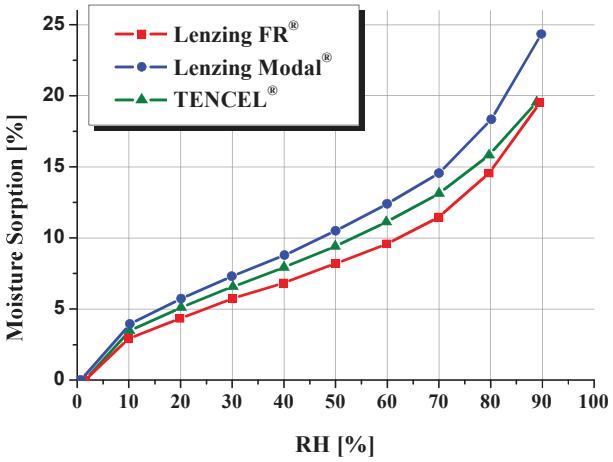

Figure 7. Sorption isotherms of cellulosics.

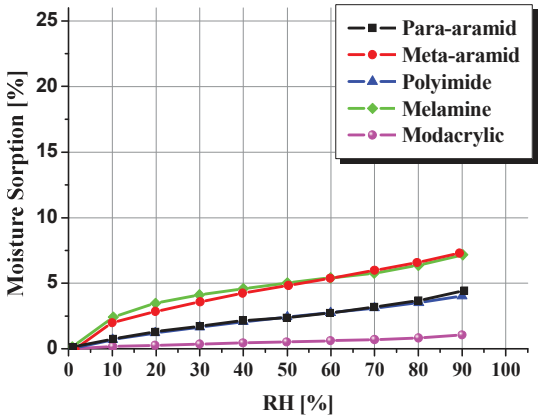

Figure 8. Sorption isotherms of synthetic FR fibres.

Water retention values (WRV)

Parallel to the vapor sorption, sorption of liquid water is measured for textile materials which refers to the porosity of the materials (Table 3 and Table 4). As TENCEL® is more porous than Lenzing Modal®, the WRV is higher. The values decrease slightly with incorporation of FR particles. Like in vapor sorption, WRV values for synthetics are significantly lower. The sorption is in this case higher for melamine and meta–aramid fibers.

Table 3. WRV of standard and modified cellulosics.

Fiber	WRV [%]
Lenzing FR®	**48.6** ± 0.16
TENCEL®	**67.1** ± 0.51
Lenzing Modal®	**57.6** ± 0.95

Table 4. WRV of synthetic FR fibers.

Fiber	WRV [%]
Para–aramid	**5.9** ± 0.19
Meta–aramid	**12.1** ± 0.80
Polyimide	**5.6** ± 0.26
Melamine	**11.8** ± 0.23
Modacrylic	**7.3** ± 0.17

From this results it can be concluded that the application of hygroscopic FR fibers in protective clothing is crucial to provide good wear comfort of protective textiles.

Visualization of burned fibers

SEM images of burned fibers support the theory about the decomposition mechanism of various FR fibers. In Figure 9 images of five mainly used protective fibers are shown. Lenzing FR® keeps shape after burning. A carbon–layer is formed on the surface and prevents the fibers from further burning. Modacrylic fibers shrink in the contact with flame and tear afterwards. FR polyester melts during heat exposure, which is not an ideal option since molten fibers can stick to the skin and skin burns are possible. Meta–aramid fibers expand during the thermal treatment, (volume increase) and form a protective barrier which prevents from further burning of the fiber.

Lenzing FR®

before burning

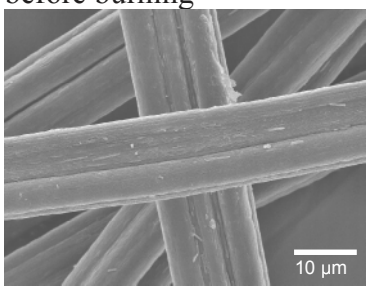

after burning

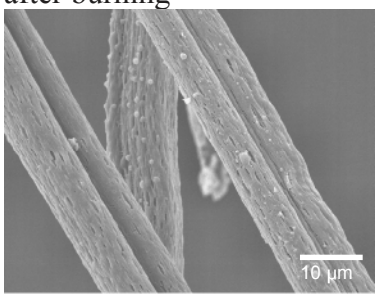

Modacrylic

before burning

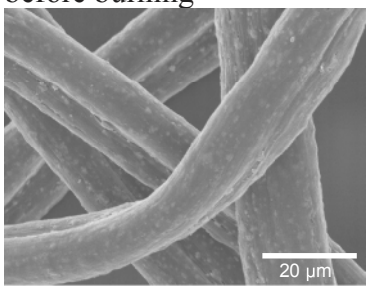

after burning

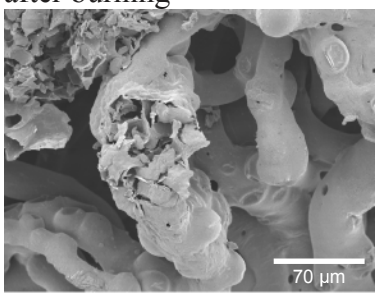

FR polyester

before burning

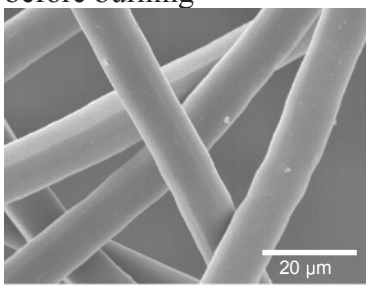

after burning

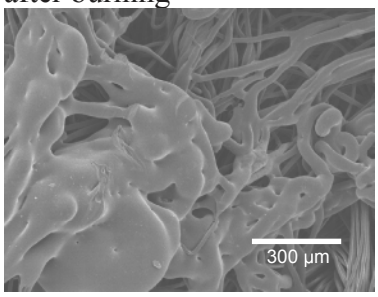

Meta–aramid

before burning

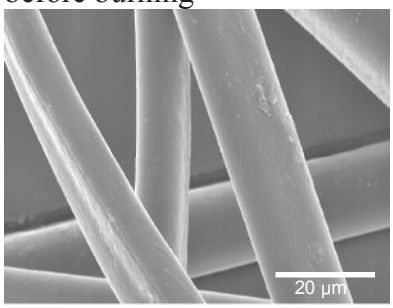

after burning

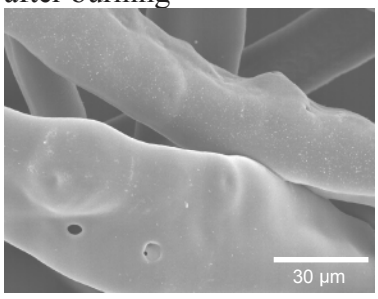

Figure 9. SEM images of FR fibers before and after burning.

Conclusions and Outlook

In this work, Lenzing FR® fibers were characterized by different analytical methods and their behavior in practical use has been investigated in comparison to other protective fibers.

Thermal methods – DSC and TGA are precise tools for observing thermal degradation – mass / energy changes with increasing temperature. The results of both thermal methods showed good correlation. Improved physiological performance of protective clothing is important and the standards for protective clothing require materials with improved comfort properties. Therefore, new developments in this segment are crucial to be at the state of the art with the market trends.

The disadvantage of using synthetic fibers is associated with poor wear comfort. The emphasis is placed on the use of Lenzing FR® in workwear as best solution between functionality and comfort. This statement is supported by the sorption isotherms showing high absorbency for cellulosics and low absorbency for synthetics.

In the field of cellulosic materials, newest developments have been focused on spun–dyed Lenzing FR®, especially in high–visibility colors for protective wear.

Acknowledgements

The authors gratefully acknowledge to Ms. Sandra Schlader (Kompetenzzentrum Holz GmbH) for SEM images and to Ms. Agnes Uwaleke (Lenzing AG) for WRV data.

References

[1] Bajaj P.: Heat and Flame Protection, in Handbook of Technical Textiles (Ed. Horrocks R. A. & Anand, S.C.), Woodhead Publishing Limited (2000), ISBN 1 85573 385 4.

[2] Hull T. R. & Kandola B. K. (Ed.): Fire Retardancy of Polymers – New Strategies & Mechanisms, © Royal Society of Chemistry 2009, ISBN 978–0–85404–149–7.

[3] Horrocks A. R., Hall M. E. & Roberts D: Environmental consequences of using flame–retardant textiles – a simple life cycle analytical model, Fire and Materials 21 (1997), pp. 229–234.

[4] http://www.lenzing.com/fasern/lenzing-fr.html (19.06.2011).

[5] Rüf H., Firgo H. & Kroner G.: Cellulosic Molded Body, Method for Manufacturing it and Use Thereof, US 2008/0233821 A1, 2008.

[6] Okubayashi S., Griesser U.J. & Bechtold T.: A kinetic study of moisture sorption and desorption on lyocell fibres, Carbohydrate Polymers 58 (2004), pp. 293–299.

[7] Aljaz L., Varga K. & Koch T.: DSC & TGA Analysis of Lenzing FR® Fibres, 41th International Symposium on Novelties in Textiles, 27–29 May 2010, Ljubljana, Slovenia.

[8] Einsele U.: Über Wirkungsweise und synergistische Effekte bei Flammschutzmittel für Chemiefasern, Lenzinger Berichte 40 (1976), pp. 102–116.

Lenzinger Berichte 89 (2011) 60-71

TENCEL® - NEW CELLULOSE FIBERS FOR CARPETS

Johann Männer*, Denitza Ivanoff, Robert J. Morley and Susanne Jary

Lenzing AG, Werkstr. 2, 4860 Lenzing, Austria

*Phone: (+43) 7672 701-3488; Fax: (+43) 7672 918-3488; Email: j.maenner@lenzing.com

Presented during the 47th Man-Made Fibers Congress, Dornbirn, 2008

Textile coverings are still the most common material for floorings. In living areas carpets used are mainly either cut or loop pile. Historically, natural fibers like wool, cotton or jute were dominant in this field. Following industrialization at the beginning of the last century viscose fibers were also introduced. The development of synthetic fibers in the 1960s caused a decrease of natural fibers and viscose. Polyamide and polypropylene, then, became the most popular materials in carpets. With the commercialization of the Lyocell process in the 1990s, a new generation of cellulose fibers was developed. Lyocell fibers branded as TENCEL® have higher tenacity, modulus and bending strength compared to viscose.

For tufted carpets fibers are typically high-dtex long staple and are processed into semi worsted or woolen yarns. TENCEL® fibers based on high dtex lyocell have now been developed. These can be processed into carpet yarns either alone or in combination with other fibers. The prime function of synthetics is utility, to some extent at the expense of comfort, whereas natural materials accentuate the comfort attributes. TENCEL® in particular exhibits excellent moisture management properties due to its internal nanofibril structure. This brings positive effects for the room climate as well as beneficial hygiene and low static properties. TENCEL® is a wood based cellulose fiber produced by a sustainable, ecological route and is bio-degradable.

Keywords: *Cellulose, carpets, lyocell, NMMO, TENCEL®*

Introduction

Most carpets used in living areas are either velour or loop pile constructions prepared as wall to wall carpets or area rugs. The most important manufacturing route for carpets makes use of tufting technology but woven constructions are also available. Coarse long staple fibers of polyamide and polypropylene are the most common fibers. Wool is also popular in living areas, especially in Western Europe. TENCEL® carpet fibers have been developed primarily in 15 dtex with cut lengths of up to 150 mm suitable for semi worsted and woolen yarn spinning. To achieve optimum resilience and abrasion resistance a blend with other fibers is preferred. The initial target sector for TENCEL® is in domestic living areas such as sleeping and children rooms. In apparel uses the excellent physiological benefits of TENCEL® and TENCEL® blends have been clearly demonstrated and widely used. These same features are equally of value in carpets such as to enhance room environments in respect of climate for humidity control, hygiene, static charge and reduced allergy. A feasibility work exhibits first experience in carpet

manufacturing, the potential and benefits of TENCEL® in this area.

Carpet market survey

A market study [1] exhibits an overview of floorings in terms of fiber consumption in the USA and Western Europe and the carpet consumption and manufacturing technologies in Western Europe.

Consumption of fibers in USA and Western Europe

The combined consumption of fibers for floorings in Europe and USA is about 1,950 to per year. Staple fibers are represented in about 30 % of soft floorings. Synthetic staple fibers are more dominant. Particularly in the USA and in Europe natural fibers (wool and cotton combined) are as common as either polyamide or polypropylene.

Table 1. Consumption of fibers in floorings in USA and Western Europe [kto/a] [1].

	Staple fibers							Filaments		
	PA	PP	Wo	Co	PES	PAN	Total	PA	PP	Total
EU	65	79	69	9	6	7	235	169	147	316
USA	259	34	14		95		402	586	423	1,009
							637			1,325
							1,962			

Distribution of floorings in Western Europe

Textile floor coverings, also called soft flooring, are the most common material in contrast to hard floorings such as ceramics or laminates. However, in living areas there are sometimes combinations of hard floor with soft area rugs used as design element. Tufting is the main method for manufacturing both, cut and loop pile carpets.

The volume of tufted products in Europe is about 645 mio m². Industry is mainly located in Belgium, also in the Netherlands, Germany and Great Britain. Great Britain and Germany are the biggest carpet users in Europe.

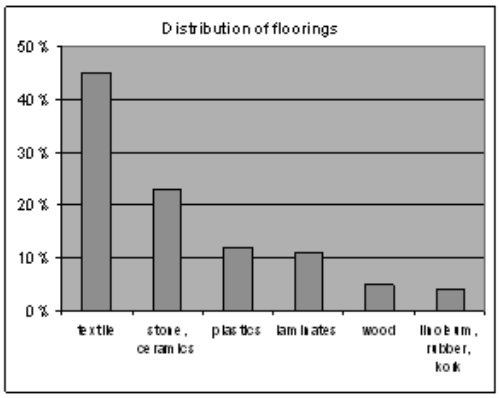

Figure 1. Distribution of floorings Western Eu.

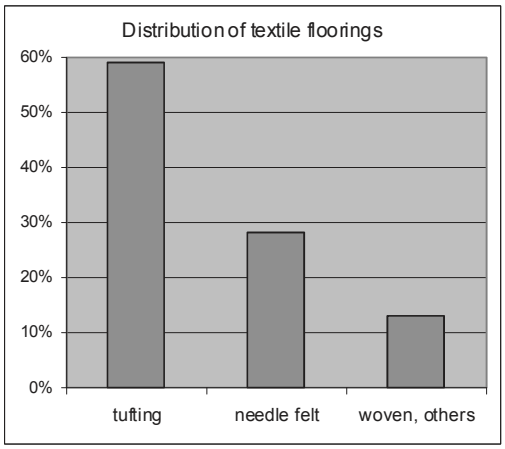

Figure 2. Distribution of textile floorings W. Eu.

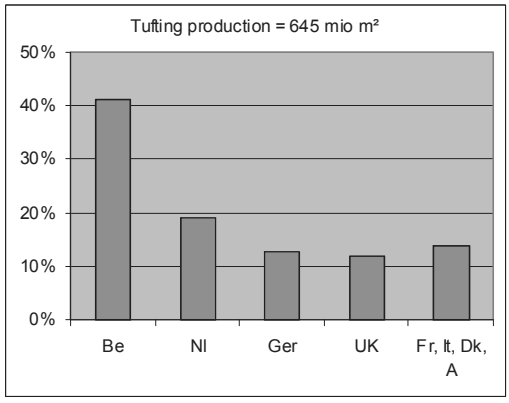

Figure 3. Tufting production, Western Europe**.**

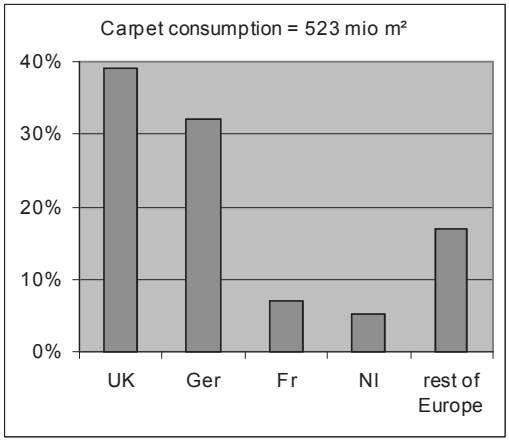

Figure 4. Carpet consumption, Western Europe.

Man made cellulose fibers in carpets

It was following the industrialization at the beginning of the last century that viscose fibers were introduced into carpets. The development of synthetic fibers in the 1960`s caused the use of viscose and natural fibers to decrease. Synthetic fibers became cheaper and the mechanical properties were greater compared to standard cellulose fibers. It also became more fashionable to use these new synthetic fibers.

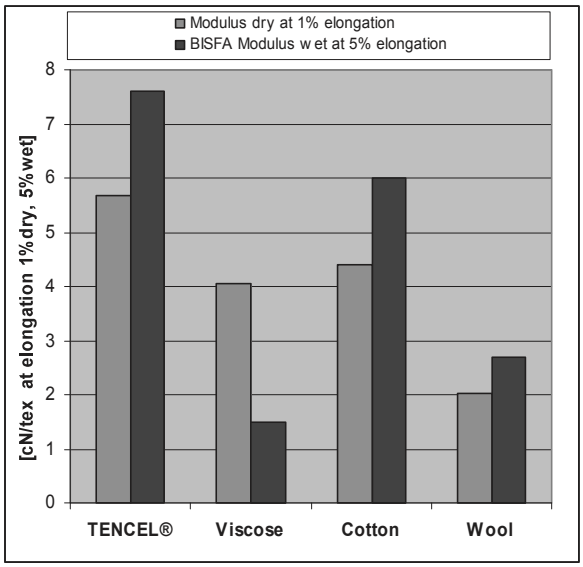

Figure 5. Fiber moduli dry and wet.

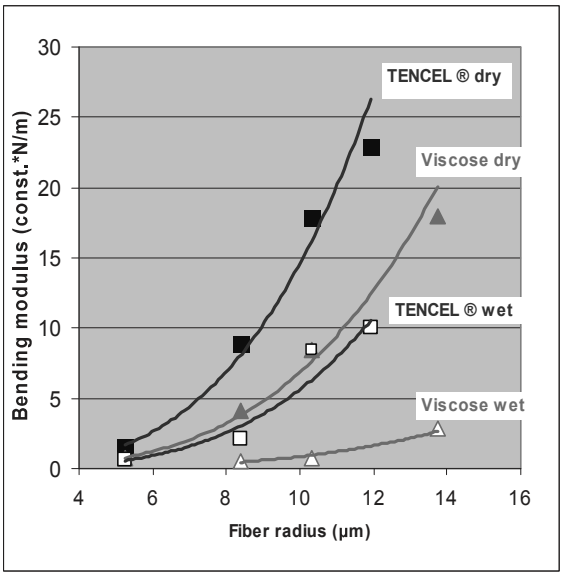

Figure 6. Fiber stiffness.

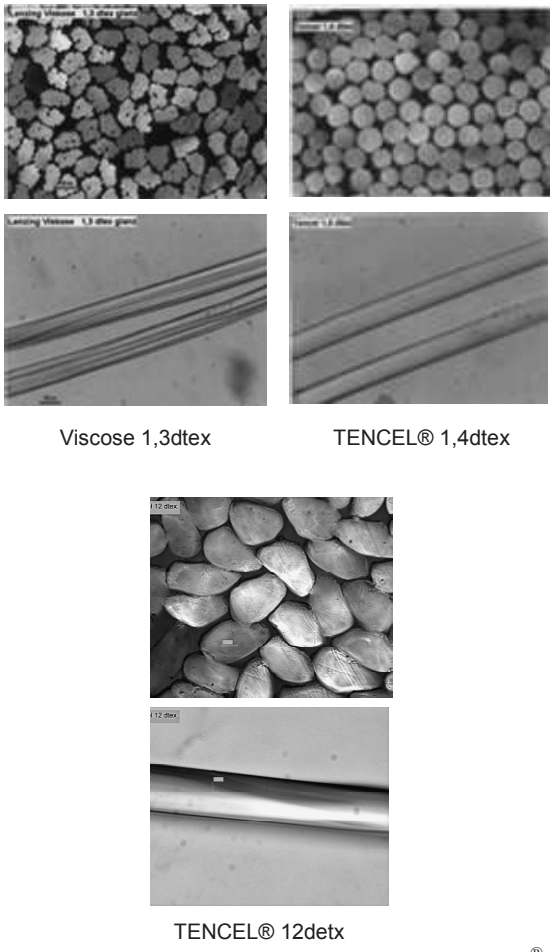

Figure 7. Cross section of viscose and TENCEL® fibers.

Nowadays, small amounts of viscose fibers are used in carpets in the dtex range 1.3 – 3 dtex as 100 % viscose and also in blends. Coarser viscose long staple up to 17dtex fiber was developed in the 1970s[s] by LENZING, though never commercialized. In the 1990s the lyocell process was developed and a new generation of cellulose fibers became available. Using this technology, coarse long staple fibers up to 15 dtex and 150 mm cut length have been developed which can be spun on either woolen or semi worsted yarn equipment. Compared with other cellulose fibers, TENCEL® has an excellent modulus which is responsible for higher fiber stiffness especially compared to viscose in wet state [2]. This means that TENCEL® fibers are more appropriate for carpets to provide the required compressibility and resilience.

The diameter of fibers correlates with the

density of the raw material:

$$D = 2 * \sqrt{V/\pi * 10000}\,;$$

$$V = titer\left[\frac{g}{10000m}\right] / \rho\left[\frac{g}{cm^3}\right]$$

For cellulose a density of 1.5 g/cm^3 is calculated. TENCEL® fibers with a titer of 1.3 dtex have a round shape and a diameter of 11 µm. 12 dtex gives a diameter of 32 µm and an irregular profile. Polypropylene has less density of 0.9 g/cm³. A titer of 12 dtex gives a diameter of 41 µm.

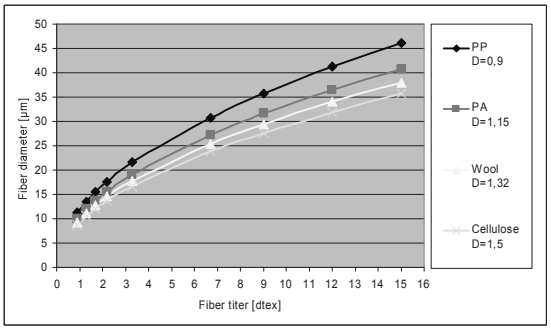

Figure 8. Correlation of fiber titer and diameter.

Carpet construction and properties

A feasibility study has been done in order to get experience in processing coarse TENCEL® fibers during dyeing, yarn spinning and carpet preparation, in cooperation with carpet experts, ASOTA and A&P.

Fiber dyeing

Different dyeing procedures are used for carpet processing. Spun dyeing is appropriate for synthetic fibers. Cellulose, wool, polyamide and acrylic fibers can be either fiber dyed or yarn dyed. Dyeing or printing of ready made carpets would also be common procedures. Most of the fibers used in carpet industry are fiber dyed. TENCEL® is wood-based and can be dyed by any of the well known procedures for dyeing cellulose, although reactive dying usually is preferred with regard to environmental aspects, compared to substantive or direct dying. TENCEL® fibers have a high inherent whiteness. Therefore, bleaching is not necessary. Compared to cotton and wool TENCEL® gives more brilliant colors in a wider range. In addition, TENCEL® has a high dyeing affinity resulting in less dyestuff consumption.

Yarn spinning

Carpet yarn counts are typically in the range of Nm 3–10 and mainly spun via the semi worsted or woolen spinning routes. For the semi worsted route fiber staple length of 130 – 150 mm are necessary. For the woolen route 100 mm cut length is suitable. The semi worsted procedure is appropriate for synthetic fibers. The woolen route is preferred for wool and wool blends because of the necessary control of air humidity during production. For TENCEL® and other cellulosic fibers climate control during spinning is desirable. If the environment is to dry, cellulose fibers become brittle and spinning behavior is impaired. However, in blend with synthetics, depending on the ratio, TENCEL® fibers can be spun without moisture control. For initial prototyping, a twisted yarn of Nm 4.5/2 in blend with wool and polypropylene low melting point fibers was used. Woolen spinning leads to a bulkier yarn than the semi worsted route.

Table 2. Examples of fiber blend and yarn construction.

Woolen yarn

Fiber blend	TENCEL® 12/100 / wool / PE 17/90 low melt 50 / 45 / 5
	TENCEL® 12/100 / PP 17/90 / PE 17/90 low melt 65 / 30 / 5
	TENCEL® 12/100 / PAN 10/100 / PE 17/90 low melt 65 / 30 / 5
Yarn	Nm 4,5/2 210 Z // 140 S

Semi worsted yarn

Fiber blend	TENCEL® 12/150 / PP 17/150 / PP 17/90 low melt 80 / 13 / 7
	TENCEL® 12/150 / PE 17/90 low melt 93 / 7
	TENCEL® 12/150 / PA 15/150 80/20 60/40
Yarn	Nm 4.5/2 190 Z // 140 S and Nm 4.5/2 190 Z // 225S

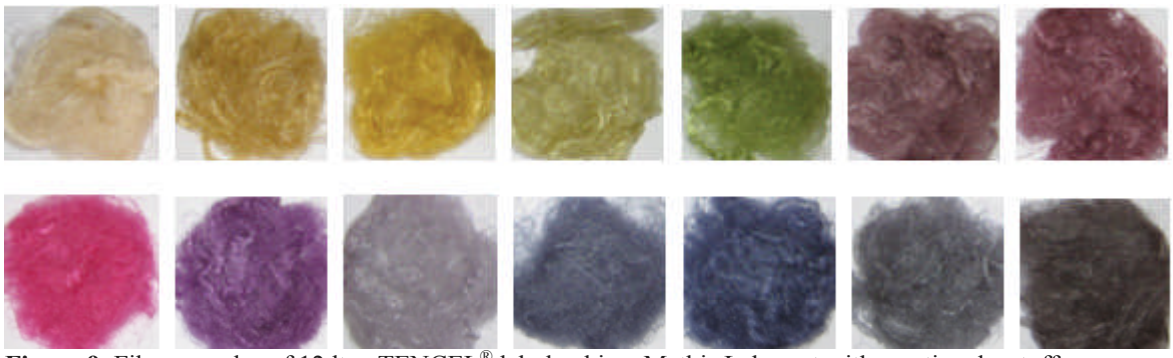

Figure 9. Fiber samples of 12dtex TENCEL® lab dyed in a Mathis Labomat with reactive dyestuff.

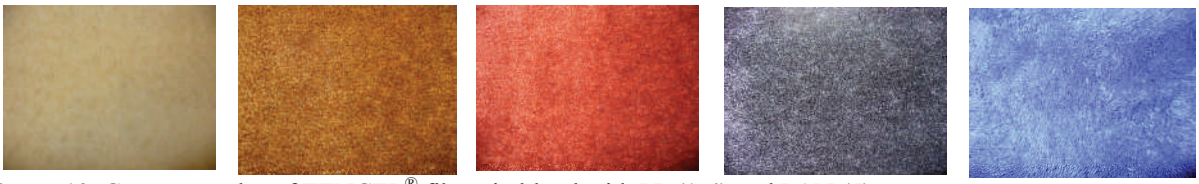

Figure 10. Carpet samples of TENCEL® fibers in blend with PP (1-4) and PAN (5).

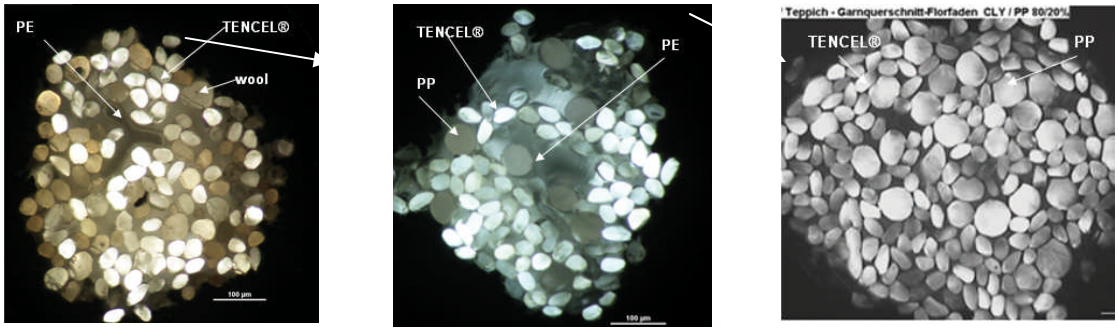

TENCEL®/wool/PE(woolen) *TENCEL®/PP/PE (woolen)* *TENCEL®/PP/PE (semi worsted)*

Figure 11. Cross section of woolen and semi worsted carpet yarns.

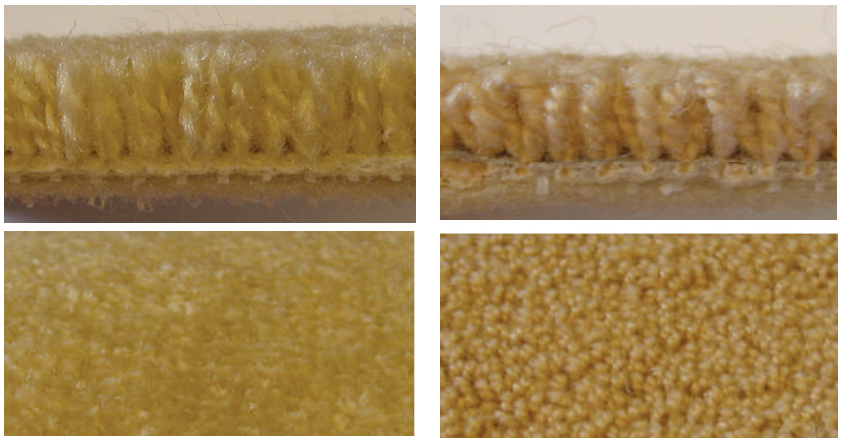

Figure 12. Cross section and surface of cut (left) loop pile (right) carpet samples.

Table 3. Applied carpet constructions [3].

		ASOTA Cut pile	A&P Loop pile
	Area weight [g/m²]	2600 - 2700	2000 - 2100
Pile	Area weight [g/m²]	1500 - 1600	800 - 850
	Height [cm]	10	7
	Gauge	1/10"	1/18"
	stitches per 10cm	37 and 45	41

Carpet properties
First prototypes of selected carpet constructions were tested independently by both, at the Austrian Textile Research Institute and ASOTA. The overall outcome shows that TENCEL® carpets give mechanical properties comparable to those made of wool. The domestic value in use is appropriate for living areas.

Table 4. Mechanical carpet data; TENCEL®/PP blend in comparison to polyamide and wool [4].

	Pile Layer	Pile Height	Lisson Test EN1963 "Tretradversuch"	
	g/m²	mm	Substance loss %	Tretrad index
TENCEL / PP 80:20	1417	10.9	18.6	5.8
PA 100%	1193	10.8	1	6.5
Wool 100%	750	5.4	18.8	4.2

Table 5. Comparison of recovery [5] of TENCEL®/wool and TENCEL®/PP cut and loop pile.

	Recovery [%] ÖNORM S1408	
	TENCEL / wool / PE 50 / 45 / 5	TENCEL / PP / PE 60 / 35 / 5
Cut pile	92	89
Loop pile	80	85

Ecological attributes of TENCEL®

TENCEL® fibers are made from a natural and renewable source: They are made from wood deriving from sustainably managed forests. The production technology was commercialized first in 1992 (Mobile/US) and is characterized by an environmentally friendly closed loop solvent spinning process. This TENCEL® process was also awarded by the European Union with the "European Award for the Environment".
During photosynthesis, the basic botanic principle, carbon dioxide and water are converted into cellulose and oxygen by means of sun light. Lenzing uses the biomass for the production of TENCEL®.

The fibers consist of 100 % cellulose, are to 100 % bio degradable and, therefore, are part of the cycle of Nature.

Physiological attributes of TENCEL® in carpets

Fibers that are spun according to the TENCEL® process have a nanofibril cellulose structure. They consist of countless fine, non swelling, crystalline microfibers that extend throughout the length of the fibers. Swelling occurs in the non-crystalline regions and capillaries between the micro- and nanofibrils. Therefore, TENCEL® fibers can be considered as a hygroscopic nano-multifilament. This feature is responsible for many of the unique characteristics of the fiber. In traditional textile applications this enables superior moisture management and contributes in many different ways towards optimizing comfort in use.

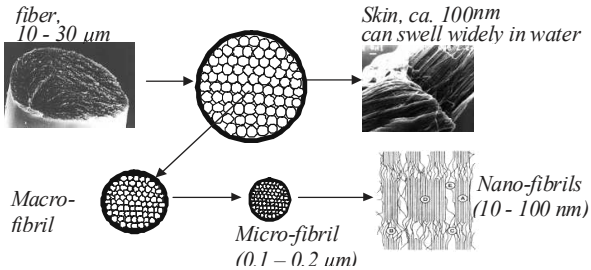

Figure 13. Model of the TENCEL® fiber structure (modified from Schuster *et* al., 2003 [6]).

Moisture distribution for hydrophilic and hydrophobic fibers
In case of hydrophobic fibers such as polyester, the moisture absorbed by the textile is found on the fiber surface between the fibers and/or yarns. In contrast, the nanofibril structure of TENCEL® fibers causes the moisture to be transported very swiftly through the nano capillaries and absorbed inside of the fibers which swell accordingly. Even at high moisture levels, a major proportion of the water is within the fiber.

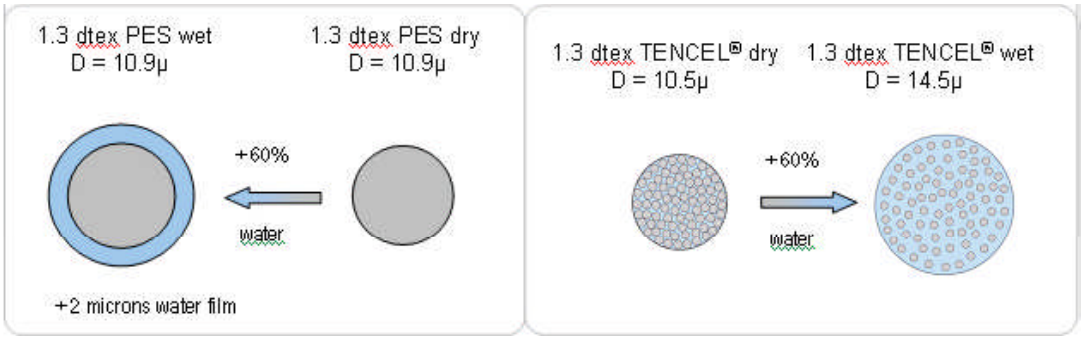

Figure 14. Model of moisture distribution on polyester and TENCEL® fibers [7].

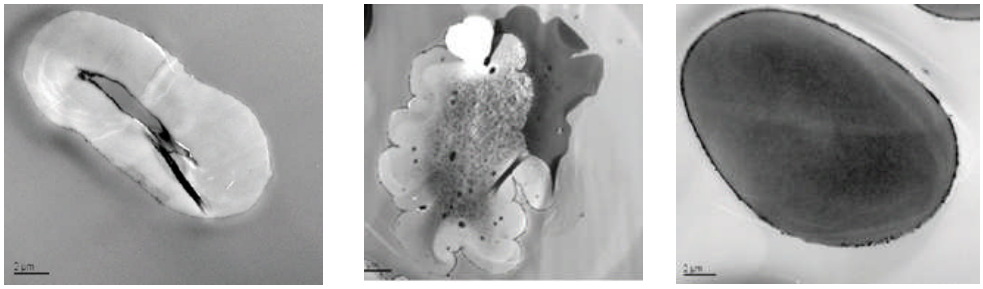

Figure 15. Moisture distribution in cellulose fibers [7].

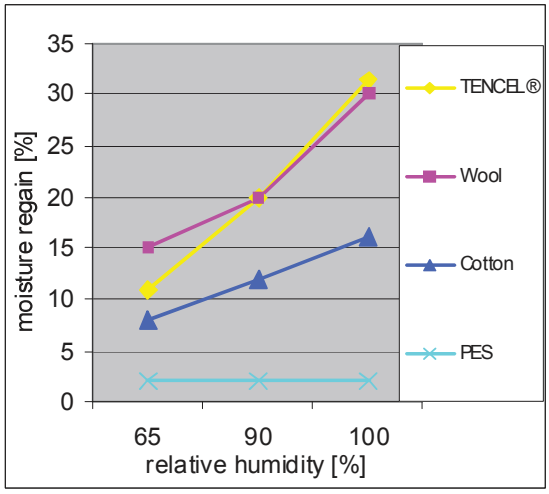

Figure 16. Equilibrium moisture regain of fibers [increasing humidity at room temperature (20 °C)].

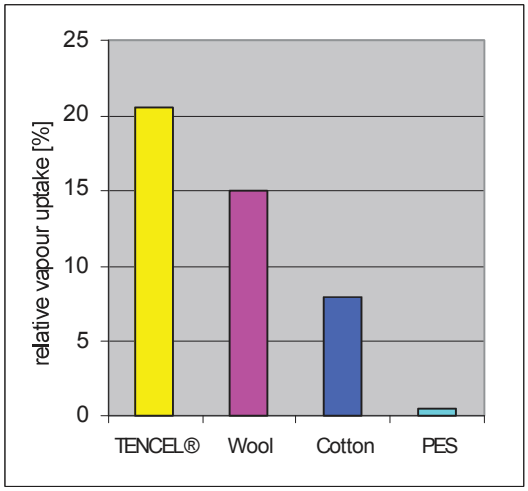

Figure 17. Change in vapor uptake at room temperature (rel. humidity increases from 65 to 100 %) [2].

Table 6. Estimated absolute vapor quantities in a common sleeping room.

Sleeping room 4x5x2,5m / 50m³	**moisture in compartment air [g]**	
Start climate	426	absolut vapour content in 50m³ air at 18°C 55%RH
Climate at dew point	773	saturation at 18°C 100%RH reached after 2 hours, without air convection
Human moisture disposal	1400	2 people, loss of moisture within 8 hours
moisture uptake		
bed textiles	40	4kg synthetics 1% buffer capacity
bed textiles	400	4kg TENCEL® : PES 50:50 10% buffer capacity
carpet (15m² active)	3000	15kg TENCEL® 20% buffer capacity

Water vapor absorbency
Hygroscopic fibers are able to absorb vapor depending on temperature and relative air humidity (%rh). At 90 %rh, TENCEL® absorbs 40 % more moisture than cotton and therefore is in the same range as wool. Non-hygroscopic fibers such as polyester adsorb only negligible amounts of moisture on the surface. At 100 %rh the total moisture content of TENCEL® is as high as that for wool. Even so TENCEL® absorbs more than wool when the air humidity changes from a standard level of 65 %rh and rises to 100 %rh. In this humidity region TENCEL® increases its absorption by 21 % which is almost twice the absorbency increase compared to that for either wool or cotton. This extra absorption by TENCEL® significantly contributes to increased moisture comfort in the room.

Enhanced room climate

For buildings it is well known that hygroscopic, naturally breathable materials like wood or clay are able to absorb water vapor, therefore, having very positive effects on the room climate. The same is significant for other materials that are also present in rooms such as furniture and textiles. Hygroscopic materials can help to keep the air humidity in a more constant range.
Personal comfort depends particularly on the temperature and mainly the relative air humidity. The comfort zone is said to be below 75 % relative humidity. Another aspect is the generation of water condensate. If the relative humidity reaches the dew point, then water will readily condense onto cold surfaces. One of the effects of this in buildings is the growth of moulds and wet spots on walls.
The superior vapor handling of TENCEL® means that carpets made from TENCEL® help maintaining the room climate at an optimized level.

Example of vapor balance in a bedroom
Nowadays, the insulation of a building is crucial in order to save energy. Also windows are airtight leading to reduced air convection and a massive change of the room climate during a sleep night. Two humans in a normal night's sleep will lose approximately 1400 mL moisture through skin and breath. For a 20m² at, say, 18 °C 55 %rh, air is able to take only 350 mL vapor before the dew point is reached. Leaving aside that air humidity is greatly increased with consequent discomfort, there is also the fact that there is over one liter of surplus water that will potentially condense on surfaces close to the sleeper. Hygroscopic materials like TENCEL® can absorb the generated moisture thus keeping the room climate more constant. Surfaces with high fiber content and large surface area such as TENCEL® carpets are the answer:

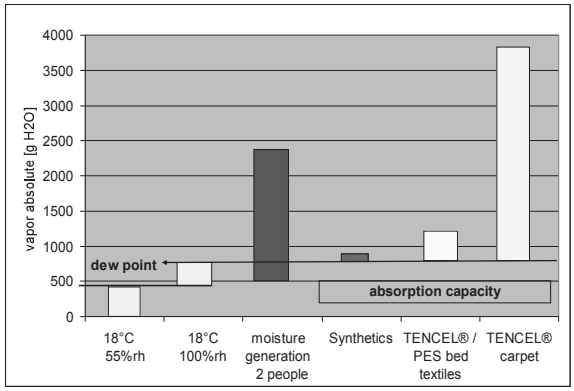

Figure 18. Estimated absolute vapor quantities in a common sleeping room.

Electrostatic charge

Electrostatic effects are of importance in carpets. The surface friction of materials results in electrostatic charge. The amount of charge built-up depends on friction intensity, conductivity, capacity and the ranking of the materials in the so-called "triboelectric series". In practice, the unpleasant effect of electrostatic charge is the spark that spurts via the hand to the door handle, or the hair-raising effect when taking off garments made of synthetic materials. On floorings the same effect happens when people walk on it. Floor coverings in rooms have to be protected against static charging especially

where sensitive electronic devices are used but also for comfort in the home. To avoid static charge in carpets, synthetic materials and wool have to be treated with antistatic additives or alternatively metal wires or carbon fibers are included in the construction.

Electrostatic behavior of textiles

The electrostatic effect of textile materials depends primarily upon the moisture present in the fabric and thus conductivity and/or resistance. The standard conditioning moisture content of TENCEL® fibers is approximately 12 %. Synthetic fibers like polyester are not hygroscopic and have conditioning moisture of less than 1 % and consequently have considerably lower conductivity.

Table 7. Electric contact resistance according to DIN 54345 for TENCEL® and polyester fabrics.

	Contact resistance [R_{DT}] Ω	
	23°C / 25% RH	23°C / 65% RH
TENCEL®	4.5×10^{10}	6.8×10^{7}
Polyester	5×10^{13}	5×10^{13}

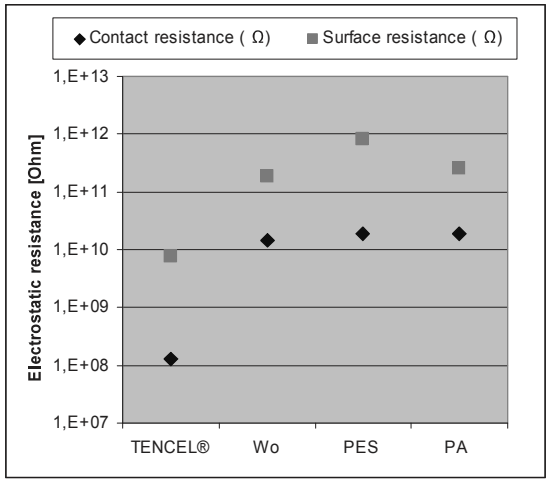

Figure 19. Static resistance of fabrics of different materials.

To evaluate the static behavior of textiles the electrostatic resistance can be determined. In order to the standard procedure, the contact and surface resistance is described at 23 °C 65 %rh. It can be found that textiles give different resistance levels. Synthetics and even wool have approximately 100 times higher resistances compared to TENCEL®. In blends with polyester reduction of fabric resistance can be achieved by at least 10x when only 10 % TENCEL fibers are used.

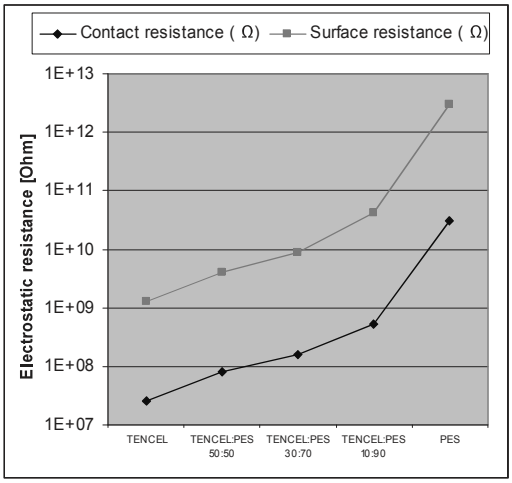

Figure 20. Static resistance of fabrics in different TENCEL PES blends.

Electrostatic charging of the human body by textile friction

The electrostatic potential caused on account of textile friction on skin was measured at the Austrian Textile Research Institute (OETI). For this purpose, different fabric materials of comparable construction were drawn over the shoulder under identical conditions in a standard climate, in order to simulate removal of a garment. The charge generated was measured by means of a hand electrode, which is used in a modified test arrangement to determine the electrostatic behavior of wall-to-wall carpeting according to DIN 66095. For polyester and polypropylene a positive potential of 3,000 Volt was measured. On account of the higher conductivity due to fiber moisture, cellulose fibers show almost no charging. With a charge of more than 1,800 volts, noticeable sparks appear when static discharge occurs to grounded objects.

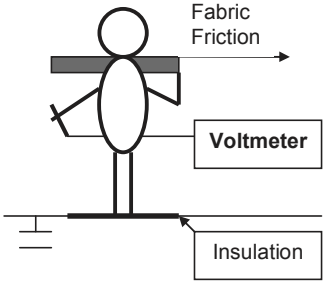

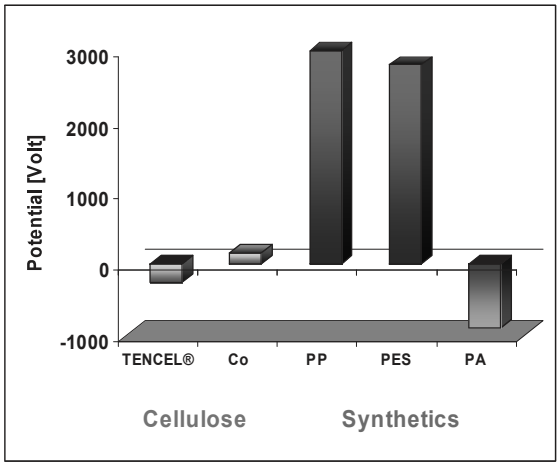

Figure 21. Electrostatic charging of the human body after a friction experiment with textiles.

Electrostatic charging of carpet samples

Carpet samples were measured by a standard walking test according to EN1815. The carpet pile of 80/20 % TENCEL®/PP gave a static charge of -0.7 kV compared to 10 kV for a polyamide. Even woolen carpets, as far as they are not anti statically treated, show a charge of more than 4 kV. To call a carpet anti-static, a charge of lower than 2 kV has to be achieved.

Table 8. Carpet Walking Test of carpets without anti-static treatment EN 1815 23 °C / 25 % RH [4].

Carpet pile	Static charge [kVolt]
TENCEL : PP 80:20	-0,7
PA	10
Wool	> 4

Moth protection without chemistry

As food stuff larva of webbing moth need keratin which is a protein in animal hairs like wool and silk. To protect wool against damage by moths, textile articles have to be treated with special chemicals. Compounds like Permethrin are the most usual additives to protect carpets against moths. Permethrin is a strong neurotoxic substance for humans and can cause allergic reaction even at very small levels.
Cellulose fibers, paper or wood become not affected by moths. Textiles made out of cellulose do not need special treatments, they are naturally moth proof.

Textile hygiene

Textile hygiene refers to the effect of textiles on the environment of the user - on the one hand the effect of the material itself with regard to the allergic potential, on the other hand the influence on skin flora and micro-organisms. A broad range of micro-organisms can be found on the skin, forming the skin flora, being essential for human health. In case of strong perspiration, sweat will transport these organisms into the textiles. Components of the sweat will be decomposed by the micro-organisms. In the course of these reactions substances such as butyric acid are formed, which are perceived as the unpleasant smell of perspiration.

Allergic potential
Due to the manufacturing process, TENCEL® fibers are very clean and free of allergic compounds and certified with the OEkoTex label class I. In comparison to other materials TENCEL® fibers do not need any chemical treatment for moth and static charge protection.

Bacterial growth on textiles
Results of the Challenge test show that bacterial growth on synthetic materials is higher than on TENCEL® by a factor of 100 to 1,000. On cotton, growth is still higher by a factor of 10, as compared to TENCEL® [8].
The considerably higher growth on synthetic fibers may be regarded as the responsible cause for the well-known stronger odor formation. The clearly

reduced growth on TENCEL®, as compared to synthetics, can be explained by the behavior of the fiber towards water. Water on the surface of synthetic fibers is fully accessible to micro-organisms. In TENCEL® materials, the water becomes absorbed almost entirely into the fiber and, therefore, offers only very limited life-sustaining basis for micro-organisms. The higher growth on cotton is though to be due to the coarser surface, to which bacteria can cling more easily, and to the higher content of residual components (cotton wax and harvesting residuals), which serve as an additional nutrient source.

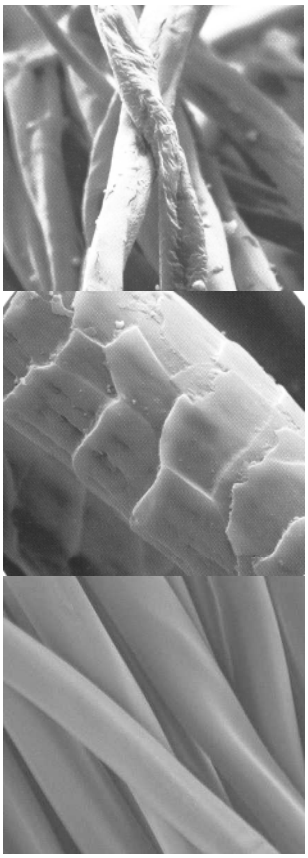

Figure 22. Scanning electron micrographs of cotton, wool and lyocell fibers.

Skin sensory perception

Receptors in the skin for temperature, changes of movement, pressure, itching irritations and pain, communicate the feeling of the skin on contact with textiles. Many people are very sensitive and suffer from "wool intolerance". The harsh surface of wool causes an itching irritation, up to atopic eczema. In case of high friction on the skin, a mechanical-toxic contact dermatitis is possible. For persons with sensitive skin, and especially those who tend to develop pathological allergic reactions such as neurodermatitis, it is important to minimize skin irritation. Under humid conditions, in cases of a major perspiration discharge, the skin has increased sensitivity to irritation. The key factors are the capacity to absorb water, the moisture permeability and the drying speed of the fabrics.
TENCEL® fibers offer an optimum comfort in wear on account of their optimum absorption capacity and their surface, which is smooth in comparison to cotton and wool.

Summary

For carpet manufacturing coarse long staple TENCEL® fibers are suited up to a titer of 15 dtex and cut length up to 150 mm. Woolen and semi worsted yarn spinning is possible also in blend with wool and synthetic fibers. First tufted carpet prototypes in cut and loop pile can be used in domestic living areas with a high comfort factor. The high moisture regain of TENCEL® fibers has positive effects on both, room climate and hygiene. TENCEL® fibers are inherently antiallergic, antistatic and moth proof. The cellulose fiber TENCEL® derives from the natural raw material wood, is produced by a sustainable process and to 100 % biodegradable, thus offering a new range of ecologically friendly carpets.

Acknowledgements

Special thanks to Mr. Struve and A&P, Mr. Linsbauer ASOTA, to all the colleagues in Lenzing, especially Karin Kämpf, Andreas Lassl, Johann Leitner, Werner Richardt and Markus Hager.

References

[1] Kunz, Michael, Diplomarbeit: Marktstudie Lenzing Lyocell – eine neue Faser für den Teppichmarkt (2003).

[2] Feilmair, W., Eichinger, D., Firgo, H., Männer, J., Krüger, P., Funktionalität von Lenzing Lyocell in Heimtextilien, TITK (2002).

[3] Applied carpet construction; ASOTA GmbH, Linz.

[4] ÖTI, Institut für Ökologie,Technik und Innovations GmbH, Vienna.

[5] ÖNORM S1408 Recovery: This test defines the recovery of the pile after a certain force and time and simulates the effect of a chair leg.

[6] K. Christian Schuster , Peter Aldred, Mario Villa, Matthias Baron, Rudolf Loidl, Olga Biganska, Stanislav Patlazhan, Patrick Navard, Hartmut Rüf and Erwin Jericha, Lenzinger Berichte, 82 (2003) 107-117.

[7] Abu-Rous, M., Ingolic, E., Schuster, K. C., Cellulose 13 (2006), 441.

[8] Prof. B. Redl et al., Medical University Innsbruck, 2004.

Lenzinger Berichte 89 (2011) 72-77

VISCOSE FIBRES WITH NEW FUNCTIONAL QUALITIES

Walter Roggenstein

Kelheim Fibres GmbH, Regensburger Str. 109, 93309 Kelheim, Germany

Phone: (+49) 9441 99-489; Fax: (+49) 9441 99-1489; Email: walter.roggenstein@kelheim-fibres.com

Presented during the 48th Dornbirn Man-Made Fibers Congress, 16 – 18th September 2009, Austria

The continued success of regenerated viscose fibres over more than 100 years has been based on a broad spectrum of fibre properties. Viscose fibre is 100 % biodegradable and produced from natural renewable pulp. The fibre properties are similar to those of natural fibres like silk and cotton but can be modified to meet specific requirements. The result is a soft, smooth and also highly absorbent fibre which is ideal for a wide range of very different applications, from apparel textiles to nonwoven materials for hygiene applications as well as special technical papers. Beside the physical modifications often used in fibre manufacture, the particular possibility of the addition of chemical functionality exists with viscose fibres on account of their chemical structure. The creation of synergistic effects in the quality profile of the viscose fibres for new areas of application without affecting their existing properties through combinations of chemical and physical modifications are demonstrated. The viscose fibres are functionalised on line in fibre production, and can therefore still be processed with existing technologies at the customer. The possibility of creating very different features with only one single fibre type is particularly interesting.

Keywords: *Viscose fibres, functionalities, modification, hygiene application, speciality papers, Kelheim Fibres*

Introduction

The continued success of regenerated viscose fibres over more than 100 years has been based on a broad spectrum of fibre properties.

Within the Man-Made Fibres, synthetic fibres are based on crude-oil, but Viscose fibres are based on the most naturally occurring organic polymer: Cellulose. It is a renewable polymer which has various molecular structures and provides the structure to the world of plants.

Viscose fibres are hydrophilic, absorbent, and skin-friendly. They provide good moisture management combined with restricted growth of micro organisms. These fibres are non-melting, mechanically and chemically stable, but if needed, they may physically and chemically be modified.

The art of manufacturing Viscose fibres is the transformation of inhomogeneous, contaminated cellulosic pulp fibres into tailor-made cellulosic Viscose fibres with well-defined physical and chemical properties at a consistent quality all the year round.

Due to their broad property spectrum, Viscose fibres are used in very different applications, from apparel over nonwovens to speciality papers.

Materials and Methods

The Viscose fibres tool box

There are multiple ways of modifying viscose fibres physically and chemically. The simplest modification is the fibre length which in general is adjusted between 2 and 130 mm according to the application. Through the change in the bending stiffness and the embedding into the fibre composite, the fibre length has a significant influence on the processing and the fibre product qualities in textile yarns, nonwovens and papers.

The fibre fineness is the mass/length and represents at a given density the cross-section area of the fibre. Usual Viscose fibre fineness values are between 0.5 and 30 dtex. Taking round cross-section fibres (Figure 1), this corresponds to a diameter between 6 and 30 µm, the human hair has a diameter of about 50 µm.

The cross section of a fibre is an ideal parameter to influence the fibre properties with the variation of the mass distribution over the cross-sectional area.

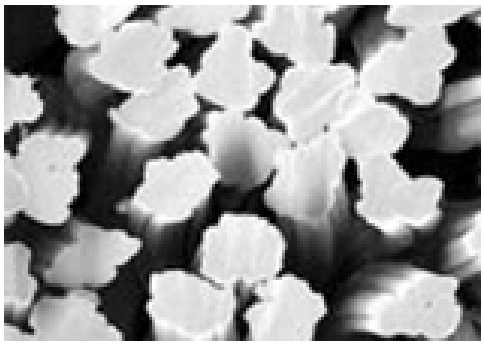

Figure 1. Round cross section Danufil.

Different cross-sections give a change of the fibre stiffness, e.g. with a flat cross-section (Figure 2). The principle is well known from science of materials where different joist profiles are used to increase the stiffness and the strength.

The Galaxy fibre (Figure 3) shows an increased fluid absorbency in a compressed fibre structure due to its higher stiffness and energy storage when compressed and forming more capillaries compared to a round cross-section when released.

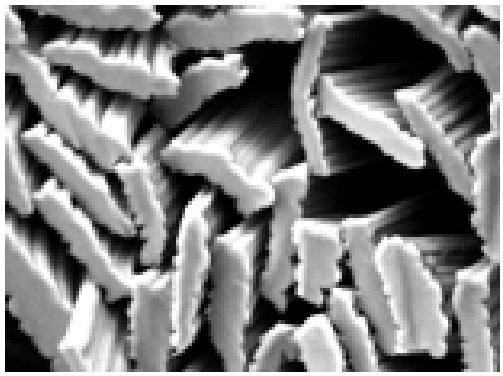

Figure 2. Flat cross section Viloft.

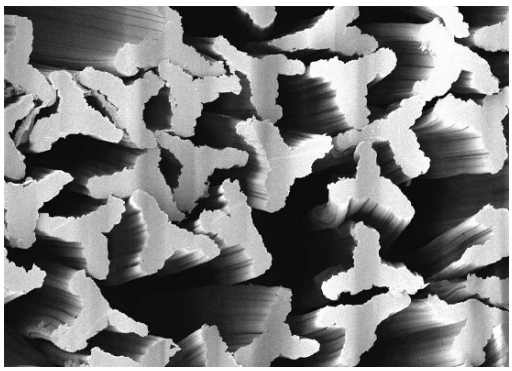

Figure 3. Y shaped cross section Galaxy.

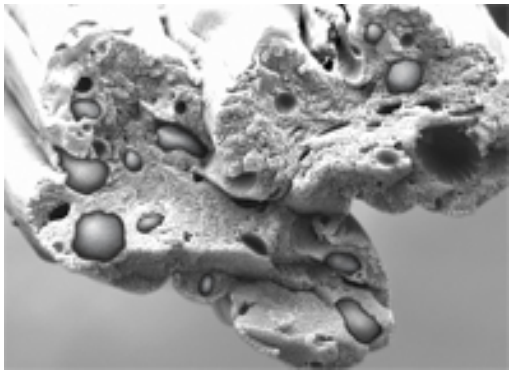

Figure 4. Viscose Outlast fibre.

The Viscose Outlast fibre (Figure 4) is a demonstrative example for the functionalisation of a Viscose fibre by the incorporation of an additive. Micro-capsules with a phase changing material (PCM) have been incorporated into the Viscose fibres by a sophisticated technology.

These fibres being transformed into a sports shirt increase the temperature comfort zone by using the latent heat capacity of the PCM.

PCM Microcapsules are only an example for the additive incorporation. It is evident that any non-viscose particle has an influence on the fibre structure and the mechanical fibre properties. It is the know-how of the fibre producer to define the right additive specification and to adapt the fibre production process for getting Viscose fibres with good processing performance and fibre product qualities.

When only the fibre surface is to be functionalized, coating is the appropriate technique. Spin finish as a coating to give the right processing performance is only one example. In many cases a homogenous continuous and thin coating film is required.

The most valuable fibre modification with Viscose fibres is the capability of bonding functional additives to the cellulosic Viscose molecule (Figure 5) by hydrogen (R_1) or covalent bonds (R_2).

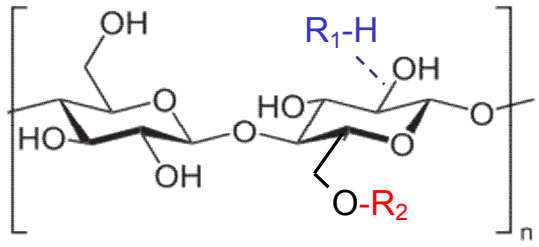

Figure 5. Cellulose molecule with hydrogen and covalent bonds.

Especially the covalent bonding of functional groups is of interest because they provide e.g. washing fastness to the fibres and the fibre products.
In consideration of the different fibre parameters and their combinations, it is obvious that there are a high number of new fibres possible.

Results and Discussion

At the end of an intensive development process, Kelheim Fibres is able to present a bundle of new functional Viscose fibres which will find their place in different applications. For better memory, these fibres are named after famous Italian artists: Verdi, Bramante, Bellini and Dante.

New modifications in Viscose fibres

The **Bellini** fibre (Figure 6) is unique in its dimensions and the surface topography.

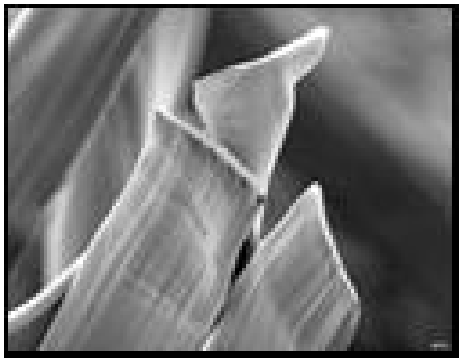

Figure 6. Flat cross section Bellini.

Through a special adaption of the spinning conditions, this specialty fibre has lost the typical crenulated surface structure. It is a fibre with a very smooth surface. The cross-section is extremely flat with an aspect ratio of 1:20 and with a thickness of about 3 µm. The recalculation of this fibre thickness into a round shaped fibre with the same diameter gives a fibre fineness of 0.1 – 0.2 dtex which is in the category of super micro fibres.

Bramante (Figure 7) is a hollow and segmented Viscose fibre, produced by a sophisticated adjustment of the spinning conditions.
The hollow segmented structure gives the Bramante fibre mechanical stability both in dry and in wet condition. Upon contact with an aqueous liquid, the hollow fibre, being collapsed when dry, fills completely with the fluid resulting in a significantly higher intrinsic absorbency. Because this

process is reversible, the fibre can also be cyclically inflated and deflated.

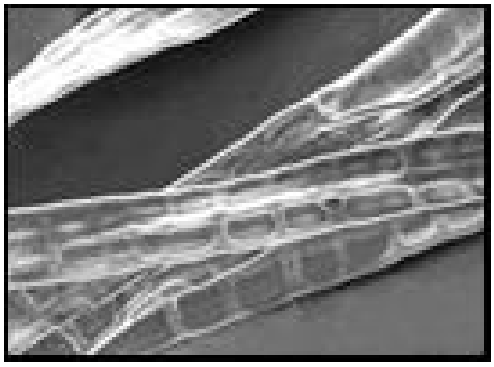

Figure 7. Segmented hollow fibre Bramante.

The **Verdi** fibre (Figure 8) is a viscose fibre with a homogeneously mixed cellulose derivative.

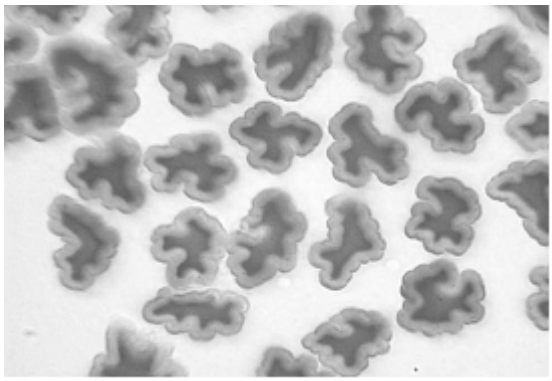

Figure 8. Verdi fibre.

Interestingly, there are four simultaneous effects with this modification. Besides increasing the absorption of aqueous fluids, these fibres disperse significantly better in water without agglomeration. In the wet state the surface of the fibre alters, resulting in a gel-like surface structure. The fourth notable effect, the fibre is self-extinguishing.
All these effects occur in parallel and can be easily controlled via the degree of modification.

The combination of Bramante with Verdi results in a new fibre, **Dante** (Figure 9).
The individual effects of each fibre are conserved, the absorbency is even activated.

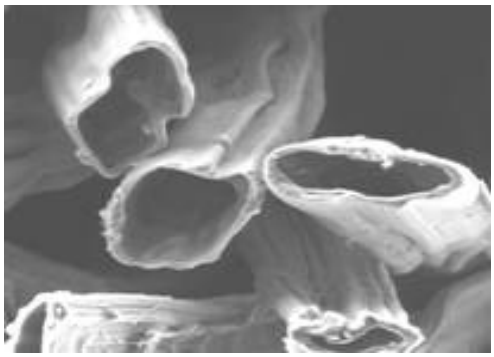

Figure 9. Dante fibre.

From fibres to applications

The transformation of the shown fibre properties into innovative product features is a challenge in fibre development. First fundamental studies already show the potential of the "Italian Fibres" to design new fibre products.

Absorbency
The water imbibition represents the absorbed water and the cohesively to the fibre bonded water. Even the flat fibre Bellini shows a slight increase in water imbibition caused by more cohesively bonded water (Figure 10). The modification with the cellulose derivative leads to around 50 % increased water imbibition on the Verdi fibre compared to a standard Viscose fibre Danufil. This is again increased to a water imbibition of 250 % with the hollow fibre structure of Bramante.

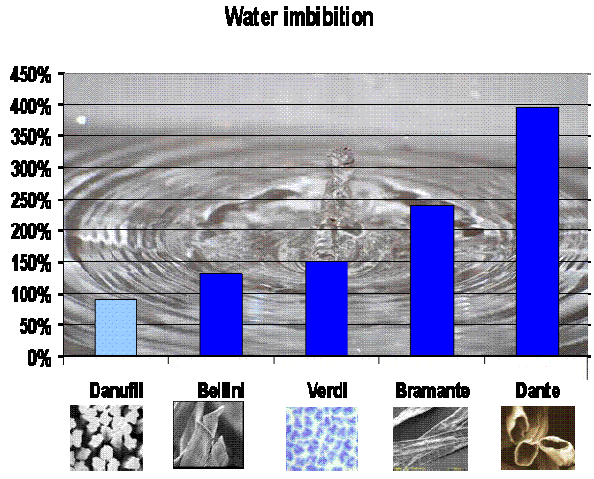

Figure 10. Water imbibition.

The Dante fibre finally reaches a water imbibition of 400 % and is hence higher by a factor of 4 compared to the standard Viscose fibre Danufil.

The absorbency increase is of interest for many applications. From simple wipes, through medical pads to hygiene tampons. The absorption capacity of sanitary tampons can be characterized with the Syngina measurement [1].

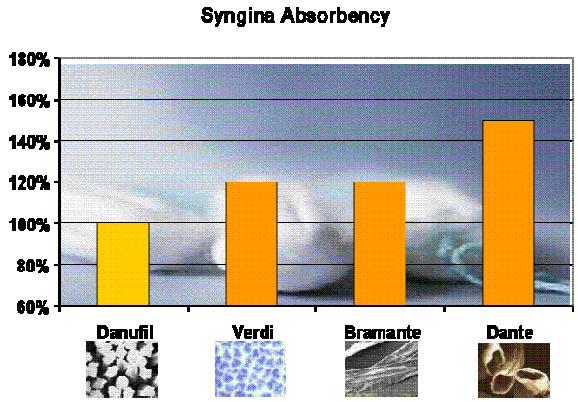

Figure 11. Syngina absorbency.

There is a significant increase in fluid absorption with the modified fibres compared to a standard Viscose fibre (Figure 11) as well. However, this increase is lower than expected by the water imbibition. The reason is the fact that the absorption of a sanitary tampon is caused only partly by the increase in the intrinsic fibre absorbency.

Fibre dispersability

In the processing of Viscose fibres to wetlaid nonwovens and specialty papers, the short-cut fibres are dispersed in water to be formed into a composite material. The main requirement of a complete separation into individual single fibres is limited by the so-called spinning effect, an agglomeration of several fibres which leads to product defects. This effect is essentially determined by the fibre bending stiffness and fibre geometry, hence the arbitrary choice of different geometries is limited.

The Verdi and Dante fibres break this limitation. The anionic charge improves the separation of the fibres. The fibre concentration when agglomeration occurs can be increased by a factor of 5 compared to standard Viscose fibres (Figure 12).

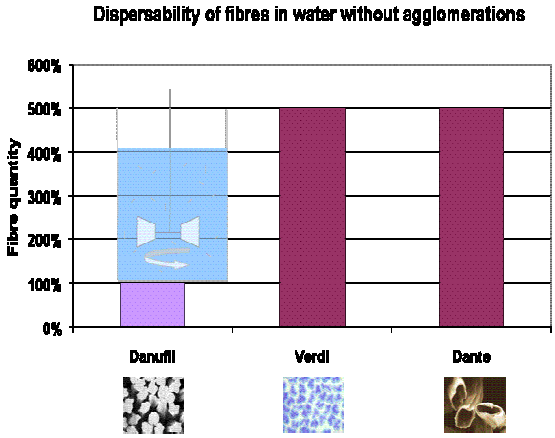

Figure 12. Fibre dispersability in water.

Paper tear resistance

The mechanical resistance of papers is characterised by the tensile strength and the tear resistance.

While it is impossible to get a paper with considerable strength out of 100% standard Viscose fibres, the use of Bramante, Verdi, Dante and especially Bellini improve significantly the tensile strength and the tear resistance in parallel (Figures 13, 14).

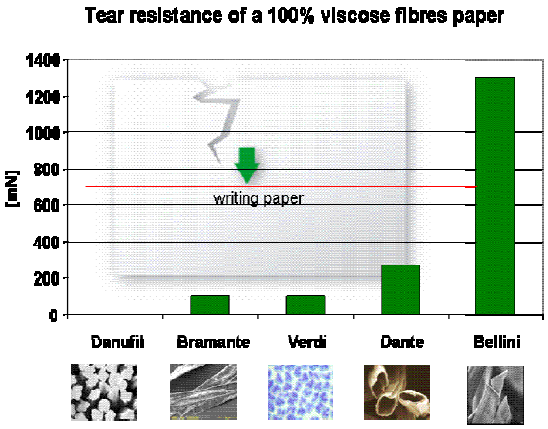

Figure 13. Paper tear resistance.

Bellini is the only Viscose fibre where a paper sheet can be formed without pulp or strengthening additive. The unique flatness, the extreme surface smoothness and the good bendability give sufficient bonding area and hydrogen bonding force for the formation of a strong paper.

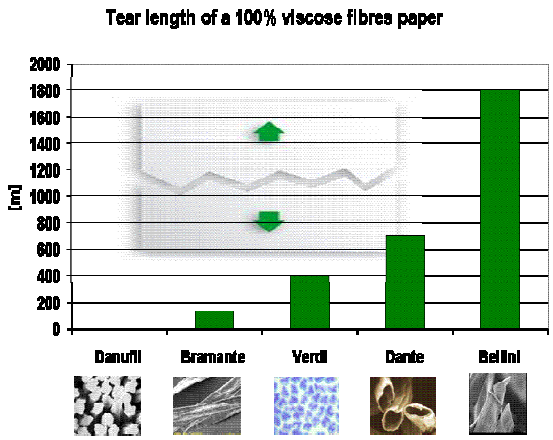

Figure 14. Paper tear length.

Self-extinguishing effect

It is expected that a cellulosic standard Viscose fibre burns totally when lightened up. Surprisingly it was discovered that the Verdi and Dante fibres extinguish after only a few seconds (Figure 15). This offers the possibility to use this fibre in textile and technical applications where fire protection is a demand.

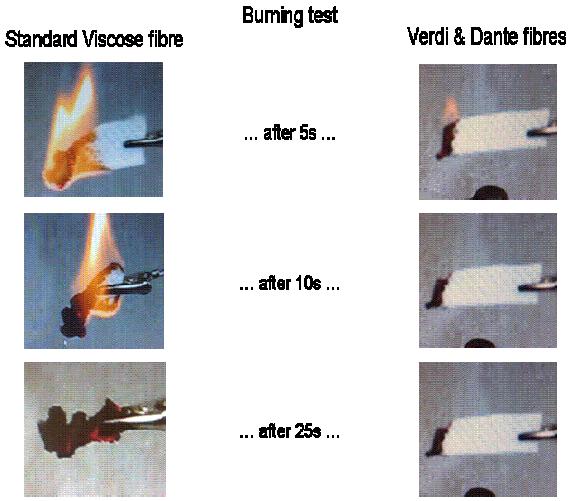

Figure 15. Burning behaviour of Viscose fibres.

Conclusions

Viscose fibres are based on the most important natural polymer, the Cellulose. Cellulose is a renewable, organic polymer with a broad spectrum of properties. Viscose fibres are tailored cellulosic fibres with unrivalled, intrinsic qualities.

Although cellulosic Viscose fibres already have a long history compared to all synthetic fibres, they still offer the opportunity of various physical and chemical modifications, additionally to standard fibre modifications.

The new Viscose–based Verdi, Bramante, Dante and Bellini fibres show ultra-high absorbency, self-bonding behaviour, high dispersability in water, a gel-like surface structure and self-extinguishing properties.

This opens up opportunities to develop new innovative fibre products and to enter into new market segments which were closed for standard viscose fibres up to now.

References

[1] INDA / EDANA Standard test methods for the nonwovens and related industries, edition 2008, WSP 350.1 (5).

Lenzinger Berichte 89 (2011) 78-85

FINE-TUNING OF PAPER CHARACTERISTICS BY INCORPORATION OF VISCOSE FIBRES

Ingo Bernt

Kelheim Fibres GmbH, Regensburger Str. 109, 93309 Kelheim, Germany

Phone: (+49) 9441 99-295; Fax: (+49) 9441 99-1295; Email: ingo.bernt@kelheim-fibres.com

Presented during Zellcheming Expo 2010, 29th June – 1st July 2010 at Rhein-Main-Hallen, Wiesbaden, Germany

Typically, the quality of paper can be controlled by using the adequate grade of pulp and auxiliary materials as well as selecting the appropriate process settings, as for example the level of refining.
In many cases, in order to achieve specific paper properties it is furthermore necessary to use blends of pulp and other fibres of natural or man-made origin. For this application viscose fibres are especially useful. As a cellulosic fibre they can be conveniently included into the paper matrix. On the other hand, as a man-made fibre they offer a very broad spectrum of possible variations, allowing a pinpoint control over the desired paper characteristics. It is detailed, which possibilities for the variation of viscose fibres exist in terms of fibre cross section, fibre dimensions and fibre functionalization.
On selected examples it is demonstrated that through the choice of the appropriate viscose fibre cross section, control over the air permeability can be achieved without loss of tear strength, while at the same time also tear resistance and a number of double folds can be improved. Furthermore, it is shown what influence the choice of the percentage of viscose fibres in the blend as well as the viscose fibre dimensions have on the ratio of tear strength to tear resistance in a paper.
Finally, the possibility to combine these effects with an additional fibre functionalization such as incorporation of functional particles, enhancement of water imbibition or anionic and cationic modifications is outlined.

Keywords: *paper, viscose, porosity, tear resistance, functionalization, Kelheim Fibres*

Introduction

The production of cellulosic fibres by the viscose process [1, 2, 3] has been introduced over one hundred years ago, but research in order to optimize these fibres for different end-uses is still ongoing. Kelheim Fibres is a producer of viscose fibres with a long experience in the production of viscose specialty fibres for various applications.
Among other man-made fibres, viscose fibres are frequently used in specialty papers in order to modify paper characteristics. Viscose fibres are produced from 100 % cellulose and can therefore conveniently be incorporated into a paper matrix having the same surface chemistry as pulp fibres.
Unlike natural cellulosic fibres, viscose fibres can be produced in a very specific length, thickness and cross-sectional shape with a very homogenous and constant quality. Apart from the well-known

standard viscose fibres Kelheim Fibres has developed several new types of viscose fibres, e.g. with a very thin and flat cross-section, which are especially suited for incorporation into papers.
Furthermore, various possibilities exist to further modify viscose fibres in order to provide additional functionality in the finished product.
In this paper, new results will be presented, highlighting the effects of the variation of different viscose fibre parameters on the characteristics of paper sheets formed from blends of pulp and viscose.

Materials and Methods

Materials
For all tests, the same batch of Eucalyptus pulp, refined to 26°SR was used.
All viscose fibres in this study were produced by Kelheim Fibres and used in the cut length as further indicated. Fibre parameters are given in Table 1.

Table 1. Viscose fibre parameters.

Fibre type	Titer [dtex]	Elongation [%]	Tenacity [cN/tex]	Work [cN*cm]	W.I. [%]
Danufil ®	3.3	24.0	21.8	2.2	83
Danufil ®	1.7	18.2	21.5	0.9	81
Galaxy ®	3.3	22.3	19.3	2.0	83
Viloft ®	3.3	25.4	19.6	2.1	84
Bramante	3.3	32.1	10.5	1.7	366
Bellini	3.3	22.1	13.9	1.5	145

Methods
Rapid-Köthen sheets of 80 g/m² were produced in the indicated composition from the materials above, without the use of any other auxiliaries. The obtained sheets were tested without seizing or other treatments. All paper testing was done following industry standard procedures.

Results and Discussion

The Viscose fibre tool box

The viscose fibre process offers a broad and versatile tool box for the modification of viscose fibres, enabling to adapt the fibre to a wide field of applications, ranging from textile over hygienic up to paper end uses.

Modification of the fibre cross section
In the viscose production, the shape of the fibre cross section can be controlled by the shape of the spinning nozzle. Round (Danufil®); flat (Viloft®) and trilobal (Galaxy®) cross sections are well-known commercially available cross sections from Kelheim Fibres.
Additionally, new cross sections have been developed, which are especially suitable for the incorporation into paper (Figure 1).

The "*Bramante*" developmental fibre features a hollow cross section in the wet state, allowing for water imbibitions (W.I.) up to four times higher than regular viscose fibres (see Table 1). When dried, the cross section collapses giving a very flexible fibre with a high specific surface area for good bonding characteristics.

The "*Dante*" fibre features the same cross sectional characteristics but is additionally anionically modified for even higher imbibition and bonding strength.

The "*Bellini*" developmental fibre shows a very smooth, thin and flat cross section with a width to thickness ratio of about 1:20. The high flexibility and surface area provides this fibre with very good bonding properties making it possible to form sheets out of 100 % viscose, using Bellini fibre.

Modification of the fibre dimensions
Like man-made fibres in general, but unlike natural fibres, viscose fibres can be produced in a constant and very specific fibre length and fibre diameter depending on the final use of the fibre. Kelheim Fibres produces short-cut viscose fibres in a range from 0.5 to 28 dtex, corresponding to an equivalent diameter of 7 to 48 micrometers for round fibre shapes. For short-cut applications, the cut length of the fibre can be selected from a range from three to twelve millimetres.

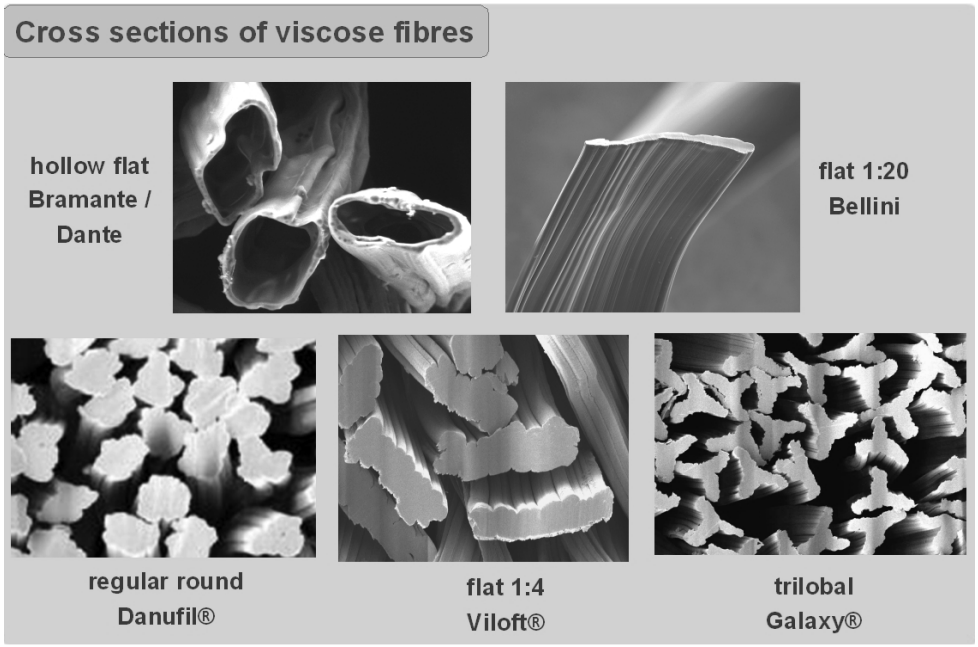

Figure 1. Options for the variation of viscose fibre cross sections.

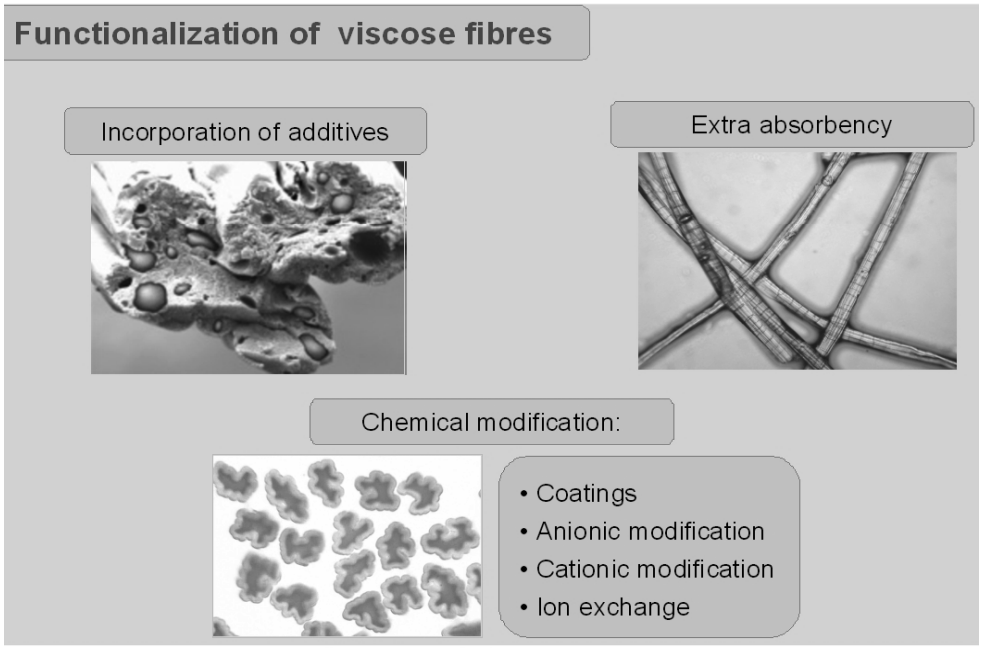

Figure 2. Options for the functionalization of viscose fibres.

Table 2. Test results of 100 % sheets.

		Pulp	Danufil ®	Galaxy ®	Viloft ®	Bramante	Bellini
Fraction	%	100%	100%	100%	100%	100%	100%
Density	g/cm²	0.679	0.355	0.380	0.414	0.602	0.641
Tear length	m	5433	34	98	30	1201	999
Tear resistance	mN	584	57	121	59	440	307

Viscose fibre functionalization
The viscose process allows the functional modification of viscose fibres in various ways (Figure 2). One possibility is the incorporation of functionalized particles, such as pigments and micro-capsules, into the cellulose matrix. Also through carefully selected spinning conditions the viscose fibre structure can be modified in order to maximize the water imbibition into the fibre. Finally by chemical modification of the fibre, anionic or cationic fibres can be produced, giving for example ion exchange properties.

Fine-tuning of paper characteristics through incorporation of viscose fibres
In order to explore the effect of the incorporation of viscose into paper with respect to the possible modifications of the viscose fibre, 80 g/m² Rapid-Köthen sheets formed from 26 SR Eucalyptus pulp were selected as a basic model system. Varying amounts of viscose fibres were blended with the pulp, while cross sections and fibre dimensions were changed independently.

Influence of the fibre cross section
a) Sheets from 100 % viscose fibre
In a first step, the influence of the fibre cross section on the paper characteristics was studied. In order to focus on the cross section alone, all viscose fibres were used in the same titer and in the same cut length (3.3 dtex; 6 mm). It is to note though, that this dtex is not the optimum choice for all fibres in a real application, especially Bellini should be used in a lower dtex.
At first, Rapid-Köthen sheets consisting of 100 % viscose fibre were formed. Test results are given in Table 2.

As expected, sheets formed of 100 % regular viscose do not show paper-like characteristics. Compared to the pulp reference, the density of the viscose sheets is 40-50 % lower and they show practically no tear strength or tear resistance. This indicates that the degree of bonding between these viscose fibres is much lower than in pulp, making it impossible to produce 100 % viscose paper from them.
With the developmental fibres Bramante and Bellini, featuring a high surface area and high flexibility, sheets with paper like characteristics were obtained. The density of these sheets is in the same range as the pulp reference paper and their strength is several times higher than that of papers from 100 % standard viscose. Higher strength values can of course be generated with lower fibre titers, giving a higher fibre count at the same weight.

Given the good results for paper strength using the Bellini and Bramante fibres, a trial was done in order to verify, whether in the same way as for pulp fibres, additional laboratory refining could increase the strength of sheets formed from these fibres. For comparison, refining was also carried out on standard Danufil® viscose fibres (Table 3).
Again as expected for viscose fibres, no mayor increase of tear strength or tear resistance was measured for the refined Danufil® fibre. For the Bellini and Bramante fibres though, a surprisingly pronounced effect of the refining was found, with an increase of tear length of up to 220 % and an increase of tear resistance of up to 285 %. This effect is attributed to a higher flexibilization of the viscose fibres, since no fibrillation was observed.
As a reference, typical values for a sheet from 100 % paper-quality Bellini in 2.1 dtex are included in Table 3 (see Ref**).

b) Sheets from blends of pulp and viscose
As shown, sheets of sufficient strength from 100 % viscose could only be formed from the Bellini and Bramante fibres. But viscose fibres are of course already used for various applications in blends with pulp fibres. Therefore, blends with 2 % and 10 % incorporation of viscose fibres were made and paper characteristics were tested (Table 4).

Table 3. Paper strength after refining of viscose fibres.

Strength of paper sheets from 100% viscose fibre.									
		Euca Pulp 26°SR	Danufil ®		Bramante		Bellini		Ref*
Fraction	%	100%	100%	100%	100%	100%	100%	100%	100%
Refining viscose	min		0	10	0	40	0	10	
Basisweight	g/m²	81	84	84	84	83	81	84	80
Density	g/cm²	0.679	0.355	0.387	0.602	0.733	0.641	0.680	0.722
Tear length	m	5433	34	130	1201	2614	999	1721	3650
Tear resistance	mN	584	57	76	440	1258	307	672	1900

Table 4. Test results of sheets made from blends of pulp and viscose fibres.

		Pulp	Danufil ®		Galaxy ®		Viloft ®		Bramante		Bellini	
Fraction Pulp	%	100%	90%	98%	90%	98%	90%	98%	90%	98%	90%	98%
Fraction Viscose	%	0%	10%	2%	10%	2%	10%	2%	90%	98%	10%	2%
Density	g/cm²	0.679	0.611	0.664	0.628	0.680	0.624	0.676	0.677	0.688	0.681	0.685
Tear length	m	5433	5025	5515	5146	5532	5552	5762	5750	5888	5445	5830
Tear resistance	mN	584	808	715	809	689	831	662	832	651	841	652
Air permeability	ml/min	1872	3488	1521	2205	1391	2248	1466	1487	1263	1301	1298
Double folds	n	203	104	260	223	357	182	320	332	355	203	354

Table 5. Test results of blends with viscose fibres for a range of fibre lengths and titers.

		Pulp	Danufil ®								
Titer	[dtex]		1.7	3.3	1.7	3.3	1.7	3.3	1.7	3.3	2.4
Fibre length	[mm]		4	4	8	8	4	4	8	8	6
Fraction pulp	[%]	100%	95%	95%	95%	95%	75%	75%	75%	75%	85%
Basisweight	[g/m²]	81	82	82	82	83	83	83	82	83	82
Density	[g/cm²]	0.679	0.654	0.646	0.651	0.650	0.561	0.550	0.552	0.543	0.643
Tear length	[m]	5433	6259	5830	5897	5646	4502	4773	4598	4519	5426
Tear resistance	[mN]	584	797	793	823	870	987	1119	1423	1569	926

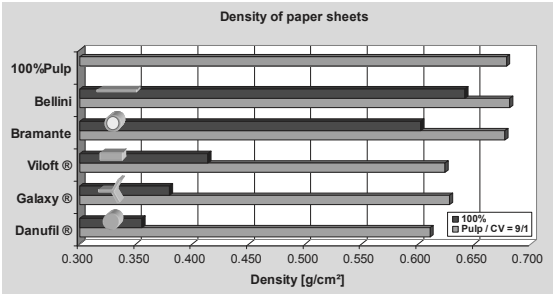

Figure 3. Density of sheets from 100 % viscose and viscose/pulp blends.

The effect of the variation of the viscose fibre on the density, porosity and strength of the formed papers was analyzed, giving the following results:

Density: In paper sheets with 10 % viscose the same order of densities is observed as found for the sheets from 100 % viscose. The lower the surface area of the fibres, the lower is the density of the sheet, with Danufil® giving the lowest density, whereas the density of blends with Bellini and Bramante was the highest, comparable with sheets from 100 % pulp (Figure 3).

Porosity: The air permeability (Bendtsen) of the sheets was studied in order to quantify their porosity (Figure 4).

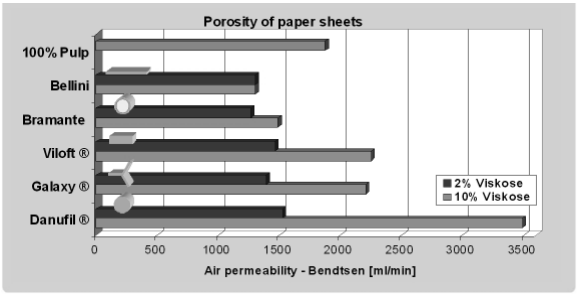

Figure 4. Porosity of sheets from viscose/pulp blends.

For the blends with 10 % incorporation the result was as expected, with those fibres giving lower densities in 100 % viscose sheets also giving higher porosities in viscose/pulp blends. By far the highest effect on air permeability with an increase of over 85 % versus the pulp reference was achieved with Danufil® fibres. Incorporation of Viloft® and Galaxy® fibres resulted in a smaller increase of air permeability of about 20 %. On the other hand, an incorporation of Bellini and Bramante fibres actually led to a decrease of air permeability of about 30 % versus the reference sheet.
In the blends with incorporation of 2 % of viscose fibres the same order of air permeabilities was found, with Danufil® fibre giving the highest and Bellini/Bramante giving the lowest permeabilities. But quite surprisingly, the air permeability for all blends with an incorporation of 2 % viscose was markedly reduced by 20-30 % compared to the permeability of the reference sheet from 100 % pulp. The reason for this decrease in permeability at low percentage incorporations of viscose is still not fully understood and under further investigation.

Tear resistance: While large differences in the tear resistance of sheets made from 100 % viscose were observed, when using different viscose cross-sections, no significant influence of the cross section was found in sheets from blends of pulp and viscose (Figure 5).

In each case, incorporation of viscose fibres results in a striking improvement of the tear resistance of the formed papers versus the reference. While by incorporation of 10 % viscose fibres tear resistance increases on average by 40 %, at an incorporation of 2 % viscose the increase in tear resistance still amounts to 15 %.

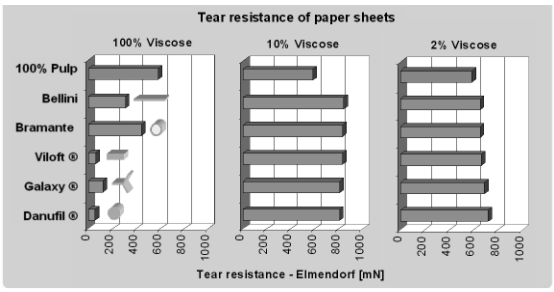

Figure 5. Tear resistance of sheets from viscose/pulp blends.

Tear strength: A marked influence of the viscose fibre cross section was found in the tear strength of sheets from viscose/pulp blends (Figure 6).

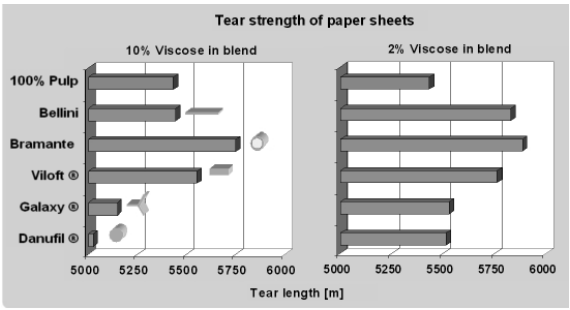

Figure 6. Tear strength of sheets from viscose/pulp blends.

At 2 % incorporation of viscose fibre, tear length of sheets with addition of Danufil® and Galaxy® fibres was only slightly higher than for the pulp reference, while incorporation Viloft®, Bramante and Bellini led to an increase in tear length of up to 8 %. A higher degree of 10 % of viscose fibre incorporation resulted in a reduction in tear length in sheets containing Galaxy® and Danufil®, whereas the incorporation of Viloft® and the developmental viscose fibre types still gave higher strength values compared to the pulp reference.

Number of double folds: Finally the number of double folds was also tested (Figure 7).

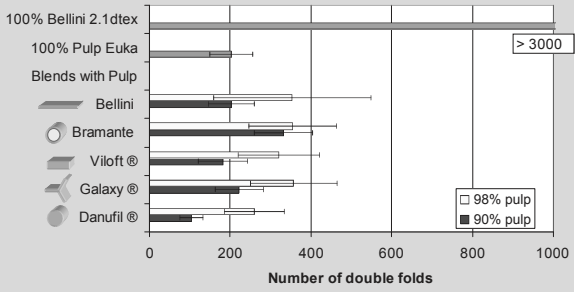

Figure 7. Number of double folds of sheets from viscose/pulp blends.

Similarly to the findings for paper strength, all fibres when incorporated at 2 % improved the number of double folds. At an incorporation of 10 % viscose, the sheets were still at or above the double fold level of the pulp reference, except for Danufil® were a lower number of double folds was observed. As a reference, a typical value for a sheet from 100 % paper-quality Bellini in 2.1 dtex, where double folds over 3000 can be achieved, was included in the graph.

Influence of the fibre length and titer

In the first part of this study it was shown that the correct choice of viscose fibre cross-section is critical to control paper porosity, strength and tear resistance. But for sure viscose fibre dimensions have an equally decisive effect on the properties of papers formed from viscose/pulp blends.

In order to get an overview over the influence of the fibre dimensions, a two-level 3-factor full-factorial experiment was carried out, where fibre length was 4 mm and 8 mm; fibre titer was 1.7 dtex and 3.3 dtex (fibre diameter 12 µm and 17 µm respectively) and the level of incorporation was 5 % and 25 %. For all experiments the "round" Danufil® cross-section was used. The results of this series, also including a central point of 6 mm length, titer 2.4 dtex and 15 % incorporation, are listed in Table 5.

As it might be expected, the biggest influence in this set of experiments is the fraction of incorporated viscose fibres. As visualized in Figure 8, incorporation of 5 % generally increases tear strength, whereas with an incorporation of 25 % viscose the tear strength of the sheets is reduced. At an incorporation of 15 % viscose, the tear strength is at the level of the pulp reference sample. At the same time, tear resistance is improved at all levels of viscose fibre incorporation.

The influence of fibre titer and cut length can be identified by comparing figures at the same levels of viscose incorporation.

At 5 % viscose the tear resistance of the viscose containing sheets is about 40 % higher than in the pulp reference sheet, with longer fibres tending to give a higher tear resistance. Also at this level of viscose incorporation shorter fibres and lower dtex result in a higher tear length, probably to be attributed to the higher number of viscose fibres in the blend. The highest tear length in this series (15 % higher than pulp reference) is consequently achieved with the incorporation of 5 % viscose of 4 mm length and 1.7 dtex titer.

At 25 % viscose incorporation, no clear trend could be observed for the tear length, but tear resistance improves with higher dtex and especially with longer fibre length. The highest tear resistance in this series (170 % higher than reference) is consequently achieved with the incorporation of 25 % viscose at 8 mm and 3.3 dtex.

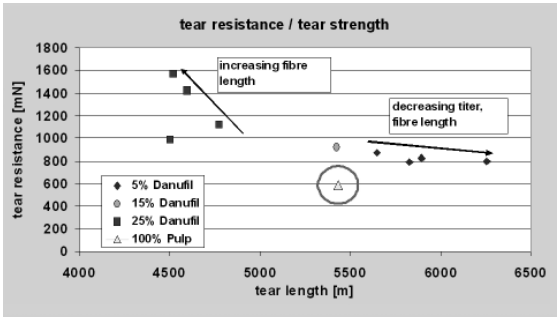

Figure 8. Ratio of tear strength and tear resistance for viscose/pulp blends.

Influence of the fibre functionalization

In general, all modifications of the physical shape of the fibres can be freely combined with a further functionalization of the fibre. Physical modifications, especially the incorporation of functional

particles, in most cases do not influence the paper forming performance of these fibres.
Chemical modification on the other hand can influence the binding behaviour of viscose fibres. An example is the anionic modification of the viscose fibre (Verdi developmental fibre), which gives a significant improvement in dry strength and also greatly improves the dispersability of these fibres.
And finally, the amount of water imbibition for a hollow fibre such as Bramante can be controlled through the choice of production conditions and the fibre titer, giving up to four times higher imbibitions than with standard viscose fibres.

Conclusion

Paper characteristics, especially porosity and tear resistance, can be controlled in a wide range by incorporation of short-cut viscose fibres. The results given here show that the correct choice of fibre cross-section, dimension and amount of incorporation is very important in order to achieve the desired paper properties. Of course the effect of viscose incorporation will vary greatly with the pulp matrix used and so for each system the best fitting viscose fibre in terms of the above modifications has to be selected.

References

[1] GB-Patent No. 8700 (1892), Charles Frederick Cross and Edward John Bevan.

[2] GB-Patent No. 1022 (1898), Charles Henry Stearn.

[3] Götze, K., Chemiefasern nach dem Viskoseverfahren. 3. Ed. 1967, Berlin, Heidelberg, New York: Springer-Verlag.

Lenzinger Berichte 89 (2011) 86-90

CATIONIC ACTIVATED VISCOSE FIBRES - DYEING OF FIBRES AND DECOLOURING OF AQUEOUS SOLUTIONS

Roland Scholz[1], Dana Dedinski[2]

[1]Kelheim Fibres GmbH, Regensburger Str. 109, 93309 Kelheim, Germany
[2]Hochschule für Angewandte Wissenschaften Hof, Abteilung Münchberg, 95213 Münchberg, Germany

Phone: (+49) 9441 99-632; Fax: (+49) 9441 99-237; Email: roland.scholz@kelheim-fibres.com

Presented with the title "Ionic activated viscose fibres" during the 49th Dornbirn Man-Made Fibers Congress, 15 – 17th September 2010, Austria

Ionic activated viscose fibres can be dyed with a high degree of efficiency. Special colour effects are obtained, for example in blends with standard cellulosic fibres. This well-known high affinity to dyestuffs provides the opportunity to employ ionic activated viscose fibres for elimination of undesired dyes in aqueous media. Focused on this application the Deep Dye fibre of Kelheim Fibres has now been further developed and its potential has been investigated. The capacity and kinetics of dye absorption is controlled by the level of ionic activation. With this directed modification of properties new fields of application for the Deep Dye fibre are possible. The functionality is brought by an in-line process into the viscose. Without any loss of activity the fibre can be converted to textile and nonwoven fabrics with standard technologies.

Keywords: *cationic activated viscose fibre, dye absorption capacity, dye absorption kinetics, dye transfer inhibition, Kelheim Fibres*

Introduction

Cationic activated viscose fibres generally feature superior dyeing properties compared to standard viscose. In the past cationic activated fibres for textile applications were developed independently by Lenzing (Rainbow Fibre) [1, 2] and Kelheim Fibres (Deep Dye Fibre) [3]. These fibres allow an efficient dyeing with anionic dyes like direct and reactive dyes.
They require shorter dyeing time, less amount of dyestuff and salt as well as lower consumption of water and energy. In total dyeing costs are reduced and environmental compatibility is improved.
The high affinity of cationic activated viscose fibres is impressively demonstrated by competitive dyeing of the activated fibre together with standard viscose in one dyeing bath. As shown in Figure 1 the activated Deep Dye fibre picks up the dyestuff "Direct Dye Blue 71" more or less completely while the standard viscose fibre remains almost uncoloured.

Figure 1. Competitive dyeing.

Special dyeing effects like bicolor or mélange patterns are achievable in a one-bath one-step dyeing procedure for fabrics consisting of activated and non-activated viscose fibres. Furthermore, homogeneous dyeing result can be obtained in a one-bath one-step dyeing procedure for blends of activated viscose and polyester [1].

In the following we will describe our recent investigations on how far cationic activated viscose fibres are applicable for decolouration of aqueous media and the capture of anionic substances in general.

Ionic Activation of Viscose Fibres

There are different principles for ionic activation of viscose fibres. Ionic functional groups can be attached to the hydroxyl groups of the cellulose via covalent bonding. In case of cationic activation generally quaternary ammonium groups are attached (Figure 2).

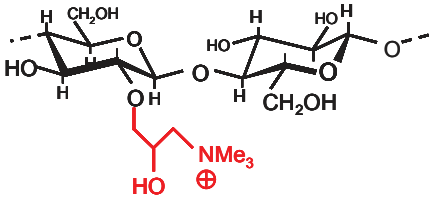

Figure 2. Cationic activation via covalent bonding.

Ionic activation is achievable by incorporation of a polyelectrolyte (Figure 3) into the spinning dope, too. The ionic additive is dispersed in the cellulose matrix of the viscose fibre.

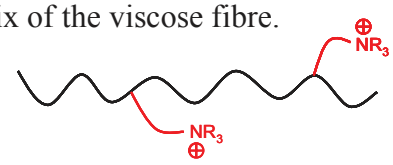

Figure 3. Cationic activation with polyelectrolyte additives.

Furthermore, coating of fibres can be used for ionic activation.

Materials and Methods

In order to investigate the potential of cationic activated viscose for decolouring of aqueous media the activation of the Deep Dye fibre was maximised.

The decolouring potential was investigated by measuring of dye absorption capacity, dye absorption speed and dye transfer.

Dye absorption and kinetic trials were carried out with direct dyes like Direct Blue 71 (Figure 4), Direct Red 80 and Direct Yellow 162. The anionic sulfonate groups of the dyes get strongly fixed to the cationic groups of the activated fibre through ionic bonds.

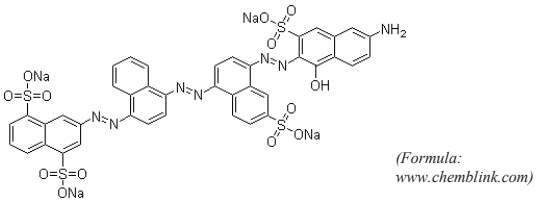

Figure 4. Direct Dye Blue 71.

Contrary to classical dyeing conditions, dye solutions without salt and alkali were used to test dye absorption capacity and kinetics. Dye solutions were treated with fibres at 60 °C. For determination of dye absorption capacity the tests were stopped after 60 min. For investigation of kinetics the trials were stopped after 10, 20 and 30 min. (Figure 5). The remaining solutions were analysed photometrically.

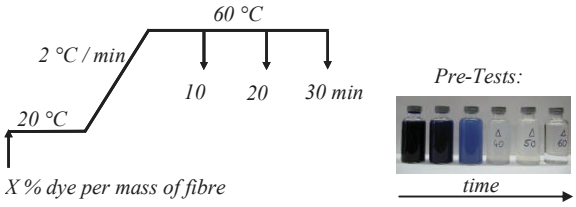

Figure 5. Trial parameters.

Dye transfer tests were carried out in accordance to DIN ISO 105-C06 "*Test for colour fastness to domestic and commercial laundering*". A bleeding fabric was sewed to an adjacent fabric consisting of six different textile types (Figure 6): Wool, Polyacrylonitrile (PAN), Polyester (PES), Polyamide (PA 6.6), Cotton, 2.5-Acetate.

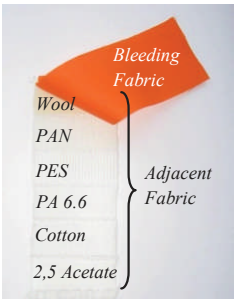

Figure 6. Bleeding fabric and adjacent fabric for dye transfer tests.

Simulation of a washing procedure was carried out by treating the textile combination with a standardised laundry detergent at 60 °C for 30 min. Steel balls were added to apply mechanical stress.

Cationic activated fibres were added to determine the extent to which a dye transfer from the bleeding fabric to the adjacent fabric could be prevented during the washing.

Results and Discussion

Dye Absorption Capacity

Ideally, a dye solution is totally decoloured after treatment with cationic activated fibres (Figure 7). Increase of dye concentration finally leads to a threshold where a defined amount of fibre will not attain complete decolouring of the solution anymore. Hence the question was how to assess this threshold, which defines the dye absorption capacity of the fibre.

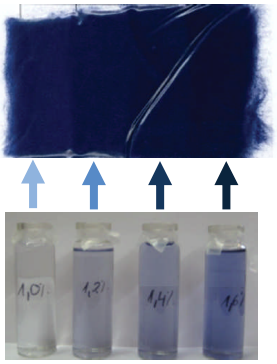

Figure 7. Dyed fibres and decoloured solutions.

For determination of the dye amount removed from the solution by the fibre, either the dye amount on the fibre itself or the remaining dye in the solution can be analysed. However, differences in colour intensity on the fibre are much more difficult to determine than intensity differences of the remaining solutions. Therefore, the colour intensity of the remaining solution was analysed via photometric measurement.

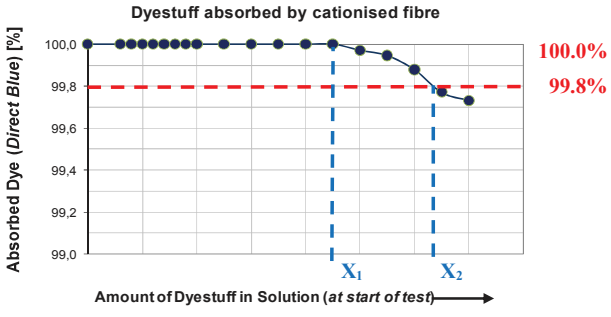

Figure 8. Defining of threshold for the determination of dye absorption capacity.

We decided to define the dye absorption capacity of a given mass of fibre as the amount x_2 of dye which is taken out of the solution to an extent of 99.8 % (Figure 8). This definition takes into account that some fibre qualities achieve decolourisation of less than but very close to 100 % over a certain range of dye concentration.

Thus, depending on the defined threshold value (e.g. 100 % or 99.8 %), the resulting dye absorption capacity of a fibre varies from x_1 to x_2.

All trials showed a direct dependency of the fibre´s dye absorption capacity on its cationic activation (Figure 9). The capacity increases sigmoidal with the level of activation. A dye absorption capacity of up to 10 % of the fibre´s own weight was achieved.

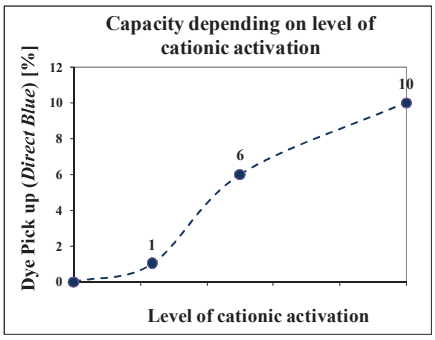

Figure 9. Dye absorption capacity depending on cationic activation of fibre.

In contrast, no dependency of absorption capacity on the total fibre surface could be observed (Figure 10).

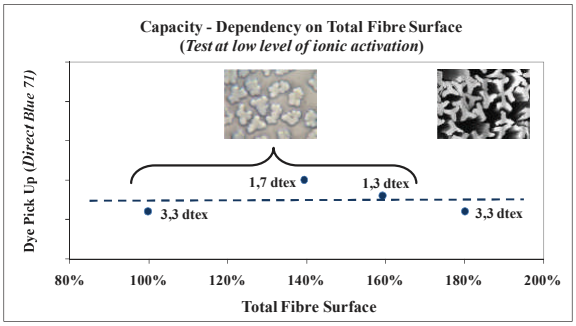

Figure 10. Dye absorption capacity of activated fibres with different total surface.

A rise of 60 % in the total fibre surface by reducing the titre of round shaped fibres from 3.3 dtex to 1.3 dtex did not increase the dye pick up. Similarly, a rise of 80 % in total fibre surface by using a trilobal shaped fibre had no impact on the dye absorption capacity.

This observation is consistent with a homogeneous distribution of the dye throughout the cationic activated fibre. Microscopic analysis of fibre cross sections

(Figure 11) prove that at low dye concentration the dyestuff is initially absorbed in the outer layers.

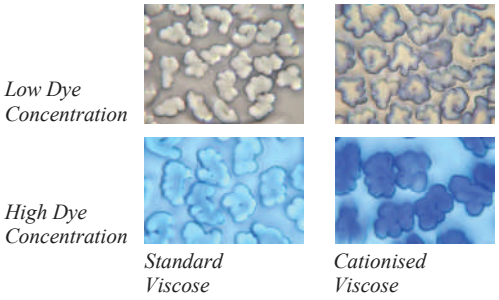

Figure 11. Cross sections of dyed fibres.

At high dye concentration the whole fibre cross section is utilised for dye absorption. The microscopic images of standard viscose show significantly less dye absorption in independent trials under same conditions.

The conversion of cationic activated fibres to spunlaced nonwovens did not change the dye absorption capacity (Figure 12). Hence in the spunlacing process no wash-out of the cationic activation took place.

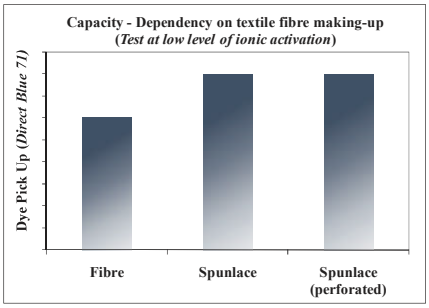

Figure 12. Dye absorption capacity of activated fibres with different fibre making up.

Basically, the dye absorption capacity of cationic activated fibres showed no significant dependency on the type of direct dyes tested (Figures 13a-c).

However, trichromic tests proved slightly varying affinity of cationic activated fibres to different direct dyes. Decolouring trials were carried out with a mixture of direct yellow, blue and red dyes giving a grey coloured trichromic solution (Figure 13d).

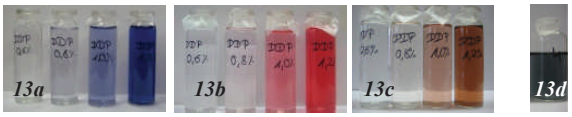

Figure 13. Decolouring of different dye solutions.

After treatment with cationic activated fibres, colourless to brown solutions remained (Figure 13c), depending on total dye concentration. This proves a slightly selective affinity of the fibre to different dyes.

The dye pick-up of cationic activated fibres is not limited to anionic dyes. As shown in Figure 14, the activated fibre absorbed even more cationic dye Victoria Blue than a standard viscose fibre. This may be explained by an interaction of the cationic activated fibre with the delocalised π-electronic system of the dye molecule.

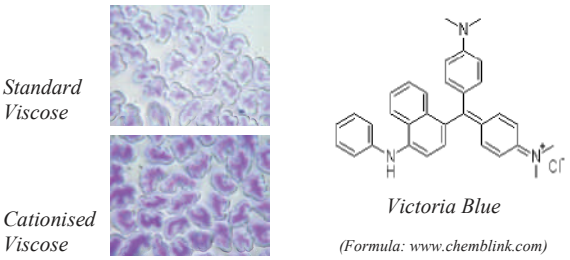

Figure 14. Fibres dyed with cationic dye.

Dye Absorption Kinetics

Time depending measurements show increasing dye absorption speed with increasing level of cationic activation of the fibre (Figure 15). An almost complete dye absorption was achieved within 10 minutes at 60 °C.

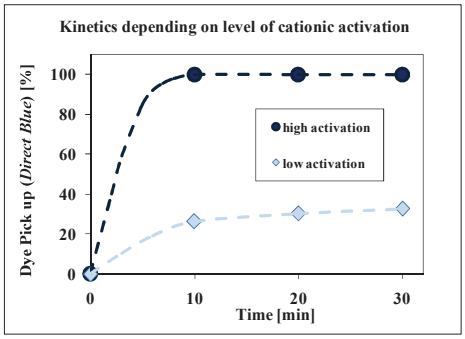

Figure 15. Time dependency of dye absorption.

Dye Transfer

A frequent problem in laundery is the bleeding of dyes from textiles which at the same time may lead to staining of other fabrics. The extent of bleeding from a textile respectively the level of staining of an adjacent fabric can be investigated in dye transfer tests. Figure 16 shows the stained adjacent fabrics of dye transfer tests

carried out with three different bleeding textile fabrics: Cotton dyed with Direct Orange 39, polyamide dyed with Acid Blue 113 and cotton dyed with Reactive Black 5. Depending on the bleeding dye different segments of the adjacent fabric were stained. For example, Acid Blue mainly stained wool, PA 6.6 and Cotton.

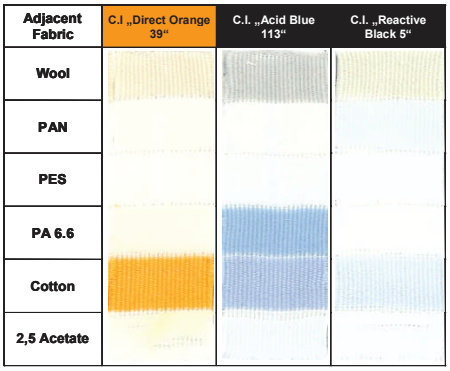

Figure 16. Dye transfer – reference trials.

In all trials the addition of cationic activated fibre reduced the dye transfer due to its high affinity to the dyes and speed of absorption. As a typical example, Figure 17 shows the results of the dye transfer with Acid Blue 113 when fibres with different level of cationic activation are added.

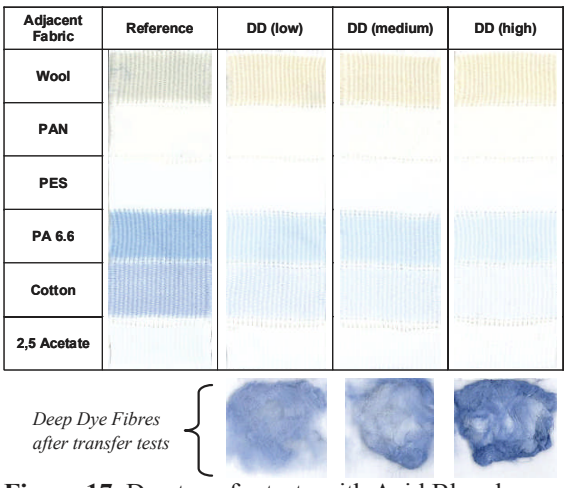

Figure 17. Dye transfer tests with Acid Blue dye.

With rising level of activation an increasing amount of bleeding dye is picked up by the fibre and accordingly the dye transfer to the adjacent fabric is reduced.

Conclusions

The described investigations regarding dye absorption capacity, kinetics and dye transfer prove the potential of the cationised Deep Dye Fibres to capture anionic substances. In addition to the superior dyeability of these fibres, the results also support their potential in applications for decolouring of aqueous media. High affinity of the cationised fibre was found for direct, reactive and acid dyes.
The level of cationic activation controls the colour absorption characteristics of Deep Dye fibres. The activation is distributed homogeneously throughout the cross section of the fibre.
A conversion of the Deep Dye fibre to textile and nonwoven fabrics without any loss of dye absorption activity and with standard equipment is possible.

Acknowledgements

We would like to thank Prof. Dr. Thomas Rauch (Hochschule für Angewandte Wissenschaften Hof, Abteilung Münchberg) for helpful discussions.

References

[1] Peter Sulek, Marina Crnoja-Cosic, Jörg Schlangen, Lenzinger Berichte 81 (2002), 22-26.

[2] M. Crnoja-Cosic, P. Sulek, G. Emlinger, J. Schlangen, Lenzinger Berichte, 82 (2003) 12-19.

[3] A. Schrell, A. von der Eltz, Hoechst Aktiengesellschaft, US Patent 5,542,955 (1996).

Lenzinger Berichte 89 (2011) 91-102

EINFLUSS DES FASERDURCHMESSERS AUF DIE STRUKTUR UND MECHANIK CELLULOSEFASER-VERSTÄRKTER PLA-KOMPOSITE

Jens Erdmann und Johannes Ganster

Fraunhofer-Institut für Angewandte Polymerforschung (IAP),
Geiselbergstr. 69, 14476 Potsdam-Golm, Deutschland
Tel.: (+49) 331 568-1252; Email: jens.erdmann@iap.fraunhofer.de,

Cellulosisches Reifencord-Garn (Rayon), welches bisher überwiegend in Form eines flächenhaften Gewebes in Hochgeschwindigkeitsreifen Anwendung findet, zeigt darüber hinaus großes Potential als biobasierte Verstärkungskomponente in thermo-plastischen Matrices. Derartige Fasern mit Durchmessern von 9, 12 und 17 µm wurden in eine thermoplastische Polymilchsäure (PLA)-Matrix eingearbeitet, der Masseanteil betrug 20 %. Der Einfluss des Faserdurchmessers auf die verarbeitungsbedingte Faserlängeneinkürzung und die resultierenden Kompositeigenschaften wurde untersucht. Die auf einem gegenläufigen Doppelschneckenextruder hergestellten Kurzfaser-verstärkten Komposite wurden hinsichtlich der Struktur und der mechanischen Eigenschaften charakterisiert. Die Analyse der Struktur umfasst sowohl die Faserlängenverteilung als auch die Bruchmorphologie. Die mechanischen Eigenschaften bei quasistatischer Belastung konnten durch den Zug- und Biegeversuch, bei schlagartiger Belastung durch den Charpy- und Durchstoßversuch bestimmt werden. Die Einarbeitung von Rayon-Fasern in PLA führt zu simultanen Verstärkungseffekten, die in Abhängigkeit des Faserdurchmessers variieren.

Stichwörter : *Komposit, Biopolymer, PLA, Cellulosefaser, Rayon*

Einleitung

Reifencord-Garn aus Cellulose (Rayon) wird seit den 60er Jahren hauptsächlich als Verstärkungskomponente in Hochgeschwindigkeitsreifen und später in Runflat-Reifen eingesetzt. Dieser Cellulosefaserstoff verstärkt in Form eines flächenhaften Gewebes die Karkasse.

Erste Versuche, derartige Fasern als Kurzfasern in thermoplastische Matrices einzuarbeiten, wurden bereits durch Amash *et* al. 1998 [1,2] unternommen. Zunächst diente Rayon verstärktes Polypropylen (PP) als Modelsystem. Systematische Untersuchungen hinsichtlich des Einflusses von Fasertyp, Fasergehalt, Haftvermittlertyp und Haftvermittlerkonzentration auf die resultierenden Kompositeigenschaften wurden von Ganster *et* al. [3,4] und Fink *et* al. [5] durchgeführt. Bereits moderate Fasergehalte im Bereich von 20 bis 30 Masse-% führen zu einer Verdreifachung der Festigkeit und des Moduls bzw. zu einer Verdopplung der Kerbschlagzähigkeit im Vergleich zu unverstärktem PP. Das Eigenschaftsniveau dieser Rayon-verstärkten PP-Komposite liegt durchaus im Bereich von Kurzglasfaser-verstärktem PP. Dabei verbessern die biobasierten, organischen Cellulosefasern nicht nur die Mechanik der PP-Matrix, sondern bieten darüber hinaus - gegenüber den konventionell zur Verstärkung eingesetzten Glasfasern - dem Compoundeur wie dem Anwender Vorteile bezüglich Gewicht, Abrasivität und Rezyklierbarkeit. Dass Rayon-verstärkte PP-Komposite das Potential besitzen, auch den Fahrzeuginnenraum u.a. in Form von Spritzgussbauteilen (z.B. Türverklei-

dungen) zu erobern, wurde bereits von Weigel *et* al. gezeigt [6]. Ausgehend von diesem Modelsystem wurden Rayon-Fasern bereits in eine Vielzahl von weiteren thermoplastischen Matrices eingearbeitet, z.B. in Polyethylen, High-Impact Polystyrol, biobasierte Polymilchsäure (PLA) oder Polyhydroxyalkanoat.
Auf Grund des biobasierten Charakters der Rayon-Faser ist diese prädestiniert zur Verstärkung von biobasierten Polymeren. Zum einen führt der Faseranteil zu einer Verbesserung des Eigenschaftsniveaus der Polymere, zum anderen bleibt der Komposit vollständig biobasiert und biologisch abbaubar. Insbesondere Polymilchsäure (PLA), welches als das kommende Commodity-Biopolymer gilt, rückt dabei mehr und mehr in den Fokus des Interesses. Das z.T. sehr geringe Schlagzähigkeitsniveau von PLA, wodurch der Einsatz für Bauteile in technischen Anwendungen noch limitiert ist, kann durch Rayon-Verstärkung deutlich angehoben werden [3,5,7-9]. Der vorliegende Beitrag behandelt durch Rayon-Verstärkung schlagzähmodifizierte PLA-Komposite. Diese wurden in einem speziell entwickelten kontinuierlichen Compoundierverfahren hergestellt und die Eigenschaften bei quasistatischer und schlagartiger Beanspruchung an Spritzgussprüfkörpern bestimmt. Als Verstärkungskomponente dienten drei Typen von Rayon-Fasern (Cordenka 610f), die sich bezüglich ihres Durchmessers im Bereich von 9 bis 17 µm voneinander unterscheiden. Der Einfluss des Faserdurchmessers auf die verarbeitungsbedingte Faserlängeneinkürzung und die resultierenden Kompositeigenschaften werden vorgestellt und diskutiert.

Materialien und Methoden

Material

Matrix
Als Matrixmaterial wurde ein für die Folienherstellung optimiertes und kommerziell erhältliches PLA vom Typ 4042D des Herstellers NatureWorks LLC verwendet. Die zahlgemittelte (M_n) bzw. massengemittelte Molmasse (M_w) dieses PLA-Typs beträgt 92.000 bzw. 170.000 g/mol. Der D-Anteil von 8 % ergibt sich aus einem optischen Drehwinkel von -144,05°. Der Schmelzflussindex (MFI), bestimmt unter einer Last von 2,16 kg bei 210°C, beträgt 18 g/10 min. Allen angegebenen Kennwerten liegen eigene Messungen zu Grunde.

Cellulosefaser
Der in diesem Beitrag verwendete Rayon Reifencord vom Typ Cordenka®610f lag im Anlieferungszustand als Multifilamentgarn vor und wurde von der Cordenka GmbH, (Obernburg, Deutschland) durch das Viskoseverfahren hergestellt. Durch Variation im Herstellungsprozess konnten drei unterschiedliche Multifilamentgarne bereitgestellt werden, die sich hinsichtlich des Durchmessers der Einzelfilamente bzw. Einzelfasern unterscheiden. Die im Beitrag berücksichtigten Multifilamentgarne, der Durchmesser bzw. Titer der Einzelfilamente mit entsprechenden Probenbezeichnungen sind in Tabelle 1 zusammengefasst. Bei der Berechnung des Einzelfaserdurchmessers unter Berücksichtigung des Titers und der Stoffdichte von 1,5 g/cm^3 wurde vereinfacht ein idealer, kreisrunder Faserquerschnitt angenommen.

Methoden

Einzelfasermessung
Die mechanischen Kennwerte Zugfestigkeit ($\sigma_{f,\,max}$), Modul und Bruchdehnung ($\varepsilon_{f,\,b}$) der Einzelfasern wurden an einer Zwick Z020 Universalprüfmaschine bestimmt, mit einer 10 N Kraftmessdose, bei 20 mm Einspannlänge und einer Prüfgeschwindigkeit von 10 mm/min entsprechend der Norm EN ISO 5079. Die in Tabelle 3 dargestellten Kennwerte wurden durch Mittelwertbildung aus mindestens 30 Einzelprüfungen bestimmt.

Vor der Prüfung wurden alle Faserproben für einen definierten Zeitraum in einem klimatisierten Prüflabor bei 23°C und 50 % relativer Luftfeuchte konditioniert, um einen einheitlichen Gleichgewichtsfeuchtegehalt von 10,5 % zu gewährleisten.

Tabelle 1. Einzelfasertiter bzw. -durchmesser mit Probenbezeichnung der verwendeten Multifilamentgarne.

Material	Proben-bezeichnung	Titer	Durchmesser, D
		[dtex]	[µm]
Cordenka 610 F 0.9	d9	0.9	8.7
Cordenka 610 F 1.8	d12	1,8	12.4
Cordenka 610 F 3.4	d17	3.4	16.9

Faserlängenverteilung
Die Isolierung der Cellulosefasern aus der PLA-Matrix erfolgte nach dem Soxleth-Verfahren unter Verwendung von Chloroform als Lösungsmittel. Nach 16-stündiger Extraktionszeit bei 60 °C waren die Fasern vollständig von Matrixmaterial befreit. Die untereinander stark verhakten Einzelfasern konnten anschließend in einem Wasserbad mit Hilfe eines Ultraschallgerätes vollständig vereinzelt werden. Eine repräsentative Menge der Wasser-Faser-Suspension wurde auf einen Objektträger präpariert und getrocknet. Somit war es möglich, die Fasern bei 5-facher Vergrößerung mit einem Jenalab Polarisationsmikroskop aufzunehmen und mit der Analysis 3.2 Bildverarbeitungssoftware hinsichtlich der Länge zu vermessen. Für die Darstellung der anzahl- ($H_{i,Anzahl}$) und volumenbezogenen ($H_{i,Volumen}$) Häufigkeitsverteilung mit einer Klassenbreite von 100 µm wurden je Probe 600 Fasern vermessen. Eine Kurvenanpassung der Häufigkeitsverteilungen konnte durch Anwendung der folgenden Peakfunktion nach Giddings realisiert werden:

$$y = y_0 + \frac{A}{w}\sqrt{\frac{x_c}{x}}\mathrm{I}_1\left(\frac{2\sqrt{x_c x}}{w}\right)e^{\frac{-x-x_c}{w}} \quad (1)$$

Compoundierung
Zur Herstellung der Granulate wurde in einem ersten Schritt ein Pultrusionsverfahren angewendet, bei dem über eine spezielle Düse 10 Multifilamentgarnstränge mit dem aufgeschmolzenen PLA ummantelt wurden. Die Anzahl der Stränge bestimmt den Faseranteil, der für alle Komposite bei 20 Masse-% lag. Nach Abkühlen des Stranges wurde dieser unter Verwendung eines Granulators (CSG 171 der Fa. Collin) auf eine Länge von 7 mm geschnitten. Nach der Trocknung für 2 h bei 85 °C wurde das nun rieselfähige Granulat in einem zweiten Schritt nochmals extrudiert, dabei homogenisiert, anschließend erneut granuliert (7 mm) und vor der weiteren Verarbeitung (Spritzguss) bei 85 °C für 4 h getrocknet. Bei beiden Verarbeitungsschritten, d.h. Ummantelung und Homogenisierung, wurde ein gegenläufiger Doppelschneckenextruder der Firma Haake (Rheocord 9000 mit PTW 25) verwendet. Die Compoundierung erfolgte bei einer maximalen Extruder- bzw. Düsentemperatur von 170 °C.

Spritzguss
Das nach dem zweiten Verarbeitungsschritt homogenisierte Granulat wurde nach DIN EN ISO 527-2 mittels einer Arburg Allrounder 270 M 500-90 Spritzgießmaschine bei einer Temperatur von 170 - 180 °C und einen Spritzdruck von 1000-1200 bar zu Normprüfkörpern in Schulterstab- (Typ 1A) bzw. Plattengeometrie verarbeitet.

Komposit-Charakterisierung
Die unter quasistatischer Beanspruchung ermittelten mechanischen Kennwerte Zugfestigkeit (σ_{max}), -modul (E_{Zug}), Reißdehnung (ε_B), und Biegemodul (E_{Biege}) wurden entsprechend der Normen DIN EN ISO 527 und 178 an einer Zugprüfmaschine Zwick 1445 ermittelt.

Die bei schlagartiger Beanspruchung ermittelten Kennwerte Charpy-Schlagzähigkeit (a_c) und Kerbschlagzähigkeit (a_{cN}) bzw. die absorbierte Durchstoßenergie (E_P), die dabei auftretende Höchstkraft (F_M) sowie das Verhältnis von Verlust- zu Speicherarbeit (Materialdämpfung, Δ), wurden unter Berücksichtigung der Normen DIN EN ISO 179 und 6603-2 an einem Pendelschlagwerk der Fa. Ohst bzw. an einem Fallwerk der Fa. Ceast bestimmt. Alle Prüfkörper wurden vor der Prüfung für einen definierten Zeitraum in einem klimatisierten Prüflabor bei 23 °C und 50 % relativer Luftfeuchte konditioniert. In Tabelle 2 sind alle verwendeten Geräte zur mechanischen Charakterisierung der Komposite sowie die ermittelten Kennwerte und die entsprechenden Normen zusammengefasst.

Tabelle 2. Zusammenfassung der mechanischen Charakterisierungsmethoden, der ermittelten Kennwerte und der berücksichtigten DIN-Normen.

Charakterisierungs-methode	Gerät	Kennwert		Norm DIN EN ISO
Zug-Versuch	Zugprüfmaschine *Zwick 1445*	Festigkeit	σ_{max}	527
		Zug-Modul	E_{Zug}	
		Bruchdehnung	ε_b	
Biege-Versuch	Zugprüfmaschine *Zwick 1445*	Biegefestigkeit	$\sigma_{f,max}$	178
		Biege-Modul	E_{Biege}	
		Biegespannung bei 3,5% Randfaserdehnung	$\sigma_{f,3.5\%}$	
Charpy-Versuch	Pendelschlagwerk *Ohst*	Schlagzähigkeit	a_c	179
		Kerbschlagzähigkeit	a_{cN}	
Durchstoß-Versuch Rebound-Versuch	Fallwerk *Fractoris*	Durchstoßenergie	E_P	6603-2
		Höchstkraft	F_M	
		Dämpfung: Verlust-/ Speicherarbeit	Δ	

Tabelle 3. Die mechanischen Eigenschaften der verwendeten Fasern, bestimmt durch Einzelfaserprüfung.

Faser	Festigkeit $\sigma_{f,max}$				Modul			Bruchdehnung	
	Ø*	s**	Ø	Ø	Ø	s	Ø	Ø	s
	[cN/tex]	[cN/tex]	[MPa]	[cN]	[cN/tex]	[cN/tex]	[GPa]	[%]	[%]
d9	51	2,5	765	4,6	1,27	0,08	19,0	10,1	0,9
d12	52	3,0	780	9,4	1,32	0,1	19,8	12,9	1,5
d17	52	3,4	780	17,6	1,34	0,08	20,1	14,5	1,4
Enka***			220				9,4	17,2	

* Mittelwert
** Standardabweichung
*** Werte aus der Literatur nach Eichhorn *et* al. [10]

Ergebnisse und Diskussion

Einzelfasereigenschaften

Die in diesem Beitrag untersuchten cellulosischen Hochleistungs-Viskosefasern (Rayon) liegen hinsichtlich ihrer mechanischen Eigenschaften (Tabelle 3) weit über dem Niveau von textilen, cellulosischen Viskosefasern (Enka). Die Festigkeiten der Rayon-Fasern schwanken im Bereich von 825 bis 735 MPa nur unwesentlich um den Mittelwert. Detaillierte Untersuchungen haben diesbezüglich Ganster *et* al. in [4] unternommen, die die Wahrscheinlichkeitsdichtefunktionen der relativen Festigkeitsverteilung ausgewertet haben. Sie stellten fest, dass die Einheitlichkeit der Eigenschaften von Cellulosefasern im Vergleich zu Natur- oder Glasfasern sehr hoch ist und dies positive Auswirkung auf die Kompositeigenschaften haben kann. Denn die Wahrscheinlichkeit für einen frühzeitigen Faserbruch, der zum Versagen des Komposites führen würde, ist sehr gering.

Mit abnehmendem Faserdurchmesser ändern sich die Fasereigenschaften nur unwesentlich, während Festigkeit und Modul nahezu unbeeinflusst bleiben, steigt die Bruchdehnung geringfügig an.

Ob die Fasern im Komposit verstärkend wirken, hängt maßgeblich von deren Länge ab. Ein ausreichender Spannungstransfer von der Matrix auf die Faser ist nur dann gewährleistet, wenn die im Komposit vorliegenden Fasern die kritische Faserlänge l_c überschreiten. Die kritische Faserlänge hängt vom Faserdurchmesser D, der Faserfestigkeit $\sigma_{f,\,max}$ und der Matrixschubfestigkeit τ_m nach folgender Beziehung ab:

$$l_{c,\,th} = \frac{\sigma_{f,\,\max}\, D}{2\tau_m} \qquad (2)$$

$$\tau_m = \frac{\sigma_{m,\,\max}}{\sqrt{3}} = 0{,}577 \cdot \sigma_{m,\,\max} \qquad (3)$$

Legt man bei der Berechnung die Matrixzugfestigkeit $\sigma_{m,\,max}$ von 70 MPa für das verwendete PLA, die ermittelten Durchmesser D (Tabelle 1) bzw. Festigkeiten $\sigma_{f,\,max}$ (Tabelle 3) der eingearbeiteten Fasern zu Grunde, ergeben sich die in Tabelle 4 zusammengefassten Werte für die kritische Faserlänge $l_{c,th}$. Der Zusammenhang nach Formel 2 gilt jedoch nur unter der Bedingung einer ideal zylindrischen Fasergeometrie sowie der idealen Faser-Matrix-Haftung. Beide Bedingungen sind in den untersuchten Rayon-PLA-Kompositen nicht erfüllt. Eine experimentelle Bestimmung der kritischen Faserlänge $l_{c,exp}$ umgeht beide Bedingungen und liefert Werte, die spezifisch für den jeweiligen Komposit sind. Die experimentelle Bestimmung von $l_{c,exp}$ geht auf eine Methode nach Ehrenstein [11] zurück und wurde wie folgt durchgeführt. Die kritische Faserlänge entspricht, für den reinen Versagensfall von gebrochenen, in Zugspannungsrichtung verstärkten Proben, der maximal auftretenden Länge der Auszugsfasern. Diese wurden an den Bruchflächen getesteter Zugprüfkörper im Bereich der höchsten Faserorientierung (Prüfkörperrand) mittels Rasterelektronenmikroskopie und der Bildverarbeitungssoftware Analysis 3.2 bestimmt und in Tabelle 4 vergleichend dargestellt.

Tabelle 4. Berechnete und experimentell bestimmte kritische Faserlänge in Abhängigkeit des Faserdurchmessers.

Faser	kritische Faserlänge theoretisch $l_{c,th}$ [µm]	experimentell $l_{c,exp}$ [µm]
d9	82	260
d12	120	275
d17	163	310

Zwar unterscheiden sich die Werte für die theoretisch und experimentell bestimmte kritische Faserlänge deutlich voneinander, jedoch ist die Tendenz hinsichtlich der Abhängigkeit vom Faserdurchmesser identisch. Jedwede Abweichung von der idealen Haftung zur Matrix sowie von der

zylindrischen Fasergeometrie resultiert in einen weniger effizienten Spannungstransfer von der Matrix auf die Faser und somit in eine Zunahme der kritischen Faserlänge. Da in den untersuchten Cellulosefaser-PLA-Kompositen auf Grund der fehlenden kovalenten Verknüpfungen zwischen Faser und Matrix keine ideale Haftung vorliegt und darüber hinaus die Fasern keinen kreisrunden, sondern einen nierenförmigen Querschnitt aufweisen, ist der deutliche Anstieg der experimentell bestimmten zur berechneten kritischen Faserlänge nicht überraschend. Mit abnehmendem Faserdurchmesser nimmt die kritische Faserlänge ab. Dünnere Fasern verstärken die PLA-Matrix demzufolge effizienter, da der Spannungstransfer von der Matrix auf die Faser auf Grund der höheren Wechselwirkungsfläche (Grenzfläche), begünstigt ist.

Faserlängenverteilung

Während der Compoundierung im gegenläufigen Doppelschneckenextruder und auch während der Formgebung der Kompositmaterialien durch das Spritzgießverfahren wirken erhebliche Kräfte auf die Fasern. Insbesondere durch Misch- und Knetelemente werden über Scherung Kräfte auf die Faser übertragen, die zwangsläufig zum Bruch führen.

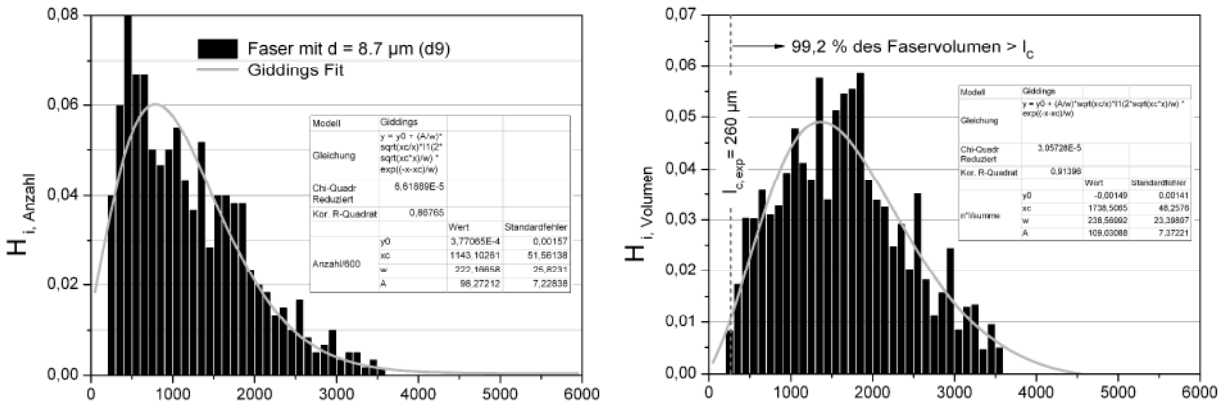

Abbildung 1a. Links anzahlbezogene ($H_{i,Anzahl}$) und rechts volumenbezogene ($H_{i,Volumen}$) Faserlängen-Häufigkeitsverteilung für Fasern unterschiedlichen Durchmessers (d9) nach Compoundierung und Spritzgießverarbeitung.

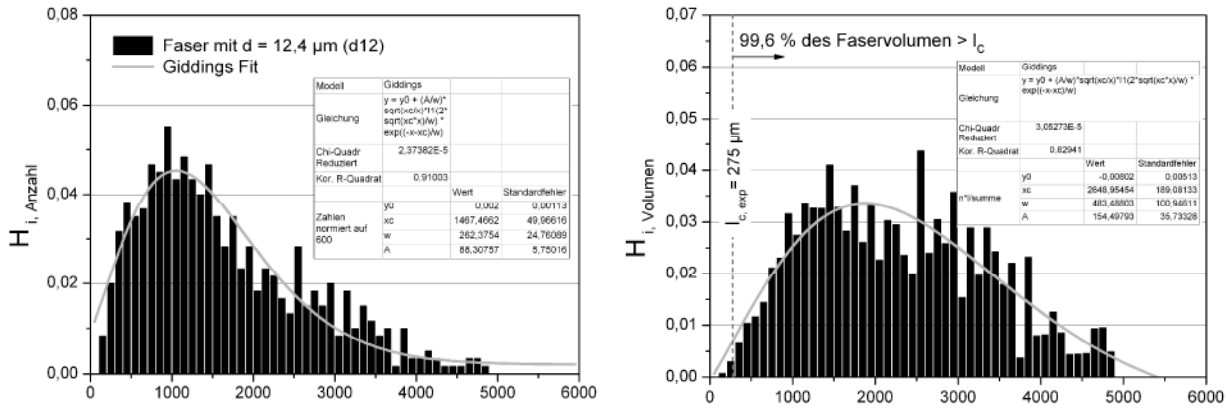

Abbildung 1b. Links anzahlbezogene ($H_{i,Anzahl}$) und rechts volumenbezogene ($H_{i,Volumen}$) Faserlängen-Häufigkeitsverteilung für Fasern unterschiedlichen Durchmessers (d12) nach Compoundierung und Spritzgießverarbeitung.

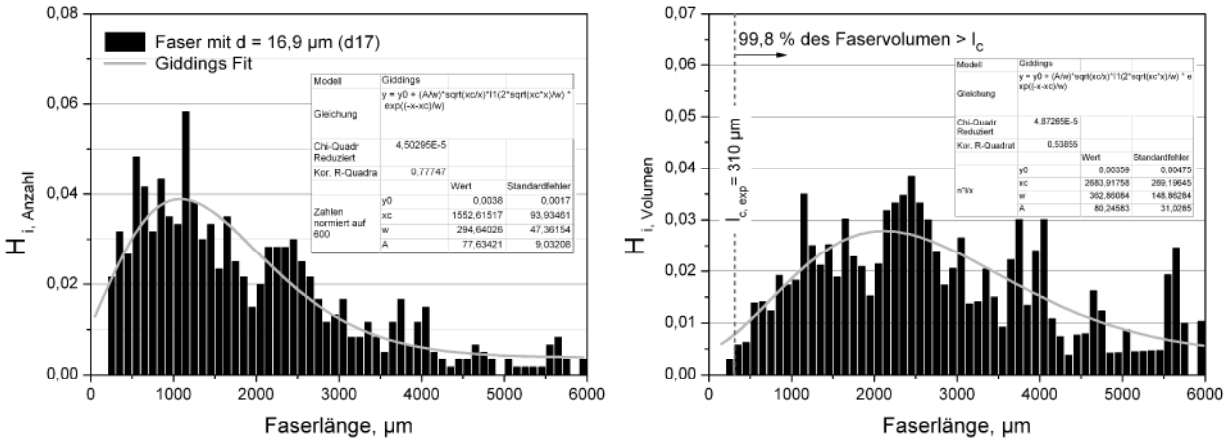

Abbildung 1c. Links anzahlbezogene ($H_{i,Anzahl}$) und rechts volumenbezogene ($H_{i,Volumen}$) Faserlängen-Häufigkeitsverteilung für Fasern unterschiedlichen Durchmessers (d17) nach Compoundierung und Spritzgießverarbeitung.

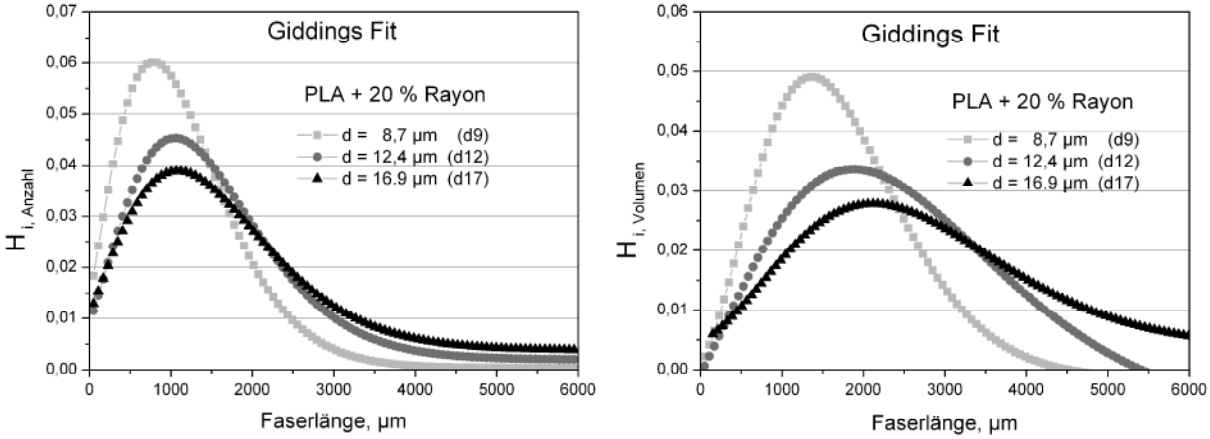

Abbildung 2. Vergleichende Darstellung der anzahl- und volumenbezogen Faserlängen-Häufigkeitsverteilung (Giddings-Fit) für Fasern unterschiedlichen Durchmessers nach Compoundierung und Spritzgießverarbeitung.

Aus der Analyse der anzahl- ($H_{i,Anzahl}$) und volumenbezogenen ($H_{i,Volumen}$) Häufigkeitsverteilungen der Faserlängen in Abbildung 1 sowie aus der Gegenüberstellung der Ausgleichsgeraden in Abbildung 2 ist in Abhängigkeit des Faserdurchmessers ein eindeutiger Trend erkennbar. Mit zunehmendem Faserdurchmesser wird die Verteilung der Faserlängen breiter, die lokalen Maxima verschieben sich hin zu höheren Werten, die Anzahl und das Volumen der kurzen Fasern sinken, während Anzahl und Volumen der längeren Fasern steigen. Liegen für d17 noch einige Fasern im Bereich zwischen 4 und 6 mm Länge, sind diese für d9 schon nicht mehr vorhanden. Auch die aus den Häufigkeitsverteilungen berechneten Kennwerte in Tabelle 5 spiegeln diesen Trend wieder.

Sind die Fasern vor der Verarbeitung im Mittel noch 7 mm lang, führt die verarbeitungsbedingte Fasereinkürzung für d17 zu einer Abnahme der mittleren Faserlänge auf 1,9 mm, für d9 sogar auf 1,2 mm. Je dünner der Durchmesser einer Faser, desto häufiger bricht diese während des Verarbeitungsprozesses. Zum einen auf Grund des geringeren mechanischen Widerstandes gegenüber den einwirkenden Kräften (Tabelle 3, d9 = 4,6 cN gegenüber d17 = 17,6 cN), zum anderen ist die Krafteinleitung durch die höhere Wechselwirkungsfläche begünstigt.

Tabelle 5. Berechnete Kennwerte aus der anzahl- und volumenbezogenen Faserlängen-Häufigkeitsverteilung in Abhängigkeit des Faserdurchmessers.

Faser	Häufigkeitsverteilung					verstärkendes Faservolumen im Komposit
	Vor	Nach der Verarbeitung				
		$H_{i,Anzahl}$		$H_{i,Volumen}$		
	Mittelwert	Mittelwert	Median	Mittelwert, l_f	Median	
	[mm]	[mm]	[mm]	[mm]	[mm]	[%]
d9	~ 7,0	1,21	1,08	1,74	0,97	99,2
d12	~ 7,0	1,66	1,44	2,26	1,23	99,6
d17	~ 7,0	1,91	1,61	2,76	1,34	99,8

Trotz der ausgeprägten Faserlängeneinkürzung während der Verarbeitung liegen für die drei untersuchten Fasertypen d9, d12 und d17 mehr als 99 % des eingearbeiteten Faservolumens über der kritischen Faserlänge $l_{c,exp}$ und wirken somit im Komposit verstärkend (siehe Abbildung 1 und Tabelle 5).

Kompositeigenschaften

Einfluss der Cellulosefaser

Bereits die ersten Versuche, PLA und Cellulosefasern miteinander zu compoundieren, brachten ohne hohen Aufwand hinsichtlich Prozess- und Rezepturoptimierung beachtliche Erfolge. Die in Abbildung 3 gezeigte Bruchfläche eines solchen Compounds verdeutlicht, dass trotz der extrem unterschiedlichen Hydrophilie der Einzelkomponenten sehr homogen strukturierte Polymer-Faser Materialien mit einer hinreichend guten Haftung erzeugt werden konnten.

Zwar bewirkt eine Kompatibilisierung des Materialsystems durch Zugabe von 1 Masse-% Hexamethylendiisocyanat eine Verbesserung der Faser-Matrix-Haftung, jedoch ist der Zugewinn der mechanischen Kompositeigenschaften hinsichtlich Festigkeit mit 15 % und der Schlagzähigkeit mit 10 % nicht signifikant [12, 13].

Auch ohne Kompatibilisierung führt ein Cellulosefaseranteil von 20 Masse-% zu einer deutlichen Verbesserung des ohnehin schon hohen Eigenschaftsniveaus von PLA. Wie Abbildung 4 veranschaulicht, steigt für den Komposit die Zug- bzw. Biegefestigkeit um 30 % bzw. 35 % auf 90 bzw. 120 MPa gegenüber unverstärktem PLA. Darüber hinaus nimmt die Materialsteifigkeit, quantifiziert durch die Kennwerte des Zug- bzw. Biegemoduls, um 40 % bzw. 50 % auf 3,7 bzw. 4,9 GPa zu.

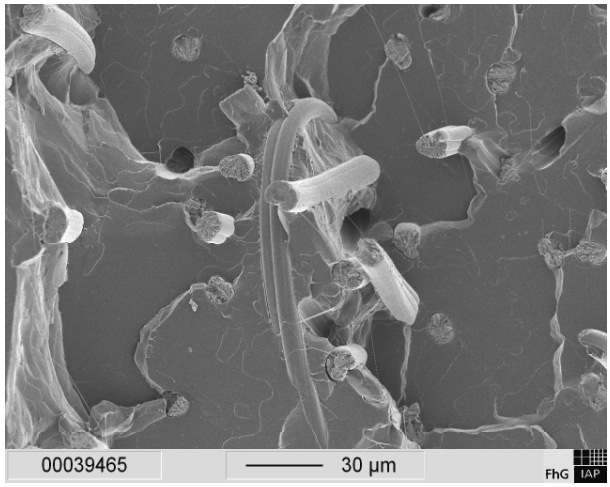

Abbildung 3. Mittels Rasterelektronenmikroskop aufgenommene Bruchfläche eines mit 20 Masse-% Cellulosefaser (d12) verstärkten PLA-Komposites.

Bemerkenswert ist, dass durch den Cellulosefaseranteil in der PLA-Matrix der Widerstand des Komposites nicht nur gegenüber quasistatischer Belastung, sondern darüberhinaus und in einem noch höheren Maße gegenüber schlagartiger Beanspruchung zunimmt. Das signifikant höhere Schlagenergieabsorptionvermögen der Komposite gegenüber der unverstärkten PLA-Matrix ist in Abbildung 5 durch die ermittelten Kennwerte aus dem Charpy-Schlag- bzw. Durchstoßversuch beziffert.

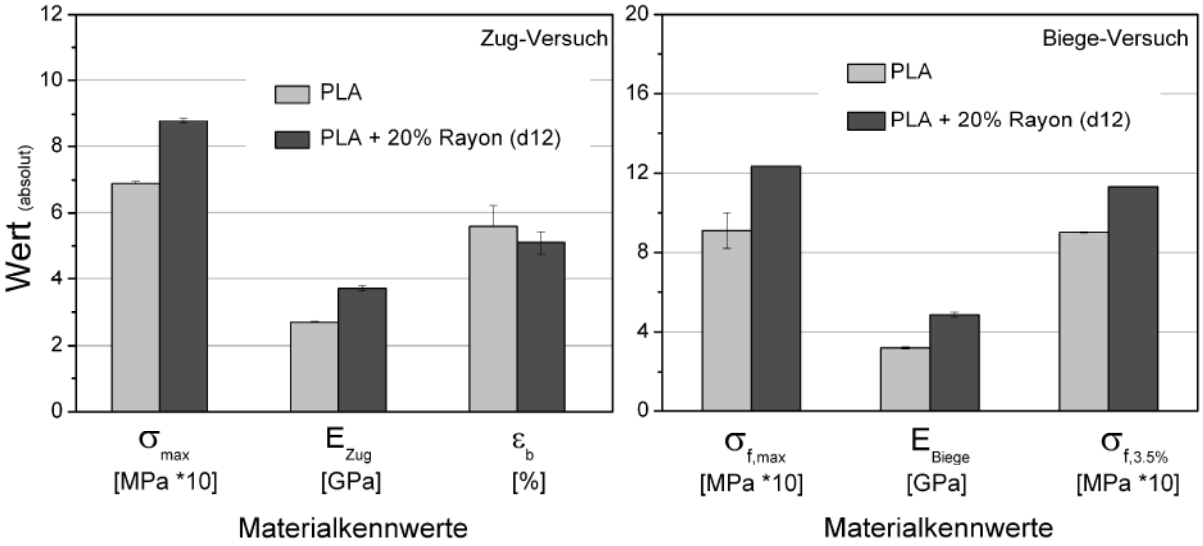

Abbildung 4. Einfluss der Cellulosefaser-Verstärkung auf die bei quasistatischer Beanspruchung ermittelten mechanischen Kennwerte aus dem Zug- und Biegeversuch.

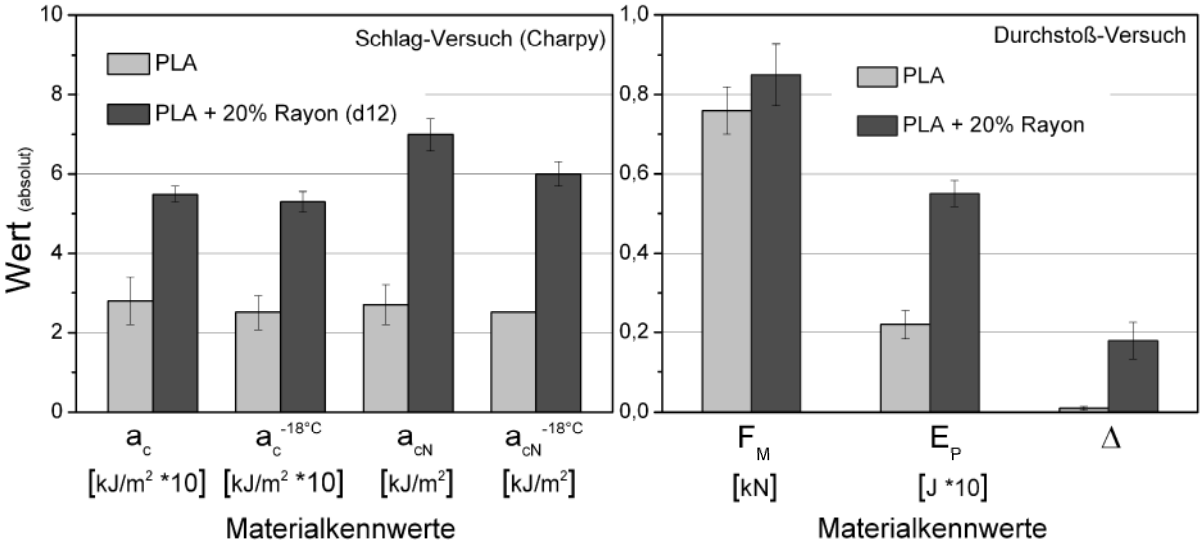

Abbildung 5. Einfluss der Cellulosefaser-Verstärkung auf die bei schlagartiger Beanspruchung ermittelten mechanischen Kennwerte aus dem Schlag- und Durchstoßversuch.

Die gekerbten und ungekerbten Charpy-Schlagzähigkeiten steigen gegenüber unverstärktem PLA sowohl bei Raumtemperatur als auch bei -18 °C auf das Zwei- bis Dreifache, die beim Fallbolzen-Durchstoß absorbierte Energie (E_P) verdreifacht sich. Der beim Rebound-Versuch (Rückprall des Fallbolzens) ermittelte Kennwert der Materialdämpfung (Δ), das Verhältnis von Verlust- zu Speicherarbeit, steigt durch die Faserverstärkung von ca. 0,01 auf 0,2. Der zusätzliche Beitrag an Verlustarbeit wird durch plastische Deformationen an der Faser-Matrix-Grenzfläche (Debonding) hervorgerufen, die jedoch nicht zum Versagen des Komposites führen.

Einfluss des Cellulosefaser-Durchmessers

In Abbildung 6 sind die mechanischen Eigenschaften der mit 20 Masse-% Rayon-verstärkten Komposite in Abhängigkeit des Faser-Aspektverhältnisses λ grafisch dargestellt. Sowohl die Faserlänge als auch der Faserdurchmesser sind für die Zug- und Biegeeigenschaften des Komposites bestimmend. Das Aspektverhältnis λ, der Quotient aus der Faserlänge und dem

Faserdurchmesser (Tabelle 1), wurde auf Basis der vorgestellten Ergebnisse ermittelt. Da für die Faserlänge der volumenbezogene Mittelwert der Häufigkeitsverteilungen (l_f, Tabelle 5) herangezogen wurde, kann λ nur als Näherung angesehen werden, steht aber in einem streng linearen Zusammenhang mit den Kompositeigenschaften. Mit steigendem Aspektverhältnis, d.h. abnehmendem Faserdurchmesser von d17 nach d9, steigt die Komposit-Zugfestigkeit von 84 auf 92 MPa (um 10 %), die Biegefestigkeit von 121 auf 126 MPa und der Biegemodul von 4,7 auf 5,1 GPa (um 10 %). Der Zugewinn dieser Kompositeigenschaften beruht auf der höheren Matrix-Faser-Wechselwirkungsfläche, wodurch ein effektiverer Spannungstransfer gewährleistet ist.

Entgegen den Erwartungen und bereits publizierten Ergebnissen nach Ganster *et* al. [4] und Thomason *et* al. [14, 15] für vergleichbare Materialsysteme (PP-Matrix) fällt der Zugmodul mit steigendem Faseraspektverhältnis λ von 3,8 auf 3,3 GPa. Dies ist möglicherweise darauf zurückzuführen, dass dünnere Fasern (im System ohne Faser-Matrix-Kompatibilisierung) während des Spritzgießprozesses weniger gut in Richtung der Prüfkörperlängsachse orientierbar sind.

Abbildung 7, links zeigt den Zusammenhang zwischen den Komposit-Kerbschlagzähigkeiten bzw. –Bruchdehnungen und der mittleren volumenbezogenen Faserlänge l_f. Diese Darstellung wurde gewählt, da die Faserlänge im Vergleich zum Faserdurchmesser in höherem Maße bestimmend für die relevanten Kompositeigenschaften ist [14-16]. Mit zunehmender Faserlänge l_f, d.h. mit steigendem Faserdurchmesser von d9 nach d17, nimmt die Kerbschlagzähigkeit der Komposite von 5,5 auf 8 kJ/m^2 um 45 % zu. Ein ähnlicher Trend wurde für Rayon-verstärktes PP gefunden und in [4] publiziert.

Mit zunehmender Faserlänge l_f (von d9 nach d17) reduziert sich die Bruchdehnung der Komposite von 5,4 auf 4,7 % Dehnung. Für den experimentellen Befund der zunehmenden Einzelfaser-Bruchdehnung von d9 nach d17 (Tabelle 3) sowie der geringeren Faseranzahl im Komposit, wodurch bruchauslösende potentielle Fehlstellen (Faserenden) im Material unwahrscheinlicher sind, wäre eine Steigerung der Komposit-Bruchdehnung zu erwarten gewesen. Hinsichtlich der Komposit-Schlagzähigkeit konnte mit 55 kJ/m^2 ein Optimum für d12 identifiziert werden.

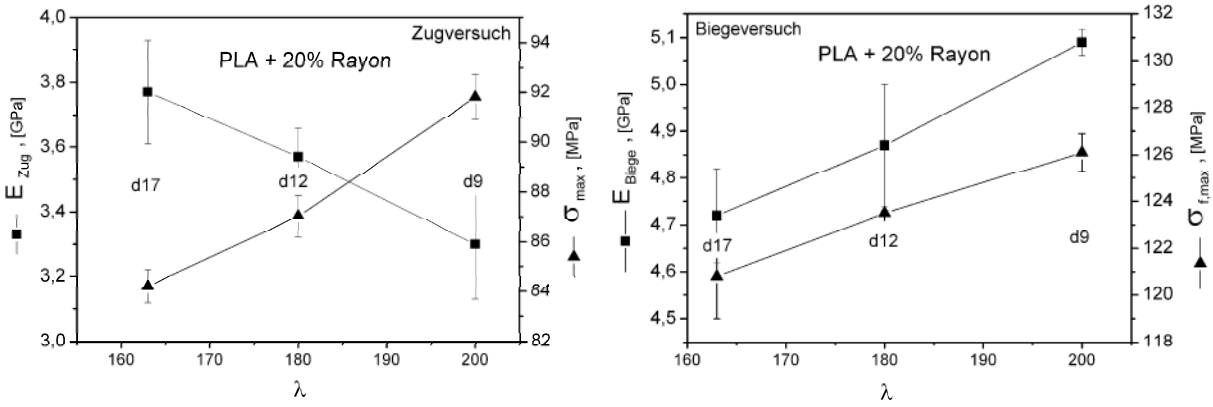

Abbildung 6. Einfluss des Cellulosefaser-Aspektverhältnisses auf die mechanischen Zug- und Biegeeigenschaften der Komposite.

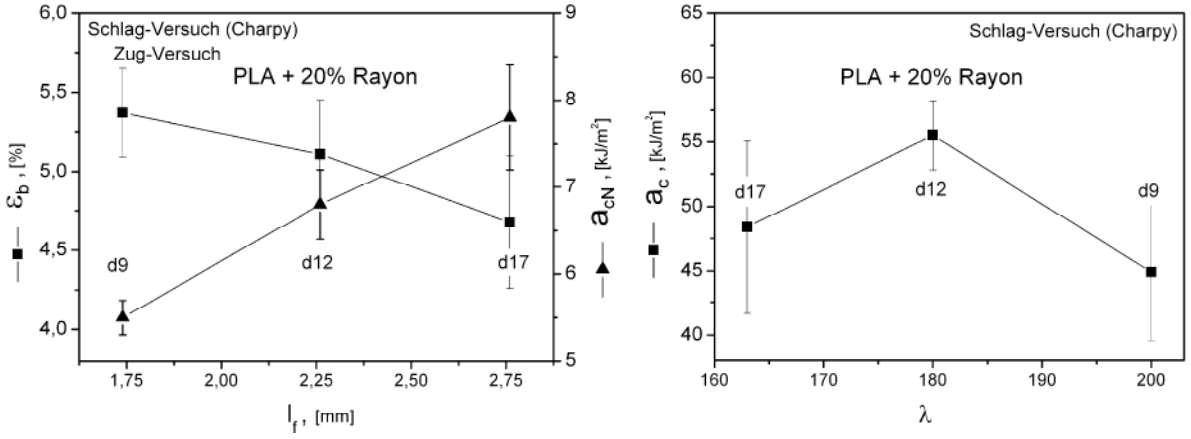

Abbildung 7. Einfluss der volumenbezogenen, mittleren Faserlänge l_f bzw. des Cellulosefaser-Aspektverhältnisses auf die Schlag- und Zugeigenschaften der Komposite.

Zusammenfassung und Schlussfolgerungen

Schon geringe Anteile von hochfesten Cellulosefasern (20 Masse-%) in der PLA-Matrix führen zu deutlichen und simultanen Verstärkungseffekten, auch ohne zusätzliche Kompatibilisierung von Faser und Matrix. Der Eigenschaftszugewinn gilt für den Widerstand der Kompositmaterialien gegenüber quasi-statischer, aber bemerkenswerterweise in viel höherem Maße gegenüber schlagartiger Beanspruchung. Ohne dass Weichmacher und/oder duktile bzw. weiche Polymere eingearbeitet werden müssen, kann durch Cellulosfaser-Verstärkung der spröde Charakter von PLA z.T. überwunden werden. Die Auswertung der im Komposit vorliegenden Faserlängen ergab, dass als Folge der Compoundierung und Spritzgießformgebung eine intensive Einkürzung der Fasern von im Mittel 7 mm auf 1,2 mm Länge stattfindet. Mit abnehmendem Faserdurchmesser verstärkt sich die verarbeitungsbedingte Faserlängeneinkürzung zusätzlich. Dennoch ist die Verstärkung für die untersuchten Komposite gegeben, da mehr als 99 % des Faservolumens über der experimentell ermittelten, kritischen Faserlänge liegt. Bei einem konstanten Faseranteil von 20 Masse-% steigen mit abnehmendem Faserdurchmesser der Biegemodul, die Biege- und Zugfestigkeit sowie die Bruchdehnung des Komposites, während die Kerbschlagzähigkeit und der Zug-Modul abfallen. Für die Komposit-Schlagzähigkeit konnte ein Optimum gefunden werden.

Danksagung

Wir danken Herrn A. Jaszkiewicz (Universität Kassel) für die Durchführung der Durchstoß- und Reboundversuche.

Literatur

[1] Amash, A.; Zugenmaier, P. Polymer Bulletin, 1998, 40, S. 251-258.
[2] Amash, A.; Zugenmaier, P. Polymer 2000, 41, S. 1589-1596.
[3] Ganster, J.; Fink, H.-P.; Pinnow, M. Composites Part A, 2006, 37, S. 1796-1804.
[4] Ganster, J.; Fink, H.-P.; Uihlein, K.; Zimmerer, B. Cellulose, 2008, 15, S. 561-569.
[5] Fink, H.-P.; Ganster, J. Macromol. Symp., 2006, 244, S. 107-118.
[6] Weigel, P.; Ganster, J.; Fink, H.-P.; Gassan, J.; Uihlein, K. Kunststoffe, 2002, 92, 5, S. 95-97.
[7] Graupner, N.; Herrmann, A.S.; Müssig, J. Composites Part A, 2009, 40, S. 810-821.
[8] Bax, B.; Müssig, J. Compos. Sci. Technol., 2008, 68, S. 1601-1607.

[9] Bledzki, A.K.; Jaszkiewicz, A. Compos. Sci. Technol., 2010, 70, S. 1687-1696.
[10] Eichhorn, S-J.; Sirichaisit, J.; Young, R-J. J. Mater. Sci., 2001, 36, S. 3129-3135.
[11] Ehrenstein, G-W. Faserverbund-Kunststoffe: Werkstoffe, Verarbeitung, 2002, ISBN 3-446-17328-5.
[12] Erdmann, J.; Ganster, J. Vortrag, Narotech, 8. Internationales Symposium, 2010, Erfurt.
[13] Ganster, J., Erdmann, J. Vortrag, 14th International Conference Polymeric Materials (P.2010), 2010, Halle-Saale, ISBN 978-3-86829-2824.
[14] Thomason, J.L.; Vlug, M.A.; Schipper, G. Composites Part A, 1996, 27, S. 1075-1084.
[15] Thomason, J.L.; Vlug, M.A. Composites Part A, 1996, 27, S. 477-484.
[16] Thomason, J.L.; Vlug, M.A. Composites Part A, 1997, 28, S. 277-288.

Lenzinger Berichte 89 (2011) 103-108

TENCELWEB™ DEVELOPMENTS

Mirko Einzmann[1], Malcolm Hayhurst[1], Marco Gallo[1] and Mengkui Luo[2]

[1] Lenzing AG, Werkstr. 1, 4860 Lenzing, Austria
[2] Weyerhaeuser Co., 32901 Weyerhaeuser Way S., WTC 2F38, Federal Way, WA 98001, USA

Phone: (+43) 7672 701-2833; Fax: (+43) 7672 918-2833; Email: m.einzmann@lenzing.com

Presented during the 49th Dornbirn Man-Made Fibers Congress, Austria, 2010

TencelWeb™ is a new technology which allows the direct manufacture of cellulosic webs from Lyocell spinning solution. In the past, melt-blown technology for cellulose proved uneconomic due to the low cellulose content of Lyocell spinning solution and resultant low output from spinning beams. Newer approaches which were developed for synthetic web manufacture suggested higher productivities and gave rise to re-assess the potential for a productive and cost-effective web formation technology based on Lyocell spinning solution. A successful development of this technology would allow the manufacture of cellulosic fine fibre products and light-weight webs.

Keywords: *TENCEL, melt-blow, lyocell, nonwovens*

Introduction

As officially announced in July 2008, Lenzing, the world market leader in cellulose staple fibres, and Weyerhaeuser, one of the world's largest forest products companies, signed a joint development agreement to investigate potential melt-blown technologies for cellulose: Weyerhaeuser contributes extensive knowledge on pulp manufacture and paper production technology while Lenzing adds over twenty years of Lyocell expertise. Both companies together have extensive intellectual property rights in the areas of interest.

Until the end of year 2008 several series of lab scale trials with small jet units were carried out. In parallel an iterative design & development programme for a pilot plant concept was driven forward. When results looked promising enough the decision was made to build a larger pilot line in order to better understand the key process economics and the unique capabilities of the TencelWeb™ process. The pilot line is located at Lenzing, Austria, and started operation in May 2009.

The line is designed for a capacity of up to 150 kg/h cellulose web with the possibility to run more than one spinning beam. Due to the importance of filament coagulation, a highly flexible arrangement of coagulation spray bars was installed between the melt-blown head and the collection belt. In order to investigate the washing efficiency as well as the mass balance for NMMO recovery the web passes several wash stations before it is collected in wet state on a winder arm. The pilot line can be operated at collection speeds up to 300 m/min; the after-treatment and web drying is carried out separately.

After commissioning in May 2009, the main development focus was laid on spinning stability and web uniformity improvement. In November 2009, sustained stable spinning combined with good web quality was achieved for the first time, and half a year later the productivity limit for half-width jet units could be raised over 30

kg/h cellulose web. In the second half of year 2010 the pilot line was scaled-up to full-width jet operation.

Results

After more than a year of pilot plant operation a better understanding of the key properties and correlations between process conditions and web properties has been achieved. Average filament diameters in the range 2-20 µm can be produced. The dope rate and the hot air through-put are the most prominent factors controlling the filament diameters: the finest filaments are obtained at low cellulose rates and high air flows (Figure 1). Another important correlation between decreasing filament diameters and increasing air velocities can be seen when air flow and cellulose through-put are combined into a single mass flux ratio (Figure 2).

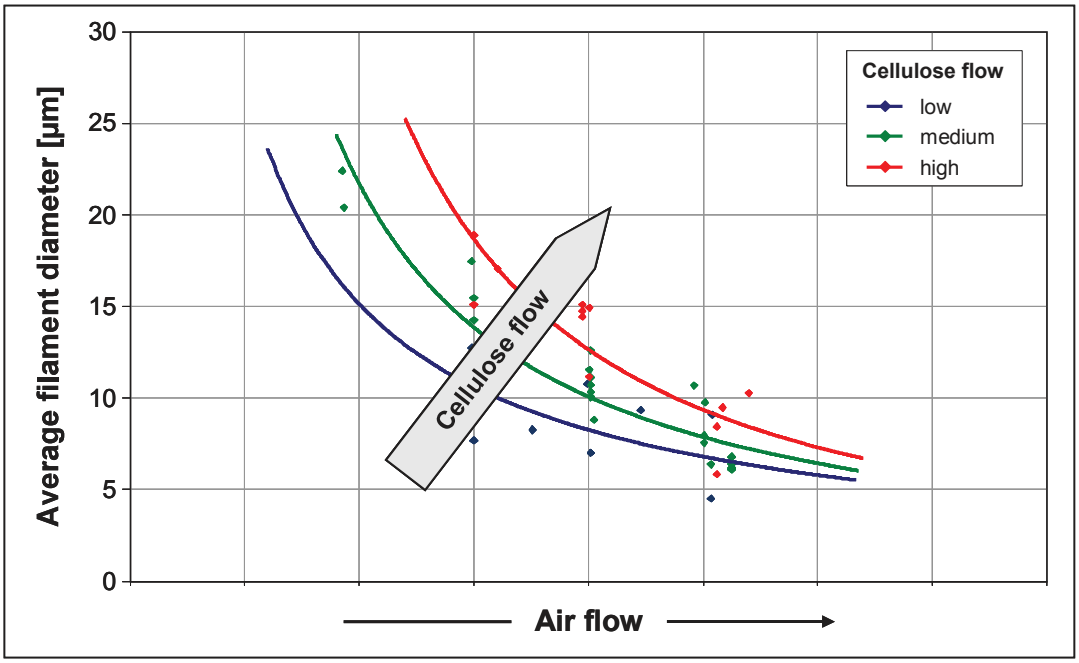

Figure 1. Filament diameter vs. air flow and cellulose flow.

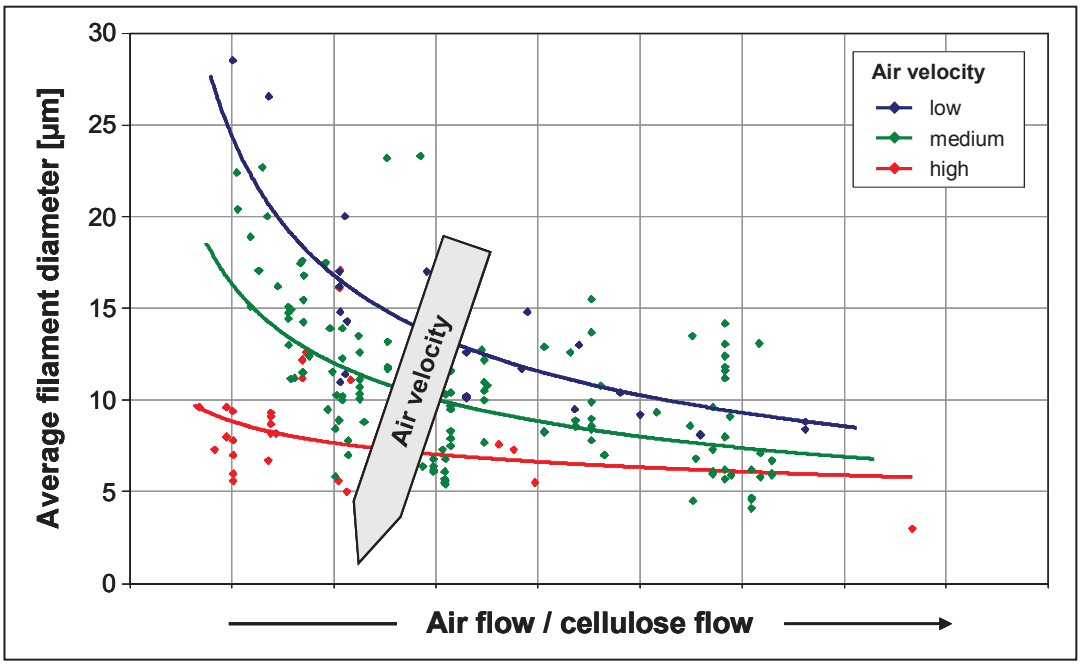

Figure 2. Filament diameter vs. mass flux ratio and air velocity.

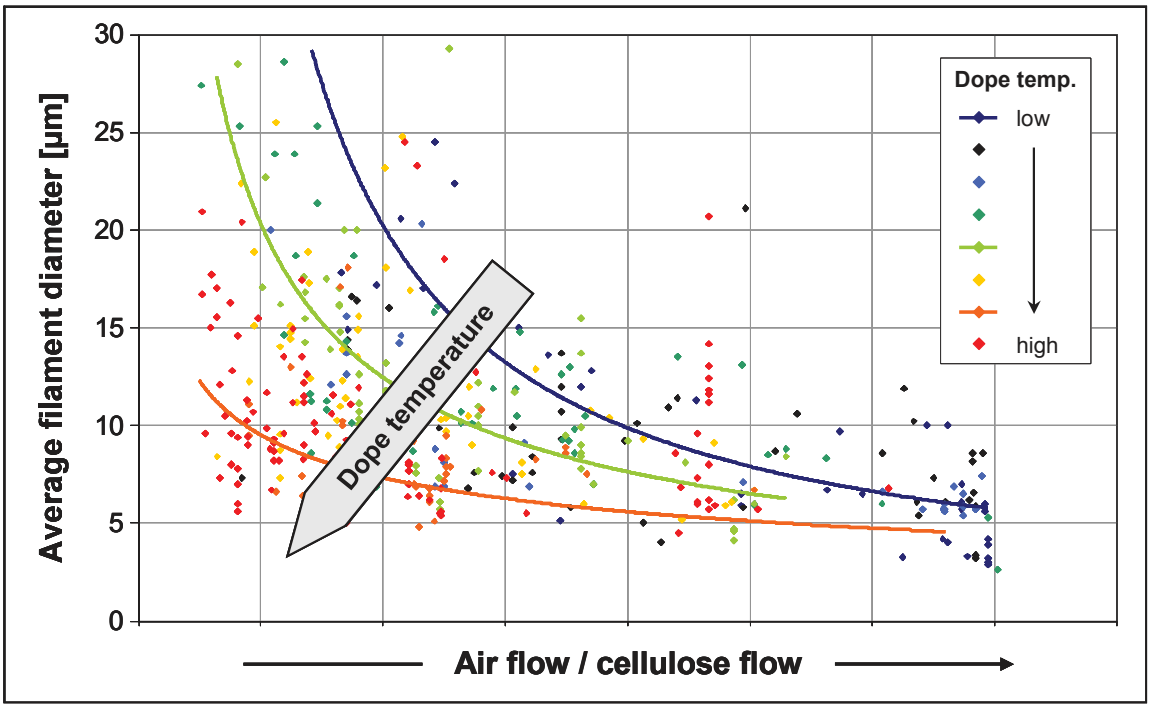

Figure 3. Filament diameter vs. mass flux ratio and dope temperature.

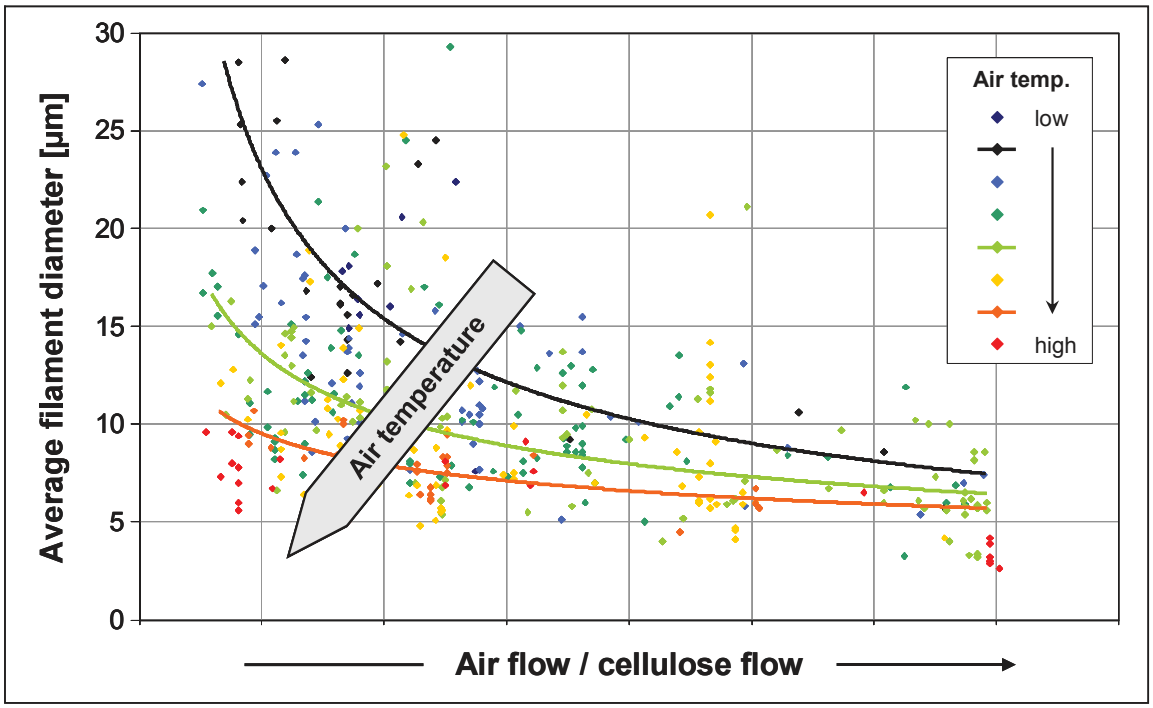

Figure 4. Filament diameter vs. mass flux ratio and air temperature.

In addition, higher temperatures of dope and air decrease the dope viscosity and result in smaller filament diameters (Figure 3 and 4).

The crystallinity of the TencelWeb™ materials was measured in a range of 30-33 % and has to be ranked between Viscose and Lyocell staple fibres. No dependency on the stretching conditions could be identified (Table 1). Depending on the coagulation conditions, web aesthetics of the TencelWeb™ products can be very different and a whole spectrum of materials ranging from fused, paper-like webs to soft, textile-like fabrics can be obtained (Figure 5).

Table 1. Crystallinities of TencelWeb™ products and cellulosic fibres.

Product	Process conditions (Air flow / cell. flow)	Crystallinity [%]
TencelWeb™	low / low	31
	low / med	32
	med - high / low	31 - 33
	med - high / med	30
Lyocell		34
Viscose		20

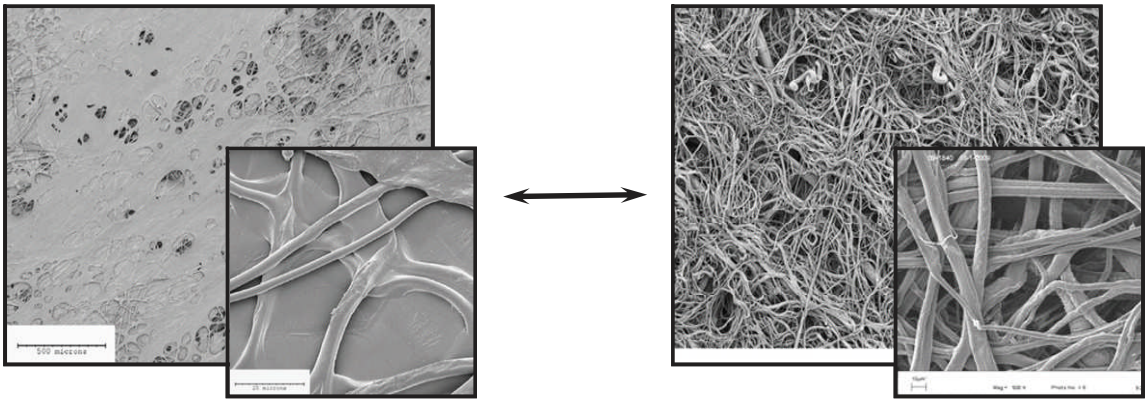

Figure 5. Web aesthetics of TencelWeb™ products.

Figure 6. Web uniformity of TencelWeb™ products.

Depending on the coagulation conditions, web aesthetics of the TencelWeb™ products can be very different and a whole spectrum of materials ranging from fused, paper-like webs to soft, textile-like fabrics can be obtained (Figure 5).

In the TencelWeb™ process, basis weights are controlled by the dope rate and belt speed. Typically, fabric weights between 5 and 150 g/m² are produced, although there is no technical reason against the manufacture of heavier products. Web uniformity and basis weight distribution are good and in line with other semi-commercial nonwoven products (Figure 6).

Table 2. Impact of the TencelWeb™ process on product properties.

Process impact	Affected product property
Jet configuration & positioning	Web uniformity, bulk density
Air flow & dope rate	Web uniformity, bulk density
Coagulation showers	Web uniformity, bonding
Collection belt & line speed	Web aesthetics, basis weight
Web de-watering & hydro-entanglement	Bulk density
Drying conditions	Web aesthetics

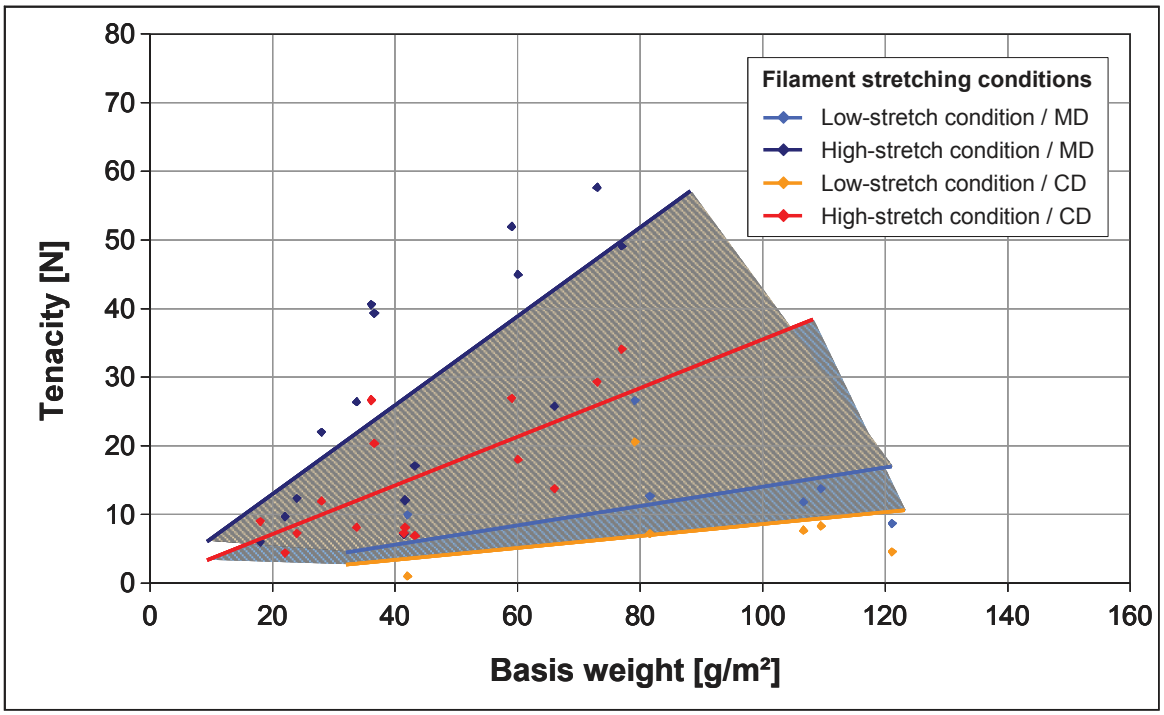

Figure 7. Tenacity vs. basis weight and stretching conditions.

An overview of the impact of the TencelWeb™ process on general web properties is shown below (Table 2).

Analogous to other textile and nonwoven materials tenacity of TencelWeb™ products increases with basis weight and filament stretch (Figure 7). In MD direction tenacity is always larger than in CD direction, but MD/CD ratio is good compared to many other products.
The sorption properties of the TencelWeb™ products are only partly comparable to other Lyocell nonwovens and textiles. On the one hand water absorption capacity decreases expectedly with the basis weight as nonwoven density increases at the same time. For a typical 30-50 g/m² dried product the absorption capacity varies between 800 and 1200 % which corresponds well with comparable staple fibre based products (Figure 8). On the other hand, water retention seems to be independent of the process conditions and relatively high values over 100 % are observed (Figure 9).

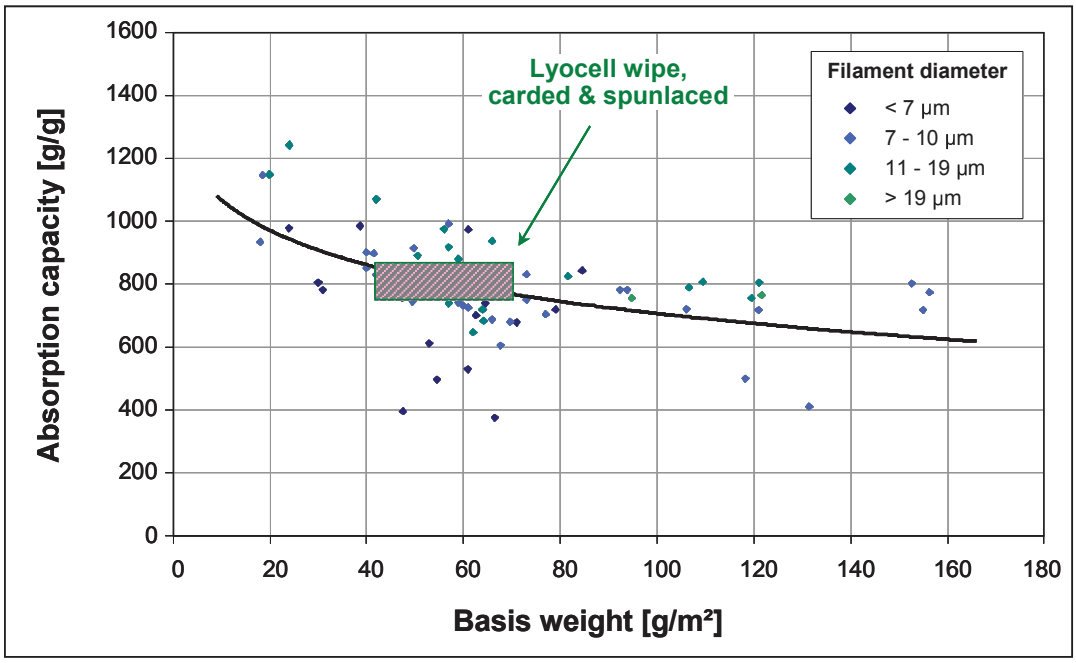

Figure 8. Water absorption capacity vs. basis weight and filament diameter.

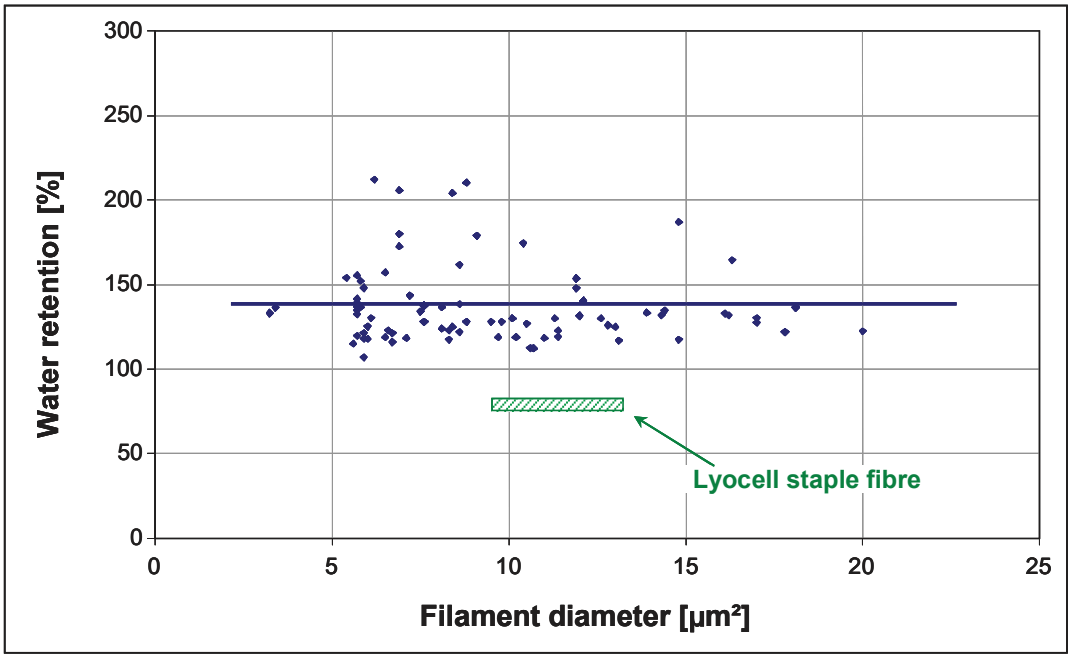

Figure 9. Water retention vs. filament diameter.

Conclusion and Outlook

Both the current product properties achieved and their correlation with process parameters suggest the technical feasibility of the TencelWeb™ process. The technology allows the manufacture of fine fibre webs and light-weight fabrics. Potential market applications include speciality wipes, hygiene and medical products as well as technical fabrics like filter media or speciality papers. Key next steps for TencelWeb™ development include further improvement on the process and productivity side, focusing on product performance development and refining estimates of process economics in advance of decisions regarding the commercialisation of the technology.

Lenzinger Berichte 89 (2011) 109-117

THE EFFECT OF DIFFERENT PROCESS PARAMETERS ON THE PROPERTIES OF CELLULOSE AEROGELS OBTAINED VIA THE LYOCELL ROUTE

Christian Schimper[1], Emmerich Haimer[1,2], Martin Wendland[2], Antje Potthast[1], Thomas Rosenau[1] and Falk Liebner[1,*]

[1] University of Natural Resources and Life Sciences, UFT Campus Tulln, Chair for Wood, Pulp and Fiber Chemistry, Department of Chemistry, Konrad-Lorenz-Str. 24, 3430 Tulln, Austria
[2] Institute of Chemical and Energy Engineering, Department of Material Sciences and Process Engineering, Muthgasse 107, 1190 Vienna, Austria

*Phone: (+43) 1-47654-6452; Fax: (+43) 1-47654-6059; Email: falk.liebner@boku.ac.at

Shaped cellulose aerogels were obtained via the Lyocell route: Dissolution of cellulose in NMMO monohydrate, molding the dopes, regeneration of cellulose and drying the lyogels using supercritical carbon dioxide ($scCO_2$). The effect of different process parameters such as cellulose content of the dope, type of antisolvent for cellulose regeneration, regeneration and $scCO_2$ drying temperature, and molding material, have been investigated. Less polar regeneration solvents such as isopropanol and hexanol were confirmed to be superior to the use of water or ethanol with respect to retaining the shape and porosity of aerogels throughout the regeneration and $scCO_2$ drying steps. Shrinking was proved to be significantly reduced when the cellulose content of the dopes was doubled from 3 to 6 w%. Elevated temperature during regeneration reduces crack formation as the steep increase of the dope's density upon cooling to room temperature for cellulose contents of up to 6 w% is prevented. Lyocell dopes cast into paper board molds were shown to resist shrinking throughout the entire regeneration and solvent exchanging process. Drying of lyogels with $scCO_2$ at temperatures above 60 °C increasingly leads to pore collapsing and shrinking.

Keywords: *Cellulose, aerogels, Lyocell, NMMO, supercritical carbon dioxide*

Introduction

Since the first steps towards highly porous aerogels from native cellulose and respective reports on the initial AEROCELL project [1], research on this class of novel biomaterials has been largely intensified [2]. Following attempts to prepare aerogels from non-derivatised cellulose via the Lyocell approach [3–6], several other cellulose solvents such as DMAc/LiCl, aqueous solutions of calcium thiocyanate, NaOH, NaOH/urea, NaOH/thiourea, LiOH/urea and ionic liquids have been investigated in this respect (for a comprehensive overview see Liebner *et* al. [2]).

Cellulose aerogels are highly porous, very lightweight materials. Depending on the applied technique, cellulose origin and cellulose content of the lyogel precursors, densities of down to approx. 5 mg cm^{-3} have been reported.

The synthesis of aerogels from non-derivatized cellulose via the Lyocell approach comprises (A) dissolution of cellulose in molten *N*-methylmorpholine-*N*-oxide monohydrate (NMMO·MH), (B) shaping of the cellulose-NMMO·MH mixture, (C) regenerating the cellulose by adding an appropriate antisolvent and (D) dry-

ing of the obtained lyogel bodies with supercritical carbon dioxide ($scCO_2$). Preservation of porosity by preventing pore collapsing is the most serious challenge in cellulose aerogel research. Lyogels from non-derivatized aerogels are highly prone to shrinking when converted into aerogels. The extent of shrinking largely depends on the employed technique of lyogel formation and subsequent conversion to aerogels. Aerogels obtained via the Lyocell approach were reported to suffer considerable shrinking [6] and the current paper will show that all of the following process steps have the potential to contribute to this undesired effect.

(A) Dissolution of cellulose in molten NMMO·MH at temperatures of 100–120 °C is the first step in aerogel preparation and is accomplished in a similar way as for fiber production (Lyocell process, TENCEL® fibers) [5]. Due to the oxidative nature of NMMO, effective stabilizing agents have been developed to prevent the cellulose solution in NMMO·MH (Lyocell dope) from undesired side reactions and to suppress both, homolytic and heterolytic degradation reactions. *N*-benzylmorpholine-*N*-oxide for example has been recently developed as a sacrificial substrate to scavenge critical NMMO derived carbonium-iminium ions that can lead to uncontrolled NMMO degradation [7, 8].

Density and crystallization behavior of NMMO·MH and its mixtures with cellulose are strongly influenced by both, temperature and cellulose content of the dope. Whereas pure NMMO·MH crystallizes at approx. 30°C, the addition of 2 or 6 wt% of cellulose shifts the crystallization range to approx. 20–25 °C and 9–12 °C, respectively. Dopes containing more than 8 wt% of cellulose do not solidify above 0 °C [9].

Upon solidification, the density of pure NMMO·MH changes considerably from approx. 1.1 to 1.2 g cm^{-3}. In particular Lyocell dopes of low cellulose content are therefore highly prone to crack formation, i.e. an effect that would decisively narrow the application potential of the subsequently obtained aerogels.

(B) The dimension of the molds used for shaping the Lyocell dopes at elevated temperature largely affects the time period necessary for cellulose regeneration and for replacing NMMO by a cellulose antisolvent. The material of the molds, the cooling rate and the relative humidity of the surrounding atmosphere are further parameters that influence at least the surface properties of the aerogels.

(C) Regeneration of cellulose and formation of a lyogel that features the same geometry and dimension as the solidified Lyocell dope is accomplished by transferring the latter in an antisolvent that dissolves NMMO but not cellulose. The type of antisolvent used for this procedure largely influences in particular the pore features of the formed cellulose aggregate structure and can lead to considerable shrinking.

(D) Drying with supercritical carbon dioxide ($scCO_2$) is considered to be the gentlest technique for converting lyogels into aerogels [5]. In particular for soft matter, $scCO_2$ drying is highly recommended as it circumvents the formation of inward forces alongside the capillary walls adjacent to the solvent menisci and hence pore collapsing. A good miscibility of the lyogels pore liquid and carbon dioxide is a prerequisite to $scCO_2$ drying. Ethanol, methanol, and acetone for example are completely miscible with carbon dioxide at pressures beyond the critical pressure for a given temperature. In case of ethanol, full miscibility is achieved at 40 °C and pressures of beyond approximately 8 MPa. Below the critical pressure of the binary system, the solubility of CO_2 in ethanol increases with increasing pressure. It has to be ensured that during drying both, temperature and pressure comply by all means with the conditions of the supercritical state to avoid surface tension and hence loss of pores. Only under these conditions — outside the phase envelop of the

binary mixture of CO_2 and CO_2-miscible solvent — it is safe to flush the CO_2-expanded solvent phase out of the drying system without affecting the fragile cellulose pore network structure. If the ethanol content is then negligible low the system can be slowly depressurized and CO_2 is subsequently replaced by air.

The current report communicates the results of a study investigating the impact of different process parameters affecting the properties of cellulosic aerogels obtained via the Lyocell approach according to the steps A–D.

Experimental

Cellulosic aerogels were prepared via the Lyocell route. Cotton linters (Cl; CCOA 4.2 μmol g^{-1} C=O; FDAM 8.8 μmol g^{-1} COOH; Mw 133.5 kg mol^{-1}) was dissolved in *N*-methylmorpholine-*N*-oxide monohydrate (NMMO·MH, technical grade) to give a final cellulose content of 3 wt% if not mentioned otherwise.
Dissolution was achieved at 110°C within 10 minutes yielding a visually clear solution. Propyl gallate and *N*-benzylmorpholine-*N*-oxide (NBnMO) were added (1 wt‰ of each) to suppress homogeneous and heterogeneous side reactions. After 10 minutes of vigorous stirring for sufficient micelle separation, the dope was cast into molds of different geometry to give cylinders or disks. Different molding materials were tested. Cellulose regeneration was accomplished by adding the respective antisolvents either prior to or after solidification, or by exhibiting the solidified dopes to an antisolvent gas phase. All solvents were purchased from Sigma Aldrich and were of puriss grade: 96 % ethanol, methanol, isopropanol, dimethylsulfoxide.

For regeneration in liquid antisolvents the solidified samples were gently shaken in the regeneration solvent (solid to liquid ratio 1:20, w/v). After every 24 hours, the samples were transferred into a second and third regeneration bath, respectively. Prior to drying, all solvents were replaced by absolute ethanol in at least two subsequent steps.

Two types of $scCO_2$ equipment were used for drying. Preliminary experiments were carried you in a laboratory-scale autoclave (Alltech Grom GmbH, Germany) as described earlier [10,11]. Briefly, the alcogels were transferred into the drying unit and then placed into an oven controlled by a Julabo LC4 controller, and temperature was set to 40 °C throughout the whole procedure. After 15 min for thermal equilibration, the system was pressurized via the bottom-valve up to 10 MPa with liquid pre-heated CO_2 using a HPLC pump (miniPump, TSP Thermal Separation Products, USA). After another 15 min of equilibration, the top-valve was opened and the bottom-valve was switched to a separator, where ethanol and CO_2 were separated by an isothermal flash. In a first step, the ethanol-rich phase was flushed out of the autoclave. In a second step, ethanol was extracted from the gel pores at constant CO_2 flow rate of 1 g min^{-1}. After 60 min, the top valve was closed and the autoclave was depressurized via the separator.

Most of the experiments were conducted in a 500 mL autoclave equipped with two separators for carbon dioxide recycling (Separex SF1, Separex, France). Wet gels were dried using a constant flow of supercritical carbon dioxide (2.5 kg CO_2 h^{-1}, 10.5 MPa, 40 °C) over a time period of one hour. In some experiments temperature and pressure were varied. After removing the entire pore liquid, the system was slowly and isothermally depressurized to prevent the occurrence of any condensation phenomena [12]. Prior to and after $scCO_2$ drying, the volume (± 0.1 mm^3) and weight (± 1 mg) of the samples were recorded.

Results and discussion

Shrinking and alteration of pore features are obviously the most serious problems in

the preparation of lightweight aerogels from non-derivatized cellulose.

Effect of the regeneration solvent

A set of six different solvents were used for regeneration of cellulose. Dopes containing 3 wt% of cotton linters were poured into respective molds to obtain cylindrical discs (2 mm x 25 mm). Regeneration of cellulose from the solidified bodies was initiated by immersing the bodies in water, 96 % ethanol (EtOH), isopropanol, hexanol, methanol or dimethyl sulfoxide (DMSO). After three times of replacing the solvent the resulting dimensional change of the samples was recorded (Table 1). Subsequently, the regeneration solvent was replaced for all samples by 96 % EtOH (3x) and then by absolute EtOH (2x) prior to supercritical drying.

Table 1 shows the decrease in diameter of the discs after (a) regeneration in the above mentioned solvents, (b) repeated solvent exchange to ethanol, and (c) $scCO_2$ drying.

Table 1. Shrinkage [%] of gels after regeneration in different solvents, solvent exchange to ethanol, and after $scCO_2$ drying.

	Shrinkage [%] after		
	regeneration	solvent replacement(EtOH)	$scCO_2$ drying
Water	8.0	32.4	36.4
EtOH	-	18.0	37.2
iso-PrOH	3.2	6.0	21.4
Hexanol	18.4	14.4	27.2
Methanol	3.2	2.4	32.6
DMSO	-1.6	32.4	46.2

With exception of hexanol and ethanol, only negligible shrinking is observed during regeneration, samples in DMSO were deformed. Methanol (2.4 %) and isopropanol (6 %) were shown to effect the lowest shrinking in the sum of regeneration and solvent exchanging steps. Ethanol as a structurally very similar homologous alcohol was surprisingly found to cause a similar high shrinking as hexanol. The highest shrinking of about 30 % was observed for the two polar compounds water and DMSO. Shrinking throughout the entire process of regeneration and drying was 20–45 % depending on the regeneration solvent used. The data clearly show that not only the extent of shrinking during regeneration and solvent exchange determines the final dimension of the aerogels but also the type of antisolvent. Methanol for example gave only minimal shrinking prior to drying but the dimensional change of these gels during $scCO_2$ drying was much more pronounced than for gels were the cellulose was regenerated with isopropanol. Interestingly, gels regenerated with isopropanol had the lowest shrinking rate throughout the entire process. However, all samples showed some deformation after $scCO_2$ drying with cracks and grooves on the surface (Figure 1).

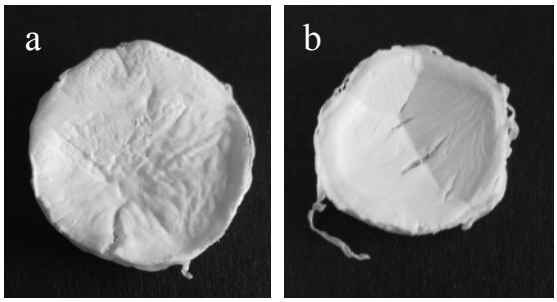

Figure 1. Pictures of cellulose aerogels from 3 w% cotton linters containing Lyocell dopes. Regeneration solvent: Isopropanol (a) and methanol (b).

Effect of the cellulose content of the dope

During solidification the density of NMMO-dopes increases considerably. This can be easily observed since the resulting crack formation by compression can be audibly recognized. Liu *et* al. [9] observed that due to this compaction phenomenon the preparation of homogeneous discs from Lyocell dopes of less than 6 wt% of cellulose is virtually impossible. The effect is more pronounced for dopes of lower cellulose content that solidify at comparatively high temperature. This effect is supposed to largely contribute to the observed shrinking and groove formation. Dopes of higher cellulose content are less prone to crack formation due to the

lower solidification temperature of the dope and a less pronounced increase in density [13]. The preparation of aerogels containing more than 6 wt% is therefore considered to be a viable strategy to avoid this problem. Even at room temperature dopes containing 6, 8 and 10 wt% of cellulose did not solidify prior to regeneration.
However, the picture regarding shrinking during the $scCO_2$-drying step is less clear. Even though the data evidence an increase of shrinking with the amount of cellulose dissolved in NMMO·MH, there seems to exist a minimum shrinking for dopes of about 6 % of cellulose (Figure 2). All samples were deformed as mentioned above; a wrinkle-free surface could be only obtained for dopes of a higher cellulose content (10 wt%), which however has the drawback of high shrinking (see insert in Figure 2). Preliminarily, this is supposed to be due to a comparatively high residual NMMO content in the lyogels and the resulting hygroscopicity of the $scCO_2$-dried aerogels as shown previously [14].

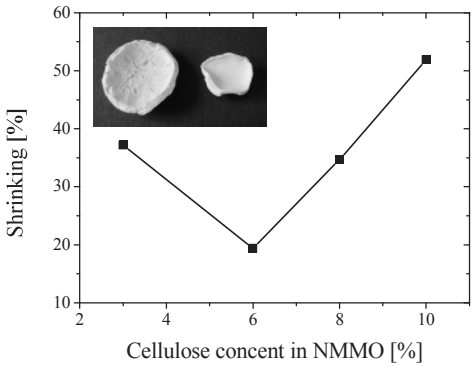

Figure 2. The effect of cellulose content on the overall shrinking [%] of shaped Lyocell dopes upon cellulose regeneration with EtOH and $scCO_2$ drying. Insert: aerogel disks with 6 wt% (left) and 10 wt% (right) cellulose.

Regeneration temperature and regeneration procedure
The solidification temperature of Lyocell dopes strongly depends on the cellulose content as described above. For a cellulose content of 3 wt% crystallization of the dope takes place at around room temperature [9]. Regeneration of cellulose above this critical range was therefore considered to be a suitable approach to prevent crack formation.

Accordingly, regeneration was started immediately after molding the dopes by adding hot ethanol (40, 60 °C) or water (40, 60, 95 °C). The molds were preheated. Subsequently, sample and regeneration solvent were allowed to cool down to room temperature. The temperature for some of the samples was kept at 60 °C for 5 hours. Other samples were exposed to hot solvent vapor (60 °C) for one hour and subsequently immersed in the same solvent. Independent on the variation of regenerating temperature and technique all samples were subjected to a final solvent exchange to abs. ethanol and $scCO_2$-drying as described above. The above presented data reveal that shrinking is less pronounced if cellulose is regenerated with water instead of ethanol.

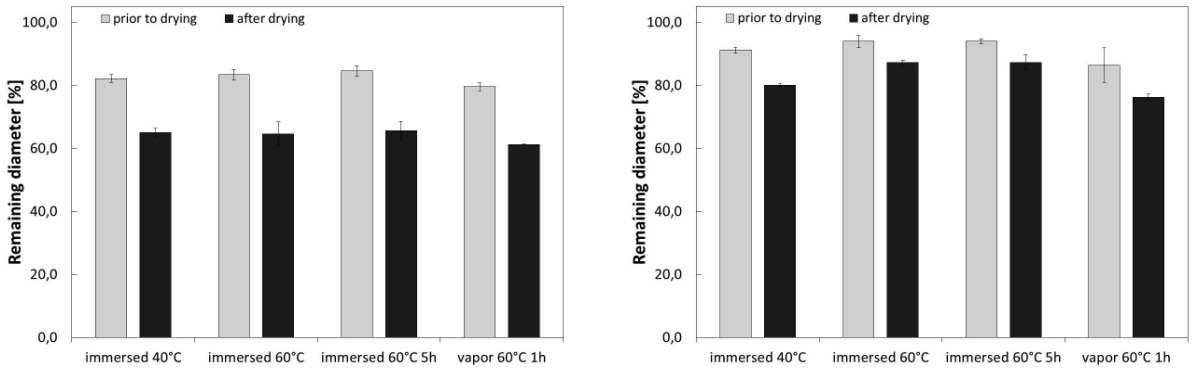

Figure 3. Remaining diameters [%] after regeneration in ethanol (left) and water (right) using different conditions during the first regeneration step.

Immersing the Lyocell dopes in water at 60 °C results in larger diameters than for 40 °C, however a similar difference was not observed for ethanol. Regeneration in solvent vapor was shown to negatively affect the dimensional stability. Higher temperature upon regeneration (95 °C, water) affords flatter samples, unfortunately at the expense of increasingly grainy and flaky surfaces of the resulting aerogels. There is evidence that the increased vapor pressure provokes a mechanical peeling effect that dimishes the advantage of reduced shrinking.

Effect of the molding material

Preliminary experiments evidenced that the molding material may also affect the final shape and dimension of the aerogels. To investigate this effect, 3 wt% cellulose containing dopes were prepared and cast into cylindrical molds prepared from a) paper board, b) Teflon, and c) butyl rubber. After solidification the shaped bodies were subjected to cellulose regeneration using 96 % ethanol (3 x), followed by solvent exchange to absolute ethanol (2 x) and $scCO_2$ drying. Figure 5 shows the remaining diameter of the samples recorded for the individual process steps in dependence on the material used for molding. It is evident that shrinking is most pronounced in the very first regeneration step whereas the following regeneration bathes and solvent exchange steps are of minor importance with regard to dimensional changes. However, a further but distinctly less pronounced contraction was observed when the 96 % EtOH was replaced by absolute EtOH. This was surprisingly not the case for Lyocell dopes that were shaped in paper board molds (see Figure 5).

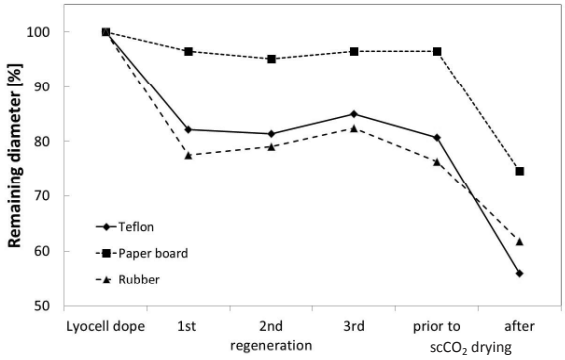

Figure 4. Dimensional changes of lyogels and aerogels in dependence on the molding material.

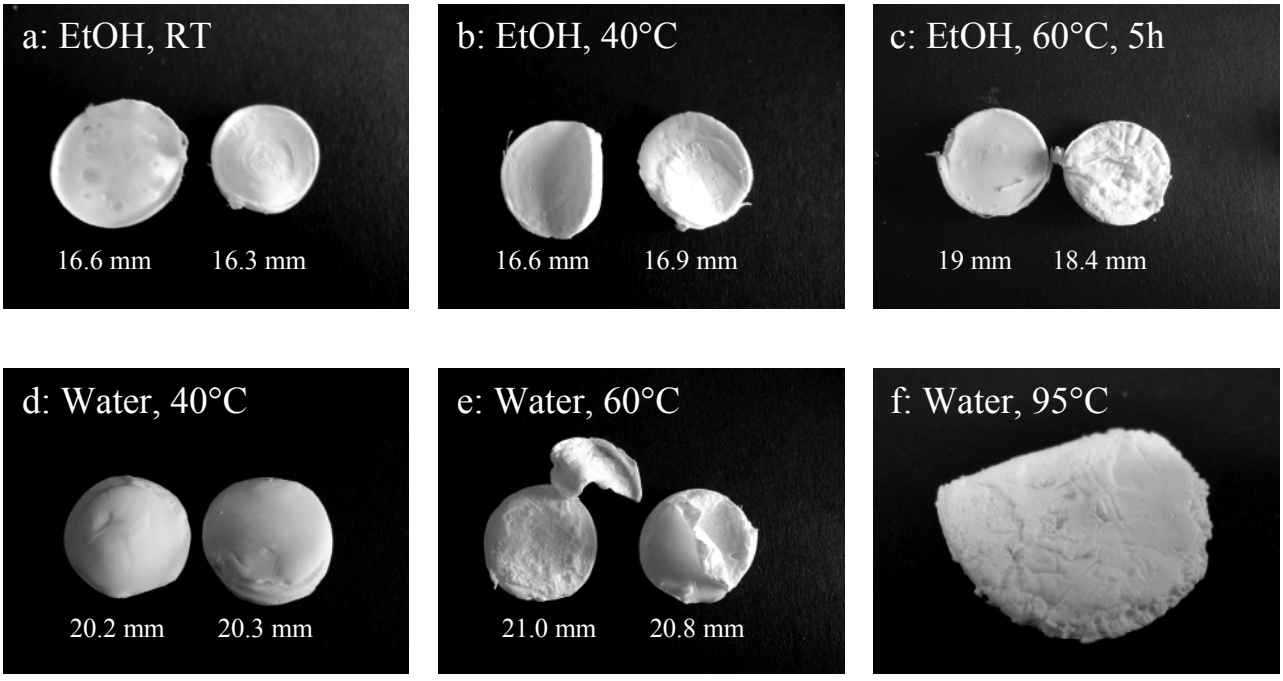

Figure 5. Photographs of $scCO_2$ dried aerogels obtained by immersing in ethanol and water during regeneration under different conditions (a-e: up- and downside).

Probably the Lyocell dope penetrated the outermost layers of the paper board upon casting. As the solidified dope remained inside the mold during the first regeneration step, the cellulose aggregate network highly likely formed a sufficiently strong crosslink with the mold surface so that the lyogels can resist shrinking. Contrary, the hydrophobic Teflon and rubber surfaces are supposed to exert a repulsive effect on the cellulose molecules in the dope which can lead to phase separation in the boundary layers between dope and mold. The latter along with the impossible penetration of the mold's surface by the dope are considered to be the main reasons for the different shrinking behavior of the gels caused by the molding material. The extent of shrinking during the final $scCO_2$ drying step was similar for the dopes cast in Teflon and paper board molds (31–32 %), however, a lower overall shrinking was obtained for the latter (see Figure 5).

All samples obtained from the Teflon and rubber molds showed typical buckling. The formation of flaky surfaces was observed for the gels from paper board molds similarly to those gels that were obtained by cellulose regeneration using hot water.

The effect of drying conditions

The equilibrium of the phase system ethanol – carbon dioxide is largely dependent on the constitution of the binary mixture, pressure and temperature. As the volume of the drying chamber and the loaded amount of ethanol per sample was largely the same for each experiment, the joint effect of temperature and pressure during $scCO_2$ drying was studied (see Table 2).

Dopes containing 3 wt% of cotton linters were cast in cylindrical molds (Ø 10 x 20 mm). After solidification the samples were removed from the mold, subjected to cellulose regeneration using 96 % ethanol which was subsequently replaced by absolute ethanol. After regeneration and solvent exchange the samples were transferred into the preheated drying chamber (initial temperature; T_i). Subsequently, the autoclave was pressurized with CO_2 (initial pressure; p_i). After 15 minutes of equilibration time, the CO_2-expanded ethanol phase was flushed out of the drying chamber by a continuous flow of $scCO_2$ (2.5 kg h^{-1}). While the drying temperature (T_w) was varied within the range of 20–80 °C, pressure (p_w) was adapted to maintain supercritical conditions. The adaptation of the $scCO_2$ pressure is supposed not to interfere with the dimensional stability of the gels as the density of $scCO_2$ hardly changes in the pressure range of 10–20 MPa which is different for subcritical conditions.

Samples A–D that were differently dried but using a starting temperature T_i of up to 60°C were shown to have a very similar remaining volume and density after $scCO_2$ drying (Table 2). Increasing the drying

Table 2. Shrinking and final density of aerogels in dependence on temperature and pressure during $scCO_2$ drying.

		$scCO_2$ drying [°C, MPa]					
Code	Scheme	T_i	T_w	p_i	p_w	Volume [%]	Density [mg cm^{-3}]
A	20 → 80	20	80	10	20	64.3	73.7
B	40	40	40	10	10	67.1	71.1
C	40 → 60	40	60	12	12	67.1	73.8
D	60	60	60	15	15	67.4	70.2
E	40 → 80	40	80	15	20	60.9	79.6
F	80	80	80	20	20	45.5	116.9

temperature T_w from 40 to 80 °C (sample A) does also not significantly change the final density of the aerogels. However, if the drying process starts at a T_i of 80 °C (sample F) considerably decreased remaining volumes and hence higher densities are obtained. Figure 6 shows a photograph of the aerogels that were obtained using the different drying conditions as listed in Table 2. Whereas the samples A–D feature an even and smooth surface, those of the samples E and F looks rather rough and uneven. We conclude that $scCO_2$ drying should be accomplished in a temperature range of 40–60°C as under these conditions the lowest shrinking and hence the lowest densities were obtained for the studied set of cellulosic gels obtained via the Lyocell route.

Summary

The preparation of cellulosic aerogels via the Lyocell route is a facile approach to highly porous, lightweight materials. Research in this field has been largely intensified during the last five years and the number of potential applications is accordingly growing. However, there are still a couple of uncertainties with regard to the reasons of shrinking which pertains in particular to the conversion of lyogels to aerogels. The present study confirmed that shrinking during the regeneration step is largely affected by the type of antisolvent used. Compared with water and ethanol, isopropanol caused less shrinking, but cracks and grooves were found for all types of solvents. Doubling the cellulose content of the dope from 3 to 6 wt% reduces the extent of shrinking significantly but not crack formation. Homogeneous, wrinkle-free surfaces could be only obtained for dopes of higher cellulose content (8, 10 wt%), however at the expense of a more pronounced shrinking. Variation of temperature during regeneration evidenced that shrinking and crack formation decreases at elevated temperature. This is due to the prevented steep increase of the dope's density upon cooling to room temperature which is critical for cellulose contents of up to 6 wt%. However, hot water (95 °C) is not suitable for cellulose regeneration due to the formation of flaked aerogel surfaces. Hydrophobic molding materials seem to intensify shrinking probably by effectuating a density gradient in the boundary layers of the dope to the molding material. Lyocell dopes cast into paper board molds were shown to resist shrinking throughout the entire regeneration and solvent exchanging process. This is most likely due to the penetration of the outermost paper board layers by the dope and the formation of a sufficiently strong cellulose network between mold and dope upon regeneration. The conducted $scCO_2$ drying experiments confirmed that a temperature range of 40–60°C is most suitable with regard to preferably low shrinking,

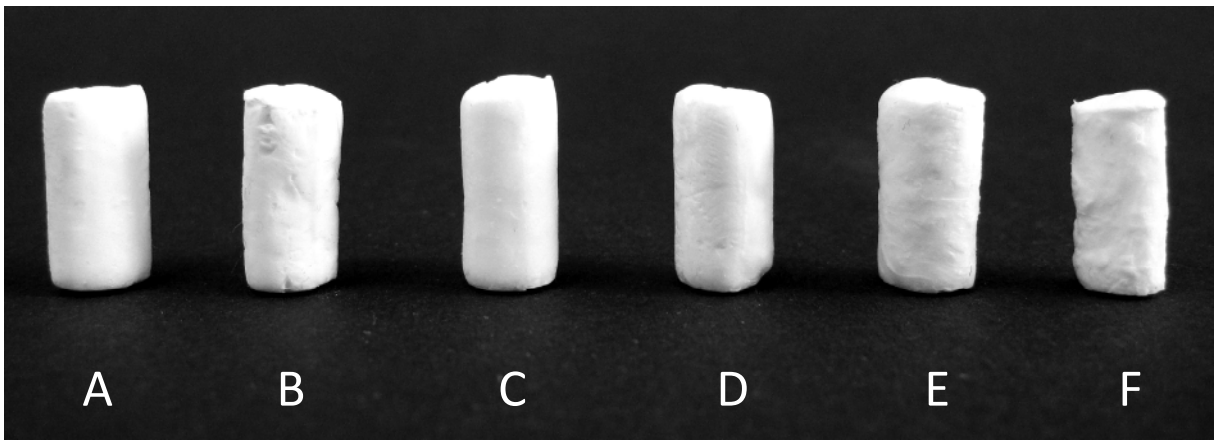

Figure 6. Photograph of cotton linters aerogels obtained under different $scCO_2$ drying conditions (see Table 2).

preservation of porosity and hence low density of the resulting aerogels.

Acknowledgement

The authors thank Melanie Leeb and Johannes Arnberger for their lab assistance. The financial support by the University of Natural Resources and Life Sciences Vienna through the BOKU DOC Grant 2009 is gratefully acknowledged.

References

[1] Innerlohinger J., Weber H. K. and Kraft G. Lenzinger Berichte 86 (2006) 137–143.

[2] Liebner F. , Haimer E., Potthast A. and Rosenau T. "Cellulosic Aerogels" in Habibi Y. and Lucia L. A. (Eds.) "Polysaccharide building blocks: a sustainable approach to renewable materials", Wiley, Hoboken, NJ, announced for autumn 2011.

[3] Innerlohinger J., Weber H. K. and Kraft G. Macromol Symp. 244 (2006) 126–135.

[4] Liebner F., Potthast A., Rosenau T., Haimer E. and Wedland M. Res Lett Mater Sci (2007) Article ID 73724.

[5] Liebner F., Potthast A., Rosenau T., Haimer E. and Wedland M. Holzforschung 62 (2008) 129–135.

[6] Liebner, F., Haimer, E., Potthast, A., Loidl, D., Tschegg, S., Neouze, M.-A., Wendland, M. and Rosenau, T. Holzforschung 63(1) (2009) 3–11.

[7] Rosenau T., Schmid P., Potthast A. and Kosma P. Holzforschung 59 (2005) 503–506.

[8] Rosenau T., Potthast A., Schmid P. and Kosma P. Tetrahedron 61 (2005) 3483–3487.

[9] Liu, R.-G., Shen, Y., Shao, H.-L., Wu, C.-X. and Hu, X.-C. Cellulose 8 (2001) 13–21.

[10] Haimer, E., Wendland, M., Schlufter, K, Frankenfeld, K., Miethe, P., Potthast, A. and Rosenau, T., Liebner, F. Macromol Symp 294(2) (2010) 64–74.

[11] Liebner, F., Haimer, E., Wendland, M., Neouze, M.-A., Schlufter, K., Miethe, P., Heinze, T., Potthast A. and Rosenau, T. Macromol Biosci 10(4) (2010) 349–352.

[12] Fischer F., Rigacci A., Pirard R., Berthon-Farby S. and Acard P. Polymer 47 (2006) 7636–7645.

[13] Chanzy H., Dube M., Marchessault RH. J Polym Sci Polym Lett Ed 17 (1979) 219–226.

[14] Schimper C. B., Aigner N., Haimer E., Nedelec J.-M., Hardy-Dessources A., Neouze M.-A., Potthast A., Henniges U., Russler A., Rosenau T. and Liebner F., Conference Proceedings, 11th EWLP, 16.08.–19.08.2010, Hamburg, Germany.

Lenzinger Berichte 89 (2011) 118-131

OVERVIEW ON NATIVE CELLULOSE AND MICROCRYSTALLINE CELLULOSE I STRUCTURE STUDIED BY X-RAY DIFFRACTION (WAXD): COMPARISON BETWEEN MEASUREMENT TECHNIQUES

Nicoleta Terinte[1], Roger Ibbett[2] and Kurt Christian Schuster[1*]

[1] Fiber Science & Development Department, Lenzing AG, Werkstr. 1, 4860 Lenzing, Austria
Email: n.terinte@lenzing.com, k.schuster@lenzing.com
[2] School of Biosciences, Division of Food Sciences, University of Nottingham, Sutton Bonington Campus, Nottingham LE12 5RD, UK, Email: roger.ibbett@nottingham.ac.uk

*Phone: (+43) 7672 701-3081; Fax: (+43) 7672 918-3081

The crystalline structure of cellulose has been studied for a long time. It is well known that crystallinity of cellulose can be measured using quite a number of methods, X-ray diffraction, solid state ^{13}C CP-MAS NMR, Fourier transform-infrared (FT-IR) spectroscopy and Raman spectroscopy. The solid state ^{13}C CP-MAS NMR and FT-IR spectroscopy considers contributions from both crystalline and non-crystalline cellulose regions resulting in relative values, while the alternative X-ray diffraction approach gives more detailed data on features of crystalline and less on the non-crystalline fraction of cellulose. Raman spectroscopy is also used to study cellulose crystallinity. This paper gives an overview on the crystallinity of three cellulose samples, cotton linters, microcrystalline cellulose (cotton linters) and Avicel powder cellulose (Avicel PH-101) determined by wide angle X-ray diffraction (WAXD). The study compares literature data with our data for the apparent crystallinity (%) of the mentioned samples from different sources to demonstrate the dissimilarities that can be obtained using different X-ray methods. For the crystallinity analysis, assumption had to be made that all cotton linters and Avicel PH-101 used in the literature were of the same quality, even though it has been reported that the quality of both samples can vary between batches and production locations. The reported crystallinity values of cotton linters were between 56-78 %, for microcrystalline cellulose (MCC), crystallinity varied within the range 65-83 % and Avicel PH-101 powder gave crystallinity values between 37-93 % dependent on the X-ray methods and experimental mode used.

Keywords: *cotton linters, microcrystalline cellulose (MCC), Avicel PH-101, crystallinity, X-ray diffraction, X-ray methods*

Introduction

The way to produce microcrystalline cellulose (MCC) from native cellulose material or pulp by acid hydrolysis has been known already for over 50 years [1]. MCC is purified partly depolymerised cellulose prepared by treating α-cellulose, obtained as a pulp from fibrous plant material, with mineral acid [2]. In the process of acid hydrolysis, the non-crystalline region is preferentially hydrolysed, so the cellulose crystals are released. In an initial stage of the hydrolysis, the degree of polymerisation (DP) of cellulose decreases dramatically, but it approaches to a constant DP value, which is known as the leveling-off degree of polymerisation (LODP). In the case of using wood pulp as a precursor of

microcrystalline cellulose, the LODP ranges from 200-300.

A series of studies were published on the application of the produced MCC and its uses in different fields. MCC from various origins has been widely used as a binder and filler in medical tablets, fat replacer and stabilizer in food industry, a composite material in wood, plastic industry [1, 3-5]. It also finds applications in cosmetics industry. The production methods, properties, and structure of microcrystalline cellulose have been studied widely. In MCC, the diameter of the cellulose fibres is in the scale of few micrometers. These fibres consist of elementary cellulose microfibrils, whose crystalline parts have a width of about 5 nm and a length of about 20 − 30 nm [6].

Among other features, crystallinity has an important effect on the physical, mechanical and chemical properties of cellulose. For example, with increasing crystallinity, tensile strength, dimensional stability and density increase, while properties such as chemical reactivity and swelling decrease. The degree of crystallinity of cellulose and the dimensions of the crystallites have been the subject of extensive investigations for many years [7]. The cellulose crystallinity is defined as the ratio of the amount of crystalline cellulose to the total amount of sample material and can be measured by a variety of methods relying on different structural features. The numerical results from the literature, which are often called “crystallinity index”, are much dependent on the choice of the X-ray instrument, data evaluation procedure applied to the measurement and on the perfectness of the sample. In this work, the concept of “apparent crystallinity” is preferable on behalf of the literature reported “crystallinity index”. The classical way of determining the degree of order (crystallinity) in a cellulose sample is using X-ray diffraction methods. Wide-angle X-ray diffraction (WAXD) has been used extensively to measure the crystallinity of cellulosic substrates [6, 8-16]. X-ray diffraction provides strong signals from the crystalline fraction of the cellulose. These signals can be used to determine crystallographic parameters, like measuring the distances in the crystalline unit cell [17]. The non-crystalline part of the cellulose structure is represented by broader and less clearly refined features in the diffraction pattern. This leads to challenges in the evaluation of the signals for a quantitative crystallinity measure.

More recently research studies showed that the degree of crystallinity can also be determined from the evaluation of the ^{13}C high-resolution cross-polarization magic angle spinning (CP-MAS) solid state NMR spectrum of the polymer [18-22]. The solid state ^{13}C CP-MAS NMR considers contributions from both, crystalline and amorphous cellulose to the NMR spectra. Information concerning the degree of crystallinity of cellulose can be obtained by other methods as well, Fourier transform-infrared (FT-IR) spectroscopy [23-25] and Raman spectroscopy [26-30]. The determination of the degree of crystallinity using FT-IR spectroscopy, thought to be the simplest method to determine the degree of order of cellulose, is a relative measurement technique which contains the same as solid state ^{13}C CP-MAS NMR spectroscopy, contributions from both crystalline and non-crystalline regions. As a result, FT-IR spectroscopy analysis gives only relative values of crystallinity. Raman spectroscopy has also been used to determine the degree of crystallinity in cellulose. Values obtained from X-ray diffraction measurements are typically comparable but not quite identical to those obtained from other methods such as ^{13}C CP-MAS NMR, FT-IR or Raman spectroscopy. These methods, other than WAXD, have limitations and these have been discussed in the literature [30 and references cited therein].

In this review, we made comparisons between different variations of WAXD techniques to measure the crystallinity of native cellulose and microcrystalline

cellulose I. Comparisons were made with literature data for the apparent crystallinity (%) of two types of cellulose - cotton linters (CL), its microcrystalline cellulose and for comparison the well-known Avicel PH-101 from different sources - to demonstrate the dissimilarities that can be obtained using different X-ray methods. Data in literature and experimental results indicated a wide range of numerical values are obtained for crystallinity using different X-ray diffraction methods for the same sample, although its interpretation is still under discussion.

Experimental

Materials

In the reviewed literature, three different types of cellulose were used: cotton linters, microcrystalline cellulose from cotton linters and the commercial Avicel powder cellulose. Cotton linters (literature: 8 in number) were purchased from different sources as shown in Table 1. The reported literature MC celluloses from cotton linters (literature: 7 in number) were prepared by mild acid hydrolysis using different concentrations of sulphuric acid (H_2SO_4) or hydrochloric acid (HCl) to prepare the MC cellulose particles. There are several different grades of the microcrystalline cellulose powders currently commercially available under the brand name Avicel. For this study, Avicel PH-101 was used. A range of 16 Avicel powder samples all called PH-101 are produced by FMC Corporation and Biochemika Fluka, as reported in literature (Table 1), obtained from different sources and probably from different production trials. The crystalline structure of cotton linters, MCC from cotton linters and of Avicel PH-101 are assigned as cellulose I. Table 1 gives specifications available from the suppliers about the reported cellulose samples, (a) cotton linters, (b) its microcrystalline cellulose and (c) Avicel PH-101 used throughout the study. Our data on Avicel PH-101 are also included in Table 1, (c).

Table 1. List of native cellulose, (a) cotton linters and MC cellulose samples tested, from (b) cotton linters and (c) Avicel PH-101.

(a) Cotton linters

No	DP	Supplier	Country	Reference
1	2200	Industrial plant Tashkent	Tashkent, Uzbekistan	6
2	-	-	-	31
3	-	Nanjing Textiles Corp. Ltd	Jiangsu, China	29
4	-	Peter Temming AG	Glückstadt, Germany	29
5	-	-	-	29
6	-	-	-	32
7	-	-	-	33
8	920	Abu Zaabal Company	Heliopolis, Cairo	34

(b) MCC (cotton linters)

No.	DP	Source	Reference
1	165	hydrolysed from (a)1	6
2	-	-	35
3	150	hydrolysed from (a)8	34
4	350	hydrolysed from (a)8	34
5	-	-	29
6	-	-	32
7	-	hydrolysed from (a)6	32

(c) Avicel PH-101

No.	DP	Supplier	Country	Reference
1	-	-	-	36
2	-	Biochemika Fluka	-	35
3	-	-	-	33
4	-	Biochemika Fluka	Switzerland	our work
5	150	FMC Corporation	New Jersey, USA	6
6	-	Biochemika Fluka	Switzerland	37, 38
7	-	Biochemika Fluka	Switzerland	29
8	-	Asahi Kasei Chem. Co.	Tokio, Japan	39
9	225	FMC Corporation	Philadelphia, PA, USA	40
10	-	FMC Corporation	Philadelphia, PA, USA	41
11	170	FMC BioPolymer Co.	-	42
12	-	Biochemika Fluka	Switzerland	37, 38
13	130-178	FMC Corporation	USA	32
14	167	FMC Corporation	Philadelphia, PA, USA	43
15	-	Biochemika Fluka	Switzerland	37, 38
16	-	Biochemika Fluka	-	44

X-ray diffraction setup

Our WAXD measurements were performed using a Bruker/Siemens D5000 system with theta-theta drive goniometer (Division of Food Sciences, University of Nottingham). The diffraction patterns were recorded using a copper K-alpha X-ray source at a voltage of 40 kV and a 40 mA power (λ = 1.541 Angstroms). The diffractometer was used in reflection mode. The WAXD data was collected at 0.05 degree (2θ) resolution, from 4 to 38 degrees (2θ). Transmission measurements were performed on a Bruker D8 Discover system, with copper K-alpha source, with parallel spot optics, with 1 mm beam diameter. After recording the diffraction patterns, the intensity as a function of the scattering angle 2θ is processed using Microsoft Excel spreadsheet tool. The tested sample, Avicel PH-101 powder, was either spread to form a flat surface in a horizontal reflection holder, or pressed into discs and mounted in a vertical transmission holder.

For the literature reported samples, diffraction patterns were obtained using various X-ray diffractometers. We report here only the experimental mode, transmission or reflection.

Determination of the cellulose degree of order (crystallinity)

The degree of crystallinity in the cellulosic materials may be measured in several ways from an X-ray diffractogram. This review compiles 5 methods to evaluate the degree of crystallinity reported in the literature, such as:

1. Peak height method [8]
2. Ruland-Vonk method [10, 16]
3. Hermans-Weidinger method [10-12]
4. Jayme-Knolle method [13]
5. Deconvolution method (curve fitting) [45]

1. The X-ray diffraction peak height method

Earlier attempts in measuring crystallinity of cellulose samples took place with the work of L. Segal and co-workers [8]. The so-called peak height method, developed by Segal and co-workers, is an empirical method being the most common and simple method to determine the degree of crystallinity. This method has been widely used for the study of crystallinity of native cellulose. In this approach, the X-ray apparent crystallinity (%) of cellulose is calculated from the height ratio between the intensity of the crystalline peak and the total intensity after the subtraction of the background signal (non-crystalline)

measured without cellulose according to the following equation:

$$C = 100 \cdot \frac{I_{200} - I_{non-cr}}{I_{200}} \ [\%]$$

where: C expresses the apparent crystallinity [%] defined by Segal and co-workers, I_{200} gives the maximum intensity of the peak corresponding to the plane in the sample with the Miller indices 200 at a 2θ angle of between 22-24 degrees and I_{non-cr} represents the intensity of diffraction of the non-crystalline material, which is taken at an angle of about 18 degrees 2θ in the valley between the peaks as it is shown in Figure 1.

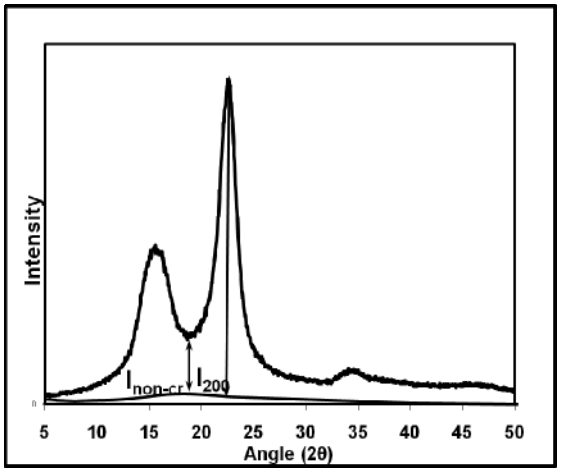

Figure 1. X-ray diffraction spectra of a cellulose I sample illustrating the peak height method.

2. Ruland-Vonk X-ray diffraction method

Another way to separate the crystalline and non-crystalline contributions to the diffracted intensity and estimate the crystallinity has been outlined by W. Ruland [9] and later on by C. G. Vonk [16]. The non-crystalline fraction of the scattering is obtained by measuring the scattering of the same sample on the non-crystalline form (Figure 2). The reflections are then scaled down below the crystalline reflections, and the fraction of integrated intensity of the crystalline phase out of total intensity including the non-crystalline background is referred to as the crystallinity of the sample. The approach is slightly similar to the amorphous (non-crystalline) subtraction method [38]. New to the amorphous (non-crystalline) subtraction method is the selection of a non-crystalline standard sample that is similar to the non-crystalline component in the sample. The non-crystalline state is defined by the criteria that the material doesn't give any indication of the lattice planes in the X-ray diffraction pattern. Various authors use different non-crystalline samples. The most used is ball milled cellulose and rarely used regenerated cellulose from dimethyl-acetamide/lithium chloride (DMAc/LiCl) solvent system or hemicelluloses to subtract the non-crystalline contribution from the diffraction profiles. The uncertainty of using ball milled cellulose, as a standard non-crystalline cellulose, is that there is no proof that are regions in a semicrystalline cellulose which have the same structure and scattering curve as ball milled cellulose [46]. After subtracting the diffractogram of the non-crystalline cellulose from the diffractogram of the whole sample, the apparent crystallinity (%) was calculated by dividing the remaining diffractogram area due to crystalline cellulose by the total area of the original diffractogram.

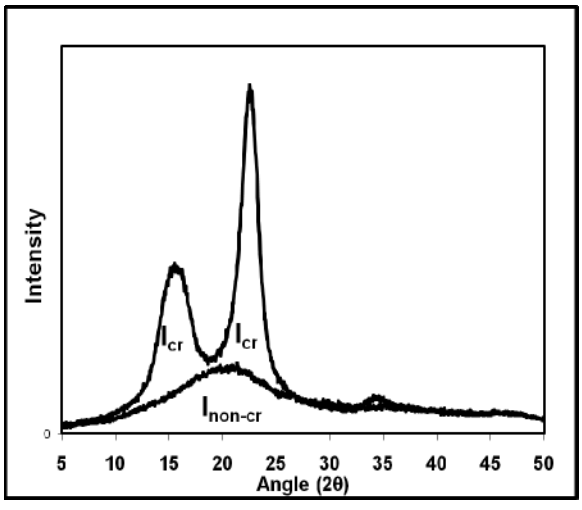

Figure 2. X-ray diffraction spectra of a cellulose I sample illustrating Ruland-Vonk's method.

The Ruland-Vonk X-ray method was further refined as the Rietveld refinement [47, 48], which uses the full diffraction

pattern in a least squares fitting numerical procedure to fit the complete X-ray diffractograms including the background or diffusive scattering due to non-crystalline regions.

3. Hermans-Weidinger X-ray diffraction method

The classical method developed by P. H. Hermans and A. Weidinger [10-12] is based on a two phase concept and it was used for the evaluation of crystallinity from X-ray intensity measurements. According to P. H. Hermans and A. Weidinger, a careful attention is given to the control of samples and of instrumental variables, and photographic recording of the diffracted beam is employed. Integration was performed by copying the traces of the photometer curves in duplicate on transparent paper of known weight per unit surface, cutting the figures out, weighing them and taking the average value. Denoting the mass of crystalline, non-crystalline fractions as M_{cr} and $M_{non\text{-}cr}$ and total mass as M respectively, the relationships between mass and cellulose apparent crystallinity is:

$$C = 100 \cdot \frac{M_{cr}}{M_{cr} + M_{non-cr}} = \left[\frac{\int I_{cr}(\theta)\, d\theta}{\int I_{cr}(\theta)\, d\theta + k_{non-cr}/k_{cr} \int I_{non-cr}(\theta)\, d\theta} \right]$$

where C is apparent crystallinity [%] defined by P. H. Hermans and A. Weidinger, k_{cr} and $k_{non\text{-}cr}$ are constants and the integrated intensities of crystalline I_{cr} and non-crystalline $I_{non\text{-}cr}$ fractions can be determined from the diffraction patterns (Figure 2). Using the above equation the following relationship [39] can be given:

$$\int I_{non-cr}(\theta)\, d\theta = -(k_{cr}/k_{non-cr}) \int I_{cr}(\theta)\, d\theta + M/k_{non-cr}$$

Using the linear relationship between $\int I_{non\text{-}cr}(\theta)\, d\theta$ and $\int I_{cr}(\theta)\, d\theta$ the value $k_{non\text{-}cr}/k_{cr}$ is given by the gradient (when different cellulose samples are taken into account). The diffraction angles were limited to the region between 7º and 42º since whole crystalline peaks are to be found in this range, and only diffuse background of the non-crystalline scattering was found at this range.

Figure 3 illustrates the X-ray diffraction spectra of a cellulose I sample presenting the X-ray method of P. H. Hermans and A. Weidinger. Evaluation of the diffuse background consists first in background correction scattered by air which is small and neglected. This portion of background radiation has to be subtracted in order to obtain a reliable measure of the quantity of the non-crystalline fraction. Background correction is still to be corrected due to thermal agitation of the atoms and Compton radiation. The background intensity of well-ordered crystals of sucrose was measured and subtracted from that of the cellulose over the range. Crystalline peaks were separated from diffuse background fraction by extrapolating smoothly the background curve near a crystalline peak and connecting the two end points of the peak. The separation of the crystalline I_{cr} and non-crystalline I_{non-cr} intensities is done usually with the help of appropriate software, Shimadzu XRD-6000 version 2.5, Japan [36].

The Hermans-Weidinger method of determining X-ray crystallinity of cellulose and the Ruland-Vonk method were found to be identical [49].

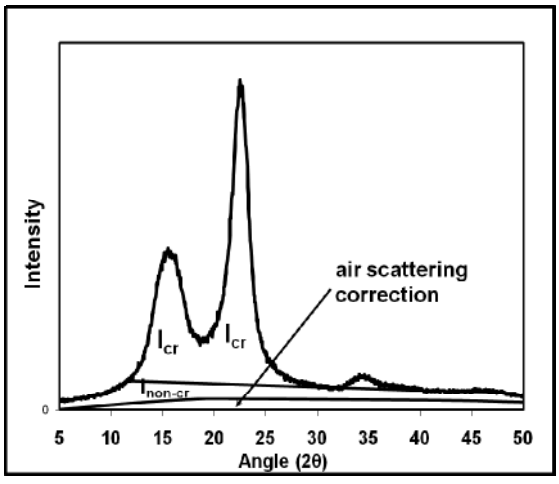

Figure 3. X-ray diffraction spectra of a cellulose I sample showing the X-ray method of P. H. Hermans and A. Weidinger.

4. Jayme-Knolle X-ray diffraction method

G. Jayme and H. Knolle [13] used two X-ray methods, Hermans-Weidinger method and of L. Segal and co-workers [8] to determine the apparent crystallinity of cellulose. The Hermans-Weidinger method is used by G. Jayme and H. Knolle by using different correction factors. No description of these correction factors is given in their publication. The peak height method is used as it is described by L. Segal and co-workers.

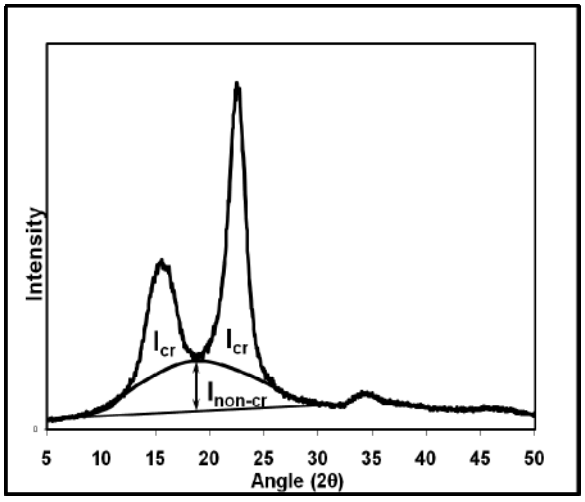

Figure 4. X-ray diffraction spectra of a cellulose I sample showing the X-ray method of G. Jayme and H. Knolle.

It must be mentioned that the Hermans-Weidinger method [12] is sensitive to the selection of the base line on the intensity trace, which is first applied to account for air scattering and non-coherent or instrumental effects. Since this was sometimes not well defined, this method should probably be given less credibility than the others. The peak height is thought to be a measure of relative estimation of the crystallinity and should not be used for estimating the absolute amount of crystalline and non-crystalline material in a cellulose sample. Out of the two mentioned X-ray methods, the authors decided for the Hermans-Weidinger method to determine cellulose crystallinity. Figure 4 shows the diffraction spectra of a cellulose I sample reflecting both X-ray methods, Hermans-Weidinger and peak height method, used by G. Jayme and H. Knolle in their publication.

G. Jayme and H. Knolle gave specific attention to the sample preparation which influences the final apparent crystallinity of cellulose.

5. The X-ray diffraction deconvolution method (curve fitting)

Given the drawbacks of the other methods, a sophisticated technique using deconvolution procedures is often applied for crystallinity measurements using suitable software or Microsoft Excel spreadsheet tool to separate the non-crystalline and crystalline contributions to the diffraction spectrum. For the curve fitting method, linear backgrounds were fitted to a simulated profile, based on the convolution of three sharp peaks, from 1-10, 110 and 200 crystalline reflections [50, 51] and one broad peak representing the non-crystalline reflection. Several shape functions can fit the complete X-ray diffractograms using least squares fitting. Gaussian functions [35, 52] are mostly often used for the deconvolution of the X-ray diffraction spectra but fitting procedures also make use of Lorentzian [53], combination of Gaussian-Lorentzian and Voigt [54] functions. Gaussian peak profiles were used for this study with free adjustment of intensity, position and breadth of crystalline peaks, and correction only of position and intensity of the non-crystalline peak. Figure 5 shows the diffraction pattern of a cellulose I illustrating the peak deconvolution method. This procedure was applied for our tested sample, Avicel PH-101, following the published method of R. Ibbett and co-workers [45]. The apparent crystallinity (%) is calculated from the ratio of the area of all crystalline peaks to the total area including non-crystalline fraction following the equation:

$$C = 100 \cdot \frac{I_{cr\ peak1} + I_{cr\ peak3} + I_{cr\ peak4}}{I_{cr\ peak1} + I_{cr\ peak3} + I_{cr\ peak4} + I_{non-cr}} \ [\%]$$

where: C is apparent crystallinity [%], $I_{cr\ peak1}$ represents the area under the first

crystalline peak in the diffraction pattern corresponding to the Miller index 1-10, $I_{cr\ peak\ 3}$ and $I_{cr\ peak\ 4}$ stand for the two areas under the second deconvoluted crystalline peak corresponding to the Miller index 110 and $I_{\text{non-cr}}$ is the area under the non-crystalline peak of the cellulose diffraction pattern.

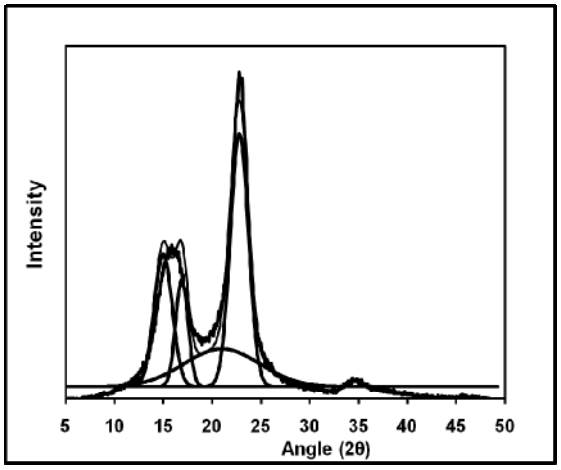

Figure 5. X-ray diffraction spectra of a cellulose I sample showing the peak deconvolution method.

Among the X-ray methods presented in this study, cellulose crystallinity can be also calculated by using the Debye calculations, described in detail by A. Thygessen and co-workers [55].

Results and discussions

Of the five X-ray methods proposed for the estimation of the crystallinity, the curve fitting method is used here to calculate apparent crystallinity (%) of our sample, Avicel PH-101. Figure 6 shows the X-ray diffraction spectra of our tested Avicel PH-101 powder cellulose measured in (a) reflection mode and (b) transmission mode illustrating the peak deconvolution method with peaks present at approximately 15, 16.5 and 22.8 degrees (2θ), corresponding to planes in the sample with Miller indices 1-10, 110, and 200 (direction "*c*" of the unit cell is along the chain axis of the polymer), showing that the crystalline component is cellulose I.

Table 2 shows the wide range of literature values for the calculated apparent crystallinity of cotton linters, its hydrolysed product and Avicel PH-101 powder categorized by the different measurement techniques and experimental modes, and it is obvious that the degree of order (crystallinity) of the same sample measured by different methods produces different results. Avicel PH-101 powder was chosen because it was the most extensively measured cellulose reported in the literature.

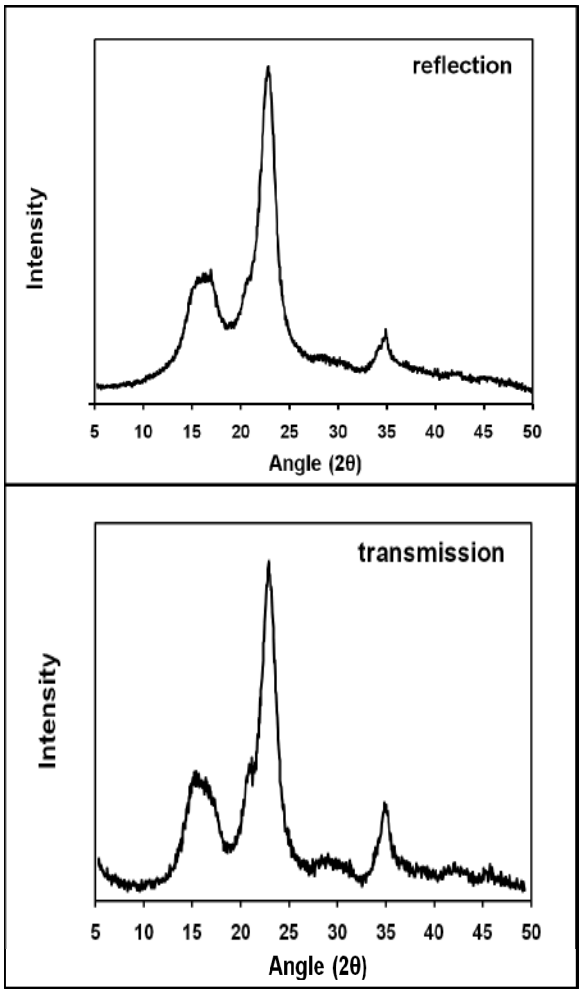

Figure 6. X-ray diffraction spectra of Avicel PH-101 powder cellulose measured in: (a, top) reflection mode and (b, bottom) transmission mode.

For the crystallinity analysis, the assumptions have to be made that all cotton linters, its microcrystalline cellulose and Avicel PH-101 used in literature studies were of the same quality, even though it has been reported that the quality of both samples can vary between batches and production locations [56, 57].

Table 2. Literature values for the apparent crystallinity of (a) cotton linters, (b) MC cellulose from cotton linters and (c) Avicel PH-101 categorized by the different measurement techniques and experimental modes.

(a) Cotton linters

No	DP	Apparent cryst. [%]	Method	Experimental mode	Reference
1	2200	- (*)	-	-	6
2	-	56-65	-	-	31
3	-	60	Ruland-Vonk	transmission	29
4	-	62	Ruland-Vonk	transmission	29
5	-	63	Ruland-Vonk	transmission	29
6	-	63	-	-	32
7	-	64-65	Ruland	-	33
8	920	78	peak height	reflection	34

(*) source for b (1), no crystallinity data given.

(b) MCC from cotton linters

No.	DP	Apparent cryst. [%]	Method	Experimental mode	Reference
1	165	65	peak deconvolution	transmission	6
2	-	67 (*)	peak deconvolution	reflection+transmission	35
3	150	72	peak height	reflection	34
4	350	76	peak height	reflection	34
5	-	77	Ruland	transmission	29
6	-	78	-	-	32
7	-	83	-	-	32

(*) the results were calculated as an average of the ones obtained by reflection and transmission measurements to minimise the effect of preferred orientation.

(c) Avicel PH-101

No.	DP	Apparent cryst. [%]	Method	Experimental mode	Reference
1	-	37 (*)	Hermans-Weidinger	-	36
2	-	54 (**)	peak deconvolution	reflection+transmission	35
3	-	55-56	Ruland	-	33
4	170 (****)	57	peak deconvolution	reflection	our work
5	170 (****)	88	peak height	reflection	our work
6	150	59	peak deconvolution	transmission	6
7	-	61 (***)	peak deconvolution	-	37, 38
8	-	61	Ruland-Vonk	transmission	29
9	-	63	Hermans- Weidinger	-	39
10	225	69	Knolle-Jayme	transmission	40
11	-	72	unknown	reflection	41
12	170	77	Vonk	reflection	42
13	-	78(**)	amorphous subtraction	-	37, 38
14	130-178	78	unknown	-	32
15	167	82	Hermans-Weidinger	transmission	43
16	-	92 (***)	peak height	-	37, 38
17	-	93	peak height	-	44

(*) calculated crystallinity data of 4 averaged measurements
(**) the results were calculated as an average of the ones obtained by reflection and transmission measurements to minimise the effect of preferred orientation
(***) standard deviations from 3 measurements
(****) by gel permeation chromatography in DMAc / LiCl

The reported cellulose apparent crystallinity results from Table 2 should be discussed and analysed with precaution in terms of the X-ray method and also of the chosen experimental mode. The relative intensities of reflections vary between transmission and reflection geometries. This may be due to various factors, including 1) the differences in angular dependence of path lengths, for each geometry, 2) differences due to preferential orientation of crystallites in transmission resulting from sample pressing, 3) effective absorption factors differing between the two geometries. It is difficult to differentiate between the two experimental modes in the X-ray diffraction experiments. The reflection geometry is thought to be more suitable for quantitative determination morphological composition [55], as the absorption factor is constant with angle and also there is less risk that the sample is perturbed by pressing.

Up to five different X-ray methods used to assess the crystalline fraction of a cellulose diffraction pattern in order to determine the cellulose crystallinity were reviewed in this study. The overall reported apparent crystallinity (%) values of cotton linters vary between 56-78 % with an average of 67 %, its microcrystalline cellulose apparent crystallinity (%) was larger than that of cotton linters between 65-83 % while the apparent crystallinity of Avicel PH-101 appears to vary quite significantly from one product to another 37-93 % dependent on the method and experimental mode used.

Compared to all X-ray diffraction approaches, peak height method gave the highest X-ray crystallinity values. With this method, apparent crystallinity (%) values for cotton linters samples reported in the literature are roughly 78 %, its hydrolysed product around 72-76 % and higher for Avicel PH-101 about 92-93 %, dependent on the experimental mode. For example, our results are consistent with the ones produced by S. Park and co-workers [38]. They used three X-ray methods (peak height, peak deconvolution and amorphous contribution subtraction) to calculate the apparent crystallinity (%) of 11 cellulose samples, including also the mentioned samples. They found that, based on a method frequency study, the peak height method gave significantly higher crystallinity values than the other methods. Due to its simple way of application, the peak height method is useful for comparing the relative differences in crystallinity between samples. However, this method is thought to be a measure of relative estimation of the crystallinity and should not be used for estimating the absolute amount of crystalline and non-crystalline material in a cellulose sample. The reasons behind these observations are presented in more details in the work of S. Park [38] and of A. Thygessen [55].

Using the Ruland-Vonk method for cotton linters samples, the reported literature values for crystallinity are in a narrow range of 60-63 % [29, 32, 33]. This method presents various disadvantages. The method is very sensitive to instrumental inaccuracies. Additional to this, the non-crystalline standard sample should be chosen in such a way that it coincides with the non-crystalline background from the tested sample, which is a difficult task. These limitations have been discussed in the literature [38, 55] although according to H. P. Fink and E. Walenta [58] and K. P. Sao and co-workers [59], the Ruland-Vonk method is thought to be the most suitable way to evaluate the crystallinity in plant fibres.

The apparent crystallinity of the hydrolysed product of the cotton linters was found to be 65-67 % by means of peak deconvolution method [6, 35] up to values of 78 and 83 % [32] by unspecified literature methods.

Measurements on the reference sample, Avicel PH-101, of different characteristics have shown different apparent crystallinity values. With Hermans-Weidinger and Ruland-Vonk methods, the results for Avicel PH-101 crystallinity vary quite a lot. These large differences can be due to

different X-ray geometries used, reflection or transmission, which can influence cellulose crystallinity and the hypothesis recommended by S. Park and co-workers [38] and G. V. Gusev [49] doesn't apply in this case. Overall, the reflection method has the most potential for quantitative crystallinity measurements. The peak deconvolution method used by different authors [6, 37, 38, our work] and different in sample geometry modes seems to give roughly similar crystallinity values for Avicel PH-101.

Conclusions

This survey intended to present approaches and literature results of WAXD in characterising apparent crystallinity of three cellulose samples. It was shown that the crystallinity for native cellulose is dependent on data evaluation procedure applied to the measurement, on the experimental mode, but should be independent of the choice of the X-ray instrument (as it is reported in literature). Among the two geometries used, reflection and transmission, reflection geometry is considered most suitable for quantitative crystallinity measurements.
Several questions in the field of X-ray diffraction remain open. There is still room for improvement concerning the developed methods and current interpretations of the crystalline structure of cellulose.

Acknowledgement

We thankfully acknowledge funding provided by the European Community's Seventh Framework Programme [FP7/2007-2013] under Grant Agreement No. 214015.

References

1. K. Fleming, D. G. Gray, and S. Matthews. Cellulose Crystallites, Chem. Eur. J. 7 (2001) 1831-1835.

2. Microcrystalline Cellulose. In: European Pharmacopoeia. 4th edition (2002), Strasbourg, France, Council of Europe.

3. M. A. S. Azizi Samir, F. Alloin, and A. Dufresne. A Review of Recent Research into Cellulosic Whiskers, their Properties and their Application in Nanocomposite Field, Biomacromolecules 6 (2005) 612-626.

4. N. E. Kotelnikova, E. F. Panarin. Cellulose Modification by Biologically Active Substances for Biomedical Applications, Cellul. Chem. Technol. 39 (2005) 437-450.

5. S. Elazzouzi-Hafraoui, Y. Nishiyama, J. L. Putaux, L. Heux, F. Dubreuil, and C. Rochas. The Shape and Size Distribution of Crystalline Nanoparticles Prepared by Acid Hydrolysis of Native Cellulose, Biomacromolecules 9 (2008) 57-65.

6. K. Leppänen, S. Anderson, M. Torkkeli, M. Knaapila, N. Kotelnikova, and R. Serimaa. Structure of Cellulose and Microcrystalline Cellulose from Various Species, Cotton and Flax Studied by X-Ray Scattering, Cellulose 16 (2009) 999-1015.

7. J. Ganster and H.-P. Fink. Polymer Handbook, 4th edition (Eds.: J. Brandrup, E. H. Immergut, E. A. Grulke, A. Abe, D. Bloch), Wiley, New York, (1999) 135-157.

8. L. Segal, J. J. Creely, A. E. Jr. Martin, and C. M. Conrad. An Empirical Method for Estimating the Degree of Crystallinity of Native Cellulose using X-ray Diffractometer, Tex. Res. J. 29 (1959) 786-794.

9. W. Ruland. X-ray Determination of Crystallinity and Diffuse Disorder Scattering, Acta Crystallogr. 14 (1961) 1180-1185.

10. P. H. Hermans and A. Weidinger. Quantitative X-Ray Investigations on the Crystallinity of Cellulose Fibers. A Background Analysis, J. Appl. Phys.19 (1948) 491-506.

11. P. H. Hermans and A. Weidinger. X-ray Studies on the Crystallinity of Cellulose, J. Polymer Sci. 4 (1949) 135-144.

12. P. H. Hermans and A. Weidinger. Relative Intensities of the Crystalline X-ray Lines in Cellulose Fibres, Textile Res. J. 31 (1961) 558-571.

13. G. Jayme, and H. Knolle. Introduction into Empirical X-ray Determination of Crystallinity of Cellulose Materials, Das Papier 18 (1964) 249-255.

14. H. Knolle and G. Jayme. Über ein digitales Verfahren zur empirischen Bestimmung der Röntgenkristallinität cellulosehaltiger Stoffe und seine Anwendung, Das Papier 19 (1965) 106-110.

15. G. Jayme. Determination and Importance of Cellulose Crystallinity, Cellul. Chem. Technol. 9 (1975) 477-492.

16. C. G. Vonk. Computerization of Ruland's X-ray Method for Determination of the Crystallinity in Polymers, J. Appl. Crystallogr. 6 (1973) 148-152.

17. P. Zugenmaier. Conformation and Packing of Various Crystalline Cellulose Fibers, Prog. Polym. Sci., 26 (2001) 1341-1417.

18. F. Horii, A. Hirai, and R. Kitamaru. CP/MAS ^{13}C NMR Spectra of the Crystalline Components of Native Celluloses, Macromolecules 20 (1987) 2117-2120.

19. R. H. Newman and J. A. Hemmingson. Determination of the Degree of Cellulose Crystallinity in Wood by Carbon-13 Nuclear Magnetic Resonance Spectroscopy, Holzforschung 44 (1990) 351-355.

20. R. H. Newman. Estimation of the Lateral Dimensions of Cellulose Crystallites using ^{13}C NMR Signal Strengths, Solid State NMR 15 (1999) 21-29.

21. P. T. Larsson, K. Wickholm, and T. Iversen. A CP/MAS ^{13}C NMR Investigation of Molecular Ordering in Celluloses, Carbohydr. Res. 302 (1997) 19-25.

22. G. Zuckerstätter, G. Schild, P. Wollboldt, T. Röder, H. K. Weber, and H. Sixta. The Elucidation of Cellulose Supramolecular Structure by ^{13}C CP-MAS NMR, Lenzinger Berichte 87 (2009) 38-46.

23. U. Richter, T. Krause, W. Schempp. Untersuchung zur Alkalibehandlung von Cellulosefasern. Teil 1. Infrarotspektroskopische und Röntgenographische Beurteilung der Anderung des Ordnungszustandes, Angew. Makromol. Chem. 185 (1991) 155-167.

24. S. H. D. Hulleman, J. M. van Hazendonk, J. E. G. van Dam. Determination of Crystallinity in Native Cellulose from Higher Plants with Diffuse Reflectance Fourier Transform Infrared Spectroscopy, Carbohydrate Res. 261 (1994) 163-172.

25. T. Baldinger, J. Moosbauer, and H. Sixta. Supermolecular Structure of Cellulosic Materials by Fourier Transform Infrared Spectroscopy (FT-IR) Calibrated by WAXS and ^{13}C NMR, Lenzinger Berichte, 79 (2000) 15 - 17.

26. B. H. Stuart. Polymer Crystallinity Studied using Raman Spectroscopy, Vib. Spectrosc. 10 (1995) 79-87.

27. R. P. Paradkar, S. S. Sakhalkar, X. He, and M. S. Ellison. Estimating Crystallinity in High Density Polyethylene Fibers using Raman Spectroscopy, J. App. Poly. Sci. 88 (2003) 545-549.

28. K. Schenzel, S. Fischer, and E. Brendler. New Method for Determining the Degree of Cellulose I Crystallinity by Means of FT Raman Spectroscopy, Cellulose 12 (2005) 223-231.

29. T. Röder, J. Moosbauer, M. Fasching, A. Bohn, H. P. Fink, T. Baldinger, and Herbert Sixta. Crystallinity Determination of Native Cellulose Comparison of Analytical

Methods, Lenzinger Berichte 86 (2006) 85-89.

30. U. P. Agarwal, R. S. Reiner, and S. A. Ralph. Cellulose I Crystallinity Determination using FT–Raman Spectroscopy: Univariate and Multivariate Methods, Cellulose 16 (2010) 721-733.

31. D. Klemm, B. Heublein, H. P. Fink, and A. Bohn. Cellulose: Fascinating and Sustainable Raw Material, Angew. Chem. Ed. 44 (2005) 3358-3393.

32. J. Schurz, and H. Klapp. Untersuchungen a mikrokristallinen und mikrofeinen Cellulosen, Das Papier 30 (1976) 510-513.

33. H. P. Fink and B. Phillip. Wide-angle X-ray Investigation of the Supermolecular Structure of Native Cellulose and Cellulosic Man-made Fibres (unpublished publication).

34. A. M. A. Nada, M. Y. El-Kady, E. S. Abd El-Sayed, and F. M. Amine. Preparation and Characterization of Microcrystalline Cellulose (MCC), BioResources, 4 (2009), 1359-1371.

35. R. Teeäär, R. Serimaa, and T. Paakkari. Crystallinity of Cellulose, as Determined by CP/MAS NMR and XRD Methods, Polym. Bull., 17 (1987) 231-237.

36. O. M. Y. Koo and P.W. S. Heng. The Influence of Microcrystalline Cellulose Grade on Shape and Shape Distributions of Pellets Produced by Extrusion-Spheronization, Chem. Pharm. Bull., 49 (2001) 1383-1387.

37. S. Park, D. K. Johnson, C. I. Ishizawa, P. A. Parilla, and M. F. Davis. Measuring the Crystallinity Index of Cellulose by Solid State ^{13}C Nuclear Magnetic Resonance, Cellulose 16 (2009) 641-647.

38. S. Park, J. O. Baker, M. E. Himmel, P. A. Parilla, and D. K. Johnson. Cellulose Crystallinity Index: Measurement Techniques and their Impact on Interpreting Cellulase Performance, Biotechnology for Biofuels 3 (2010) 1-10.

39. Y. Nakai, E. Fukuoka, and S. Nakajima. Crystallinity and Physical Characteristics of Microcrystalline Cellulose, Chem. Pharm. Bull. 25 (1977) 96-101.

40. P. Kleinebudde, M. Jumaa, and F. El Saleh. Influence of Degree of Polymerisation on Behaviour of Cellulose during Homogenisation and Extrusion/Spheronization, AAPS Pharmasci. 2 (2000) 1-10.

41. V. Kumar and S. H. Kothari. Effect of Compressional Force on the Crystallinity of Directly Compressible Cellulose Excipients, Int. J. Pharm., 177 (1999) 173–182.

42. M. Ioelovich, A. Leykin, and O. Figovski. Study of Cellulose Paracrystallinity, BioResources 5 (2010) 1393-1407.

43. E. Doelker and R. Gurny. Degrees of Crystallinity and Polymerization of Modified Cellulose Powders for Direct Tableting, Powder Technology 52 (1987) 207-213.

44. F. Dourado, F. M. Gama, E. Chibowski, and M. Mota. Characterization of Cellulose Surface Free Energy, J. Adhesion Sci. Technol., 12 no. 10 (1998) 1081-1090.

45. R. Ibbett, D. Domvoglou, and D. A. S. Phillips. The Hydrolysis and Recrystallisation of Lyocell and Comparative Cellulosic Fibres in Solutions of Mineral Acid, Cellulose 15 (2008) 241-254.

46. J. Mann. Modern Methods of Determining Crystallinity in Cellulose, Pure Appl. Chem. 5 (1962) 91-106.

47. H. M. Rietveld. Line Profiles of Neutron Powder-diffraction Peaks for Structure Refinement, Acta Cryst. 22 (1967) 151-152.

48. H. M. Rietveld. A Profile Refinement Method for Nuclear and Magnetic Structures. J. Appl. Cryst. 2 (1969) 65-71.

49. G. V. Gusev. Hermans-Weidinger X-ray Diffraction Technique for

Determining Polymer Crystallinity and the Use of the Ruland Ratio, Polym. Sci. 20 (1978) 1295-1297.

50. F. J. Kolpak, and J. Balckwell. Determination of the Structure of Cellulose II, Macromolecules 9 (1976) 273-278.

51. A. Sarko, and A. J. Stipanovic. Packing Analysis of Carbohydrates and Polysaccharides. 6. Molecular and Crystal Structure of Regenerated Cellulose II, Macromolecules 9 (1976) 851-857.

52. L. E. Hult, J. Iversen, and J. Sugiyama. Characterization of the Supramolecular Structure of Cellulose in Wood Pulp Fibres, Cellulose 10 (2003) 103-110.

53. J. He, S. Cui, and S-Y. Wang. Preparation and Crystalline Analysis of High-grade Bamboo Dissolving Pulp for Cellulose Acetate, J Appl. Polym. Sci. 107 (2008) 1029-1038.

54. C. J. Garve, I. H. Parker, and G. P. Simon. On the Interpretation of X-ray Diffraction Powder Patterns in Terms of the Nanostructure of Cellulose I Fibres, Macromol. Chem. Phys. 206 (2005) 1568-1575.

55. A. Thygessen, J. Oddershede, and H. Lilholt. On the Determination of Crystallinity and Cellulose Content in Plant Fibres, Cellulose 12 (2005) 563-576.

56. M. Landin, R. Martinezpacheco, J. L. Gomezamoza, C. Souto, A. Concheiro, and R. C. Rowe. Effect of Country of Origin on the Properties of Microcrystalline Cellulose, Int. J. Pharm. 91 (1993) 123-131.

57. R. C. Rowe, A. G. McKillop, D. Bray. The Effect of Batch and Source Variation on the Crystallinity of Microcrystalline Cellulose, Int. J. Pharm. 101 (1994) 169-172.

58. H. P. Fink and E. Walenta. Röntgenbeugungsuntersuchungen zur übermolekularen Struktur von Cellulose im Verarbeitungsprozeß, Das Papier 48 (1994) 739-748.

59. K. P. Sao, B. K. Samantaray, and S. Bhattacherjee. Analysis of Lattice Distortions in Ramie Cellulose, J. Appl. Polym. Sci. 66 (1997) 2045-2046.

Lenzinger Berichte 89 (2011) 132-141

^{13}C-NMR SPECTROSCOPICAL INVESTIGATIONS OF THE SUBSTITUENT DISTRIBUTION IN CELLULOSE XANTHATES

Katarzyna Dominiak[1,2], Horst Ebeling[1], Jürgen Kunze[1] and Hans-Peter Fink[1*]

[1] Fraunhofer Institute for Applied Polymer Research, Geiselbergstr. 69, 14476 Potsdam-Golm, Germany
[2]Cordenka GmbH, 63784 Obernburg, Germany

*Phone: (+49) 331 568-1112; Fax: (+49) 331 568-3000; Email: hans-peter.fink@iap.fraunhofer.de

A new method has been developed for determining the distribution of xanthate groups of viscose that uses ^{13}C-NMR spectroscopy to investigate stabilized cellulose xanthate. The xanthate groups are stabilized by converting the cellulose xanthate with diethylchloracetamide or benzyl bromide.

The substituent distribution in the cellulose xanthates was analyzed under the aspect of varying carbon disulfide input and, additionally, in the specific case of using frozen alkali cellulose. The varying input of carbon disulfide results in cellulose xanthates ranging in DS from 0.5 to 1.65 and showing always a clearly preferred substitution at the C-6 position. Further, the primary hydroxyl groups show the highest relative reactivity as compared to the C-2 and C-3 positions at the lowest total degree of substitution (approx. 0.5) which is close to technical viscose. When frozen alkali cellulose was used there was a reduction in the overall degree of substitution of the cellulose xanthates compared to the case of freshly alkalized alkali cellulose. This is the result of a partial phase transition to Na-cellulose II by the low temperature and a reduction in alkali cellulose activity of Na-cellulose II as compared to Na-cellulose I with regard to xanthation. In terms of the relative distribution of the xanthate groups, we observed a decrease in substitution in the hydroxyl groups in the C-2 position.

Keywords: *Viscose process, cellulose xanthate stabilization, ^{13}C-NMR spectroscopy, distribution of substituents, CS_2 input, alkali cellulose*

Introduction

The viscose process introduced more than 100 years ago still achieves a production volume of more than 2.5 million tons annually despite its well-known environmental issues and it remains the primary technology used for producing cellulose fibers and filaments.

Cellulose activated with sodium hydroxide is converted to cellulose xanthate with carbon disulfide. Cellulose xanthate is dissolved in diluted sodium hydroxide forming the so-called viscose from which fibers and filaments are spun using the wet spinning process [1, 2]. The processing properties of the viscose and the resulting fiber properties are influenced by the quality of the viscose which, among others, is determined by the distribution of the xanthate groups within the anhydroglucose unit as well as along and between the polymer chains. The distribution of the substituents in the cellulose xanthate is determined by the synthesis process and is subject to fundamental changes during the viscose's ripening process. The processes that lead to changes in the xanthation pattern during viscose ripening have been controversially debated in the past and continue to be a topic of scientific discussion. One reason for this is undoubtedly that xanthate groups are unstable making them difficult to be determined accurately [3-5].

It has been established that NMR spectroscopy is very useful for determining the overall degree of substitution of polymers and, especially, for ascertaining the substituent distribution. NMR investigations of viscose with regard to the substitution of hydroxyl groups at C-2, C-3, and C-6 position have already been described by König [3] and Kamide [4]. Due to the well-known instability of cellulose xanthates, changes in the substituent distribution during the storage of viscose as well as during NMR measuring have to be considered. König reduced the measuring time by using ^{13}C enriched CS_2, which, however, only led to relative degrees of substitution.
Converting cellulose xanthates into stable derivatives, introduced by H. Fink *et* al. [6] as early as 1934, may offer the possibility of investigating viscose provided that good solution conditions and thus a residue-free dissolution of the derivatives can be achieved. With this aim in mind, methyl cellulose xanthate was synthesized and a ^{13}C-NMR spectrum of this solution was made by Takahashi [7] as early as 1986. However, as there were no visible substitution effects in the spectrum interval of the cellulose ring C atoms, there was no way of determining the substitution pattern of the cellulose xanthate. A ^{13}C-NMR investigation of diethylacetamide cellulose xanthate has been further described [8], however, it did not indicate any substitution of secondary hydroxyl groups. Thus a numerical evaluation of the substitution pattern from this NMR spectrum was not possible.
Russler *et* al. [5, 9] developed a method based on converting cellulose xanthates into stable iodine-acetanilide derivatives, however, without publishing NMR results on the substituent distribution so far.
Quite recently, Schwaighofer *et* al. [10] investigated the xanthate group distribution of viscose by ^{1}H-NMR spectroscopy, with the xanthate groups stabilized by allyl bromide.

Our paper introduces methods for stabilizing technical viscose and determining the stabilized xanthate group distribution by ^{13}C-NMR spectroscopy. The new method has been applied to elucidate the average distribution of substituents i) as a function of the degree of xanthation due to varying CS_2 input in the reaction, and ii) as a function of varying alkali cellulose structures with emphasis on frozen alkali cellulose.

Experimental

Viscose preparation and characterization

As cellulose raw material we used commercial dissolving pulp (softwood sulfite pulp) with a degree of polymerization (DP) of approx. 700. The cellulose was mixed into a slurry in 18 % NaOH at 50 °C and 20 °C in a solid to liquor ratio of 1:30. After an alkalization period of 45 min the cellulose was squeezed. The alkali cellulose that formed was composed of 30-34 % cellulose and 14-16 % sodium hydroxide. The alkali cellulose was shredded and preripened in the rotary pistons of a rotary evaporator at 54 °C and 28 °C to the required degree of polymerization. Then the alkali cellulose was reacted with carbon disulfide in a rotary evaporator. The alkali cellulose was heated to 28 °C under vacuum and reacted with varying amounts of carbon disulfide (28 %, 32 %, and up to 200 % in relation to the cellulose). The xanthation period was usually 1.5 h. This time period was extended to up to 3 h for the highly-substituted viscose, whereby after a 1.5 h sulfurization period 100 % CS_2 was added in a second step. The reaction mixture was kept at 28 °C in a water bath. The resulting cellulose xanthate (CX) was then dissolved at 8 °C in diluted sodium hydroxide creating a viscose with a composition of 8.5 % cellulose and 6 % sodium hydroxide. As a routine, the γ-values as the average degree of substitution (DS) multiplied with 100 was determined according to the Fock-method (see in [1]).

Stabilizing the viscose

Stabilization of the viscose was performed by two different stabilizing reactions based on i) diethylchloracetamide according to

[6], and ii) benzyl bromide. Approximately 50 ml of ice-cooled water was added little by little to between 5 g and 7 g of viscose and stirred with a glass stirrer until a low viscosity solution was formed. After adding phenolphthalein as an indicator, the viscose solution was neutralized with diluted acetic acid under constant stirring and then 2.5 moles of diethylchloracetamide on the one hand and benzyl bromide per 1 mole AGU on the other hand were added. Approximately 4 moles of the stabilizing reagent were added to the highly-substituted cellulose xanthates. After precipitating the polymer, the reaction mixture was stirred at low temperature for one hour. The stabilized cellulose xanthate was transferred as a precipitate to a G-2 frit, washed multiple times with distilled water and then with 50 ml of ethanol and 10 ml of diethyl ether and dried in a vacuum exsiccator at room temperature [6,11].

Investigation of the alkali cellulose formation by ^{13}C-CP/MAS-NMR

High-resolution solid state ^{13}C-NMR is well suitable for the investigation of alkali cellulose [12, 13]. In the present paper we used a NMR spectrometer from VARIAN (Unity 400) at a resonance frequency of 100.57 MHz. High-resolution spectra of the wet solid state alkali cellulose were obtained by the cross polarization / magic angle spinning (CP/MAS) method. Sample rotation was 5 to 6 kHz, contact time was 1 ms and the interval between experiments was 3 s.

The samples treated with sodium hydroxide were mechanically pressed for the ^{13}C-CP/MAS-NMR measurements. Around 0.1 cm³ of each substance was filled in a sample rotor. Measuring time was around 20 h.

Measuring the ^{13}C-NMR spectra of the stabilized viscose

The NMR spectra from the solutions were obtained by a Unity Inova 500 spectrometer (VARIAN) at a measuring frequency of 125 MHz for the ^{13}C atoms and a ^{1}H decoupling frequency of 499.8 MHz under quantitative measuring conditions (inverse gated decoupling technique). For the measurements, approximately 100 mg of the polymer was solubilized in 1 ml of DMSO-d_6 at 80 °C each time and then transferred to a 5 mm diameter NMR sample tube. The measurements were also performed at a temperature of 80° C. In order to achieve a sufficient signal-to-noise ratio, approx. 12,000 – 32,000 accumulations were carried out per measurement. An acquisition time of 0.4 s and a relaxation delay of 5 s resulted in measuring times of 18 h to 24 h per spectrum.

The calibration of the ^{13}C-NMR spectra was done externally using tetramethylsilane (δ_{TMS}=0 ppm).

The processing and evaluation of the spectra, as well as signal integration, were performed using the spectrometer internal VNMR software.

Results and discussion

The xanthate groups were stabilized through alkylation by diethylacetamide and benzyl bromide according to Figure 1, leading to the stable compounds diethylacetamide cellulose xanthate (DACX) and benzyl cellulose xanthogenate (CXBE), respectively. We found a rather good agreement between γ-values (divided by 100), DS values from wet chemical analysis, and the DS-values obtained from the ^{13}C-NMR spectra.

Peak assignment in ^{13}C-NMR spectra of stabilized cellulose xanthate

The signal assignment of the ^{13}C-NMR spectrum for stabilized CX, using DACX as an example, can be seen in Figure 2. The spectrum was interpreted under the rules of the NMR line shifts using model substances with differing degrees of substitution and with the aid of literature.

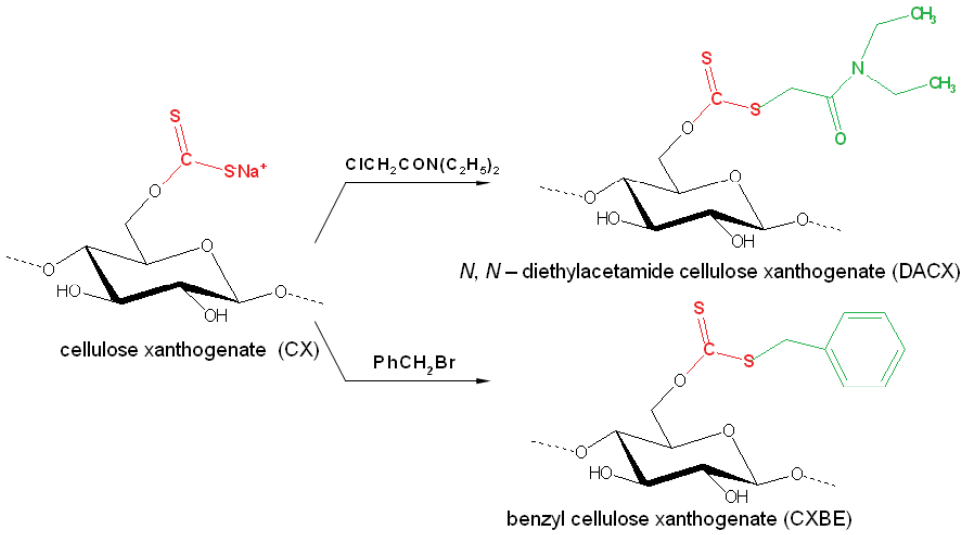

Figure 1. Derivatization of cellulose xanthate.

The ^{13}C-NMR spectrum of the DACX displays intensive signals for the functional groups as well as for the AGU of the cellulose between 10 und 220 ppm. The lines C-1 to C-6 of the cellulose structure are found between 50 ppm and 110 ppm.
At 212-214 ppm line E, representing the carbon atom of the dithiocarbonate group, was shifted farthest downfield. The peak of the carbamoyl carbon atom C is located around 164 ppm. The two well-separated lines (A) between 10 and 20 ppm, which are generated by the two methyl groups, are of interest for quantitative analysis. They make it possible to analyse the total degree of substitution which can be related to the γ value.

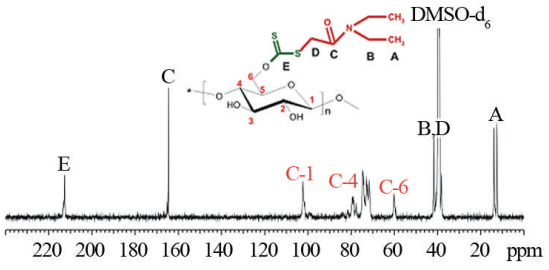

Figure 2. ^{13}C-NMR spectrum of DACX in DMSO-d6 with the formula for a monomer unit.

Partial degrees of substitution, e.g. the substitution at C-2, C-3, and C-6 of the AGU of the cellulose, can only be derived from the changes in the region of the C-1 to C-6 lines.

Figure 3 shows in a magnification the ^{13}C-NMR spectra in the region of the cellulose lines for C-1 to C-6 for unmodified cellulose and a DACX sample.
The spectrum of unmodified cellulose serving as a reference shows the ^{13}C lines of the non-substituted AGU. The six carbon atoms of the anhydroglucose ring correspond to the well known lines at 60 ppm (C-6), in the range of 70-75 ppm as poorly separated lines of C-2, C-3, C-5, at 80 ppm (C-4), and at 100 ppm (C-1).

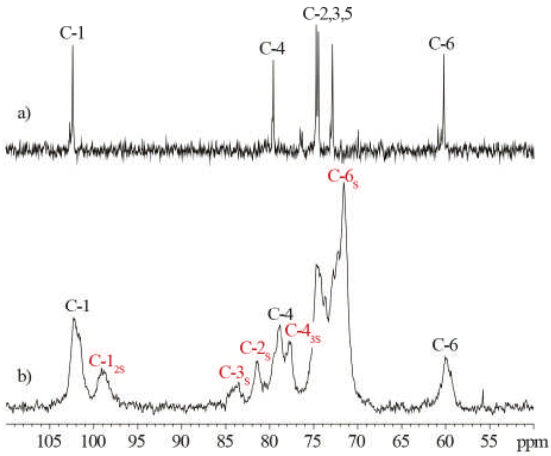

Figure 3. ^{13}C-NMR spectra of cellulose and DACX in the range of the cellulose carbon atoms.
a) Cellulose (reference) in DMSO-d6
b) DACX in DMSO-d6

As to be expected, the ^{13}C-NMR spectrum of DACX reveals considerable changes in

the chemical shift of some lines as compared to the spectrum of non-substituted cellulose. The substitution of a proton by a xanthate group or stabilized xanthate group within the hydroxyl group of a specific carbon atom of the AGU is expressed in a downfield shift of the affected carbon resonance by a few ppm. Accordingly, the substitution in the C-6 atom provokes a resonance shift downfield by ~11 ppm. The functionalization of the hydroxyl groups of the C-2 and C-3 carbon atoms causes a downfield shift by 8 to 9.5 ppm. This is reflected in the ^{13}C-NMR spectrum by the appearance of additional peaks for C-2, C-3 and C-6 (Figure 3).

The signals of the C atoms neighboring the carbon atom of the substituted hydroxyl group experience a slight shift upfield (due to the gamma-effect). As a result, the corresponding resonance lines split up. The ^{13}C-NMR spectrum seen in Figure 3b clearly shows that the substitution at C-2 and C-3 results in the separation of the C-1 and C-4 signals into two signals (C-1 and C-1_{2s} as well as C-4 and C-4_{3s}).

Comparing the ^{13}C-NMR spectra of cellulose and stabilized cellulose xanthate one can see that the DACX spectrum exhibits broader resonance peaks. This is the result of lower molecular mobility in the solution due to the higher DP and the cellulose substitution.

Calculating the degree of substitution from the ^{13}C-NMR Spectrum

The quantitative analysis of the ^{13}C-NMR spectra is performed by integrating the suitable peaks, i.e. each degree of substitution is calculated from the area of the corresponding signal. The areas of the peaks are unbiased when the measurement is performed with no NOE effect.

The equations used to calculate the degree of substitution are summarized as follows. The designation of the NMR signals is according to Figure 2 and Figure 3. DX_{CX} represents the overall (or total) degree of substitution. DS_2, DS_3, and DS_6 are the partial degrees of substitution of the corresponding C atom.

In order to calculate the partial and overall degrees of substitution (DS_i and DS_{CX}), the area of the suitable peaks is related to the area of the C-1 peak [equations (1) to (4)].

$$(1) \qquad DS_2 = \frac{I_{C-1_{2s}}}{I_{C-1} + I_{C-1_{2s}}}$$

$$(2) \qquad DS_3 = \frac{I_{C-3_s}}{I_{C-1} + I_{C-1_{2s}}}$$

$$(3) \qquad DS_6 = 1 - \frac{I_{C-6}}{I_{C-1} + I_{C-1_{2s}}}$$

$$(4) \qquad DS_{CX} = \frac{I_{\frac{A}{2}}}{I_{C-1} + I_{C-1_{2s}}}$$

The following normalization also applies:

$$(5) \qquad DS_{CX} = DS_2 + DS_3 + DS_6$$

In case of evaluating the partial degree of substitution for C-3, it should be noted that the signal (C-3) caused by the substitution in the hydroxyl groups in the C-3 position often is small and poorly separated especially in the case of low-substituted cellulose xanthates. Consequently, since a direct determination of the DS_3 in the case of cellulose xanthates with a very low degree of esterification is error-prone, the degree of substitution in C-3 is better given as the difference between the reliable overall degree of substitution and the partial degrees of substitution in C-2 and C-6, i.e. by applying of equation (5).

The numerical evaluation of the ^{13}C-NMR spectra of CXBE is performed the same way as for DACX.

Substituent distribution of cellulose xanthate produced at varying CS_2 contents during xanthation

As already mentioned, the substituent distribution of cellulose xanthate influences the processing properties of the viscose and the properties of the regenerated fibers. In turn, the substituent distribution of the cellulose xanthate is governed by the process parameters, first of all the amount of carbon disulfide in the xanthation reaction. Using the NMR methodology presented here we examined the distribution of the xanthate groups as a function of the amount of bound carbon disulfide.

To this end viscoses with increasing γ-values in the range from 50 to 170 are synthesized and examined in terms of the distribution of the xanthate groups within the AGU. Figure 4 shows the ^{13}C-NMR spectra of these DACX samples in the frequency range of the AGU (DACX dissolved in DMSO-d_6).

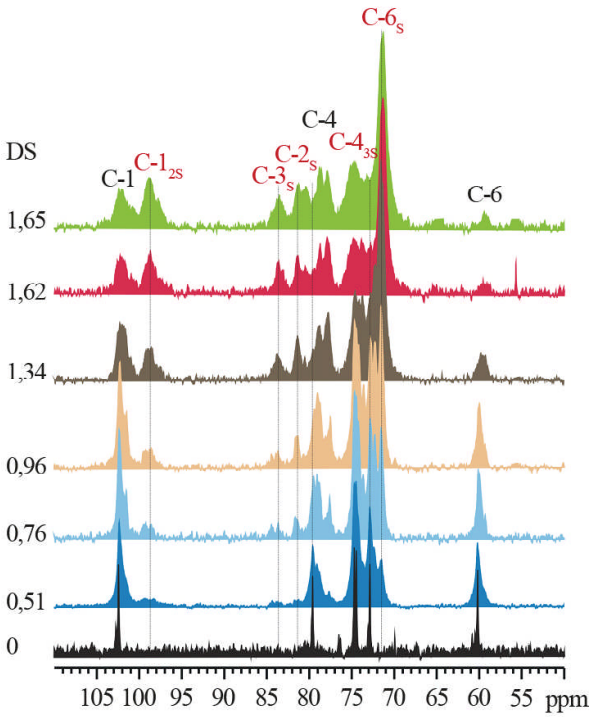

Figure 4. 13C-NMR spectra of DA xanthates with varying degrees of substitution.

A visual inspection of these spectra reveals that the intensity of some peaks increases with increasing overall degree of substitution (C-2$_s$, C-1$_{2s}$, C-3$_s$, C-4$_{3s}$ and C-6$_s$). The functionalization of the primary hydroxyl groups can be indirectly identified by the clear reduction in signal area for the non-substituted C-6 carbon atom. Generally, the changes of these spectra as a function of the DS confirm the peak assignment discussed above.

The distribution of the xanthate groups in the AGU, arising from the numerical evaluation and based on the overall degree of substitution DS$_{CX}$, is presented in Figure 5.

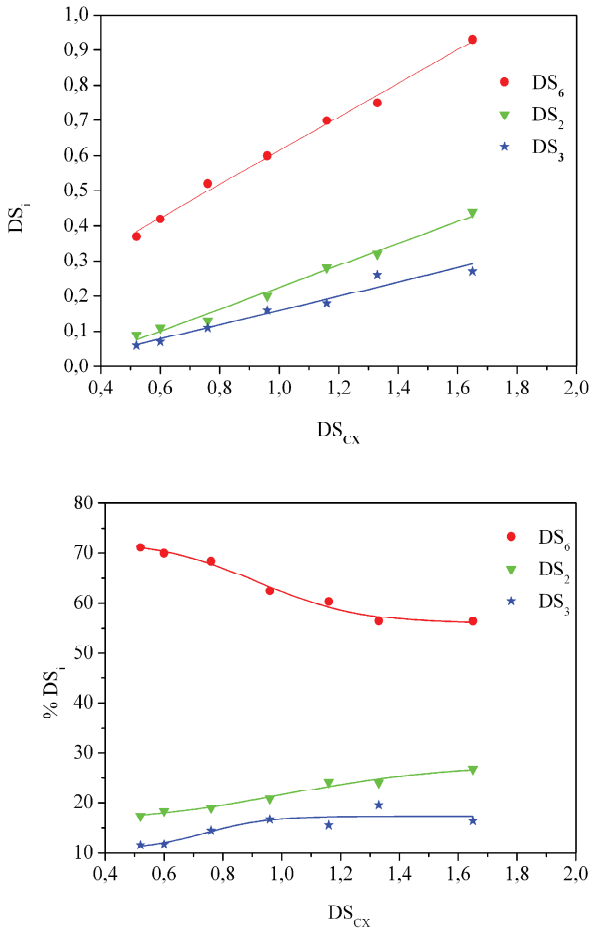

Figure 5. Partial degrees of substitution DS$_i$ as a function of the overall DS$_{CX}$ of the stabilized cellulose xanthate (DACX) (above), and as percentages of DS$_{CX}$ (below).

As depicted in Figure 5, there is a preferred C-6 substitution throughout the entire DS range investigated and not an intense substitution at the secondary hydroxyl groups of the AGU as it is often postulated. Furthermore, we can see that the relative reactivity of the primary hydroxyl groups is on the highest level at the lowest degree of substitution of the cellulose xanthates. While approx. 60 % of the xanthate groups are located in the primary hydroxyl

groups for highly substituted cellulose xanthates, the relative degree of substitution DS_6 is approximately 70 % for practical viscoses ($DS_{CX} \approx 0.5$).

The increased amount of C-2,3 substitution for the higher substituted cellulose xanthates is obviously the result of the approached saturation of the primary hydroxyl groups for $DS_6=1$.

The viscose for the present investigations was stabilized via DACX. The published findings of Kamide *et* al. [4] and König *et* al. [3], for comparison, were also determined using ^{13}C-NMR spectroscopy but without stabilizing the cellulose xanthate. Our own results as well as the results from [3, 4] are shown in Figure 6 to allow a better overview.

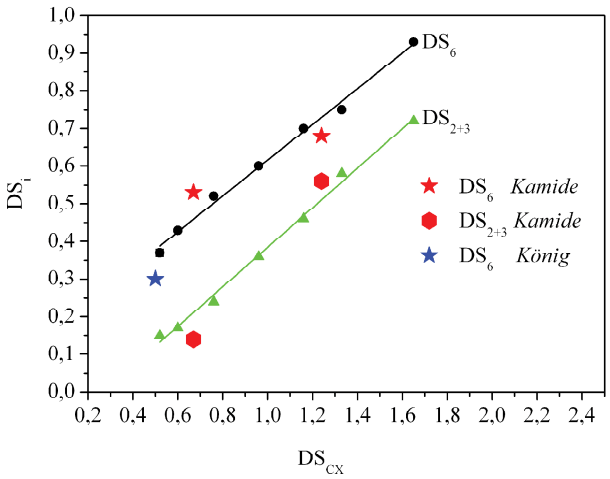

Figure 6. Partial degrees of substitution D_i as a function of the overall DS_{CX} of stabilized cellulose xanthates (full circles and triangles – this work) compared to the published values [3, 4] determined by ^{13}C-NMR spectroscopy as well.

Figure 6 shows that the values taken from literature fit well into the series of findings of our work. It should be noted that both types of viscose investigated by Kamide differ in terms of the method of xanthation (dry and wet sulfidation) and in the amount of carbon disulfide used for the sulfidation reaction. Kamide used a higher amount of carbon disulfide for the dry sulfidation process. Accordingly, these xanthates have a higher degree of substitution. Further, Kamide et al. observed that the higher substituted cellulose xanthates from dry sulfidation exhibit a stronger substitution in the secondary OH groups compared to the cellulose xanthates sulfidized in a solution. The authors explained this finding by a preferred interaction of the sodium hydroxide with the hydroxyl groups at the C-2 and C-3 positions of alkali cellulose.

On the other hand, the variation in substituent distribution could also be the result of a transesterification of the xanthate groups of the C-6-OH groups in a solution state. Kamide's absolute DS values should be discussed with care since the decomposition of the cellulose xanthate during the long measuring period is certainly of significance and the quality of the spectra in sodium hydroxide is notably worse than in DMSO-d_6.
König et al. found the same range for C-6, although it was somewhat lower than in the present work. Approximately 55-66 % of the xanthate groups were established in the primary hydroxyl groups for a viscose with a DS of 0.5.
Recent results from ^{1}H-NMR investigation of stabilized viscose by Schwaighofer *et* al. [10] agree qualitatively with our ^{13}C-NMR result of a dominating substitution at the C-6 position.

Viscose from frozen alkali cellulose

By freezing the alkali cellulose, preripening is interrupted, i.e. the depolymerization of the cellulose is largely reduced. This produces the prospect of preserving the alkali cellulose by storing it at low temperatures (between -16 °C and -20 °C) to be ripened and processed into viscose at a later point in time.
It has been shown in a phase diagram [14, 15] that the structure of alkali cellulose depends on alkali concentration and temperature. However, the question remained unanswered as to what extent this influences the reactivity of the alkali cellulose in the viscose process. Literature shows some evidence that the state of the alkali

cellulose, i.e. its crystalline modification, is important for the course of sulfidation. Xanthation of sodium cellulose II, for example, should require considerably higher reaction temperatures than sodium cellulose I (at least at 60 °C) in order to obtain a soluble cellulose xanthate [1].

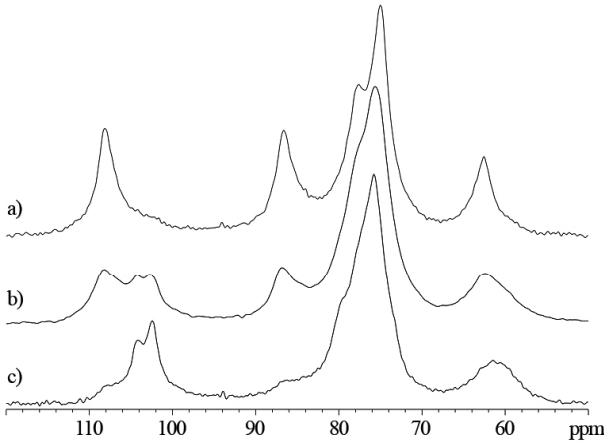

Figure 7. ^{13}C-CP/MAS-NMR spectra of alkali cellulose generated in different ways.
a) AC_18_fresh
b) AC_18_ frozen
c) AC_25_ fresh

In order to analyze the possible impact that freezing the alkali cellulose has on the substitution of the cellulose xanthate, freshly alkalized cellulose and afore frozen alkali cellulose were converted to viscose. Both forms of viscose were investigated in terms of substitution. Na-cellulose II, which was formed by treating the same dissolving pulp with 25 % sodium hydroxide at room temperature, was included as a reference. The structure of each sample of alkali cellulose was investigated by solid state ^{13}C-CP/MAS-NMR spectroscopy according to [12]. The alkali cellulose samples were reacted with carbon disulfide under identical conditions and solubilized to viscose. The substitution of the cellulose xanthates was characterized by the γ-values and the distribution of the stabilized xanthate groups in solution by the appropriate ^{13}C-NMR-method as described above. Figure 7 compares the ^{13}C-CP/MAS-NMR spectra of the variously prepared alkali celluloses. As earlier shown in a comprehensive WAXS and NMR study of slack cellulose alkalization [16], treatments of the cellulose in 18 % and 25 % aqueous sodium hydroxide at room temperature result in Na-cellulose I and Na-cellulose II, respectively. This is confirmed by spectra a and c in Figure 7, which clearly represent Na-cellulose I and II in accordance with our earlier published data [12, 13, 16]. By comparing spectrum b with spectra a and c in Figure 7 we can clearly see that part of the Na-cellulose I was transformed into Na-cellulose II as a result of freezing. After thawing, the frozen alkali cellulose I is still a mixture of Na-cellulose I and Na-cellulose II, i.e. the latter does not reconvert to Na-cellulose I at room temperature.

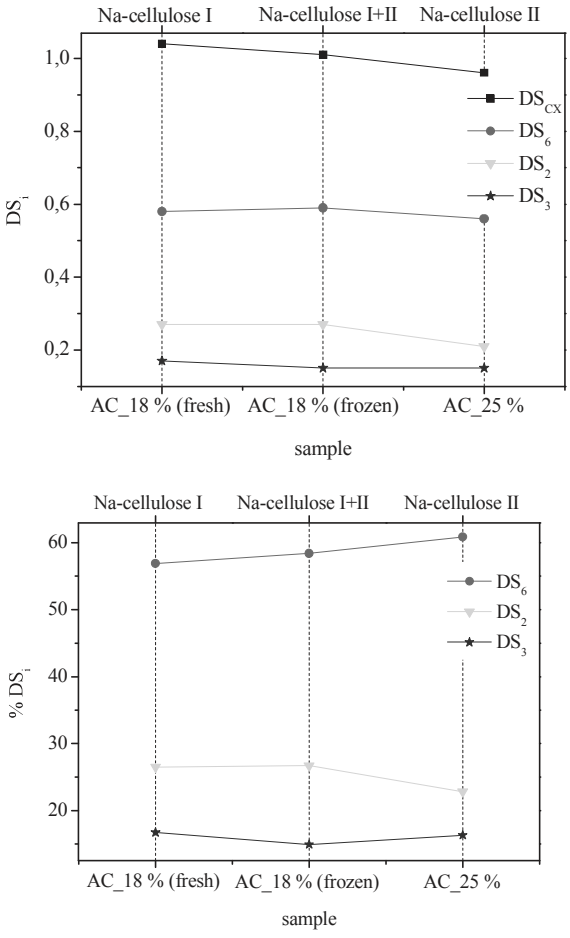

Figure 8. Substitution of cellulose xanthates made from alkali cellulose formed in different ways; Stabilizing reagent: DEAA.

Figure 8 shows an overview of the substituent distribution of the xanthates that are produced from different types of alkali

cellulose. It becomes clear that the crystalline modification (and the related composition) of the alkali cellulose has a significant impact on the formation of xanthate. The viscose produced from Na-cellulose I (AC 18% fresh) exhibits the highest DS or γ-value. The γ-value decreases with increasing Na-cellulose II content. This result corresponds to earlier published results.

The lower reactivity of Na-cellulose II can be explained by the less expanded crystal lattice and a lower amount of bound water as compared to Na-cellulose I. The presence of bound water is essential for carbon disulfide to react quickly with NaOH and Na-cellulose [17]. Also, one must keep in mind that a lower degree of substitution for cellulose xanthates can occur due to by-product formation which is fostered by the higher alkali content of the noncrystalline portion of alkali cellulose and also by adhering lye of higher concentration after a treatment in 25 % aqueous NaOH.

With regard to the distribution of the xanthate groups, it can be seen that, in the case of Na-cellulose II, there is a decrease in substitution in the C-2 positions and an increase in substitution in C-6 when compared with the alkali cellulose I values used as a reference.

In addition to the changes in the substitution pattern, deviating cellulose xanthate properties can be observed. In the investigations involving the frozen alkali cellulose, the resulting stabilized cellulose xanthates (in the form of BCX) were shown to possess a poorer dissolving behaviour in DMSO. This poor dissolvability is all the more striking since it involves highly-substituted viscose (DS_{CX} approx. 1) that was stabilized to a derivative which already exhibited good dissolvability at low substitution. Thus, with regard to the Na-cellulose II case, we concluded that potentially two differently substituted phases are formed (i.e. low crystalline - high noncrystalline) which in summary provide a rather high average DS, but includes one badly dissolving phase.

Summary

This paper presents a method for determining the average substituent distribution in cellulose xanthates, which is based on ^{13}C-NMR spectroscopic investigations of stabilized cellulose xanthates. This methodology allows to investigate the viscose process parameters with regard to the effects on the xanthation pattern. In the present paper we analysed the changes of the substituent distribution at varying amounts of carbon disulfide in the sulfidation stage, and in the specific case that frozen alkali cellulose is used. In a forthcoming paper, the change in xanthate group distribution during ripening as well as its influence on the spinnability of the viscose will be investigated.

Acknowledgements

The work was carried out as part of two projects funded by the Agency of Regrowing Resources (FNR) of the German Federal Ministry BMELV (FKZ 22016703 und FKZ 22003307), co-funded by the viscose companies Kelheim Fibres GmbH, ENKA GmbH & Co. KG, Lenzing AG, and Glanzstoff Austria GmbH & Co. KG.

References

[1] Götze, K., Chemiefasern nach dem Viskoseverfahren. 3. Ed. 1967, Berlin, Heidelberg, New York: Springer-Verlag.

[2] Rogovin, Z.A., Chemiefasern. Chemie - Technologie. 1982, Stuttgart, New York: Wilhelm Albrecht, Georg Thieme Verlag.

[3] König, L.D., R.; Postel, S., ^{13}C-NMR-Untersuchungen an ^{13}C-markierten Cellulosexanthaten. Das Papier, 1993. 11: p. 641-644.

[4] Kamide, K., K. Kowsaka, and

K. Okajima, C-13 NMR-Study on the Distribution of Substituent Groups on Trihydric Alcohol Units in Cellulose Xanthate. Polymer Journal, 1987. 19(2): p. 231-240.

[5] Russler, A., Lange, T., Potthast, A., Rosenau, T., Berger-Nicoletti, E., Sixta, H. and Kosma, P., A novel method for analysis of xanthate group distribution in viscoses. Macromolecular Symposia, 2005. 223: p. 189-199.

[6] Fink, H., Stahn, R., and Matthes, A. Reifebestimmung und Ultrafiltration von Viscose. Angewandete Chemie, 1934. 47(34): p. 602-607.

[7] Takahashi, S.-I., et al., Journal of Polymer Science 1986. 24: p. 2981-2993.

[8] Nehls, I., W. Wagenknecht, and B. Philipp, C-13-NMR spectroscopic studies of cellulose in various solvent systems. Cellulose Chemistry and Technology, 1995. 29(3): p. 243-251.

[9] Russler, A., Potthast, A., Rosenau, T., Lange, T., Saake, B., Sixta, H. and Kosma, P., Determination of substituent distribution of viscoses by GPC. Holzforschung, 2006. 60(5): p. 467-473.

[10] Schwaighofer, A., Zuckerstätter, G., Schlagnitweit, J., Sixta, H., Müller, N.: Determination of xanthate group distribution on viscose by liquid state ^{1}H-NMR spectroscopy. Anal. Bioanal. Chem., 2010 (400) 2449-2456.

[11] Willard, J.J. and Pacsu, E.; Journal of the American Chemical Society, 1960. 82(16): p. 4350-4352.

[12] Kunze, J. and Fink, H.-P.: Characterization of cellulose and cellulose derivatives by high resolution solid state C-13-NMR-spectroscopy. Das Papier, 1999. 53(12): p. 753-764.

[13] Kunze, J. and Fink, H.-P.: Structural changes and activation of cellulose by caustic soda solution with urea. Macromolecular Symposia, 2005. 223: p. 175-187.

[14] Sobue, H., H. Kiessig, and K. Hess, Zeitschrift für Physikalische Chemie, 1939. B43: p. 309-328.

[15] Krässig, H.A.: Cellulose - Structure, Accessibility and Reactivity. 1993: Yverdon: Gordon and Breach Sci. Publ. S.A.

[16] Fink, H.-P., Walenta, E., Kunze, J., Mann, G.: Wide angle X-ray and solid state 13C-NMR studies of Cellulose Alkalization. in Cellulose and cellulose derivatives: Physico-chemical aspects and industrial applications. Eds. Kennedy, Phillips, Williams, Piculell, Woodhead Publishing Ltd., Cambridge (1995) p. 523-528.

[17] Philipp, B., Zur Kinetik der Xanthogenatreaktion der Cellulose. Faserforschung und Textiltechnik, 1957. 8(2): p. 45-53.

Lenzinger Berichte 89 (2011) 142-151

THE HITAC-PROCESS (HIGH TEMPERATURE ADSORPTION ON ACTIVATED CHARCOAL) – NEW POSSIBILITIES IN AUTOHYDROLYSATE TREATMENT

Jenny Sabrina Gütsch[1] and Herbert Sixta[2,3]

[1] Kompetenzzentrum Holz GmbH, St.-Peter-Str. 25, 4021 Linz, Austria
[2] Lenzing AG, Werkstr. 1, 4860 Lenzing, Austria
[3] Department of Forest Products Technology, Aalto University School of Science and Technology, P.O. Box 16300, Vuorimiehentie 1, Espoo, Finland; Email: herbert.sixta@aalto.fi

Water prehydrolysis of wood is an interesting process for the recovery of xylooligosaccharides and derivatives thereof, while at the same time cellulose is preserved to a large extent for subsequent dissolving pulp production. The recovery of value-added products out of autohydrolysates is frequently hindered by extensive lignin precipitation, especially at high temperatures. In this study, a new high temperature adsorption process (HiTAC process) was developed, where lignin is removed directly after the autohydrolysis, which enables further processing of the autohydrolysates. The suitability of activated charcoals as a selective adsorbent for lignin under process relevant conditions (150 and 170 °C) has not been considered up to now, because former experiments showed decreasing efficiency of the adsorption of lignin onto activated charcoals with increasing temperature in the range of 20 – 80 °C. In contrast to these results, we demonstrated that the adsorption of lignin at 170 °C directly after autohydrolysis is even more efficient than after cooling the hydrolysate to room temperature. The formation of lignin precipitation and incrustations can thus be efficiently prevented by the HiTAC process. The carbohydrates in the autohydrolysis liquor remain unaffected over a wide charcoal concentration range and can be further processed to yield valuable products.

Keywords: activated charcoal (AC), adsorption, autohydrolysis, desorption, *Eucalyptus globulus*, HiTAC process (high temperature adsorption on activated charcoal), lignin, precipitation, prehydrolysis, xylooligosaccharides

Introduction

Globally, the alkaline kraft process constitutes the principal pulping process. It accounts for 89 % of the chemical pulp production. Alkaline pulping processes, however, are not capable of selectively removing hemicelluloses as a prerequisite for the production of high-purity dissolving pulps [1]. Autohydrolysis in water is the process of choice for the extraction of the hemicelluloses from wood biomass for the subsequent production of a dissolving pulp. The extracted hemicelluloses are an interesting feedstock for food additives and pharmaceuticals. Thus, autohydrolysis may contribute to the profitability of the pulping process [2-4]. One major challenge during autohydrolysis of wood is the partial dissolution of highly reactive lignin components. These components cause high turbidity of the autohydrolysate and form resinous precipitates during heating and storage at high temperatures. The precipitates were specified as a highly

condensed form of the colloidal dissolved lignin fraction [5]. Further processing of the autohydrolysate such as heat recovery, isolation or hydrolysis of oligosaccharides as well as the separation of acetic acid and furanic compounds is impaired by extensive lignin precipitation. However, the formation of these insoluble precipitates cannot be avoided completely [6]. In order to circumvent the precipitation problems and to simultaneously benefit from autohydrolysis, steam prehydrolysis is conducted in industrial practice. A disadvantage of this technique is the immediate neutralisation of the hydrolysates with cooking liquor, which renders impossible the isolation of hydrolysed sugar components because of severe carbohydrate degradation and the small quantity of hydrolysis liquor [1, 7].

Thus, finding suitable technologies for the quantitative removal of the insoluble components and their precursors (soluble lignin) from autohydrolysates is one of the prerequisites for the commercialization of water autohydrolysis for the parallel production of high purity dissolving pulps and sugar-based by-products. The lignin separation step needs to be performed immediately after the drainage of the hydrolysates from the reactor in order to completely avoid incrustation problems. The separation of lignin at temperatures exceeding 100 °C has not been a research topic so far, however, lignin separation from hydrolysates at ambient temperature has found some interest, especially in respect of the removal of inhibitors for fermentative purposes. Inhibitors in this context are lignin, lignin degradation products, and furanic compounds that are toxic to microorganisms in higher concentrations and therefore need to be removed prior to fermentation of the carbohydrate containing liquors [8-12].

A large variety of purification methods has already been studied in this respect. Some adsorbent materials, such as ion exchange resins and activated charcoals, have proven to be applicable for the removal of lignin and sugar degradation products from carbohydrate containing liquors [13]. Even polymeric resins showed good efficiency in lignin removal, although they were not utterly selective as large amounts of carbohydrates were adsorbed, too [14]. Among the adsorbent materials, activated charcoals showed a rather good selectivity towards lignin and lignin degradation products [15, 16]. However, along with lignin removal, substantial co-adsorption of sugars can be observed. Therefore, an optimal charcoal concentration was proposed, where sugar adsorption was still low.

In general, adsorption of lignin on activated charcoals is highest at low pH values, a condition typically met in untreated autohydrolysates [17]. Nevertheless, a neutralisation step is often applied prior to adsorption, as neutral pH is required for subsequent fermentative treatments. In addition to neutralization, filtration and evaporation stages are often proposed to remove volatile compounds and to purify the hydrolysates before an adsorption step [8, 18-20]. However, it is strongly recommended to remove the sticky and reactive lignin prior to the application of additional treatment steps, because lignin inevitably hampers the treatment by continuous precipitation.

The objective of this study was to develop a process for the removal of lignin and lignin degradation products from the autohydrolysis liquor immediately after its discharge from the pressurized reactor. In order to prevent excessive precipitation, the critical substances should be removed by adsorption on activated charcoal. The efficiency and selectivity of this HiTAC process (high temperature adsorption on activated charcoal) should be investigated in detail. Within a temperature range of 20 °C to 170 °C, the effects of adsorption temperature, adsorption time and the type and amount of activated charcoal will be examined. Furthermore desorption of the lignin components from the charcoal will be investigated, in order to reuse the charcoal.

Material and Methods

Wood chips

Eucalyptus globulus wood chips from plantations in Uruguay were supplied by ENCE (Huelva, Spain). The chips were ground with a Retsch-type grinding mill and fractionated. The fraction with particle sizes between 2.5 and 3.5 mm was collected and used for the prehydrolysis experiments. The dry content of the wood chips (82.9 %) was measured after drying at 104 °C until constant weight (48 h). The carbohydrate content and composition were analyzed after a two-stage total hydrolysis by high performance anion exchange chromatography with pulsed amperometric detection [21]. Klason lignin and acid soluble lignin were measured according to Tappi T222om 98 [22].

Autohydrolysis

Autohydrolysis was carried out in a lab-scale Parr reactor station with a reactor volume of 450 ml, mechanical stirring and temperature control. 50 g of wood were placed inside the reactor. Deionised water was added to achieve a liquor-to-wood ratio of 5:1. The reactor was heated up to 170 °C within 30 min (minimum heating time), the temperature was maintained until a prehydrolysis-factor (P-Factor) of 600 h (corresponding to approximately 60 min). The P-factor was calculated from the recorded temperature/time data according to Sixta [1] based on an activation energy of 125.6 kJ mol^{-1}. The prehydrolysate was subsequently separated from the wood residue by displacement with nitrogen to a preheated second reactor containing saturated steam with a temperature of 170 °C following the protocol of Leschinsky [6]. The isothermal phase separation recovered all components that are dissolved in the prehydrolysate at 170 °C, particularly the components that are insoluble at lower temperatures. During this separation step, no temperature and pressure drop occurred. The experiments were split into reference and adsorption experiments. For reference measurements, the second reactor was filled with steam only, while for the adsorption experiments, activated charcoal was added. The corresponding reactor scheme is shown in Figure 1.

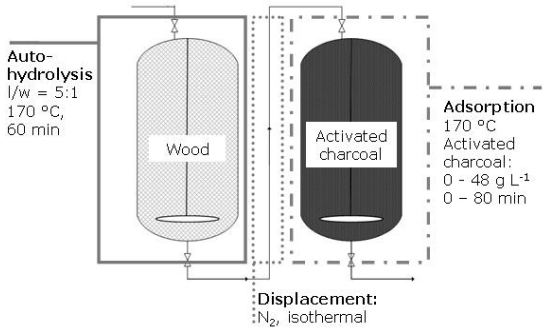

Figure 1. Autohydrolysis' reactor system.

Reference experiments

In the reference experiments the hydrolysates were subjected to a temperature treatment at 170 °C for 0, 20, 40 and 80 min after isothermal phase separation. Then, the reactors were cooled to room temperature with ice water. Precipitates that had built up during this treatment on the equipment were solubilised in 0.1 M NaOH with short heating to over 100 °C and were quantified via standard TOC measurements.

Adsorption experiments

Sources of charcoal: Sigma decolorizing charcoal, Norit® granular charcoal purchased from Sigma-Aldrich, Carbopal Gn-AZ from Donau Carbon and activated coke HOC Super, kindly supplied by Rheinbauer Brennstoff GmbH. Norit® granular charcoal was ground, while the other charcoal samples were used as supplied. The activated charcoal concentration is given as the ratio to the liquid phase during prehydrolysis in (g L^{-1}). For adsorption experiments at 170 °C the second reactor was held at 170 °C, for adsorption experiments at 150 °C, the batch was cooled with the reactor's internal cooling system immediately after liquid transfer from the first reactor. The temperature was maintained until the required adsorption time was accomplished. After the adsorption, the reactor was immediately

cooled down to below 40 °C with ice water. Adsorption time of 0 min represents the minimal adsorption time possible to record. The minimum adsorption time at 170 °C is estimated to be less than 2 min, followed by a cooling time to below 40 °C of 10 - 15 min. Adsorption at 20 °C was conducted after isothermal liquid transfer and ice cooling. The adsorbent was separated from the prehydrolysate via vacuum filtration using a 0.45 µm membrane.

Table 1. BET surface area, pH and ash content of the activated charcoals.

Type of activated charcoal	BET / $m^2\ g^{-1}$	pH	Ash / %
Carbopal Gn-AZ	1270	5.9	n.d.
Sigma decolorizing	880	6.7	1.1
Norit® (Sigma)	560	6.0	12
HOC Super	280	11.2	8.7

Desorption Experiments

1 g of spent activated carbon (adsorption paramenters: 20 g L^{-1} AC, adsorption at 170 °C, 20 min adsorption time, 410 mg lignin per g AC) was subjected to 5 mL of solvent [0.5 N NaOH, acetone/ water 5:1 (v/v), ethanol, acetic acid, DMSO] and shook overnight. AC was separated via a 0.45 µm filter and washed with 100 mL deionised water.

Analytical methods

Lignin and turbidity analysis were conducted immediately after the prehydrolysis experiments. The samples were then stored at 4 °C. Lignin content was analysed via UV/VIS-spectrometry (absorption coefficient of 110 L g^{-1} cm^{-1} at 205 nm according to Tappi um-250, [23]). Turbidity was measured on a Hach 2100P turbidimeter. Furfural and hydroxylmethyl-furfural (HMF) were quantified via HPLC on a Hypersil ODS column with UV detection at 277 nm with 14 % (v/v) acetonitrile as eluent at a temperature of 65 °C. Acetic acid was determined via HPLC on a Rezex ROA column with RI and UV detection and 0.005 M H_2SO_4 as eluent at a temperature of 65 °C. The carbohydrate content and the composition of the samples were analyzed before and after a two-stage total hydrolysis with sulphuric acid by high performance anion exchange chromatography with pulsed amperometric detection [21]. Size exclusion chromatograms (SEC) were obtained on a PSS MCX 1000 (8x300) column coupled with RI detection and 0.1 M NaOH as eluent. BET was measured on a BELsorp mini II from BEL Inc., Japan according to Brunauer *et al.* [24] and IUPAC recommendations [25]. Nonlinear regression was analysed by means of the Statgraphics Centurion XV software. The ash content of the ACs was measured according to DIN 38 409 H1-3 [26] at a temperature of 850 °C. The ash content of the activated charcoals and the pH in water at a concentration of 50 g L^{-1} are given in Table 1. Charcoal samples have been examined by high-resolution scanning electron microscopy after coating with a thin layer of Au/Pd at a 7000x magnification with a Hitachi S4000 SEM (FE-SEM) applying an acceleration voltage of 6 kV.

Results and discussion

Reference experiments

During autohydrolysis, mainly the xylan in the wood is degraded and solubilised in the aqueous phase, whereas the cellulose is depolymerised - depending on prehydrolysis intensity - but practically no water soluble fractions are formed. The main components of the crude autohydrolysate are oligomeric and monomeric sugars (25.2 g L^{-1}), mainly xylose (20.5 g L^{-1} xylose corresponding to 11.3 % odw) and less than 1 g L^{-1} of glucose (0.5 % odw). 68 % of the xylose in solution was still in oligomeric form due to the rather mild conditions of autohydrolysis. Additionally, the carbohydrate degradation products furfural and hydroxymethylfurfural (HMF) as well as acetic acid derived from the hydrolysis of the acetyl groups attached to the xylan backbone were detected in the autohydrolysate (1166, 113 and

2814 mg L^{-1}, respectively). Parallel to sugar dissolution from wood, some lignin also solubilises in the hot hydrolysate. A part of it precipitates upon cooling. The total lignin in the hydrolysate accounts for 5.6 % odw (10.1 g L^{-1} in hydrolysate), 30 % thereof can be separated by centrifugation. If the crude hydrolysate is further exposed to the reaction temperature of 170 °C, the oligomeric sugars are hydrolysed to monosugars and subsequently dehydrated to furanic compounds in an extent depending on the treatment intensity.

Table 2. Composition of the hydrolysates after activated charcoal (AC, BET 880 m^2 g^{-1}) treatment at 170 °C.

AC / g L^{-1}	Adsorp. time / min	Lignin / mg L^{-1}	Total sugars / mg L^{-1}
8	0*	5674	23685
	20	5634	23712
	40	5099	20722
	80	5326	17170
12	20	4391	23631
	40	4215	21421
	80	4847	14021

*minimum adsorption time

Additionally, a drop in lignin concentration was observed with increasing treatment time (Table 2) which can be attributed to the formation of incrustations due to polycondensation reactions [27]. These sticky incrustations lead to serious problems in the processability of autohydrolysates because they contribute to scaling in all downstream equipment, especially in the heat exchanging devices.

Influence of activated charcoal

The addition of activated charcoal (AC), even in amounts far lower than those recommended in the literature (minimum 8 g AC per litre hydrolysate versus 100 g AC per kg hydrolysate [15]), could prevent the formation of incrustations efficiently. Adsorption time had only a minor effect on lignin adsorption at 170 °C (Table 3). As sugar decomposition at 170 °C started to be significant when exceeding 20 min of treatment time, the adsorption time was set to 20 min for further experiments.

The turbidity of an aqueous system correlates with the amount of colloidal matter in solution indicating an increase in insolubles with rising turbidity. This measuring principle can be adopted for the autohydrolysis liquor to track the concentration of colloidal lignin compounds causing the formation of sticky precipitates. Crude autohydrolysates exhibited a turbidity of more than 10 000 NTU. Vacuum filtration, using a 0.45 µm membrane, still resulted in a turbidity higher than 1000 NTU indicating an insufficient removal of the colloidal lignin compounds, while the treatment with the minimal amount of AC (8 g L^{-1}) resulted in a turbidity of 23 NTU only. An increase in AC concentration lowers turbidity to below 10 NTU. This turbidity value remained constant during a period of more than three weeks, stored at room temperature or 4 °C, indicating no further lignin precipitation over time as confirmed by lignin content measurements. With the highest AC concentration in the hydrolysate tested, 48 g L^{-1}, the lignin content in the hydrolysate decreased by 96 % (Table 4). Carbohydrates were not affected up to AC concentrations of 24 g L^{-1} corresponding to a lignin removal of 85 %. However, at an AC concentration

Table 3. Reference experiments: Composition of autohydrolysates after temperature treatment at 170 °C.

Adsorp. time / min	Lignin / mg L^{-1}	Xylose oligo[1] / mg L^{-1}	Xylose mono[2] / mg L^{-1}	Furfural / mg L^{-1}	HMF / mg L^{-1}	Acetic acid / mg L^{-1}	Incrust.[3] / mg L^{-1}
0	10114	13945	6557	1166	113	2814	–
20	9680	11212	7664	1555	172	3083	430
40	7546	8121	8678	2304	237	3743	2570
80	6870	3489	10207	4257	426	4743	3240

[1] oligomeric fraction: difference in sugar content before and after total hydrolysis, [2] before total hydrolysis,
[3] incrustations from the reactor equipment dissolved in NaOH

of 48 g L^{-1}, a concomitant adsorption of 19 % of the carbohydrates, mainly present in their polymeric form, occurred.
The same tendencies were found by size exclusion chromatography (SEC). SECs of the crude hydrolysates showed a bimodal molecular weight distribution (Figure 2). The low molecular weight peak is considered as monomeric sugars mainly, the higher molecular weight peak is composed of lignin and oligomeric sugars.
With increasing charcoal concentration, the UV active lignin is constantly removed and accounts for the reduction of the high molecular weight peak for the most part. UV detection showed a bimodal molecular weight distribution of lignin compounds, where lignin with a higher molecular mass is removed prior to low molecular mass lignin. The C_5- and C_6-sugar dehydration products furfural and HMF were increasingly removed from autohydrolysis liquor with rising charcoal concentrations. At the maximum charcoal concentration investigated (48 g L^{-1}), 85 % of furfural and 72 % of HMF were removed from the autohydrolysis liquor. Acetic acid concentration was not reduced by AC, but was rather significantly increased at high AC concentrations.
A theoretically possible catalysis of the cleavage of acetyl groups from the xylan backbone by activated charcoal and the concomitant release of free acetic acid into the hydrolysate needs further investigation. Anyway, a release of free acetic acid would promote further hydrolysis of the oligosaccharides to monomeric sugars and would therefore explain the increase in monomeric sugars (Table 4).

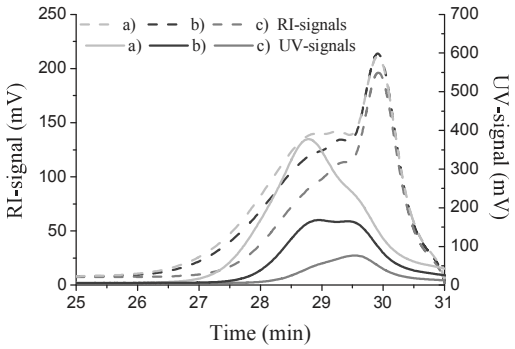

Figure 2. Size exclusion chromatograms of the autohydrolysates after adsorption on a) 12 g L^{-1}, b) 24 g L^{-1}) and c) 48 g L^{-1} activated charcoal (BET 880 m^2 g^{-1}) for 20 min at 150 °C.

An interesting field of application for water prehydrolysates is the fermentative and enzymatic conversion of the carbohydrates (xylan, xylooligosaccharides and xylose) to xylitol, bioethanol, and other fermentation products. Lignin, furfural and HMF are inhibitors for most of the enzymes in question. The amounts of lignin, furfural and HMF in *E. globulus* water prehydrolysates, subjected to the HiTAC process, are at a sufficiently low level for fermentation processes [8-12].

Adsorption isotherms

Lignin adsorption on activated charcoal is fairly efficient at 170 °C, adsorption at 170 °C is even better than at room temperature. The measurement of the exact equilibrium adsorption time of lignin in autohydrolysate at high temperatures is not possible due to the high amount of side reactions of carbohydrates and furfural. Nevertheless, it was shown that the lignin concentration in the hydrolysate did not

Table 4. Composition of prehydrolysates after 20 min adsorption onto activated charcoal (BET 880 m^2 g^{-1}) at 170 °C.

AC[1]	Lignin	Sugar total[2]	Sugar oligo[3]	Xylose oligo[3]	Xylose mono[4]	Glucose oligo[3]	Glucose mono[4]	Furfural	HMF	Acetic acid	Incrust.[5]
/g l^{-1}	/mg l^{-1}	/mg l^{-1}	/mg l^{-1}	/mg l^{-1}	/mg l^{-1}	/mg l^{-1}	/mg l^{-1}	/mg l^{-1}	/mg l^{-1}	/mg l^{-1}	/mg l^{-1}
0	9680	23368	13119	11212	7664	515	293	1555	172	3083	430
8	5634	23711	12680	10810	8231	588	326	1477	153	3341	-
12	4391	23631	13108	11218	7796	579	324	1167	127	3531	-
20	2972	23398	13661	11609	7190	585	274	1068	137	3557	-
24	1559	22184	11574	9678	7918	572	335	720	118	3496	-
32	921	20732	10481	8965	7595	436	293	333	71	3182	-

[1]Activated charcoal, [2]after total hydrolysis, [3] oligomeric fraction: difference in sugar content before and after total hydrolysis
[4] before total hydrolysis, [5] incrustations from the reactor equipment dissolved in NaOH

decrease steadily with adsorption times exceeding 20 min. Therefore, an adsorption time of 20 min was chosen for the adsorption experiments. Adsorption equilibrium at room temperature is known to be attained only after several hours of adsorption time [17].

The adsorption behaviour of the hydrolysis lignin can be approximated by isotherms of type I, although there is a slight tendency of increasing coverage at higher lignin concentrations (Figure 3). High surface coverage at high concentrations indicates the formation of multilayers at the adsorbens' surface. However, within the concentration range investigated, this couldn't be unambiguously confirmed. The study of higher lignin concentrations or lower activated charcoal concentrations was not possible, owing to the formation of lignin incrustations at lower AC concentrations at high temperatures. Type I isotherms can be modelled according to the theories of Freundlich and Langmuir. The Langmuir isotherm describes adsorption in a monomolecular layer, where adsorption of a particle is independent of the degree of surface coverage according to equation 1:

$$\frac{C_e}{q_e} = \frac{1}{Q_0 \cdot \beta} + \frac{C_e}{Q_0} \qquad (1)$$

where q_e is the amount of lignin adsorbed per unit mass of activated carbon (mg g^{-1}), C_e is the equilibrium concentration of lignin in solution (mg L^{-1}), Q_0 is the maximum lignin uptake per unit mass of carbon (mg g^{-1}), and β is the Langmuir constant (L mg^{-1}).

The Freundlich adsorption isotherm additionally relates the concentration of the solute on the surface of the adsorbent to the concentration of the solute in the liquid phase in a logarithmical relationship. The Freundlich equation can be written as:

$$q_e = k_f \cdot C_e^{1/n} \qquad (2)$$

where q_e and C_e correspond to the Langmuir terms, k_f is the Freundlich constant related to the adsorption capacity [mg g^{-1} (mg $L^{-1})^n$], and n is a dimensionless empirical parameter representing the heterogeneity of the surface.

Both, Freundlich and Langmuir isotherm models, gave good correlation with the measured lignin adsorption data. Nonlinear regression was performed in order to attain the Freundlich and Langmuir coefficients (Table 5).

Figure 3 shows the Freundlich isotherms for three different adsorption temperatures (20, 150, 170 °C). Notably, the amount of lignin adsorbed per unit mass of adsorbent (q_e) significantly increased at elevated temperatures, indicating more efficient adsorption. We therefore suggest that the lignin in solution at 170 °C exhibits a different structure than at room temperature or even is in liquid state. The arrangement of hydrophilic and hydrophobic groups in this state might favour the adsorption onto activated charcoal. Validation of these assumptions will require further research in this area. Furthermore, we propose that the adsorption of lignin on AC at high temperatures follows a chemisorption process as indicated in the literature [17] and in our own preliminary desorption experiments with limited success. Elevated temperatures might provide the activation energy required for a chemisorptive process. We further suspect a change in the

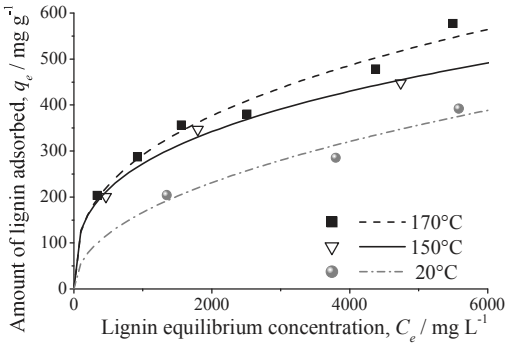

Figure 3. Freundlich isotherms (curves) and experimental adsorption data (individual points) of lignin on activated charcoal (BET surface area 880 m^2 g^{-1}) at different temperatures (20, 150 and 170 °C). q_e amount of lignin adsorbed per unit mass of AC, C_e equilibrium concentration of lignin in solution.

adsorption mechanism at temperatures beyond 100 °C, as Parajo found that in the range between 20 and 60 °C the adsorption efficiency decreased significantly with increasing temperature [19].

Due to the long adsorption times at 20 °C, it can be assumed that no significant lignin adsorption occurred during the cooling phase. Furthermore, after 80 min of adsorption at 170 °C and a charcoal amount exceeding 12 g L^{-1} no incrustations were formed (Table 4). Thus, lignin was not available for condensation reactions. This also indicates that the lignin was already adsorbed before cooling. Reference measurements without activated charcoal at the same conditions, however, yielded an amount of incrustations higher than 3.2 g L^{-1}.

Effect of activated charcoal type

Four activated charcoals with BET surface areas of 280, 560, 880 and 1270 $m^2 g^{-1}$ were tested for lignin adsorption. The adsorption behaviour of the different charcoals was modelled in terms of Freundlich and Langmuir isotherms, whereby the fit of the former was slightly better (mean R^2 of 0.94 compared to 0.92). The best adsorption results were obtained using the charcoal with the highest BET surface area (1270 $m^2 g^{-1}$, Figure 4). All charcoals investigated showed small mesopore diameters (data not shown). The volume of mesopores was almost equal for the charcoals with a BET surface area of 560 and 880 $m^2 g^{-1}$, but significantly higher for the charcoal of BET 1270 $m^2 g^{-1}$.

The micropore volume was higher for the AC of BET 880 $m^2 g^{-1}$ than for 560 $m^2 g^{-1}$. The micropore diameters of the AC of BET 1270 $m^2 g^{-1}$ were larger than for the other charcoals. The AC of BET 280 $m^2 g^{-1}$ exhibited only small volumes of meso- and micropores.

In terms of lignin adsorption, a decrease of the BET surface from 1270 to 880 $m^2 g^{-1}$ resulted in a 150 % higher demand of AC to yield a comparable lignin reduction. A further decrease of the BET surface area to 280 $m^2 g^{-1}$ required twelve times the amount of AC to achieve the equivalent adsorption efficiency. Taking into account the total surface area of the adsorption system as the surface area ($m^2 g^{-1}$) of the AC times the amount of AC (g L^{-1}), it can be seen that the smallest surface is needed, for the charcoal with the high volume of mesopores and larger micropores (BET 1270 $m^2 g^{-1}$). A 70 % higher total surface area is needed for the charcoals with BET 560 and 880 $m^2 g^{-1}$. For the charcoal of minor microporosity (AC with BET 280 $m^2 g^{-1}$) almost three times the total surface area is needed for similar lignin removal. Thus, not only the total surface area is a criterion for lignin adsorption, but also the distribution and volume of meso- and microporosity and assumingly surface functionalities. A potential effect of the ash content and the alkalinity of the ACs on the lignin adsorption is possibly superimposed by the high differences in BET surface

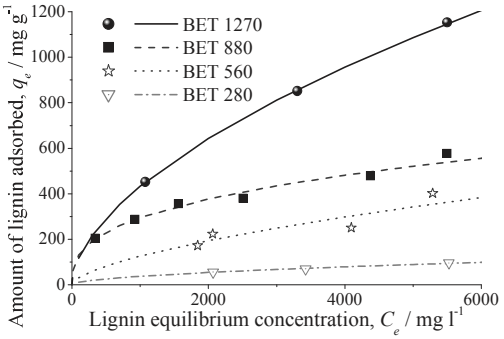

Figure 4. Freundlich isotherms (curves) and experimental adsorption data (individual points) of lignin on activated charcoals of BET surface areas of 1270, 880, 560, 260 $m^2 g^{-1}$ for 20 min at 170°C. q_e amount of lignin adsorbed per unit mass of AC, C_e equilibrium concentration of lignin in solution.

Table 5. Freundlich and Langmuir coefficients calculated by nonlinear regression.

Temp. / °C	BET / $m^2 g^{-1}$	Freundlich			Langmuir		
		k	1/n	R^2	Q	β	R^2
170	1270	8.32	0.57	1,00	1849.59	3503.8	0.98
170	880	22.83	0.37	0.97	617.70	1052.5	0.89
150	880	28.00	0.33	0.99	512.55	767.8	0.99
20	880	6.36	0.47	0.93	530.43	2456.1	0.88
170	560	1.02	0.69	0.81	884.41	7498.0	0.79
170	280	0.72	0.57	0.99	174.25	4700.1	0.97

area. The alkalinity of the AC might affect the stability of carbohydrates during the adsorption process.

Spent activated charcoal

After adsorption of lignin on an activated carbon of BET surface area 880 $m^2 g^{-1}$ at 170 °C the surface area decreases drastically to 70 $m^2 g^{-1}$. SEM images (Figure 5) show the structured surface of the activated carbon. After the adsorption process a smooth surface covered with lignin is imaged.

Table 6. BET surface after solvent desorption of lignin.

Solvent	dissolved lignin / % lignin on AC	BET / $m^2 g^{-1}$
Reference before desorption		70
NaOH (0.5 N)	10	109
Acetone/water (5/1)	21	122
Ethanol	10	95
Acetic acid	18	106
DMSO	n.d.	134

Desorption of this lignin (Table 6) using solvents yields up to 18 % of the lignin on the charcoal. However, the active surface area is not positively affected, probably due to the high binding strength of remaining lignin to the charcoal and due to the inaccessibility of lignin in the pores. This is also in agreement with the literature [28].

Conclusions

Adsorption of lignin and lignin degradation products from autohydrolysates on activated charcoals at prehydrolysis temperature is a suitable method for the prevention of scaling. The so-called HiTAC process exhibits a fairly good selectivity towards lignin adsorption without concomitant adsorption of carbohydrates up to a lignin removal of 85 % at 170 °C. At higher charcoal concentrations oligomeric sugars are increasingly adsorbed, while monomeric sugars remain unaffected. The carbohydrate dehydration products, furfural and HMF, are removed during the AC treatment to a concentration sufficiently low which allows an uninhibited fermentation of the hydrolysate. The equilibrium adsorption time is reached within a rather short period of time. Surprisingly, it could be shown that adsorption is significantly more efficient at autohydrolysis temperature (150 and 170 °C) than at room temperature, which is advantageous for purifying the hydrolysate during its discharge from the digester. The choice of an activated charcoal of high microporosity and surface area is indispensable for a successful implementation in commercial practice. It was demonstrated that the addition of activated charcoal to the hydrolysate prevents the formation of sticky precipitates efficiently. Clearly, a cost effective regeneration process for the charcoal is needed for a commercial realisation. Solvent desorption of lignin is yet not possible. Thus, it is our goal to develop an appropriate recycling strategy for the exhausted charcoal.

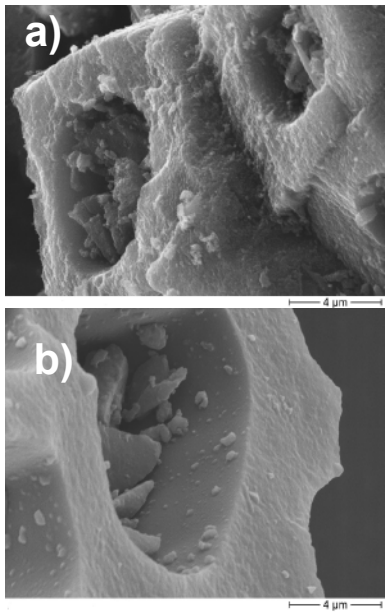

Figure 5. SEM images of activated charcoal a) before, b) after lignin adsorption.

Acknowledgement

Special thanks to the Wood Analytic Center Lenzing (WAL) and Sandra Schader for SEM imaging. Financial support was provided by the Austrian

government, the provinces of lower Austria, upper Austria, and Carinthia as well as by Lenzing AG. We also express our gratitude to the Johannes Kepler University, Linz, the University of Natural Resources and Applied Life Sciences, Vienna, and Lenzing AG for their in-kind contributions.

References

[1] H. Sixta, Handbook of Pulp. 1st ed. Vol. 1. 2006, Weinheim: Wiley-VCH. 3-1352.
[2] G. Garrote, H. Dominguez, and J.C. Parajo, J. Chem. Technol. Biotechnol. 74 (1999) 1101-1109.
[3] H.-J. Huang and S. Ramaswamy, Sep. Purif. Methods 62 (2008) 1-21.
[4] M.J. Vázquez, J.L. Alonso, H. Dominguez, and J.C. Parajo, Food Sci. Technol. 11 (2000) 387-393.
[5] M. Leschinsky, R. Patt, and H. Sixta. in PulPaper Conference 2007. 2007. Helsinki.
[6] M. Leschinsky, thesis, University of Hamburg, Faculty of Mathematics, Informatics and Natural Sciences, (2009).
[7] W. Wizani, A. Krotscheck, J. Schuster, and K. Lackner (1994) WO 93-AT183 19931202.
[8] M.L.M. Villarreal, A.M.R. Prata, M.G.A. Felipe, and J.B. Almeida E Silva, Enzym. Microb. Technol. 40 (2006) 17-24.
[9] J.M. Cruz, J.M. Domingues, H. Domingues, and J.C. Parajó, Food Chem. 67 (1999) 147-153.
[10] C.V.T. Mendes, C.M.S.G. Baptista, J.M.S. Rocha, and M.G. Carvalho, Holzforschung 63 (2009) 737-743.
[11] F.A.J. Keller and Q.A. Nguyen (2001) US 6,498,029 B2.
[12] J.C. Parajó, V. Santos, and M. Vázquez, Biotechnol. Bioeng. 59 (1998) 501-506.
[13] Moure, P. Gúllon, H. Domímguez, and J.C. Parajo, Process Biochem. 41 (2006) 1913-1923.
[14] T.J. Schwartz and M. Lawoko, Bioresour. 5 (2010) 2337-2347.
[15] J.C. Parajó, H. Domínguez, and J.M. Domínguez, Bioresour. Technol. 57 (1996) 179-185.
[16] D. Montané, D. Nabarlatz, A. Martorell, V. Torné-Frernández, and V. Fierro, Ind. Eng. Chem. Res. 45 (2006) 2294-2302.
[17] S. Venkata Mohan and J. Karthikeyan, Environ. Pollut. 97 (1997) 183-187.
[18] L. Canilha, J.B.d.A.e. Silva, and A.I.N. Solenzal, Process Biochem. 39 (2004) 1909-1912.
[19] J.C. Parajó, H. Dominguez, and J.M. Dominguez, Bioprocess Eng. 16 (1996) 39-43.
[20] E. Sepúlveda-Huerta, S.J. Tellez-Luis, V. Bocanegra-Garcia, J.A. Ramírez, and M. Vázquez, J. Sci. Food Agric. 86 (2006) 2579-2586.
[21] H. Sixta, N. Schelosky, W. Milacher, T. Baldinger, and T. Röder. in 11th ISWPC. 2001. Nice, France.
[22] Tappi, Acid-insoluble lignin in wood and pulp. 1998, standard.
[23] Tappi, Acid-soluble lignin in wood and pulp. 1991, standard.
[24] S. Brunauer, P.H. Emmet, and E.J. Teller, J. Am. Chem. Soc. 60 (1938) 309-319.
[25] J. Rouquerol, D. Avnir, C.W. Fairbridge, D.H. Everett, J.H. Haynes, N. Pernicone, J.D.F. Ramsay, K.S.W. SIing, and K.K. Unger, Pure Appl. Chem. 66 (1994) 1739-1758.
[26] Deutsche-Norm, Bestimmung des Gesamttrockenrückstandes, des Filtrattrockenrückstandes und des Glührückstandes. 1987.
[27] M. Leschinsky, G. Zuckerstätter, H.K. Weber, R. Patt, and H. Sixta, Holzforschung 62 (2008) 645-652.
[28] A. Dabrowski, P. Podkoscielny, Z. Hubicki, and M. Barczak, Chemosphere 58 (2005) 1049 - 1070.

Lenzinger Berichte 89 (2011) 152-160

DISSOLVING PULPS FROM ENZYME TREATED KRAFT PULPS FOR VISCOSE APPLICATION

Verena Gehmayr[1] and Herbert Sixta[2,3]

[1]Kompetenzzentrum Holz GmbH, St.-Peter-Str. 25, 4021 Linz, Austria
[2]Department of Forest Products Technology, Aalto University School of Science and Technology, P.O. Box 16300, Vuorimiehentie 1, Espoo, Finland; Email: herbert.sixta@aalto.fi
[3]Lenzing AG, Werkstr. 1, 4860 Lenzing, Austria

The purpose of this study was to illuminate enzymatic treatments as process steps for the efficient conversion of paper-grade pulps to dissolving pulps in terms of process economics. The challenge of pulp refinement comprises the selective removal of hemicelluloses and the precise adjustment of the pulp viscosity, while maintaining the reactivity of the pulp as required for viscose application.

A commercial oxygen-delignified *E. globulus* paper-grade kraft pulp was subjected to xylanase (X) pre-treatment combined with cold caustic extraction (CCE) at reduced alkali concentration and to endoglucanase (EG) post-treatment after TCF-bleaching. The xylanase pre-treated pulp showed increased reactivity towards xanthation and high viscose dope quality in terms of particle content in comparison to the pulp after cold caustic extraction at elevated alkali concentration.

The dependence of cellulose chain scission upon endoglucanase treatment on certain pulp qualities was analyzed in detail, and this allowed precise viscosity reduction as well as reactivity increase. The qualities of the spun fibers from the differently treated pulps were very similar to those viscose fibers from commercial dissolving pulps.

Keywords: *Dissolving pulp, endoglucanase, enzyme, filterability, reactivity, viscose fiber, xylanase*

Introduction

Demands for dissolving pulp and fibers have boomed world-wide within the last decade and thus nowadays much effort is put into the production of dissolving pulps from paper-grade pulps besides the dissolving pulp production from the commonly applied technologies such as the acid sulfite process and the alkaline pre-hydrolysis kraft process.

The main challenges in the conversion of a paper-grade pulp to overcome are the selective removal of hemicelluloses while ensuring high pulp reactivity.

For the viscose application the removal of the alkali soluble hemicelluloses is necessary, because otherwise they are dissolved in the steeping lye and impair the viscose process. A well-known method for the removal of hemicelluloses is the cold caustic extraction, CCE, which is an alkaline extraction at moderate temperatures from 25 to 45 °C and alkali concentrations from 5-10 % (w/w) NaOH in the lye [1]. Anyhow, pulp treatment at elevated alkali concentration induces the formation of the cellulose modification II [2]. The cellulose II crystal lattice is characterized by an increased number of inter-planar hydrogen bonds compared to cellulose I [3, 4]. Upon drying, inter-fibrillar spaces of mercerized pulps collapse and thus mercerized dried pulps

show intensely decreased surface area and pore volume [2, 5-8]. This results in reduced pulp reactivity towards derivatization and is called hornification [9, 10]. The reactivity of a pulp is determined by the accessibility of the OH-groups at C_6 and C_2 of the glucose monomer units to the reactants [11] and the reactivity determines the processability of a dissolving pulp for the viscose process [12]. Many treatments such as swelling, solvent exchange, degradation procedures [13] and chemical modification [8] were investigated for increasing the reactivity of a pulp.

Within the last few years, the monocomponent endoglucanase (EG) treatment to increase pulp reactivity and, as a side effect, precisely adjust the viscosity of a pulp has been the focus of much work [14-19].

Endoglucanase preferably degrades amorphous cellulose located on the fiber surface and in-between the microfibrils, which leads to increased crystalline surface exposure and to increased swelling ability and reactivity of the pulp [15]. Additionally, cellulose II is attacked by endoglucanase [20, 21], which was speculated to play a role in reactivity increase of the pulp after endoglucanase treatment [14, 15].

In this study, the applicability of enzyme treatment steps within a full bleaching sequence in relation to process conditions was thoroughly investigated. For removal of hemicelluloses, a commercial oxygen-delignified *E. globulus* kraft pulp was treated with xylanase (X) and CCE prior to TCF (total chlorine free) bleaching. Finally, the pulp was subjected to an endoglucanase (EG) treatment in order to adjust the final viscosity and to increase the pulp reactivity. The experimental bleaching and purification sequence of choice was O-(X)-CCE-A-Z-P-EG, with and without xylanase treatment. Additionally, an ECF-bleached (elemental chlorine free) *E. globulus* kraft pulp was subjected to acid hydrolysis for comparative reasons concerning final pulp reactivity.

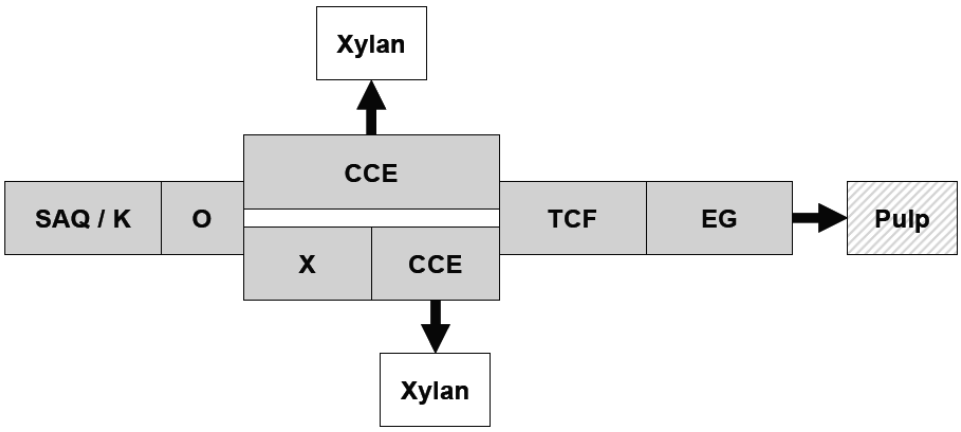

Figure 1. Concept of the Hem-Extra-process.

Table 1. Parameters of the HW-O and HW-ECF starting pulps and differently bleached pulps with optional xylanase pre-treatment.

	Kappa (--)	B (%)	[η] (mL g^{-1})	R18 (%)	Xylan (%)
HW-O	10.3	58.8	895	89.5	22.5
With X-pre-treatment [a]					
X	6.4	67.4	945	90.9	12.1
CCE70	3.6	70.6	1025	96.8	4.9
A	3.6	71.7	1020	96.9	n.d.
Z-3.3	0.9	85.3	720	96.8	n.d.
P	0.4	91.8	585	96.9	4.8
EG20	0.4	91.7	420	95.9	4.7
Without X-pre-treatment [b]					
CCE100	3.9	68.0	1015	98.3	4.2
A	3.4	68.7	945	98.2	n.d.
Z-2.9	0.9	84.2	675	97.9	n.d.
P	0.5	90.2	645	97.8	4.0
EG15	0.5	90.6	330	96.8	4.5
HW-ECF	6.0	90.1	750	91.5	19.1
CCE100	1.4	92.3	860	97.1	6.3
P	2.0	93.3	695	97.1	7.0
A (pH 1.5)	1.2	n.d.	410	n.d.	7.1

[a] CCE 70 g NaOH L^{-1}, Z-bleaching 3.3 kg ozone t^{-1}, EG-treatment 20 ECU g^{-1}
[b] CCE 100 g NaOH L^{-1}, Z-bleaching 2.9 kg ozone t^{-1}, EG-treatment 15 ECU g^{-1}

Experimental

Pulps and enzyme preparations

E. globulus kraft pulps after oxygen-delignification (HW-O) and after final ECF-bleaching (HW-ECF) were kindly supplied by ENCE (Table 1). Both pulps were prepared from wood chips from Uruguay in the pulp mill in Huelva, Spain. The xylanase preparation Pulpzyme® HC and the monocomponent endoglucanase preparation Novozym® 476 were kindly supplied by Novozymes, Denmark. Both preparations are produced by submerged fermentation of genetically modified microorganism.

Enzyme treatments

Enzyme treatments and the washing procedure for enzyme inactivation were performed according to Köpcke *et al.* [16] at 3 % consistency in a phosphate buffer pH 7 (11 mM NaH_2PO_4, 9 mM Na_2HPO_4; deionised water) at 60 °C for 120 min (xylanase treatment) and at 50 °C for 60 min (endoglucanase treatment), respectively. A detailed description of the handling of the enzyme treatments is given in our previous work [19].

Caustic extraction and TCF-bleaching of HW-O

The substrate pulp was subjected to cold caustic extraction with a target residual xylan content of 4.5-5 %. After xylanase-treatment, alkaline extraction with 70 g NaOH L^{-1} (CCE70) was performed while CCE100 (100 g NaOH L^{-1}) was necessary without enzyme pre-treatment to reach the target hemicellulose content (30 min, 30 °C, 10 % consistency). Hot acid treatment (A) was conducted at pH 3.5 adjusted with sulfuric acid at 90 °C for 60 min at 10 % consistency [22]. Final pulp bleaching comprised an ozone stage (Z) followed by hydrogen peroxide bleaching (P). Ozone bleaching was carried out in a medium-consistency high-shear mixer at 50 °C for 10 s at pH 2.5 and 10 % consistency. The ozone charge was adjusted to the viscosity target of 700-750 mL g^{-1}. Peroxide bleaching was performed at 80°C for 120 min at 10 % consistency applying 10 kg NaOH t^{-1} odp, 8 kg H_2O_2 t^{-1} odp and 1 kg $MgSO_4.7H_2O$ t^{-1} odp. The final bleached pulps were acidified with diluted sulfuric acid prior to testing and analytical characterization.

Caustic extraction and acid hydrolysis of HW-ECF

Alkaline extraction was performed with 100 g NaOH L^{-1} at 30 °C for 30 min at 10 % consistency. Peroxide bleaching was performed at 70 °C for 120 min at 10 % consistency applying 5 kg NaOH t^{-1} odp, 4 kg H_2O_2 t^{-1} odp and 1 kg $MgSO_4.7H_2O$ t^{-1} odp. Hot acid treatment of the pulp was performed at 90 °C for 60 min at 3 % consistency and at varying pH values from 1-3.

Viscose preparation and fiber production

Viscose preparation and characterization in terms of particle content and filterability were performed according to a modified method by Treiber *et al.* [23]. Particles in a range of 3 to 155 µm were measured on a Pamas device operating according to the light blockade principle (sensor model HCB25/25, serial number W-2525-2). Viscose solution was extruded through a 20-hole spinneret into a spinning bath on a bench-scale unit. The fibers were cut to staples with a length of 40 mm and were washed to remove acid, salts and occluded sulfur.

Table 2. Structural properties and results of the application tests of the differently treated pulps, analysis of the viscose dopes and fiber characteristics (given for stretching 60 %). The crystallinity index CrI represents the crystallinity of the samples containing cellulose I and II.

	HW-O	HW-O X-CCE70-EG20	HW-O CCE100-EG15
Cell II (%)	n.d.	8	13
CrI (%)	n.d.	54	54
M_w (kg $mole^{-1}$)	450	183	128
PDI (--)	4.9	3.3	2.3
FV (--)	n.d.	171	119
Particle (ppm)	n.d.	23	18
WRV (%)	151	113	120
Tenacity (cN tex^{-1})	n.d.	24.7	25.1
Elongation (%)	n.d.	17.2	17.5
Working capacity (cN tex^{-1} %)	n.d.	430	440

Analytical methods

Carbohydrate content was measured after a two stage total hydrolysis by high performance anion exchange chromatography with pulsed amperometric detection [24]. Water retention value (WRV) was determined according to Zellcheming [25], kappa number according to TAPPI [26], brightness according to ISO [27], intrinsic viscosity [η] according to SCAN-CM [28] and alkali resistance according to DIN [29]. The degree of polymerization (DPv) was calculated from the intrinsic viscosity according to Marx-Figini [30]. Fock-reactivity was measured according to a slightly modified method of Fock *et al.* [31, 32].

Molecular weight distribution was measured by size exclusion chromatography (SEC) with multi-angle light scattering (MALLS) detection in LiCl/DMAc solution according to Schelosky *et al.* [33]. The degree of crystallinity (CrI) and the cellulose II content (Cell II) were determined with FT-Raman [34, 35]. FT-Raman measurements were done using a Bruker IFS66 with Raman module FRA106, Nd:YAG Laser 500 mW; Laser wavenumber 9394 cm^{-1} (1064 nm), liq. N_2 cooled Ge-Detektor, 3500-100 cm^{-1}, resolution 4 cm^{-1}, 100 scans, 4 measurements of each sample. The sample of 300 mg was pressed with 6 t cm^{-1} for approximately 10 min. Analysis was performed with a chemometric model, WAXS data were used as a standard for calibration and comparison.

FE-SEM pictures were accomplished at the Wood Analytics Centre Lenzing (WAL), Lenzing, Austria. The sample was coated with a thin layer of Au/Pd and examined by high-resolution scanning electron microscopy (10,000 x magnification) with a Hitachi S4000 FE-SEM using an acceleration voltage of 10 kV and a working distance of 12 mm.

Results and discussion

Converting the paper-grade pulp HW-O into a dissolving pulp

Xylanase (X) pre-treatment of the starting pulp solubilized 46 % of the initial xylan to a content of 12.1 % (Table 1) which is in good agreement with the results found by Köpcke *et al.* [16]. During X-pre-treatment, the molecular weight of the residual xylan in the pulp was substantially decreased, as can be verified by SEC of the pulps. Xylan chain degradation during X-pre-treatment was further confirmed by the analysis of the beta-cellulose fractions from the CCE-lyes (data not shown) [19]. Consequently, owing to the high degree of xylan chain degradation, xylanase pre-treatment is only recommended for use when the xylan fraction in the caustic lye is not further needed as polymeric reusable material. In contrast, xylan is solubilized in CCE-lyes as high molecular weight polymeric material and thus can be utilized for many additional applications, as described by the principles of modified kraft cooking [36] and the Hem-Extra-process (Figure 1). These process-concepts describe the conversion of paper-grade pulps into dissolving pulps by extraction of hemicelluloses, TCF-bleaching and adjustment of final pulp viscosity and reactivity increase by endoglucanase treatment. The extracted hemi-fraction might be purified and separated into monomers and oligomers by filtration or re-utilized in the cooking or O-bleaching stage of a kraft paper pulp cook in order to attain increased paper pulp fiber strength. Subsequent to TCF-bleaching, DP-adjustment with endoglucanase (EG) was applied as the final treatment step aiming at about 450 mL g^{-1} (DPv = 1050), the target viscosity for viscose staple fiber kraft pulps. Final EG-treatment decreased the viscosity of the X-pre-treated pulp to 420 mL g^{-1} odp at an enzyme concentration of 20 ECU g^{-1} (EG20) and the viscosity of the reference pulp without X-pre-treatment to 330 mL g^{-1} at an

enzyme concentration of 15 ECU g^{-1} (EG15). The elevated chain degradation of the CCE100-treated pulp might be traced back to its increased cellulose II content, which is preferably degraded by the enzymes. The final pulp properties, spinning dope qualities and the fiber characteristics are shown in Table 2. A FE-SEM picture of the pulp HW-O-X-CCE70-EG20 is shown in Figure 2. The CCE100-treated pulp was of high purity (R18 96.8 %) and thus showed a narrower molecular weight distribution, expressed as very low polydispersity index. The reactivity of the pulps was determined by measuring the filterability of the viscose dope as filter clogging value (FV). The X-pre-treated pulp HW-O-X-CCE70-EG20 had a higher reactivity (171) compared to HW-O-CCE100-EG15 (119). Both enzyme treated pulps revealed higher filter values in comparison to other alkali extracted kraft pulps [37, 38], indicating an increase in reactivity caused by enzyme treatment. Drying or intense dewatering of pulps after treatment at high alkalinity is known to induce the formation of molecular aggregates by inter- and intra-fibrillar hydrogen bonding of the cellulose microfibrils, which is known as hornification. In terms of reactivity towards xanthation in the viscose process, the influence of drying is not yet clear. In order to quantify hornification, the water retention value, which provides information about the integral pore volume of a pulp and the content of hydrophilic groups, was determined as an indicator of the swelling capacity of a pulp. High swelling capacity enables homogeneous penetration of the dissolving lye into the pulp, uniform sorption and swelling of the pulp and a low particle content of the final viscose dope. This hypothesis is in good agreement with the results of this study. The never-dried pulp HW-O-X-CCE70-EG20 showed a slightly lower WRV (113 %), but a higher dope particle content (23 ppm) in comparison to the pulp HW-O-CCE100-EG15 (WRV 120 %, particle 18 ppm). Mechanical fiber properties expressed in terms of tenacity, elongation and working capacity of the staple fibers made thereof were comparable (Table 2), also to those made of commercial PHK pulps (not shown).

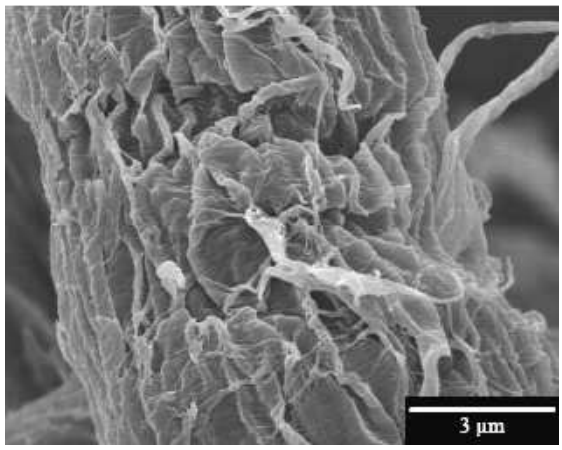

Figure 2. FE-SEM picture of the endoglucanase treated pulp HW-O-X-CCE70-EG20; destroyed surface structure visible.

Comparison of enzyme and acid degradation

In order to investigate the activating effect of an endoglucanase treatment, the reactivity according to Fock [31] of the enzymatically degraded pulp was measured and compared to an acidly degraded industrial HW-ECF paper-grade pulp of same viscosity after CCE100- and P-treatment (Table 1). The change in viscosity is shown in Figure 3. The Fock-method describes a lab-scale viscose process upon which an alkaline pulp suspension is mixed with carbon disulfide in order to get a viscose-like solution. From this solution, cellulose is regenerated by acidification and quantified by an oxidation- and titration-procedure. The Fock-reactivity given in weight percentage describes the amount of pulp which was dissolved in the viscose-like solution. Consequently, high Fock-reactivity indicates high pulp reactivity. Following the trend of the filter values, the pulp

HW-O-X-CCE70-EG20 showed a higher Fock-reactivity (26.8 %) compared to HW-O-CCE100-EG15 (22.9 %). The pulp degraded at pH 1.5 had an even lower Fock-reactivity of 19.1 % and a broader molecular weight distribution (PDI 2.9) compared to the other CCE100-treated pulp (PDI 2.3) was observed.

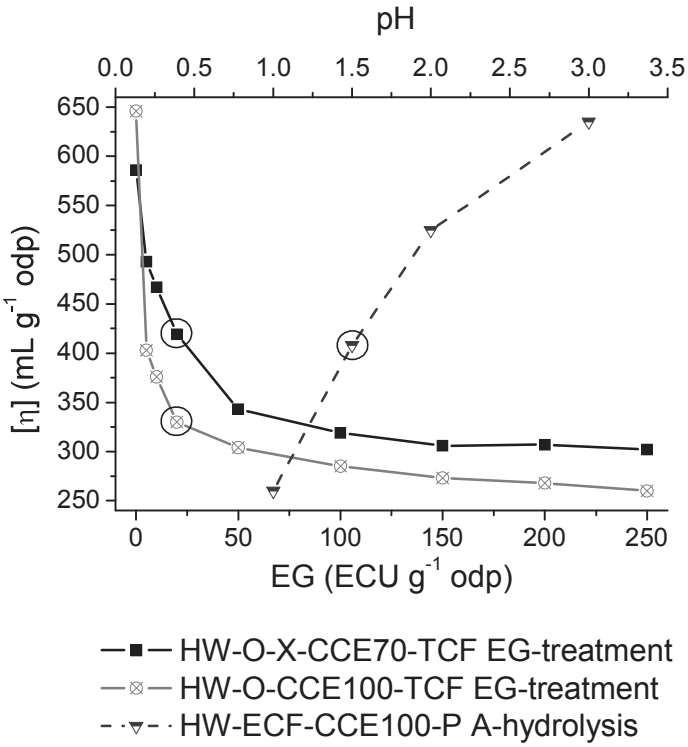

Figure 3. Comparison of cellulose degradation upon endoglucanase treatment and acid hydrolysis: EG-treatment of the dissolving pulps converted from the paper-grade pulp HW-O; A-hydrolysis of the HW-ECF paper-grade pulp after CCE100- and P-treatment; Encircled: pulps for Fock-reactivity measurement.

Conclusions

The present study revealed beneficial effects of xylanase pre-treatment and endoglucanase post-treatment in the production of novel high-purity dissolving pulps following the Hem-Extra-process scheme. A commercial oxygen delignified *E. globulus* kraft pulp was subjected to a (X)-CCE-A-Z-P-EG treatment, with and without xylanase pre-treatment, revealing the following effects:

- Xylanase (X) pre-treatment removed almost 50 % of the initial xylan of the pulp and thus subsequent CCE at reduced alkalinity was adequate to reach the target residual xylan content of the pulp.
- Xylan recovered from CCE-lye after X-pre-treatment was highly degraded and so the xylan fraction in the caustic lye was not useable anymore as polymeric material.
- The adjustment of the final average degree of polymerization was accomplished by endoglucanase treatment and a direct correlation between the cellulose II content and the chain cleavage of the pulps upon enzymatic degradation was confirmed.
- The xylanase pre-treated pulp showed an increased reactivity towards xanthation determined as

filter value and as Fock-reactivity because of the lower degree of fiber hornification.

- A comparison of enzymatically degraded pulps with an acidly hydrolyzed pulp showed higher Fock-reactivity for the enzyme-treated pulps, indicating an opening effect of the enzyme treatment on the fiber pore structures - this being apparent in increased water retention values, resulting in a more homogeneous penetration of carbon disulfide and dissolving lye into the fibers after enzyme treatment due to an enlarged capillary system.
- The differently treated pulps fulfilled the main characteristics as required for viscose application and the mechanical fiber properties expressed in terms of tenacity, elongation and working capacity of the staple fibers made thereof were comparable to those made of commercial PHK pulps.

The commercial benefit of the new Hem-Extra-pulps compared to a conventional prehydrolysis-kraft pulp is constituted by a substantial higher yield at a given R18 content, ranging between 4 % and 8 % on oven dried wood depending on the wood source [39]. This yield advantage is based on the high selectivity of the CCE treatment towards cellulose, while prehydrolysis of wood introduces new reducing end groups through cellulose depolymerization which in turn initiates a substantial cellulose yield loss during subsequent alkaline cooking owing to peeling reactions.

Acknowledgements

Financial support was provided by the Austrian government, the provinces of lower Austria, upper Austria, and Carinthia as well as by Lenzing AG. We also express our gratitude to the Johannes Kepler University, Linz, the University of Natural Resources and Applied Life Sciences, Vienna, and Lenzing AG for their in-kind contribution.

References

[1] G. Jayme, E. Roffael, Das Papier 23 (1969) 405-412.
[2] H. A. Krässig, Das Papier 38 (1984) 571-582.
[3] J. Blackwell, F. J. Kolpak, K. H. Gardner, Tappi J. 61 (1978) 71-72.
[4] F. J. Kolpak, J. Blackwell, Macromol. 9 (1976) 273-278.
[5] T. N. Kleinert, Holzforschung 29 (1975) 134-135.
[6] B. Kyrklund, H. Sihtola, Papper och Trä 4 (1963) 131-134.
[7] T. Oksanen, J. Buchert, L. Viikari, Holzforschung 51 (1997) 355-360.
[8] K. D. Sears, J. F. Hinck, C. G. Sewell, J. Appl. Polym. Sci. 27 (1982) 4599-4610.
[9] N. M. S. El-Din, F. F. A. El-Megeid, Holzforschung 48 (1994) 496-500.
[10] G. Jayme, U. Schenck, Das Papier 3 (1949) 469-476.
[11] H. Sixta, Pulp purification. In: H. Sixta (ed) Handbook of Pulp - Volume 2, 1st edn. Wiley-VCH, Weinheim, pp 933-966 (2006).
[12] H. Sixta, Pulp properties and applications. In: H. Sixta (ed) Handbook of Pulp - Volume 2, 1st edn. Wiley-VCH, Weinheim, pp 1009-1069 (2006).
[13] H. A. Krässig, Methods of activation. In: H. A. Krässig (ed) Cellulose: Structure, accessibility and reactivity, 1st edn. Gordon and Breach Science Publishers, Amsterdam, The Netherlands, pp 215-276 (1993).
[14] A.-C. Engström, M. Ek, G. Henriksson, Biomacromol. 7 (2006) 2027-2031.
[15] G. Henriksson, M. Christiernin, R. Agnemo, J. Ind. Microbiol. Biotechnol. 32 (2005) 211-214.
[16] V. Köpcke, D. Ibarra, M. Ek, Nordic Pulp Pap. Res. J. 23 (2008) 363-368.

[17] M. Luo, Enzymatic treatment of pulp for lyocell manufacture. Weyerhaeuser-Company. Patent PCT/US2008/086367.
[18] D. Ibarra, V. Köpcke, P. T. Larsson, A.-S. Jääskeläinen, M. Ek, Bioresour. Technol. 101 (2010) 7416-7423.
[19] V. Gehmayr, G. Schild, H. Sixta, Cellulose 18 (2011) 479-491.
[20] L. Rahkamo, L. Viikari, J. Buchert, T. Paakkari, T. Suortti, Cellul. 5 (1998) 79-88.
[21] R. H. Atalla, Conformational effetcs in the hydrolysis of cellulose. In: R. D. Brown Jr., L. Jurasek (ed) Hydrolysis of cellulose: Mechanisms of enzymatic and acid catalysis, 1st edn. American Chemical Society, Washington D. C., pp 55-69 (1979).
[22] T. Vuorinen, P. Fagerstroem, J. Buchert, M. Tenkanen, A. Teleman, J. Pulp Pap. Sci. 25 (1999) 155-162.
[23] E. Treiber, J. Rehnström, C. Ameen, F. Kolos, Das Papier 16 (1962) 85-94.
[24] H. Sixta, N. Schelosky, W. Milacher, T. Baldinger, T. Röder, Characterization of alkali-soluble pulp fractions by chromatography. In: The 11th ISWPC, Nice, France, June 11-14 (2001).
[25] Zellcheming Merkblatt IV/33/57, Bestimmung des Wasserrückhaltevermögens (Quellwertes) von Zellstoffen (1957).
[26] TAPPI T 236 cm-85, Kappa number of pulp (1993).
[27] ISO 2470-1, Paper, board and pulps - Measurement of diffuse blue reflectance factor - Part 1: Indoor daylight conditions (ISO brightness) (2009).
[28] SCAN-CM 15:99, Viscosity in cupriethylenediamine solution (1999).
[29] DIN 54355, Bestimmung der Beständigkeit von Zellstoff gegen Natronlauge (Alkaliresistenz) (1977).
[30] M. Marx-Figini, Angew. Makromol. Chemie 72 (1978) 161-171.
[31] W. Fock, Das Papier 13 (1959) 92-95.
[32] N. Kvarnlöf, Activation of dissolving pulps prior to viscose preparation. Dissertation, Karlstad University (2007).
[33] N. Schelosky, T. Röder, T. Baldinger, Das Papier 53 (1999) 728-738.
[34] T. Röder, J. Moosbauer, M. Fasching, A. Bohn, H.-P. Fink, T. Baldinger, H. Sixta, Lenzinger Berichte 86 (2006) 85-89.
[35] W. Ruland, Acta Crystallogr. 14 (1961) 1180-1185.
[36] H. Sixta, A. Promberger, A. Borgards, R. Möslinger, Verfahren zur Herstellung eines Zellstoffes. Lenzing-Aktiengesellschaft. Patent PCT/AT2007/000225.
[37] G. Schild, H. Sixta, Cellul. Online First™, April 16 (2011)
[38] R. Wollboldt, G. Zuckerstätter, H. Weber, P. Larsson, H. Sixta, Wood Sci. Technol. 44 (2010) 533-546.
[39] G. Schild, H. Sixta, V. Gehmayr, Production of a novel generation of sulphur-free dissolving pulps. In: Zellcheming Cellulose-Symposium, Wiesbaden, Germany, June 29-30 (2010).